Immune Evasion by *Staphylococcus aureus*: Expanding the Repertoire

Nienke Wilhelmina Maria de Jong

Immune Evasion by *Staphylococcus aureus*: Expanding the Repertoire
PhD thesis, Utrecht University, the Netherlands

ISBN: 978-94-6295-866-1
Cover-design: Dr. Ron Gorham
Lay-out: Nienke de Jong
Printing: ProefschriftMaken || www.proefschriftmaken.nl

Photograph of the author (page 209) by Kobus Bosman

Printing of this thesis was financially supported by the Netherlands Society of Medical Microbiology (NVMM) and the Royal Netherlands Society for Microbiology (KNVM); Infection and Immunity Center Utrecht; Chipsoft BV; Stichting voor Afweerstoornissen; and the University Medical Center Utrecht.

Immune Evasion by *Staphylococcus aureus*: Expanding the Repertoire

Ontsnapping aan het Immuunsysteem door *Staphylococcus aureus*:
Uitbreiding van het Arsenaal

(met een samenvatting in het Nederlands)

Proefschrift

ter verkrijging van de graad van doctor aan de Universiteit Utrecht op gezag van de rector magnificus, prof.dr. G.J. van der Zwaan, ingevolge het besluit van het college voor promoties in het openbaar te verdedigen op donderdag 29 maart 2018 des middags te 12.45 uur

door

Nienke Wilhelmina Maria de Jong

geboren op 10 maart 1988
te Waalre

Promotor
Prof.dr. J.A.G. van Strijp

Copromotor
Dr. K.P.M. van Kessel

Voor mijn ouders

Leescommissie
Prof.dr. L. Koenderman
Prof.dr. H.P. Haagsman
Prof.dr. J.P.M. van Putten
Prof.dr. W. Bitter
Dr. M. Vrieling

Paranimfen
Kirsten J. Koymans
Seline A. Zwarthoff

TABLE OF CONTENTS

Chapter 1

GENERAL INTRODUCTION - Immune evasion by *Staphylococcus aureus*

Nienke W. M. de Jong[1], Kok P. M van Kessel[1], Jos A. G. van Strijp[1]

[1] Department of Medical Microbiology, University Medical Center Utrecht, Utrecht University, Utrecht, the Netherlands

Manuscript accepted for publication:
Adapted from Gram-positive pathogens, 3rd Edition, Section III: the Staphylococcus Novick R. et al., Eds.

ABSTRACT

Staphylococcus aureus has become a serious threat for human health. Next to having an increased antibiotic resistance, the bacterium is a master in adapting to its host by evading almost every facet of the immune system, the so-called immune evasion proteins. Many of these immune evasion proteins target neutrophils, the most important immune cells in clearing *Staphylococcus aureus* (*S. aureus*) infections. The neutrophil attacks pathogens via a plethora of strategies. Therefore, it is no surprise that *S. aureus* has evolved numerous immune evasion strategies at almost every level imaginable. In this review we discuss step by step the different aspects involved in neutrophil-mediated killing of *S. aureus* such as neutrophil activation, migration to the site of infection, bacterial opsonization, phagocytosis and subsequent neutrophil-mediated killing. After each section we discuss how *S. aureus* evasion molecules are able to resist the neutrophil attack of these different steps. To date, around forty immune evasion molecules of *S. aureus* are known, but its repertoire is still expanding due to the discovery of new evasion proteins and addition of new functions to already identified evasion proteins. Interestingly, as the different parts of neutrophil attack are redundant, the evasion molecules display redundant functions as well. Knowing how and with which proteins *S. aureus* is evading the immune system is important in understanding the pathophysiology of this pathogen. This knowledge is crucial for development of therapeutic approaches that aim to clear staphylococcal infections.

1. INTRODUCTION

The Gram positive bacterium *Staphylococcus aureus* (*S. aureus*) is considered a commensal bacterium as roughly one third of the human population is colonized by this bacterium without developing disease (1). Colonization occurs in the human nose whereby host nasal microbiota plays a major role in promoting or inhibiting *S. aureus* colonization (2). Despite the fact that *S. aureus* is considered a commensal, nasal carriage of *S. aureus* is linked to bacteremia (3). Once infected with *S. aureus*, the bacterium may cause a range of infections, from cellulitis and superficial skin disease to abscesses, bacteremia, sepsis, endocarditis, and pneumonia (4). Moreover, *S. aureus* has shown to adapt in the interaction with humans by increasing resistance against methicillin among staphylococci and is currently a leading cause of human bacterial disease worldwide. Methicillin-resistant *S. aureus* (MRSA) was identified in the 1960s as a nosocomial pathogen, when hospitalized patients showed distinct risk factors for acquisition (5). The prevalence of methicillin resistance among nosocomial *S. aureus* isolates has increased from 2.1% in 1975 to 35% in 1991 (6). MRSA epidemiology changed in the 1990s when infections of healthy individuals outside hospitals were reported. These increased virulence strains were the first reports of community-acquired (CA) MRSA (7, 8). Now, *S. aureus* has been reported as the leading cause of bacterial infections in the bloodstream, skin, soft tissue, and lower respiratory tract in the developed countries (9). As a consequence, research interest in the pathophysiology of *S. aureus* has extended.

This extensive research during the last decades resulted in the identification and characterization of around forty proteins which are able to evade various processes of the innate and adaptive immune system (10), the so called immune evasion proteins. Proteomics have shown that around 100-200 proteins of *S. aureus* are secreted, many with a still unknown function (11). These unknown secreted proteins are potential evasion molecules, demonstrating that the identification and characterization of new evasion proteins is not completely known yet and will most likely expand in the future.

Many evasion proteins are targeted against neutrophils. This is not a surprise as neutrophils are the most prominent leukocytes in blood, covering 60% of the leukocyte population and play a prominent role in fighting *S. aureus* infection. They are equipped with various granules with specific content to kill both Gram-negative and Gram-positive bacteria (12, 13). Neutrophils originate and mature in the bone marrow and are afterwards released into blood vessels. There, these end-stage cells will circulate and migrate toward the site of infection by chemotactic signals produced both by the bacteria themselves as well as by host cells (13). Upon arrival at the infection site, neutrophils are able to 'eat' micro-organisms that are opsonized (labeled) by the complement system or immunoglobulins (antibodies). The complement system is especially important in clearing staphylococcal infections. Mice deficient in complement C5 showed decreased clearance of *S. aureus* after pulmonary and bloodstream infections (14, 15). In addition, antibodies play an important role in fighting staphylococcal

Abbreviation	Full name	Evades process
Aur	Aureolysin	III, V
CHIPS	Chemotaxis inhibitory protein of *Staphylococcus*	II
Cna	*Staphylococcus* aureus collagen adhesion	III
Eap and EapH	Extracellular adherence protein-homologue	I, V
Ecb	Extracellular complement-binding protein	III
Efb	Extracellular fibrinogen-binding protein	III
FLIPr	FPR2 inhibitory protein	II
Hla	Hemolysin-alpha	V
Hlg	Hemolysin-gamma	V
Hmp	Flavohemoglobin	V
Ldh	L-lactate dehydrogenase	V
Luk	Leukocidin	V
MMP	Matrix metalloproteinase	II
Nuc	Nuclease	IV
PSMs	Phenol-soluble modulins	V
SAgs	Superantigens	V
SAK	Staphylokinase	III, V
Sbi	Staphylococcal binding of IgG	III
SCIN	Staphylococcal complement inhibitor	III
ScpA	Staphopain A	II
SdrE	Surface-associated serine-aspartate repeat protein E	III
SElX	Staphylococcal enterotoxin-like X	I
SpA	Staphylococcal protein A	III
SPIN	Staphylococcal peroxidase inhibitor	V
SSL	Staphylococcal superantigen-like	I, II, III

Table 1: Abbreviations from staphylococcal immune evasion proteins and the processes they evade.

Different processes of neutrophil-mediated killing:

I Neutrophil extravasation
II Priming, chemotaxis and activation of neutrophils
III Opsonization and phagocytosis
IV NET formation
V Bacterial killing by neutrophils

infections. Opsonization of bacteria subsequently leads to phagocytosis and ultimately killing of microbes, because neutrophils release the content of their antimicrobial granules and the produce reactive oxygen species (ROS) (13).

Impaired neutrophil function is linked to staphylococcal infections, as shown in multiple studies. For instance, patients suffering from congenital neutropenia deficiencies often have severe infections, including staphylococcal infections, which can be fatal (16). Patients with chronic granulomatous disease (CGD) have defects in their NADPH oxidase which leads to impaired formation of ROS. Especially catalase-positive micro-organisms, such as *S. aureus*, cause recurrent infections in these patients because catalase breaks down the bacterial hydrogen peroxide and thereby prevents the generation of ROS (17). Another example where *S. aureus* infections play a major role, is in burn patients. The burn wound is especially susceptible to bacterial colonization and infection, because neutrophils are known to be decreased in burn patients (18, 19). From these observations we can conclude that neutrophil-mediated killing in healthy individuals is crucial in the defence against *S. aureus*.

After the first response, the acquired immune system comes in the picture. However, this part of the immune system has an insignificant role in acute infection. Nonetheless, antibodies are important on the long term with recurrent staphylococcal infections, but antibodies against staphylococcal proteins do not show effective protection, since high levels of circulating antibodies against different *S. aureus* proteins are not protective enough from acquiring *S. aureus* infections (20).

In this chapter we discuss the different facets of the innate immune system to *Staphylococcus aureus*. First, we describe the mechanisms of neutrophil extravasation through the endothelium. Second, we give an overview of the proteins and receptors involved in neutrophil priming, chemotaxis, and activation. Third, we describe the processes involved in bacterial opsonization and phagocytosis by neutrophils. Fourth, we provide an overview of the processes involved in bacterial killing by neutrophils. After each section we describe the various evasion molecules intervening that specific process. Finally, we discuss why *S. aureus* has evolved so many evasion proteins and therapeutic implications against staphylococcal infections. Thus, we will give an overview of what we know so far about *S. aureus* immune evasion and what lessons we can draw from this knowledge.

2. NEUTROPHIL EXTRAVASATION THROUGH THE ENDOTHELIUM

Once pathogens cause infections in tissues, neutrophils leave the bloodstream and migrate toward the site of infection. This multistep process is called extravasation and includes neutrophil rolling, crawling and firm adhesion to the endothelial cells, extravasation through the endothelium (diapedesis), and migration to the infection site over a chemokine gradient (21). An overview of this process is shown in **Figure 1**.

First, the neutrophils in the bloodstream slow down near the site of infection. This is initiated by changes on the endothelial surface by inflammatory mediators (e.g. histamine, cytokines

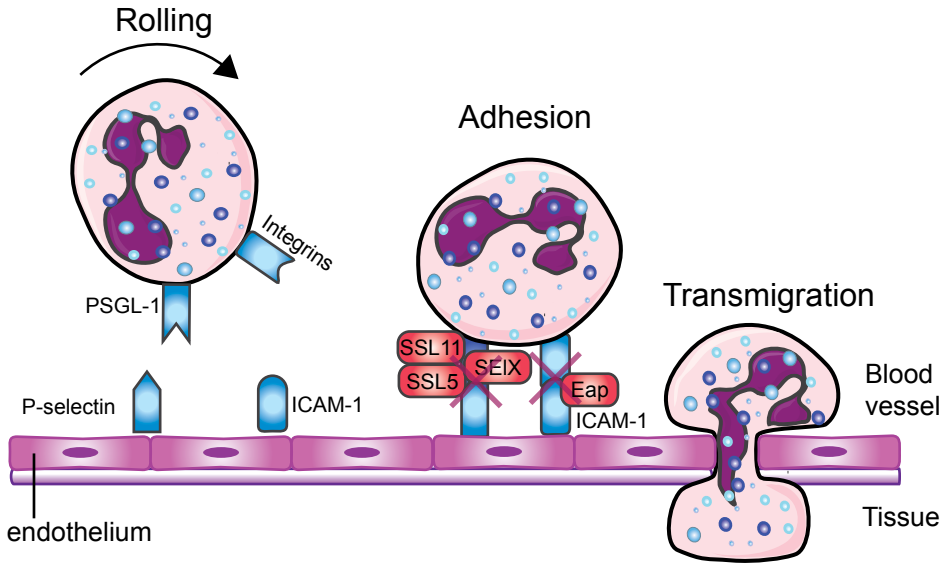

Figure 1: Evading neutrophil extravasation to the infection site. Mechanisms by which *Staphylococcus aureus* evades the different steps in neutrophil extravasation. Neutrophils start to roll on the activated endothelium, which leads to firm adhesion and subsequently transmigration through the endothelium. Red boxes indicate staphylococcal proteins whereas blue boxes indicate host proteins. Abbreviations: PSGL-1, P-selectin glycoprotein 1; SSL, staphylococcal superantigen-like protein; ICAM-1, intracellular adhesion molecule 1; Eap, extracellular adherence protein; SEIX, staphylococcal enterotoxin-like X. The figure was adapted from Servier Medical Art.

and leukotrienes) (22). The endothelial cells are activated and start to express P-selectin and E-selectin which interact with P-selectin glycoprotein ligand-1 (PSGL-1) on the surface of neutrophils (23). This leads to the tethering (capturing) of freely moving neutrophils to the endothelial surface as they start to roll along the vessel in the direction of the blood flow. In the second step the neutrophils adhere and 'crawl' along the vessel wall by the interaction between intercellular adhesion molecule 1 (ICAM-1) on endothelial cells and ß2 integrins (such as LFA-1 and Mac-1) on the surface of phagocytes (24–26). Neutrophils express constitutively high levels of ß2 integrins, which undergo conformational change upon either intracellular activation ligand binding (outside-in signaling) or integrin adhesiveness (inside-out signaling). ß2 integrins are re-localized to the cell surface upon activation by chemokines (27, 28). The neutrophils enter the arrested state after expressing high levels of ICAM-1. This leads to the initiation of transendothelial cell migration through a paracellular (passing through the endothelium between the cells) or a transcellular (movement through the endothelial cell) pathway. Leukocytes mainly migrate via the paracellular route, but follow the transcellular route in the central nervous system and in various inflammatory settings (29). After extravasation, the neutrophils continue their journey toward the infection site via chemotaxis.

3. EVADING NEUTROPHIL EXTRAVASATION

An overview of the molecules evading the extravasation of neutrophils is shown in **Figure 1**. *S. aureus* is able to modulate the first step in neutrophil extravasation, rolling of neutrophils on endothelial cells, by secreting staphylococcal superantigen-like 5 (SSL5). SSL5 directly binds PSGL-1 on leukocytes and human HL-60 leukemia cells. This prevents the interaction of PSGL-1 with its natural ligand, P-selectin, in a sulfation- and sialylation dependent manner (30, 31). Co-crystallization data revealed SSL5 in complex with tetrasaccharide sialyl Lewis X (sLeX), a key posttranslational modification of PSGL-1 binding to P-selectin (32). SSL5 is part of a larger group of 14 structurally related proteins (SSL1-14), which are involved in innate immune evasion. SSL11 shares the highest amino acid sequence identity to SSL5 out of all the SSLs and also shows binding to sLeX by looking at the co-crystal structure of the complex. SSL11 also binds other sialic acid-containing glycoproteins, such as FcαRI, the Fc receptor for IgA (33). *S. aureus* secretes another immune evasion molecule, named SElX, which also interacts with PSGL-1 in a glycosylation-dependent manner (34). Before the molecular mechanism was identified, SElX was previously described to possess superantigenic activity and was associated with a virulence factor in MRSA necrotizing pneumonia (35). Recently, SElX was also found to have the sialylated-glycan-dependent active site, similar to a sub-family in SSLs (SSL2-4 and SSL6) (36). This leads to binding of neutrophils and monocytes via multiple glycosylated neutrophil surface receptors and thereby disrupting IgG-mediated phagocytosis and contributing to pathogenesis in a necrotizing pneumonia rabbit infection model (37, 38).

The second step of extravasation, the adhesion of neutrophils to endothelial cells, is also targeted by *S. aureus*. The pathogen secretes extracellular adherence protein (Eap) that directly binds ICAM-1 and thereby inhibits neutrophil recruitment to the infection site (39).

4. PRIMING, CHEMOTAXIS AND ACTIVATION OF NEUTROPHILS

When neutrophils have migrated through the endothelial barrier, they are primed, recruited toward the site of infection by various chemoattractants and activated by multiple inflammatory stimulants. Here we will discuss various sets of proteins and receptors involved in this process. An overview is shown in **Figure 2**.

Priming is when a neutrophil is exposed to a primary priming stimulus and therefore enhances neutrophil's functional response (for example adhesion, phagocytosis, degranulation, and superoxide production (40)), whereby the priming stimulus does not give the functional response itself (41). This is dependent on the concentration of the stimulus, because chemotaxis is promoted at higher concentrations. Examples of known priming molecules for neutrophils are: complement components C3a and C5a (42), interleukin-8 (IL-8) (43), granulocyte colony-stimulating factor (G-CSF) (43), tumor-necrosis factor-α (TNF-α) (44), and interferon-γ (IFN-γ)

(45).

Chemoattractants are chemokines and bacteria- and complement-derived products and they will activate phagocytes by interacting with receptors at the surface of neutrophils which belong to the superfamily of G protein-coupled receptors (GPCRs) (46). These GPCRs also belong to the rhodopsin subfamily of GPCRs which is a seven-transmembrane receptor with seven helical membrane-spanning regions connected by six extramembrane loops, as shown with crystallizing studies (47). The mechanism of stimulation of the GPCR depends on type of ligand. For example small peptides (e.g. fMLP) and lipid-derived stimuli (e.g. platelet-activating factor and leukotriene B4) primarily activate their GPCRs through the transmembrane regions. Larger stimuli (e.g. chemokines and anaphylatoxins) activate GPCRs via a two-step model, whereby the stimulus binds the N-terminus of the specific GPCR, whereupon conformational change of the receptor leads to activation by the interaction with the pocket formed by the transmembrane domains (48). CXC chemokine receptors expressed on the surface of various immune cells also belong to the family of GPCRs and to date, seven receptors have been described (named CXCR1 trough CXCR7). They interact with chemokines, a large family of 8-12 kDa proteins. The CXC chemokines are one of the most prominent groups and are mostly chemotactic for neutrophils, such as CXCL8 (also known as IL8) (49).

Newly synthesized bacterial proteins contain formylated methionine, thus bacteria secreted a lot of N-formylated proteins and peptides, which were identified as chemoattractants in 1975 (50). These formylated peptides interact with formyl peptide receptor 1 (FPR1) and 2 (FPR2) (FPR2 is also known as FPRL1) on neutrophils (51), both belonging to the GPCR family. The prototype N-formyl-peptide, fMLP, binds with higher affinity to FPR1 than its homologue FPR2 (52). Neutrophils and monocytes express FPR1 and FPR2, whereas the third homologue, FPR3 (also known as FPRL2), is only expressed in monocytes (52). Staphylococci produce phenol-soluble modulins (PSMs) in addition to formyl peptides. PSMs are important secreted staphylococcal toxins but they are also sensed by FPR2, which leads to activation and attraction of leukocytes (53).

Two complement receptors (CRs) on neutrophils also belong to the family of GPCRs, namely C3a receptor (C3aR), and C5a receptor (C5aR). Their ligands are the small complement components C3a and C5a, formed during complement activation. C5a and C3a are commonly also called anaphylatoxins and are both chemoattractants by attracting phagocytes to the site of infection (54).

Neutrophils express also another class of innate immune receptors that are involved in pathogen recognition, the Toll-like receptors (TLRs). The discovery of these proteins in the mid-1990s revealed that pathogen recognition by the innate immune system is actually specific by recognizing different parts of foreign pathogens, which are called pathogen-associated molecular patterns (PAMPs). PAMPs important for staphylococcal infections are

bacterial lipoproteins (recognized by TLR1, TLR2, TLR6) and unmethylated CpG sequences in DNA molecules (recognized by TLR9) (55). Ligand binding to the extracellular domains of TLRs causes dimerization of the receptor complexes and triggers recruitment of MyD88 to the intracellular TIR domains, which ultimately leads to the activation of transcription factor NF-κB (56). Most TLRs appear to function as homodimers, although TLR2 forms heterodimers with TLR1 or TLR6. TLR1/2 recognizes triacylated lipoproteins, whereas TLR2/6 specifically respond to diacylated lipoproteins (57). TLRs are not directly involved in chemotaxis but they contribute in phagocytosis.

Another class of proteins important for controlling inflammation are the matrix metalloproteinases (MMPs). This family of 23 different endopeptidases is secreted by numerous cells and is important in the recruitment and migration of neutrophils during bacterial infections. They breakdown extracellular matrix components, so neutrophils can migrate toward the infection, but they also stimulate pro-inflammatory signals and cleave chemokines. This leads to an enhanced inflammation and improved bacterial clearance. The two main neutrophil MMPs are MMP8 (also known as neutrophil collagenase) and MMP9 (also known as neutrophil gelatinase B) (58).

5. EVADING PRIMING, CHEMOTAXIS AND ACTIVATION OF NEUTROPHILS

Studies thus far have not shown whether *S. aureus* can directly modulate neutrophil priming to influence the function of neutrophils. Additional studies are necessary to understand the influence of *S. aureus* on neutrophil priming (59). However, more knowledge is gained about the impact of *S. aureus* on neutrophil chemotaxis and activation. Here we describe the function of the evasion proteins SSL5, SSL10, SSL3 and SSL4, Staphopain A, CHIPS, FLIPr, and FLIPr-like in their role in evading neutrophil chemotaxis and activation, as shown in **Figure 2**.

SSL5 binds to PSGL-1, to evade neutrophil extravasation, but it also binds glycosylated N-termini GPCRs, thereby inhibiting the ligands that require the N-terminus of the receptor for activation. Therefore, it binds but does not interfere with the activation of FPR1 and FPR2, leukotriene B4 receptor, platelet-activating factor receptor, and nucleotide receptor P2Y2, since ligands of these receptors are small and signal via the transmembrane domains of the GPCRs (60). Pretreating neutrophils with SSL5 leads to inhibited activation induced by C3a and C5a, because chemokines and anaphylatoxins bind the N-termini of their receptors. SSL5 also inhibits activation and neutrophil migration induced by IL-8 which interacts with CXCR1 and CXCR2, but it also targets the response induced by chemokine ligand 1 (CXCL1) that acts only on CXCR2 (60). SSL5 together with SSL1 inhibit neutrophil migration through breakdown of collagen and potentiation of IL-8 by inhibiting cleavage of the neutrophil specific MMP8 (neutrophil collagenase) and MMP9 (neutrophil gelatinase B) as well as other members of the MMP family (MMP1, 2, 7, 12, 13, and 14) (61, 62). Additionally, SSL5 activates and aggregates

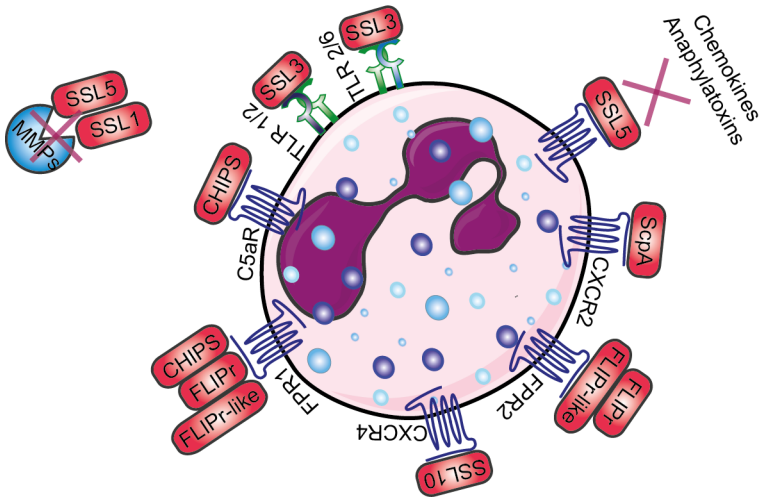

Figure 2: Schematic overview how *S. aureus* evades priming, chemotaxis, activation of neutrophils. Red boxes indicate staphylococcal proteins whereas proteins shown in blue indicate host proteins. Abbreviations: TLR, Toll-like receptor; CXCR, chemokine receptor; ScpA, Staphopain A; SSL, staphylococcal superantigen-like protein; FPR, formyl peptide receptor; FLIPr, FPR2 inhibitory protein; C5aR, C5a receptor; CHIPS, chemotaxis inhibitory protein of Staphylococcus; MMP, matrix metalloproteinase. The figure was adapted from Servier Medical Art.

platelets by interacting with platelet membrane receptor GPIbα and collagen receptor GPVI, leading to a beneficial environment for staphylococcal colonization (63, 64).

SSL10 targets another chemokine receptor, CXCR4, expressed on neutrophils and cancer cells. It binds to human T-cell acute lyphoblastic leukemia, lymphoma, and cervical carcinoma cell lines and inhibits calcium mobilization and cell migration induced by the ligand of CXCR4; CXCL12 (also known as stromal cell-derived factor-1 α, SDF-1α) (65).

SSL3 binds the extracellular domain of TLR2 and inhibits its activity on human and murine neutrophils and monocytes (66, 67). The co-crystal structure of SSL3 in complex with TLR2 reveals that SSL3 blocks ligand binding and prevents TLR heterodimerization of TLR1 and TLR6 and downstream signaling by interacting with an already formed TLR2-lipopeptide complex (68). SSL4 shares the highest homology with SSL3 and also blocks TLR2 activation, albeit less potent compared to SSL3. Therefore it remains unknown if this is the primarily function of SSL4, because SSL4 also showed to bind myeloid cells in a glycan-dependent manner (66, 69). Recently, antibodies against SSL3 and SSL4 were detected in human serum, showing that both evasion proteins are secreted *in vivo*. SSL3 is able to bind both murine and human TLR2, therefore SSL3 was investigated in an intravenous murine infection model where it showed to be more virulent. To circumvent low expression rates of SSL3 in mice, an SSL3-overproducing strain was used (70).

S. aureus also secretes a protease that interferes with chemokine signaling. Staphopain A cleaves the N-terminus of CXCR2 and thereby cause unresponsive neutrophils to activation by CXCR2. The protease also hampers neutrophil migration toward CXCR2 chemokines (71). Mature Staphopain A has a broader substrate specificity, because it is also able to degrade elastin fibers. However, it is also prone to autolytic degradation, which could explain the loss of activity of Staphopain A over time (71, 72).

S. aureus supernatant showed chemotaxis-inhibiting properties by targeting fMLP and C5a response of neutrophils (73). Later the protein responsible in the supernatant was identified and this 14.1 kDa evasion protein was named chemotaxis inhibitory protein of Staphylococcus (CHIPS). CHIPS binds and inhibits the GPCRs FPR1 and C5aR on neutrophils and monocytes. Thus, it blocks these receptors for their ligands, namely C5a and fMLP, and thereby impairs the activation and chemotaxis of phagocytes (74, 75). N-terminal peptides of CHIPS inhibited FPR1, while the activity of C5aR was unaffected (76). This showed that the N-terminus of CHIPS is specific for its activity toward FPR1 and that CHIPS probably had another binding site for C5aR. Indeed, CHIPS targets with its C-terminal domain specifically the N-terminus of C5aR through binding to amino acids 10-18 and thereby prevents the binding of C5a to its receptor (77, 78). Especially arginine 44 and lysine 95 of CHIPS appear to be highly important in the antagonism of C5aR (78).

The importance of CHIPS as a potential virulence factor led to the search of homologous excreted proteins in the genome of *S. aureus*. This resulted in the discovery of FPRL1 (FPR2) inhibitory protein (FLIPr), which showed 49% homology with the gene for CHIPS (chp). Similar to CHIPS, FLIPr is able to inhibit FPR1, but can additionally also inhibit FPR2, whereas binding with FPR3 was not observed (79). Later, the evasion protein FLIPr-like was discovered by a BLAST search through sequenced *S. aureus* genomes with FLIPr as reference sequence. FLIPr and FLIPr-like are two allelic variants of the same gene with 73% homology on amino acid level. The function of FLIPr-like is also similar compared to FLIPr, because it is an antagonist of both FPR1 and FPR2 (80). Moreover, FLIPr and FLIPr-like also target FcγR, the receptors for IgG, where FLIPr is almost exclusively restricted to class II receptors, with a preference for FcγRIIa, while FLIPr-like binds to most FcγR isoforms (81).

6. OPSONIZATION AND PHAGOCYTOSIS

6.1. Opsonization

The next step in clearing a bacterial infection, after neutrophils have been attracted to the site of infection, is uptake of the pathogens by phagocytes. In order for this phagocytosis to be effective, bacteria have to be opsonized, coated with components of the complement system, immunoglobulins, or other innate immune components. We will first describe opsonization by the complement system, followed by opsonization by immunoglobulins.

6.1.1. Opsonization by complement system

Complement is a proteolytic cascade comprising more than 30 proteins in plasma that can: (i) opsonize bacteria by depositing complement activation products at the surface of bacteria; (ii) attract and activate other immune cells by formation of chemoattractants; (iii) lyse and kill Gram-negative bacteria directly by the formation of the membrane attack complex (54). The complement system can be activated via three separate pathways that differ in their way of recognition but come together at one central step: formation of C3 convertase which cleaves C3. The lectin pathway is activated upon recognition of conserved microbial sugars such by ficolins and mannan-binding lectin. Activation of the classical pathway is primarily initiated by the interaction of C1q with antigen-antibody complexes (54). The third pathway, the alternative pathway, is initiated on surfaces of neutral or positively charged pathogens that do not contain complement inhibitors. This is due to the spontaneous 'tick-over' reaction of C3 with water to form hydrolyzed C3, and it exists in an activated state at all times. Importantly, this pathway serves as an amplification loop after C3b is formed on bacterial cells via the lectin and classical pathway (54). C3 convertases are enzyme complexes with proteolytic activity to cleave C3. The classical and lectin C3 convertase is formed by cleavage of C4 by C1s to C4b, where after C4b covalently attaches to the bacterial surface and binds C2. C1s is then able to cleave C2 as well, thereby forming the C3 convertase C4b2a. The alternative pathway C3 convertase is different by containing a surface-bound C3b molecule attached to protease Bb, a subunit of factor B. Factor H controls complement activation by stimulating the decay of Bb from the alternative pathway convertase (C3bBb) and is a cofactor for Factor I-mediated cleavage and inactivation of C3b (82).

Cleavage of C3 results in the formation of chemoattractant C3a and the deposition of C3b at the bacterial surface. C3b can be cleaved to the proteolytic inactive product iC3b by factor I on the surface of bacteria. iC3b is still able to opsonize bacteria, but it cannot associate with Bb (83). Both C3 convertases can bind an additional C3b molecule to form C5 convertases and this convertase can cleave C5 into C5a and C5b. C5a is a chemoattractant and has been shown to have a protective role during staphylococcal bloodstream infections in mice (15). C5b together with C6, C7, C8 and multiple copies of C9 will form the membrane attack complex (54). The membrane attack complex is able to directly lyse Gram-negative bacteria, whereas Gram-positive bacteria stay unaffected due to their thick peptidoglycan layer (84). However, the complement system is important in the opsonization process by depositing C3b on the surface of Gram-positive bacteria, such as *S. aureus*. Together this sequence of events results in efficient rapid detection and elimination of bacterial invaders.

6.1.2. Opsonization by immunoglobulins

Immunoglobulins (Igs) are a class of proteins that enable highly efficient opsonization, but are also involved in agglutination, neutralization of toxins and other virulence factors and inhibition of adhesion. After binding to antigens on pathogens via their Fab fragments, they

are recognized by Fc receptors on the surface of phagocytes via their Fc region. The four isotypes of Igs vary in complement activation and are recognized by their own Fc receptor (FcγR, FcαR, FcεR, FcμR). IgG, IgA and IgM play roles in controlling infections, whereas IgE is more important in immunity to parasites. IgM is especially effective at opsonization through complement activation due to its polymeric structure (85). IgG consists of four subclasses (IgG1, IgG2, IgG3, and IgG4) and the differences in effector functions between the four IgGs are caused by differences in structure, especially the length and flexibility between the variable Fab fragments and the stable Fc fragment (86). Therefore the different subclasses of IgG bind differently to C1q, which is at the start of the classical pathway cascade. IgG3 binds the strongest, after which IgG1 and IgG2 bind weaker (IgG1 > IgG2). IgG4 completely lacks to activate the complement system (87).

6.2. PHAGOCYTOSIS

Phagocytosis is a process by which other cells, cell fragments and micro-organisms are engulfed by white blood cells and end up in an internal compartment called the phagosome. As described above, opsonized micro-organisms bind to specific receptors on the phagocyte surface. Subsequently invagination of the cell membrane causes envelopment of the bacterium. This uptake is aided and highly enhanced by factors such as C5a; TLR ligands on the surface of the bacterium; and ligands for C-type lectins (such as DC-SIGN, Dectin-1, and the mannose receptor on the surface of neutrophils (88).

Crosslinking of FcγR by ligand binding on the surface of neutrophils activates several effector functions directed toward killing of pathogens and an inflammatory response (16). FcγRs are members of the immunoglobulin superfamily and they are capable of binding the Fc region of IgG antibodies. There are several activating receptors (FcγRI/CD64, FcγRIIa/ CD32a, FcγRIIc/CD32c and FcγRIIIa/CD16a), one inhibitory receptor (FcγRIIb/CD32b), and one glycosylphosphatidylinositol anchored receptor that contains no signal motif (FcγRIIIb/ CD16b) (89). Human neutrophils express only two FcγRs; FcγRIIa and FcγRIIIb, of which FcγRIIa induces mainly phagocytosis (89).

CR1 (CD35) is found on circulating monocytes, neutrophils and B-lymphocytes. This receptor binds C4b, C3b, and iC3b and induces phagocytosis (90). CR3 (CD11b/CD18, Mac-1) and CR4 (CD11c/CD18, p150/95) are heterodimeric glycoproteins from the integrin family with a shared β-chain (CD18). They bind the iC3b fragment and to a lesser extend also C3b (91). Stimulation of neutrophils and monocytes via CR3 and CR4 results in induction and enhancement of phagocytosis, degranulation and generation of ROS (91).

7. EVADING OPSONIZATION AND PHAGOCYTOSIS

S. aureus has evolved numerous molecules that evade the different parts of the complement cascade, immunoglobulins and elements of the phagocytic process. These molecules are illustrated in **Figure 3**. Evasion of these aspects will result in a highly effective delay or reduction of the immune response and will create a beneficial situation for the bacterium to survive and multiply within its host.

7.1. Capsule production

The best way for the bacterium to prevent phagocytosis is to hide the antigenic or immunogenic proteins at the surface of bacterial cell wall with a polysaccharide capsule. Up to ~75% of all clinical *S. aureus* isolates have a capsule or microcapsule whereby most of them contain capsular polysaccharide 5 (CP5) and capsular polysaccharide 8 (CP8). These bacteria grown under optimal capsule production conditions showed resistance in opsonophagocytosis and thus killing (92). However, the capsule of *S. aureus* does not completely block deposition of complement components at the bacterial surface or binding of specific antibodies (93). Other bacteria, such as Streptococcus pneumoniae, are known to produce a very thick capsule (94).

7.2. Proteins targeting immunoglobulins

The first evasion molecule described to have anti-opsonic properties, is staphylococcal protein A (SpA). SpA is linked to the staphylococcal cell wall via its LPXTG anchor, but can be released upon hydrolysis during growth (95, 96). This protein contains four or five immunoglobulin-binding domains capable of binding the Fc part of IgG, which leads to blockage of FcR-mediated phagocytosis (97). Spa also binds to the Fab domain of Variable Heavy 3 (VH3) type B cell receptors of IgM, which serves as a B cell antigen by stimulating B cell activation (98–100). Consequently, this shows that SpA effectively interferes with the adaptive response. Recently, guinea pigs were shown to be a good model to test this therapeutic approach *in vivo* (101).

Staphylococcus aureus binder of IgG (Sbi) is a second IgG-binding protein, which was identified through a phage display screen against immobilized human IgG (102). Same as SpA, Sbi is also expressed at the staphylococcal cell surface and is secreted during bacterial growth (103, 104). Sbi has also two binding targets because it is able to bind to another serum component, ß2-glycoprotein I, also known as apolipoprotein H. This was similarly identified by phage display and the binding site was clearly different from the IgG-binding domain (103). However in contrast to SpA, Sbi can only interact with the Fc domain of IgG (105). Furthermore, the extracellular region of Sbi consists of four globular domains, where domain I and II are immunoglobulin-binding domains and domain III and IV are able to bind complement component C3 and factor H where it forms a stable tripartite complex (Sbi:C3:Factor H) (106, 107). Together, Sbi is a versatile evasion protein interfering with the innate immune system by binding IgG and apolipoprotein H, as well as the complement components Factor H and C3.

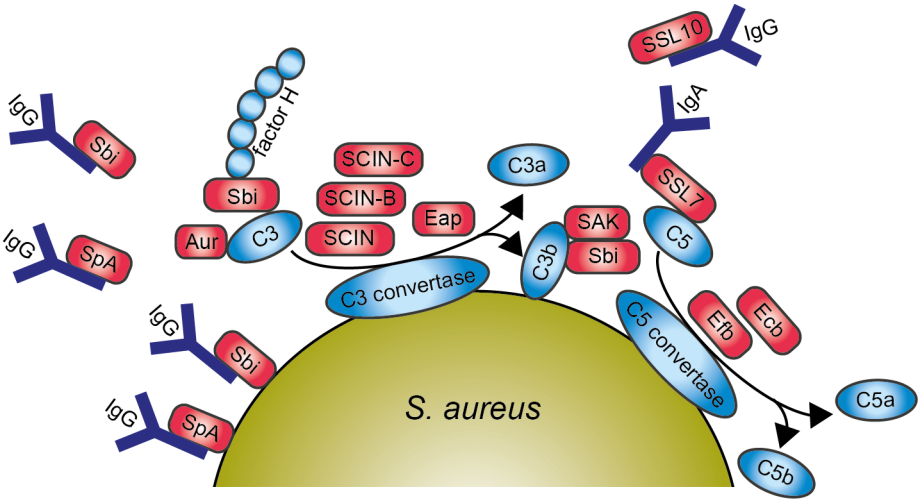

Figure 3: Schematic representation of *S. aureus* evading opsonization and phagocytic uptake by neutrophil. Red boxes indicate staphylococcal proteins whereas blue boxes indicate host proteins. Abbreviations: IgG, immunoglobulin G; SpA, Staphylococcal protein A; Sbi, staphylococcal binding of IgG; SCIN, staphylococcal complement inhibitor; SAK, staphylokinase; Aur, aureolysin; SSL, staphylococcal superantigen-like protein; Efb, extracellular fibrinogen-binding protein; Ecb, extracellular complement-binding protein. The figure was adapted from Servier Medical Art.

SSL10 is yet another evasion protein able to bind IgG1 (108). This leads to the inhibition of complement activation via the classical pathway and this is the second function of SSL10, since it is also a CXCR4 antagonist. The N-terminus of SSL10 binds to the Fc domain of IgG1, preventing association with C1q and FcγRs leading to inhibition of FcγR-mediated phagocytosis (109). Furthermore, SSL10 also targets prothrombin and Factor Xa to inhibit blood coagulation (110) binds to phosphatidylserine, and recognizes apoptotic cells (111). Finally, *S. aureus* secretes a serine protease, V8, which is able to cleave immunoglobulins (112).

7.3. Proteins targeting complement system

Not all known evasion proteins interfering with opsonization target immunoglobulins. Some of them are specialized in evading the complement system. For example; the secreted metalloprotease aureolysin cleaves the central complement component C3 in a zinc-dependent manner. The cleavage site on C3 of aureolysin differs by two amino acids from the C3 convertase cleavage site generating active C3a' and C3b'. This suggests that aureolysin mimics C3 convertases, but it also degrades the cleaved C3b' together with factor I and factor H, making this cleavage *in vivo* more effective because it is more effective in serum than without serum. Aureolysin is a secreted protease, thus it can cleave C3 away from the bacterial surface, creating a C3 free micro-environment and thus preventing C3b' to covalently attach with its thioester to bacteria (113).

Staphylococcal complement inhibitor (SCIN) inhibits all three complement pathways: the

alternative, classical and lectin pathway. SCIN stabilizes and inhibits surface-bound C3 convertases and this results in decline of C3b deposition and release of chemoattractant C5a, which results into the inhibition of phagocytosis (114). Later, SCIN-B, SCIN-C and open reading frame (ORF)-D were identified in *S. aureus* genome. Characterization of these homologues shows that SCIN-B and SCIN-C also inhibit complement, whereas ORF-D shows no inhibitory activity (115). Co-crystallization studies of SCIN with C3 convertase reveals that SCIN inhibits convertase activity via three ways: (i) SCIN prevents Bb mobility, which prevents Bb to access substrate C3 (116); (ii) SCIN may dimerize two C3 convertases and thereby prevents substrate binding (116); (iii) By binding to a single C3b molecule, SCIN slows the rate of factor B loading onto C3b and thus lowers the amount of C3 convertase formation (117). This all leads to inhibition of phagocytosis, C3b deposition, and C5a generation (114). Furthermore, a new SCIN variant was recently identified in equid *S. aureus* isolates. This equine SCIN (eqSCIN) has adapted to horses by inhibiting the equine complement system (**Chapter 7**).

Extracellular fibrinogen-binding protein (Efb) and extracellular complement-binding protein (Ecb) are two homologues proteins (118). The first characteristic described for Efb was that it binds with its N-terminus to fibrinogen, hence its name (119). Efb can also bind to platelets, as identified by phage display, interferes with platelet aggregation and contributes to the virulence in wound infections and delays the healing process in rats (120–122). Additionally, the C-terminus of Efb is able to bind C3 and its cleavage products containing the thioester domain (C3d) (123, 124). Efb blocks phagocytosis *in vitro* of *S. aureus* by neutrophils in plasma and human whole blood, as well as *in vivo* in a mouse peritonitis model. This evasion protein forms a unique bridge between complement and coagulation system, since it can bind both C3 and fibrinogen. Efb cover bacteria with a thick layer of fibrinogen, which leads to shielding of surface-bound C3b and antibodies from recognition by phagocytic receptors (125). This mechanism to shield the bacterial surface from phagocytosis together with the formation of a capsule enhance the evasion of *S. aureus* against phagocytosis (126).

Ecb (also known as Ehp) compared to Efb lacks fibrinogen binding activity, but it does inhibit the complement system like Efb by binding the C3d domain of C3 (118, 127). This results in blocking of C3 convertases of the alternative pathway and C5 convertases of all three complement pathways (128). The binding of Ecb to C3d is stronger than Efb to C3d, because Ecb contains a second, lower affinity, C3 binding site. This results in enhanced complement inhibitory effect of Ecb compared to Efb (127). The function of many evasion molecules is restricted to the human host, however, Ecb and Efb efficiently inhibit the complement system in both humans and mice. Therefore, the importance of Ecb and Efb could be examined *in vivo* in a murine infection model. Mice experienced higher mortality rates in an intravenous model with wild-type bacteria (79%) compared to an isogenic ΔEcbΔEfb mutant (21%). In addition, Ecb and Efb promoted bacterial survival and blocked neutrophil influx in the lungs. These results indicate that Ecb and Efb are essential to *S. aureus* virulence *in vivo* and could be attractive targets for vaccine development (129).

S. aureus recruits factor H to its surface with the surface-associated serine-aspartate repeat protein E (SdrE) and this leads to inhibition of the alternative pathway of the complement system (130). Recombinant SdrE recognizes its ligand via a unique 'close, dock, lock and latch' mechanism as determined by crystallographic studies (131). Moreover, factor H bound to SdrE retains its activity for factor I-mediated cleavage of C3b to iC3b (130). Factor I is directly targeted by the full length cell wall component clumping factor A (ClfA) as well as a secreted part of around 50 kDa. Binding of ClfA to factor I promotes cleavage of C3b to iC3b, which results in disruption of opsonophagocytosis (132, 133).

Extracellular adherence protein (Eap) has a variety of functions in evading the immune system. We already discussed the binding of Eap to ICAM-1 with impaired function in neutrophil extravasation (39), but Eap is also able to inhibit the complement system. C4b is targeted by Eap and this leads to inhibition of C2 binding to C4b and thus formation of an active C3 convertase of the lectin and classical pathway (134).

Staphylokinase (SAK) is also an anti-opsonic immune evasion protein by converting human plasminogen into the active bacterium-bound serine protease plasmin. Plasmin degrades IgG and C3b from the bacterial surface, resulting in decreased phagocytosis by human neutrophils (135).

SSL7 is able to inhibit opsonization via two ways; it selectively binds both IgA and complement C5 (136). The binding of SSL7 to the Fc region of IgA is mediated via its N-terminus, which causes interference with antibody recognition (137), whereas the C-terminus binds to C5 and thereby inhibits terminal complement activation and cleavage of C5 by interfering with binding to C5 convertases (138). SSL7 also showed to be important *in vivo* by inhibiting complement-induced neutrophil influx in a murine inflammatory model (138).

S. aureus has also evolved a protein attached to the cell wall to inhibit specifically the classical pathway of the complement system. *Staphylococcus aureus* collagen adhesion (Cna) is a cell wall-anchored protein that belongs to the MSCRAMM (microbial surface component recognizing adhesive matrix molecules) family of adhesins. Cna binds C1q and thus inhibits classical pathway activation. Cna is part of the structurally related Cna-like family, which is found in many other Gram-positive bacterial species. Thus, the function of Cna-like MSCRAMMs to inhibit the classical pathway could be used as an immune evasion strategy by numerous Gram-positive pathogens (139).

8. NET FORMATION

Neutrophils have recently been shown to have another defense mechanism whereby they

release their DNA associated with antimicrobial peptides, histones and proteases to form a network of extracellular fibers, which entrap and kill various microbes. This results in the formation of neutrophil extracellular traps (NETs) (140). There are currently studies to address the molecular mechanism behind NET formation, but more research is needed to fully understand this (141). The formation of NETs *in vitro* is activated via different pro-inflammatory stimuli, including hydrogen peroxide, phorbol myristate acetate (PMA), lipopolysaccharide (LPS), IL-8, and different bacteria such as *S. aureus* (142). The importance of NETs has also been shown *in vivo*, where intravascular NETs were observed in the liver during sepsis induced by *S. aureus* (143).

9. EVADING NET FORMATION

A secreted nuclease of *S. aureus*, Nuc, is important in the breakdown of NETs. This is shown both *in vitro* as *in vivo*, whereby an isogenic nuclease knock-out of *S. aureus* shows impaired degradation of NETs compared to the wild-type strain. This leads to the linkage of nuclease production to delayed bacterial clearance in the lung and increased mortality after intranasal infection *in vivo* (144). Thus, Nuc helps staphylococci to escape from the extracellular fibers and prevents getting killed by antimicrobial peptides and proteases. Nuc also showed to play a role in immune cell death together with adenosine synthase. These two enzymes are able to convert NETs to deoxyadenosine, which triggers the caspase-3–mediated death of immune cells (145).

10. BACTERIAL KILLING BY NEUTROPHILS

Neutrophils are end-stage cells with high concentration of antimicrobial proteins safely stored within different granules. They are able to kill pathogens by releasing their granules containing antimicrobial proteins into the phagosome (also called degranulation) and generating ROS (also known as the oxidative burst) upon phagocytosis of bacteria. Phagocytes, especially macrophages, form also reactive nitrogen species (RNS) via the oxidation of nitric oxide (NO•) which is produced by an inducible nitric oxide synthase (iNOS) (146). The granules of neutrophils can be divided into three different groups; the primary or peroxidase-positive granules, secondary or specific granules, and the tertiary or gelatinase granules. The peroxidase-positive granules are also called azurophilic granules due to the affinity for the basic dye azure A (12). The secretory vesicles are often also mentioned as an additional granule group, however their origin may differ from the other granule types since they contain plasma proteins and are therefore suggested to be formed by endocytosis (12). Azurophilic granules contain a variety of antimicrobial proteins, such as pore-forming peptides (α-defensins), neutrophil serine proteases (NSPs; proteinase 3 and 4, cathepsin G, and elastase), myeloperoxidase (MPO), the bactericidal/permeability-increasing (BPI) protein, and lysozyme. Secondary granules contain

hCAP-18, lactoferrin, neutrophil gelatinase-associated lipocalin (NGAL), and also lysozyme. Tertiary granules contain a number of metalloproteases, such as MMP-8 (collagenase) and MMP-9 (gelatinase). Secretory vesicles contain plasma proteins and membrane-associated receptors essential at the earliest phase of neutrophil-mediated inflammatory response, such as the extremely rapid upregulation of ß2-integrin CD11b/CD18, CR1, and FPR1 and FPR2 (147). However, it should be mentioned that heterogeneity exists between the different granules and that their granule contents overlap, because they are sequentially formed during myeloid cell differentiation (148).

10.1. Oxygen-independent killing by neutrophils

Oxygen-independent killing mechanisms by neutrophils greatly contribute to microbial killing. This is proven by the fact that neutrophils can still kill substantial amounts of certain microbes under anaerobic conditions, wherein there is no functional NADPH oxidase (149). Agents that contribute to oxygen-independent microbicidal activity include antimicrobial peptides and proteins such as lactoferrin, lysozyme, α-defensins, cathelicidins such as hCAP-18, azurocidin, proteinase 3, cathepsin G, and neutrophil elastase (12). The C-terminal part of hCAP-18, named LL-37, forms an amphipathic α-helix and has antimicrobial properties against Gram-negative and Gram-positive bacteria, such as *S. aureus* (150). LL-37 is effective against both intra- and extracellular *S. aureus* (151). Other antimicrobial peptides are α-defensins (also known as human neutrophil peptide-1, HNP-1). These peptides are antimicrobial by the formation of multimeric pores and apply this on various micro-organisms (152). The structurally related serine proteases (cathepsin G, elastase, and proteinase 3 and 4) have various functions by cleaving bacterial factors, regulating immune responses by cleaving receptors and chemokines, or they are able to kill bacteria in the extracellular milieu after being secreted (153). The serine proteases also proved to be important *in vivo*, since mice lacking cathepsin G showed impaired clearance of *S. aureus* during infection (154). Lactoferrin and calprotectin are chelating proteins; lactoferrin sequesters iron needed for microbial growth and calprotectin chelates zinc and manganese and thereby inhibits staphylococcal growth (155). Calprotectin is located in the cytoplasm of neutrophils and comprises more than 60% of the proteins in the cytosol (156). Lysozyme is a cationic antimicrobial peptide and is present in all granule subsets with a peak concentration in secondary granules. Lysozyme cleaves bacterial cell wall peptidoglycan polymers by breaking the β-1,4 glycosidic bonds between N-acetylmuramic acid (MurNAc) and N-acetylglucosamine (GlucNAc) (157). This results in lysis of various bacteria, such as Bacillus subtilis in human plasma (158).

10.2. Oxygen-dependent killing by neutrophils

Upon phagocytosis of bacteria, the azurophilic granules are the first to fuse with the phagosome and this leads to assembly of the five essential parts of the NADPH oxidase complex and activation of the complex (159). Active NADPH oxidase transfers electrons across the phagosomal membrane from cytosolic NADPH to intraphagosomal molecular oxygen to produce superoxide, which is compensated for by an influx of cations or protons. Although

superoxide has limited direct microbicidal capacity, the molecule is involved in generating secondary derived ROS such as hypochlorous acid, chloramines, hydroxyl radicals and singlet oxygen, which do directly contribute to PMN microbicidal activity. The superoxide anion is spontaneously converted to hydrogen peroxide or by the help of superoxide dismutase. MPO catalyzes the reaction of hydrogen peroxide with chloride to form the highly bactericidal agent hypochlorous acid (HOCl) (160, 161). Chlorine, chloramines (e.g. monochloramines, dichloramines, and taurine chloramine), singlet oxygen, hydroxyl radicals, and ozone are subsequently formed in secondary reactions and are also competent antimicrobial compounds (162).

11. EVADING KILLING

Here we give an overview of evasion factors that are involved in staphylococcal survival from oxygen-dependent and -independent killing. These proteins are summarized in **Figure 4**. Then, the various staphylococcal toxins will be discussed. An overview of these toxins is shown in **Figure 5**.

11.1. Evading oxygen-dependent killing by neutrophils

S. aureus' surname is derived from the fact that this bacterium has "a jacket of the golden pigment", staphyloxanthin. This staphyloxanthin serves as an antioxidant and is protective in killing by hydrogen peroxide and singlet oxygen. Bacteria lacking staphyloxanthin showed impaired survival *in vitro* as well as *in vivo* (163). The genes crtM (dehydrosqualene synthase) and crtN (dehydrosqualene desaturase) are essential in the biosynthetic pathway to produce staphyloxanthin. Therefore, synthetic inhibitors of CrtM are interesting new virulence factor-based therapies by targeting the biosynthesis of staphyloxanthin (164, 165).

S. aureus has developed other proteins that contribute in the resistance against ROS. The bacterium produces two superoxide dismutases, sodA and sodM, that convert the harmful superoxide radicals into hydrogen peroxide and oxygen (166). Isogenic sodA and/or sodM knock-out bacteria had reduced virulence in a mouse abscess model, showing that both sodA and sodM contribute to the virulence of *S. aureus* (166). Probably sodA has the major SOD activity in *S. aureus* throughout all growth stages, but sodM becomes active under oxidative stress during late exponential and stationary growth phase (167). The hydrogen peroxide generated by the neutrophil is degraded into water and oxygen by the presence of KatA, a staphylococcal catalase, which is described to be a major virulence factor (168). However, studies with a catalase mutant strain showed no difference in virulence in a murine abscess infection model (169). Another catalase-like protein produced by *S. aureus* is alkyl hydroperoxide reductase (AhpC). Catalase appears to be important for protection against external oxidative stress, whereas AhpC clears endogenously produced hydrogen peroxide. In that study, AhpC and KatA were not required for virulence of *S. aureus*, but AhpC or/and KatA

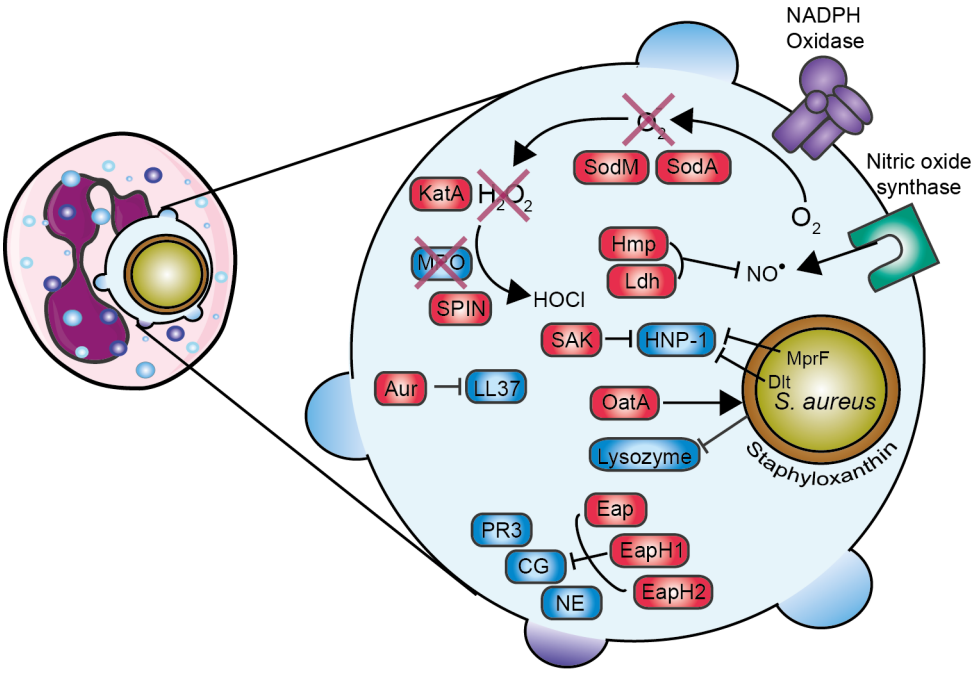

Figure 4: Overview of evasion proteins that are involved in evading neutrophil killing. Enlargement of the phagosome is shown on the right. Red boxes indicate staphylococcal proteins whereas blue boxes indicate host proteins. Staphyloxanthin provides a protective shield against, KatA neutralizes hydrogen peroxide (H_2O_2) into water (H_2O) and oxygen (O_2), and SPIN inhibits MPO activity. MprF and Dlt operon leads to an increase in positive charge of bacterial surface. Abbreviations: SOD, superoxide dismutase; SAK, staphylokinase; KatA, catalase; MPO, myeloperoxidase; SPIN, staphylococcal peroxidase inhibitor; Aur, aureolysin; Hmp, Flavohemoglobin; Ldh, L-lactate dehydrogenase; Eap and EapH, extracellular adherence protein-homologue; PR3, proteinase 3; CG, cathepsin G; NE, neutrophil elastase. The figure was adapted from Servier Medical Art.

is/are important for nasal colonization (170). Another yet unknown virulence factor regulated via the SaeR/S two-component system was suspected to play a role in decrease of hydrogen peroxide and hypochlorous acid production. This factor was independent of SOD and catalase, since their expression is not regulated by SaeR/S (171). Later, this factor was identified as Staphylococcal Peroxidase Inhibitor (SPIN), a secreted protein of 8.4 kDa which is able to bind and inhibit MPO. From crystallographic studies, we know that SPIN acts as a molecular plug that prevents access of substrate hydrogen peroxide to the MPO active site. Despite the controversy in importance of MPO in bacterial clearance, SPIN protects *S. aureus* from MPO-mediated killing (172). Zooming into the structure-function relationships of SPIN revealed that the N-terminus is absolutely required for inhibiting MPO and that this N-terminus is unstructured in the unbound state (**Chapter 5**).

S. aureus has also evolved two proteins to resist nitric oxide stress produced in activated phagocytes. Flavohemoglobin (Hmp) scavenges host-derived NO• and the NO•-inducible

L-lactate dehydrogenase (Ldh) produces L-lactate, which maintains redox homeostasis during nitrosative stress (173, 174).

11.2. Evading oxygen-independent killing by neutrophils

S. aureus contains two independent loci (dltABCD and mprF) that are involved in susceptibility to defensins and other cationic pore-forming peptides by modifying the net charge of the cell wall envelope. The dlt operon is responsible for the incorporation of D-alanine into teichoic acids and this leads to a decrease in negative charge on the bacterial surface and tolerance of high concentrations of positively charged antimicrobial peptides (175). Dlt knock-out mutant was more susceptible to killing by defensin peptides and human neutrophils, even in absence of a functional respiratory burst. As a control, there was no difference in killing between wild-type and Dlt knock-out bacteria when using monocytes, which do not produce defensins (176). The mprF (multiple peptide resistance factor) gene encodes a lysylphosphatidylglycerol synthetase on its membrane which is involved in modification of membrane phosphatidylglycerol with L-lysine, which also results in reduction of negatively charged membrane surface (177, 178). In contrast to most defensins, cathelicidin-derived bactericidal peptides, such as LL-37, have substantial activity against staphylococci. However, *S. aureus* has also evolved a protein to evade antimicrobial effects of LL-37 by degrading and thereby inactivating LL-37 by the staphylococcal metalloproteinase aureolysin (which is also involved in the opsonization process by cleaving C3) (179). As described earlier, lysozyme degrades the cell wall peptidoglycan layer. Nonetheless, *S. aureus* is resistant to lysozyme by expressing the enzyme O-acetyltransferase A (OatA). OatA causes O-acetylation of the peptidoglycan and this leads to resistance to the muramidase activity of lysozyme. OatA is regarded as a virulence factor since it is only expressed in pathogenic, lysozyme-resistant staphylococci (for example *S. aureus*, S. epidermidis, S. lugdunensis) (180, 181).

Eap inhibits the activity of NSPs (neutrophil elastase, cathepsin G and proteinase 3). Its homologues, EapH1 and EapH2, contain one EAP domain, whereas the earlier described Eap contains most often four or five EAP repeats. One single EAP domain already impairs the function of NSPs, therefore also EapH1 and EapH2 inhibit NSP activity (182). Recently, the interaction between EAP/NSPs was investigated and despite the homology between EapH1 and EapH2, they form different complexes with NSPs (183). *S. aureus* protects its own immune evasion arsenal from degradation and cleavage by inhibiting these NSPs (184). For example, the N-terminus of SPIN is susceptible to proteolysis of NSPs, which results in a loss-of-function to inhibit MPO, but it is protected again by Eap (**Chapter 5**). SAK is not only involved in evading opsonization by cleaving plasminogen to active plasmin (135), it also binds and inhibits α-defensin (HNP-1) and thereby neutralizes the bactericidal effect of HNP-1 (185).

11.3. Escape by toxins

S. aureus also protects itself by the secretion of toxins (**Figure 5**). Toxins can directly lyse and thereby kill (immune) cells by disrupting the cell membrane of host cells and protecting the

pathogen both before and after engulfment by neutrophils. These lytic toxins can be divided into two groups, based on their structure: the ß-barrel pore-forming toxins like α-hemolysin and leukocidins and the small α-helical peptides as the PSMs. A different group of toxins, the superantigens, activate T-cells by crosslinking MHC class II and T-cell receptors, resulting in massive non-specific activation of T-cells. This temporarily overactivation of a large population of T cells causes secondary inhibition of adaptive immune system and thereby contributes to immune escape.

β-Barrel pore-forming toxins target eukaryotic cells expressing specific factors. Hemolysin-alpha (Hla, also known as α-toxin) is secreted as a monomer, which forms a homo-heptameric pore upon binding to its receptor the zinc-dependent metalloprotease ADAM-10 (186). Hla also upregulates ADAM10 on endothelial and epithelial cells, causing disruption of the endothelial and epithelial barrier (187, 188). Hla does not lyse granulocytes (e.g. neutrophils) but it does lyse other immune cells such as erythrocytes, macrophages and subpopulations of lymphocytes (189). Other β-barrel pore-forming toxins are leukocidins. These toxins consist of two independent secreted monomers and form octamer pores of four F (fast) and four S (slow) subunits in membranes of host cells (190). Currently, seven leukocidins of *S. aureus* have been

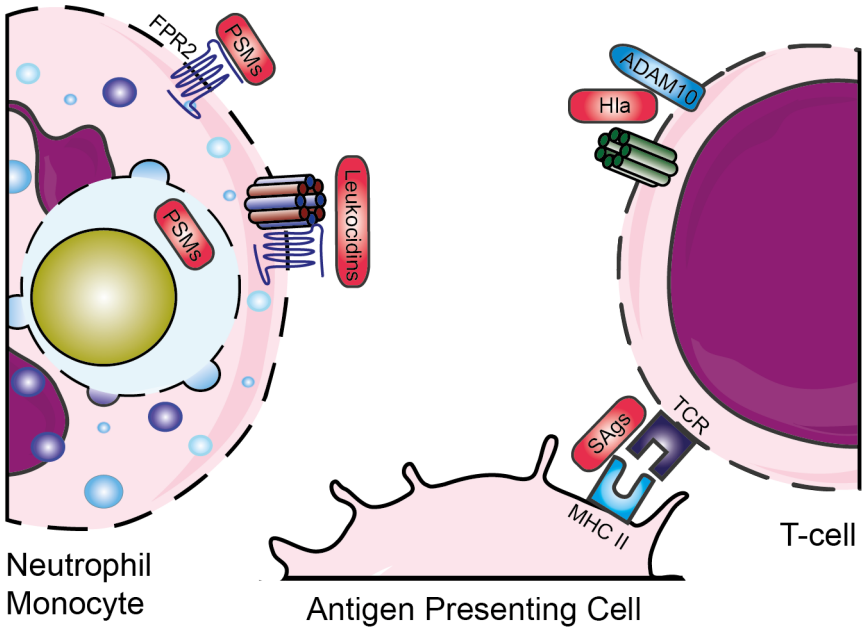

Figure 5: Evasion by staphylococcal toxins. Various leukocidins bind specific GPCRs after which they form a pore and lyse host cells. PSMs are released inside the phagosome and can bind via FPR2. SAgs cross-link MHC class II and T-cell receptors. Abbreviations: GPCR, G-protein-coupled receptor; FPR, formyl protein receptor; PSMs, phenol-soluble modulins; Hla, hemolysin-alpha; SAgs, superantigens; MHC II, major histocompatibility complex II; TCR, T-cell receptor. The figure was adapted from Servier Medical Art.

described: five in human associated strains; LukAB (also known as LukGH), LukSF (also known as PVL), LukED, and two γ-hemolysins (HlgAB and HlgCB). Two animal associated leukocidins (LukPQ (191) and LukMF' (192)) were recently added to the arsenal (193). The receptors for these leukocidins have recently been identified and this explains the cellular tropism and biological consequences for these pore forming toxins during infection (194).Their receptors, all GPCRs and almost exclusively chemoattractant receptors are located on different immune cells, but mainly on phagocytes. This indicates that the major role of these toxins is in immune evasion. They are "designed" to kill those cells that are crucial in eliminating staphylococci. HlgAB and LukED however, also target the Duffy antigen receptor for chemokines (DARC) expressed on erythrocytes, which leads to release of hemoglobin and promotes bacterial growth (195). Furthermore, LukAB has shown to play a role in intracellular lysis of neutrophils, thereby promoting bacterial replication and outgrowth (196). Interestingly, the presence of these leukocidins in the genome of *S. aureus* is highly diverse. For example, the HlgACB and lukAB genes are located in the core genome and are present in more than 95.5% of human *S. aureus* isolates, whereas PVL is located on a phage and is found in less than 2% of all clinical isolates, but it is found in the majority of community-acquired MRSA strains in the United States (197).

The other class of toxins are PSMs, which are small α-helical peptides. These peptides are associated with enhanced virulence in community-acquired MRSA and are produced at high concentrations. PSMs contain a common amphipathic α-helical region which is responsible for disrupting the cell membrane, nonetheless they are categorized in two groups; the β-type PSMs (around 44 amino acids in length), and the shorter α-type PSMs (20-25 amino acids long) which have more enhanced toxic characteristics (198). The function of PSMs are inhibited by serum lipoproteins, which are present in large quantities in human serum (199). Therefore, their function is mainly intracellular, where they are able to lyse phagocytes from the inside out. The critical concentration for PSM transcription is easily reached inside the condensed phagosome (200). Through the interaction between PSMs and FPR2 (see section 'opsonization'), PSMs cannot only lyse neutrophils, but also attract and activate leukocytes via FPR2 (53).

S. aureus also encodes a variety of toxins that modulate the adaptive immune system. There are around 20 serologically distinct staphylococcal superantigens known, which are divided into enterotoxins, enterotoxin-like, and TSS toxin-1 (TSST-1). Their nomenclature is distinguished based on proven emetic activity when orally ingested (enterotoxins, SEA-E, G-J, and S-T) or unconfirmed of this activity (enterotoxin-like, SEIK-R, U and U2, V, and X-Y) (201). Superantigens are able to crosslink MHC class II and T-cell receptors. This causes massive non-specific activation of T-cells and increase of many cytokines to toxic levels, which leads to damage of tissue and organs. This is called the, often lethal, toxic shock syndrome (202). The SSLs were first annotated as SET proteins for 'staphylococcal enterotoxin-like' but were later renamed to staphylococcal superantigen-like (SSL) since these proteins lack enterotoxic

activity (201). Even though their enterotoxic activity is lacking, the SSLs have distinct functions in evading the innate immune system.

12. CONCLUDING REMARKS

Staphylococcal immune evasion is very important for the bacterium, especially to fight the immune system during acute infection. Therefore, most evasion proteins are directed against this initial attack by neutrophils. This review gave an overview of the different evasion proteins and their function(s) during infection. Interestingly, the repertoire is still expanding by recent discovery of novel proteins and new functions of existing evasion molecules. It is an important field of research, since functional therapeutics against staphylococcal infections are still lacking, while the economic burden increases. But, with the current speed of experiments, our knowledge is growing every year and most likely it will only be a matter of time before we will find the appropriate therapeutics for prophylaxis or treatment of this extremely clever bacterium.

13. AIM AND OUTLINE OF THE THESIS

In this thesis we aim to further explore the staphylococcal repertoire to evade the innate immune system. To date, around forty proteins are identified and characterized, but this number is only the tip of the iceberg if we look at predictions (11). Neutrophils are important for clearing infections caused by *S. aureus*, but *S. aureus* can survive within these neutrophils and even use these phagocytes to travel away from the site of infection as so called 'Trojan Horses' (203). Before we searched for unidentified evasion proteins targeting one of the granular proteins of neutrophils, we needed to develop tools to study fluorescently labeled bacteria intracellular. Thus in **Chapter 2**, we present integration vectors of *S. aureus* encoding fluorescent reporters for 6 different colors. This paper describes a method to markerless integrate the different fluorescent reporters or use reporter plasmids to study any other promoter of interest for expression studies. In **Chapter 3**, we detect that there is an unknown factor interfering with neutrophil ROS production. We therefore set out a screening method with secretome phage display to discover novel immune evasion proteins targeting the degranulate of neutrophils. There we identified and characterized a protein we named Staphylococcal Peroxidase INhibitor (SPIN), which is a potent blocker of MPO, as described in **Chapter 4**. Thus, the unknown factor observed in **Chapter 3** is most likely SPIN. The presence of SPIN in *S. aureus* is important for bacterial survival after phagocytosis by neutrophils, thus SPIN interferes with MPO-mediated killing. Crystallization studies with SPIN/MPO showed that SPIN acts as a molecular plug to prevent H_2O_2 substrate access to the active site of MPO. In **Chapter 5**, we further explored the structure/function relationship between SPIN and MPO. Various mutant of SPIN showed that the C-terminal region is important for binding to MPO, whereas the N-terminal region is

dispensable for MPO binding. The N-terminal region is necessary, but not sufficient regarding MPO inhibition. In **Chapter 6**, we looked at SPIN homologs in other staphylococci to further understand the molecular features that determine the specificity of SPIN proteins to MPO. There we observed that SPIN from *S. delphini* is also able to inhibit human MPO, although it shares only ~50% identity to SPIN from *S. aureus*. Furthermore in **Chapter 7**, we identified another staphylococcal evasion protein, a novel variant of Staphylococcal Complement INhibitor (SCIN), which is known to interfere with the activation of the complement system and leads to reduced C3b deposition and subsequently phagocytosis. This equine variant of SCIN (eqSCIN) showed to be a potent blocker of the horse complement system and is thereby the first animal-adapted SCIN variant. Modification of this phage-encoded complement inhibitor plays a role in the host adaptation of *S. aureus*. Finally, we discuss the role of these newly identified evasion proteins and their the therapeutic implications in **Chapter 8**.

14. ACKNOWLEDGMENTS

We would like to thank Kobus Bosman and Seline Zwarthoff for useful discussions and critical review of the manuscript. This work was supported by ZonMw Grant 205200004 from the Netherlands Organization for Health Research and Development (to J.A.G.v.S.).

15. REFERENCES

1. Gorwitz, R. J., Kruszon-Moran, D., McAllister, S. K., McQuillan, G., McDougal, L. K., Fosheim, G. E., Jensen, B. J., Killgore, G., Tenover, F. C., and Kuehnert, M. J. (2008) Changes in the Prevalence of Nasal Colonization with *Staphylococcus aureus* in the United States, 2001–2004. J. Infect. Dis. 197, 1226–1234
2. Krismer, B., Weidenmaier, C., Zipperer, A., and Peschel, A. (2017) The commensal lifestyle of *Staphylococcus aureus* and its interactions with the nasal microbiota. Nat. Rev. Microbiol. 15, 675–687
3. Von Eiff, C., Becker, K., Machka, K., Stammer, H., Peters, G., and Grp, S. (2001) Nasal carriage as a source of *Staphylococcus aureus* bacteremia. N. Engl. J. Med. 344, 11–16
4. Lowy, F. D. (1998) *Staphylococcus aureus* infections. N. Engl. J. Med. 339, 520–532
5. Barrett, F. F., McGehee, R. F., and Finland, M. (1968) Methicillin-Resistant *Staphylococcus aureus* at Boston City Hospital. N. Engl. J. Med. 279, 441–448
6. Panlilio, A. L., Culver, D. H., Gaynes, R. P., Banerjee, S., Henderson, T. S., Tolson, J. S., Martone, W. J., and System, N. N. I. S. (1992) Methicillin-Resistant *Staphylococcus aureus* in U.S. Hospitals, 1975-1991. Infect. Control Hosp. Epidemiol. 13, 582–586
7. DeLeo, F. R., Otto, M., Kreiswirth, B. N., and Chambers, H. F. (2010) Community-associated meticillin-resistant *Staphylococcus aureus*. Lancet. 375, 1557–1568
8. DeLeo, F. R., Diep, B. A., and Otto, M. (2009) Host Defense and Pathogenesis in *Staphylococcus aureus* Infections. Infect. Dis. Clin. North Am. 23, 17–34
9. Diekema, D. J., Pfaller, M. A., Schmitz, F. J., Smayevsky, J., Bell, J., Jones, R. N., and Beach, M. (2001) Survey of Infections Due to Staphylococcus Species: Frequency of Occurrence and Antimicrobial Susceptibility of Isolates Collected in the United States, Canada, Latin America, Europe, and the Western Pacific Region for the SENTRY Antimicrobial Surveillanc. Clin. Infect. Dis. 32, S114–S132
10. Goldmann, O., and Medina, E. (2017) *Staphylococcus aureus* strategies to evade the host acquired immune response. Int. J. Med. Microbiol. 10.1016/j.ijmm.2017.09.013

11. Kusch, H., and Engelmann, S. (2014) Secrets of the secretome in *Staphylococcus aureus*. Int. J. Med. Microbiol. 304, 133–141
12. Faurschou, M., and Borregaard, N. (2003) Neutrophil granules and secretory vesicles in inflammation. Microbes Infect. 5, 1317–1327
13. Rigby, K. M., and DeLeo, F. R. (2012) Neutrophils in innate host defense against *Staphylococcus aureus* infections. Semin. Immunopathol. 34, 237–59
14. Cerquetti, M. C., Sordelli, D. O., Ortegon, R. a., and Bellanti, J. a. (1983) Impaired lung defenses against *Staphylococcus aureus* in mice with hereditary deficiency of the fifth component of complement. Infect. Immun. 41, 1071–1076
15. Von Köckritz-Blickwede, M., Konrad, S., Foster, S., Gessner, J. E., and Medina, E. (2009) Protective role of complement C5a in an experimental model of *staphylococcus aureus* bacteremia. J. Innate Immun. 2, 87–92
16. Amulic, B., Cazalet, C., Hayes, G. L., Metzler, K. D., and Zychlinsky, A. (2012) Neutrophil function: from mechanisms to disease. Annu. Rev. Immunol. 30, 459–89
17. Winkelstein, J. A., Marino, M. C., Johnston, R. B., Boyle, J., Curnutte, J., Gallin, J. I., Malech, H. L., Holland, S. M., Ochs, H., Quie, P., Buckley, R. H., Foster, C. B., Chanock, S. J., and Dickler, H. (2000) Chronic Granulomatous Disease: Report on a National Registry of 368 Patients. Medicine (Baltimore). 79, 155–169
18. Cook, N. (1998) Methicillin-resistant *Staphylococcus aureus* versus the burn patient. Burns. 24, 91–98
19. Church, D., Elsayed, S., Reid, O., Winston, B., and Lindsay, R. (2006) Burn wound infections. Clin. Microbiol. Rev. 19, 403–434
20. Verkaik, N. J., de Vogel, C. P., Boelens, H. a, Grumann, D., Hoogenboezem, T., Vink, C., Hooijkaas, H., Foster, T. J., Verbrugh, H. a, van Belkum, A., and van Wamel, W. J. B. (2009) Anti-Staphylococcal Humoral Immune Response in Persistent Nasal Carriers and Noncarriers of *Staphylococcus aureus*. J. Infect. Dis. 199, 625–632
21. Vestweber, D. (2007) Adhesion and signaling molecules controlling the transmigration of leukocytes through endothelium. Immunol. Rev. 218, 178–196
22. Kolaczkowska, E., and Kubes, P. (2013) Neutrophil recruitment and function in health and inflammation. Nat. Rev. Immunol. 13, 159–75
23. Moore, K. L., Patel, K. D., Bruehl, R. E., Fugang, L., Johnson, D. a, Lichenstein, H. S., Cummings, R. D., Bainton, D. F., and McEver, R. P. (1995) P-selectin glycoprotein ligand-1 mediates rolling of human neutrophils on P-selectin. J. Cell Biol. 128, 661–671
24. Phillipson, M., Heit, B., Colarusso, P., Liu, L., Ballantyne, C. M., and Kubes, P. (2006) Intraluminal crawling of neutrophils to emigration sites: a molecularly distinct process from adhesion in the recruitment cascade. J. Exp. Med. 203, 2569–75
25. Smith, C. W., Marlin, S. D., Rothlein, R., Toman, C., and Anderson, D. C. (1989) Cooperative interactions of LFA-1 and Mac-1 with intracellular adhesion molecule-1 in facilitating adherence and transendothelial migration of human neutrophils *in vitro*. J. Clin. Invest. 83, 2008–2017
26. Diamond, M. S., Staunton, D. E., de Fougerolles, a R., Stacker, S. a, Garcia-Aguilar, J., Hibbs, M. L., and Springer, T. a (1990) ICAM-1 (CD54): a counter-receptor for Mac-1 (CD11b/CD18). J. Cell Biol. 111, 3129–3139
27. Kim, M., Carman, C. V, and Springer, T. a (2003) Bidirectional transmembrane signaling by cytoplasmic domain separation in integrins. Science. 301, 1720–5
28. Jones, D. H., Anderson, D. C., Burr, B. L., Rudloff, H. E., Smith, C. W., Krater, S. S., and Schmalstieg, F. C. (1988) Quantitation of intracellular Mac-1 (CD11b/CD18) pools in human neutrophils. J. Leukoc. Biol. 44, 535–44
29. Ley, K., Laudanna, C., Cybulsky, M. I., and Nourshargh, S. (2007) Getting to the site of inflammation: the leukocyte adhesion cascade updated. Nat. Rev. Immunol. 7, 678–89
30. Bestebroer, J., Poppelier, M. J. J. G., Ulfman, L. H., Lenting, P. J., Denis, C. V., Van Kessel, K. P. M., Van Strijp, J. A. G., and De Haas, C. J. C. (2007) Staphylococcal superantigen-like 5 binds PSGL-1 and inhibits P-selectin-mediated neutrophil rolling. Blood. 109, 2936–2943

31. Walenkamp, A. M. E., Bestebroer, J., Boer, I. G. J., Kruizinga, R., Verheul, H. M., van Strijp, J. a G., and de Haas, C. J. C. (2010) Staphylococcal SSL5 binding to human leukemia cells inhibits cell adhesion to endothelial cells and platelets. Cell. Oncol. 32, 1–10

32. Somers, W. S., Shaw, G. D., and Camphausen, R. T. (2001) Insights into the molecular basis of leukocyte tethering and rolling revealed by structures of P- and E-selectin bound to SLeX and PSGL-1 (Cell 103:3 (467-479)). Cell. 105, 971

33. Chung, M. C., Wines, B. D., Baker, H., Langley, R. J., Baker, E. N., and Fraser, J. D. (2007) The crystal structure of staphylococcal superantigen-like protein 11 in complex with sialyl Lewis X reveals the mechanism for cell binding and immune inhibition. Mol. Microbiol. 66, 1342–1355

34. Fevre, C., Bestebroer, J., Mebius, M. M., de Haas, C. J. C., van Strijp, J. a G., Fitzgerald, J. R., and Haas, P. J. A. (2014) *Staphylococcus aureus* proteins SSL6 and SElX interact with neutrophil receptors as identified using secretome phage display. Cell. Microbiol. 16, 1646–1665

35. Wilson, G. J., Seo, K. S., Cartwright, R. a., Connelley, T., Chuang-Smith, O. N., Merriman, J. a., Guinane, C. M., Park, J. Y., Bohach, G. a., Schlievert, P. M., Morrison, W. I., and Fitzgerald, J. R. (2011) A novel core genome-encoded superantigen contributes to lethality of community-associated MRSA necrotizing pneumonia. PLoS Pathog. 10.1371/journal.ppat.1002271

36. Baker, H. M., Basu, I., Chung, M. C., Caradoc-Davies, T., Fraser, J. D., and Baker, E. N. (2007) Crystal Structures of the Staphylococcal Toxin SSL5 in Complex with Sialyl Lewis X Reveal a Conserved Binding Site that Shares Common Features with Viral and Bacterial Sialic Acid Binding Proteins. J. Mol. Biol. 374, 1298–1308

37. Tuffs, S. W., James, D. B. a., Bestebroer, J., Richards, A. C., Goncheva, M. I., O'Shea, M., Wee, B. a., Seo, K. S., Schlievert, P. M., Lengeling, A., van Strijp, J. a., Torres, V. J., and Fitzgerald, J. R. (2017) The *Staphylococcus aureus* superantigen SElX is a bifunctional toxin that inhibits neutrophil function. PLOS Pathog. 13, e1006461

38. Langley, R. J., Tian, Y., Clow, F., Young, P. G., Radcliff, F. J., Choi, M., Sequeira, R. P., Holtfreter, S., Baker, H., and Fraser, J. D. (2017) Staphylococcal enterotoxin-like X (SElX) is a unique superantigen with functional features of two major families of staphylococcal virulence factors. PLoS Pathog. 13, e1006549

39. Chavakis, T., Hussain, M., Kanse, S. M., Peters, G., Bretzel, R. G., Flock, J.-I., Herrmann, M., and Preissner, K. T. (2002) *Staphylococcus aureus* extracellular adherence protein serves as anti-inflammatory factor by inhibiting the recruitment of host leukocytes. Nat. Med. 8, 687–93

40. Ellis, T. N., and Beaman, B. L. (2004) Interferon-γ activation of polymorphonuclear neutrophil function. Immunology. 112, 2–12

41. Swain, S. D., Rohn, T. T., and Quinn, M. T. (2002) Neutrophil priming in host defense: role of oxidants as priming agents. Antioxid. Redox Signal. 4, 69–83

42. Skjeflo, E. W., Christiansen, D., Espevik, T., Nielsen, E. W., and Mollnes, T. E. (2014) Combined inhibition of complement and {CD14} efficiently attenuated the inflammatory response induced by *Staphylococcus aureus* in a human whole blood model. J. Immunol. {(Baltimore,} Md. 1950). 192, 2857–2864

43. Mitchell, G. B., Albright, B. N., and Caswell, J. L. (2003) Effect of interleukin-8 and granulocyte colony-stimulating factor on priming and activation of bovine neutrophils. Infect. Immun. 71, 1643–1649

44. Rainard, P., Riollet, C., Poutrel, B., and Paape, M. J. (2000) Phagocytosis and killing of *Staphylococcus aureus* by bovine neutrophils after priming by tumor necrosis factor-?? and the des-arginine derivative of C5a. Am. J. Vet. Res. 61, 951–959

45. Edwards, S. W., Say, J. E., and Hughes, V. (1988) Gamma interferon enhances the killing of *Staphylococcus aureus* by human neutrophils. J. Gen. Microbiol. 134, 37–42

46. Bestebroer, J., De Haas, C. J. C., and Van Strijp, J. a G. (2010) How microorganisms avoid phagocyte attraction. FEMS Microbiol. Rev. 34, 395–414

47. Chalovich, J. M., and Eisenberg, E. (2005) G Protein–Coupled Receptor Rhodopsin. Biophys. Chem. 257, 2432–2437

48. Allen, S. J., Crown, S. E., and Handel, T. M. (2007) Chemokine:Receptor Structure, Interactions, and Antagonism. Annu. Rev. Immunol. 25, 787–820

49. Tecchio, C., and Cassatella, M. a. (2016) Neutrophil-derived chemokines on the road to immunity. Semin. Immunol. 28, 119–128

50. Schiffmann, E., Corcoran, B. a, and Wahl, S. M. (1975) N-formylmethionyl peptides as chemoattractants for leucocytes. Proc. Natl. Acad. Sci. U. S. A. 72, 1059–62

51. Dahlgren, C., Gabl, M., Holdfeldt, A., Winther, M., and Forsman, H. (2016) Basic characteristics of the neutrophil receptors that recognize formylated peptides, a danger-associated molecular pattern generated by bacteria and mitochondria. Biochem. Pharmacol. 114, 22–39

52. Le, Y., Oppenheim, J. J., and Wang, J. M. (2001) Pleiotropic roles of formyl peptide receptors. Cytokine Growth Factor Rev. 12, 91–105

53. Kretschmer, D., Gleske, A.-K., Rautenberg, M., Wang, R., Köberle, M., Bohn, E., Schöneberg, T., Rabiet, M.-J., Boulay, F., Klebanoff, S. J., van Kessel, K. a., van Strijp, J. a., Otto, M., and Peschel, A. (2010) Human Formyl Peptide Receptor 2 Senses Highly Pathogenic *Staphylococcus aureus*. Cell Host Microbe. 7, 463–473

54. Gasque, P. (2004) Complement: A unique innate immune sensor for danger signals. Mol. Immunol. 41, 1089–1098

55. Kawai, T., and Akira, S. (2010) The role of pattern-recognition receptors in innate immunity: update on Toll-like receptors. Nat. Immunol. 11, 373–384

56. O'Neill, L. a. J., and Bowie, A. G. (2007) The family of five: TIR-domain-containing adaptors in Toll-like receptor signalling. Nat. Rev. Immunol. 7, 353–364

57. Jin, M. S., Kim, S. E., Heo, J. Y., Lee, M. E., Kim, H. M., Paik, S. G., Lee, H., and Lee, J. O. (2007) Crystal Structure of the TLR1-TLR2 Heterodimer Induced by Binding of a Tri-Acylated Lipopeptide. Cell. 130, 1071–1082

58. Rodríguez, D., Morrison, C. J., and Overall, C. M. (2010) Matrix metalloproteinases: What do they not do? New substrates and biological roles identified by murine models and proteomics. Biochim. Biophys. Acta - Mol. Cell Res. 1803, 39–54

59. Guerra, F. E., Borgogna, T. R., Patel, D. M., Sward, E. W., and Voyich, J. M. (2017) Epic Immune Battles of History: Neutrophils vs. *Staphylococcus aureus*. Front. Cell. Infect. Microbiol. 7, 1–19

60. Bestebroer, J., Van Kessel, K. P. M., Azouagh, H., Walenkamp, A. M., Boer, I. G. J., Romijn, R. a., Van Strijp, J. a. G., and De Haas, C. J. C. (2009) Staphylococcal SSL5 inhibits leukocyte activation by chemokines and anaphylatoxins. Blood. 113, 328–337

61. Itoh, S., Hamada, E., Kamoshida, G., Takeshita, K., Oku, T., and Tsuji, T. (2010) Staphylococcal superantigen-like protein 5 inhibits matrix metalloproteinase 9 from human neutrophils. Infect. Immun. 78, 3298–3305

62. Koymans, K. J., Bisschop, A., Vughs, M. M., van Kessel, K. P. M., de Haas, C. J. C., and van Strijp, J. a. G. (2016) Staphylococcal superantigen-like protein 1 and 5 (SSL1 & SSL5) limit neutrophil chemotaxis and migration through MMP-inhibition. Int. J. Mol. Sci. 17, 1–16

63. De Haas, C. J. C., Weeterings, C., Vughs, M. M., De Groot, P. G., Van Strijp, J. a., and Lisman, T. (2009) Staphylococcal superantigen-like 5 activates platelets and supports platelet adhesion under flow conditions, which involves glycoprotein Ibα and αIIbβ3. J. Thromb. Haemost. 7, 1867–1874

64. Hu, H., Armstrong, P. C. J., Khalil, E., Chen, Y. C., Straub, A., Li, M., Soosairajah, J., Hagemeyer, C. E., Bassler, N., Huang, D., Ahrens, I., Krippner, G., Gardiner, E., and Peter, K. (2011) GPVI and GPIBα mediate Staphylococcal superantigen-like protein 5 (SSL5) induced platelet activation and direct toward glycans as potential inhibitors. PLoS One. 6, 1–9

65. Walenkamp, A. M. E., Boer, I. G. J., Bestebroer, J., Rozeveld, D., Timmer-Bosscha, H., Hemrika, W., van Strijp, J. a. G., and de Haas, C. J. C. (2009) Staphylococcal Superantigen-like 10 Inhibits CXCL12-Induced Human Tumor Cell Migration. Neoplasia. 11, 333–344

66. Bardoel, B. W., Vos, R., Bouman, T., Aerts, P. C., Bestebroer, J., Huizinga, E. G., Brondijk, T. H. C., Van Strijp, J. a G., and De Haas, C. J. C. (2012) Evasion of Toll-like receptor 2 activation by staphylococcal superantigen-like protein 3. J. Mol. Med. 90, 1109–1120

67. Yokoyama, R., Itoh, S., Kamoshida, G., Takii, T., Fujii, S., Tsuji, T., and Onozaki, K. (2012) Staphylococcal superantigen-like protein 3 binds to the toll-like receptor 2 extracellular domain and inhibits cytokine production induced by *Staphylococcus aureus*, cell wall component, or lipopeptides in murine macrophages. Infect. Immun. 80, 2816–2825

68. Koymans, K. J., Feitsma, L. J., Brondijk, T. H. C., Aerts, P. C., Lukkien, E., Lossl, P., van Kessel, K. P. M., de Haas, C. J. C., van Strijp, J. A. G., and Huizinga, E. G. (2015) Structural basis for inhibition of TLR2 by

staphylococcal superantigen-like protein 3 (SSL3). Proc. Natl. Acad. Sci. U. S. A. 112, 11018–11023

69. Hermans, S. J., Baker, H. M., Sequeira, R. P., Langley, R. J., Baker, E. N., and Fraser, J. D. (2012) Structural and functional properties of staphylococcal superantigen-like protein 4. Infect. Immun. 80, 4004–4013

70. Koymans, K. J., Goldmann, O., Karlsson, C. a. Q., Sital, W., Thänert, R., Bisschop, A., Vrieling, M., Malmström, J., van Kessel, K. P. M., de Haas, C. J. C., van Strijp, J. a. G., and Medina, E. (2017) The TLR2 Antagonist Staphylococcal Superantigen-Like Protein 3 Acts as a Virulence Factor to Promote Bacterial Pathogenicity *in vivo*. J. Innate Immun. 10.1159/000479100

71. Laarman, A. J., Mijnheer, G., Mootz, J. M., van Rooijen, W. J. M., Ruyken, M., Malone, C. L., Heezius, E. C., Ward, R., Milligan, G., van Strijp, J. a. G., de Haas, C. J. C., Horswill, A. R., van Kessel, K. P. M., and Rooijakkers, S. H. M. (2012) *Staphylococcus aureus* Staphopain A inhibits CXCR2-dependent neutrophil activation and chemotaxis. EMBO J. 31, 3607–3619

72. Nickerson, N., Ip, J., Passos, D. T., and McGavin, M. J. (2010) Comparison of Staphopain A (ScpA) and B (SspB) precursor activation mechanisms reveals unique secretion kinetics of proSspB (Staphopain B), and a different interaction with its cognate Staphostatin, SspC. Mol. Microbiol. 75, 161–177

73. Veldkamp, K. E., Heezius, H. C. J. M., Verhoef, J., Van Strijp, J. A. G., and Van Kessel, K. P. M. (2000) Modulation of neutrophil chemokine receptors by *Staphylococcus aureus* supernate. Infect. Immun. 68, 5908–5913

74. De Haas, C. J. C., Veldkamp, K. E., Peschel, A., Weerkamp, F., Wamel, W. J. B. Van, Heezius, E. C. J. M., Poppelier, M. J. J. G., Kessel, K. P. M. Van, and Van Strijp, J. a G. (2004) Chemotaxis Inhibitory Protein of *Staphylococcus aureus* , a Bacterial Antiinflammatory Agent. J. Exp. Med. J. Exp. Med. 03687900, 687–695

75. Postma, B., Poppelier, M. J., van Galen, J. C., Prossnitz, E. R., van Strijp, J. a. G., de Haas, C. J. C., and van Kessel, K. P. M. (2004) Chemotaxis Inhibitory Protein of *Staphylococcus aureus* Binds Specifically to the C5a and Formylated Peptide Receptor. J. Immunol. 172, 6994–7001

76. Haas, P.-J., de Haas, C. J. C., Kleibeuker, W., Poppelier, M. J. J. G., van Kessel, K. P. M., Kruijtzer, J. a W., Liskamp, R. M. J., and van Strijp, J. a G. (2004) N-terminal residues of the chemotaxis inhibitory protein of *Staphylococcus aureus* are essential for blocking formylated peptide receptor but not C5a receptor. J. Immunol. 173, 5704–11

77. Postma, B., Kleibeuker, W., Poppelier, M. J. J. G., Boonstra, M., Van Kessel, K. P. M., Van Strijp, J. a. G., and De Haas, C. J. C. (2005) Residues 10-18 within the C5a receptor N terminus compose a binding domain for chemotaxis inhibitory protein of *Staphylococcus aureus*. J. Biol. Chem. 280, 2020–2027

78. Haas, P. J., De Haas, C. J. C., Poppelier, M. J. J. C., Van Kessel, K. P. M., Van Strijp, J. a. G., Dijkstra, K., Scheek, R. M., Fan, H., Kruijtzer, J. a. W., Liskamp, R. M. J., and Kemmink, J. (2005) The structure of the C5a receptor-blocking domain of chemotaxis inhibitory protein of *Staphylococcus aureus* is related to a group of immune evasive molecules. J. Mol. Biol. 353, 859–872

79. Prat, C., Bestebroer, J., de Haas, C. J. C., van Strijp, J. a. G., and van Kessel, K. P. M. (2006) A New Staphylococcal Anti-Inflammatory Protein That Antagonizes the Formyl Peptide Receptor-Like 1. J. Immunol. 177, 8017–8026

80. Prat, C., Haas, P.-J., Bestebroer, J., de Haas, C. J. C., van Strijp, J. a G., and van Kessel, K. P. M. (2009) A homolog of formyl peptide receptor-like 1 (FPRL1) inhibitor from *Staphylococcus aureus* (FPRL1 inhibitory protein) that inhibits FPRL1 and FPR. J. Immunol. 183, 6569–6578

81. Stemerding, A. M., Köhl, J., Pandey, M. K., Kuipers, A., Leusen, J. H., Boross, P., Nederend, M., Vidarsson, G., Weersink, A. Y. L., van de Winkel, J. G. J., van Kessel, K. P. M., and van Strijp, J. a G. (2013) *Staphylococcus aureus* formyl peptide receptor-like 1 inhibitor (FLIPr) and its homologue FLIPr-like are potent FcγR antagonists that inhibit IgG-mediated effector functions. J. Immunol. 191, 353–62

82. Ferreira, V. P., Pangburn, M. K., and Cortés, C. (2010) Complement control protein factor H: The good, the bad, and the inadequate. Mol. Immunol. 47, 2187–2197

83. Cunnion, K. M., Hair, P. S., and Buescher, E. S. (2004) Cleavage of Complement C3b to iC3b on the Surface of *Staphylococcus aureus* Is Mediated by Serum Complement Factor I Cleavage of Complement C3b to iC3b on the Surface of *Staphylococcus aureus* Is Mediated by Serum Complement Factor I. 72, 2858–2863

84. Mueller-Eberhard, H. J. (1986) The membrane attack complex of complement. Annu. Rev. Immunol. 4, 503–528

85. Wellek, B., Hahn, H., and Opferkuch, W. (1976) Opsonizing activities of IgG, IgM antibodies and the C3b inactivator-cleaved third component of complement in macrophage phagocytosis. Agents Actions. 6, 260–262

86. Mantovani, B. (1975) Different roles of IgG and complement receptors in phagocytosis by polymorphonuclear leukocytes. J. Immunol. 115, 15–7

87. Radaev, S., and Sun, P. (2013) Structural Recognition of Immunoglobulins by Fcγ Receptors. in Antibody Fc: Linking Adaptive and Innate Immunity, pp. 131–144, 38, 131–144

88. Stuart, L. M., and Ezekowitz, R. A. B. (2005) Phagocytosis: Elegant complexity. Immunity. 22, 539–550

89. Rosales, C. (2017) Fcγ receptor heterogeneity in leukocyte functional responses. Front. Immunol. 8, 1–13

90. McGreal, E., and Gasque, P. (2002) Structure-function studies of the receptors for complement C1q. Biochem Soc Trans. 30, 1010–1014

91. Todd, R. F. (1996) The continuing saga of complement receptor type 3 (CR3). J. Clin. Invest. 98, 1–2

92. O'Riordan, K., Lee, J. C., Riordan, K. O., and Lee, J. C. (2004) *Staphylococcus aureus* Capsular Polysaccharides. Clin. Microbiol. Rev. 17, 218–234

93. Cunnion, K. M., Lee, J. C., and Frank, M. M. (2001) Capsule production and growth phase influence binding of complement to *Staphylococcus aureus*. Infect. Immun. 69, 6796–6803

94. Rajagopal, M., and Walker, S. (2015) Envelope Structures of Gram-Positive Bacteria. in Current Topics in Microbiology and Immunology, pp. 1–44, 404, 1–44

95. Schneewind, O., Model, P., and Fischetti, V. a. (1992) Sorting of protein a to the staphylococcal cell wall. Cell. 70, 267–281

96. Becker, S., Frankel, M. B., Schneewind, O., and Missiakas, D. (2014) Release of protein A from the cell wall of *Staphylococcus aureus*. Proc. Natl. Acad. Sci. 111, 1574–1579

97. Forsgren, A., and Sjöquist, J. (1966) "Protein A" from *S. aureus*. I. Pseudo-immune reaction with human gamma-globulin. J. Immunol. 97, 822–7

98. Falugi, F., Kim, H. K., and Missiakas, D. M. (2013) Role of Protein A in the Evasion of Host Adaptive Immune Responses. MBio. 4, 1–9

99. Goodyear, C. S., and Silverman, G. J. (2003) Death by a B Cell Superantigen. J. Exp. Med. 197, 1125–1139

100. Pauli, N. T., Kim, H. K., Falugi, F., Huang, M., Dulac, J., Henry Dunand, C., Zheng, N.-Y., Kaur, K., Andrews, S. F., Huang, Y., DeDent, A., Frank, K. M., Charnot-Katsikas, A., Schneewind, O., and Wilson, P. C. (2014) *Staphylococcus aureus* infection induces protein A–mediated immune evasion in humans. J. Exp. Med. 211, 2331–2339

101. Kim, H., Falugi, F., Thomer, L., Missiakis, D., and Schneewind, O. (2015) Protein A Suppresses Immune Responses during *Staphylococcus aureus* Bloodstream Infection in Guinea Pigs. MBio. 6, 1–11

102. Zhang, L., Jacobsson, K., Vasi, J., Lindberg, M., and Frykberg, L. (1998) A second IgG-binding protein in *Staphylococcus aureus*. Microbiology. 144, 985–991

103. Zhang, L., Jacobsson, K., Strom, K., Lindberg, M., and Frykberg, L. (1999) *Staphylococcus aureus* expresses a cel I surface protein that binds both IgG and. Microbiology. 145, 177–183

104. Ebner, P., Prax, M., Nega, M., Koch, I., Dube, L., Yu, W., Rinker, J., Popella, P., Flötenmeyer, M., and Götz, F. (2015) Excretion of cytoplasmic proteins (ECP) in *Staphylococcus aureus*. Mol. Microbiol. 97, 775–789

105. Atkins, K. L., Burman, J. D., Chamberlain, E. S., Cooper, J. E., Poutrel, B., Bagby, S., Jenkins, a. T. a, Feil, E. J., and van den Elsen, J. M. H. (2008) *S. aureus* IgG-binding proteins SpA and Sbi: Host specificity and mechanisms of immune complex formation. Mol. Immunol. 45, 1600–1611

106. Burman, J. D., Leung, E., Atkins, K. L., O'Seaghdha, M. N., Lango, L., Bernado, P., Bagby, S., Svergun, D. I., Foster, T. J., Isenman, D. E., and Van Den Elsen, J. M. H. (2008) Interaction of human complement with Sbi, a staphylococcal immunoglobulin-binding protein: Indications of a novel mechanism of complement evasion by *Staphylococcus aureus*. J. Biol. Chem. 283, 17579–17593

107. Haupt, K., Reuter, M., Van Den Elsen, J., Burman, J., Hälbich, S., Richter, J., Skerka, C., and Zipfel, P. F. (2008) The *Staphylococcus aureus* protein Sbi acts as a complement inhibitor and forms a tripartite complex with host complement factor H and C3b. PLoS Pathog. 10.1371/journal.ppat.1000250

108. Itoh, S., Hamada, E., Kamoshida, G., Yokoyama, R., Takii, T., Onozaki, K., and Tsuji, T. (2010) Staphylococcal

superantigen-like protein 10 (SSL10) binds to human immunoglobulin G (IgG) and inhibits complement activation via the classical pathway. Mol. Immunol. 47, 932–938

109. Patel, D., Wines, B. D., Langley, R. J., and Fraser, J. D. (2010) Specificity of staphylococcal superantigen-like protein 10 toward the human IgG1 Fc domain. J. Immunol. 184, 6283–6292

110. Itoh, S., Yokoyama, R., Kamoshida, G., Fujiwara, T., Okada, H., Takii, T., Tsuji, T., Fujii, S., Hashizume, H., and Onozaki, K. (2013) Staphylococcal superantigen-like protein 10 (SSL10) inhibits blood coagulation by binding to prothrombin and factor Xa via their γ-carboxyglutamic acid (Gla) domain. J. Biol. Chem. 288, 21569–21580

111. Itoh, S., Yokoyama, R., Murase, C., Takii, T., Tsuji, T., and Onozaki, K. (2012) Staphylococcal superantigen-like protein 10 binds to phosphatidylserine and apoptotic cells. Microbiol. Immunol. 56, 363–371

112. Prokešová, L., Potužníková, B., Potempa, J., Zikán, J., Radl, J., Hachová, L., Baran, K., Porwit-Bbr, Z., and John, C. (1992) Cleavage of human immunoglobulins by serine proteinase from *Staphylococcus aureus*. Immunol. Lett. 31, 259–265

113. Laarman, A. J., Ruyken, M., Malone, C. L., van Strijp, J. a. G., Horswill, a. R., and Rooijakkers, S. H. M. (2011) *Staphylococcus aureus* Metalloprotease Aureolysin Cleaves Complement C3 To Mediate Immune Evasion. J. Immunol. 186, 6445–6453

114. Rooijakkers, S. H. M., Ruyken, M., Roos, A., Daha, M. R., Presanis, J. S., Sim, R. B., van Wamel, W. J. B., van Kessel, K. P. M., and van Strijp, J. A. G. (2005) Immune evasion by a staphylococcal complement inhibitor that acts on C3 convertases. Nat. Immunol. 6, 920–927

115. Rooijakkers, S. H. M., Milder, F. J., Bardoel, B. W., Ruyken, M., van Strijp, J. a G., and Gros, P. (2007) Staphylococcal complement inhibitor: structure and active sites. J. Immunol. 179, 985–994

116. Rooijakkers, S. H. M., Wu, J., Ruyken, M., van Domselaar, R., Planken, K. L., Tzekou, A., Ricklin, D., Lambris, J. D., Janssen, B. J. C., van Strijp, J. a G., and Gros, P. (2009) Structural and functional implications of the alternative complement pathway C3 convertase stabilized by a staphylococcal inhibitor. Nat. Immunol. 10, 721–727

117. Garcia, B. L., Ramyar, K. X., Tzekou, A., Ricklin, D., McWhorter, W. J., Lambris, J. D., and Geisbrecht, B. V. (2010) Molecular Basis for Complement Recognition and Inhibition Determined by Crystallographic Studies of the Staphylococcal Complement Inhibitor (SCIN) Bound to C3c and C3b. J. Mol. Biol. 402, 17–29

118. Jongerius, I., Köhl, J., Pandey, M. K., Ruyken, M., van Kessel, K. P. M., van Strijp, J. a. G., and Rooijakkers, S. H. M. (2007) Staphylococcal complement evasion by various convertase-blocking molecules. J. Exp. Med. 204, 2461–2471

119. Bodén, M. K., and Flock, J. I. (1994) Cloning and characterization of a gene for a 19 kDa fibrinogen-binding protein from *Staphylococcus aureus*. Mol.Microbiol. 12, 599–606

120. Palma, M., Shannon, O., Quezada, H. C., Berg, A., and Flock, J. I. (2001) Extracellular Fibrinogen-binding Protein, Efb, from *Staphylococcus aureus* Blocks Platelet Aggregation Due to Its Binding to the α-Chain. J. Biol. Chem. 276, 31691–31697

121. Heilmann, C., Herrmann, M., Kehrel, B. E., and Peters, G. (2002) Platelet-binding domains in 2 fibrinogen-binding proteins of *Staphylococcus aureus* identified by phage display. J.Infect.Dis. 186, 32–39

122. Palma, M., Nozohoor, S., Schennings, T., Heimdahl, a., and Flock, J. I. (1996) Lack of the extracellular 19-kilodalton fibrinogen-binding protein from *Staphylococcus aureus* decreases virulence in experimental wound infection. Infect. Immun. 64, 5284–5289

123. Lee, L. Y. L., Höök, M., Haviland, D., Wetsel, R. a, Yonter, E. O., Syribeys, P., Vernachio, J., and Brown, E. L. (2004) Inhibition of Complement Activation by a Secreted *Staphylococcus aureus* Protein. J. Infect. Dis. 190, 571–579

124. Hammel, M., Sfyroera, G., Ricklin, D., Magotti, P., Lambris, J. D., and Geisbrecht, B. V (2007) A structural basis for complement inhibition by *Staphylococcus aureus*. Nat. Immunol. 8, 430–437

125. Ko, Y. P., Kuipers, A., Freitag, C. M., Jongerius, I., Medina, E., van Rooijen, W. J., Spaan, A. N., van Kessel, K. P. M., Höök, M., and Rooijakkers, S. H. M. (2013) Phagocytosis Escape by a *Staphylococcus aureus* Protein That Connects Complement and Coagulation Proteins at the Bacterial Surface. PLoS Pathog. 9, 1–13

126. Kuipers, A., Stapels, D. a C., Weerwind, L. T., Ko, Y. P., Ruyken, M., Lee, J. C., van Kessel, K. P. M., and Rooijakkers, S. H. M. (2016) The *Staphylococcus aureus* polysaccharide capsule and Efb-dependent

fibrinogen shield act in concert to protect against phagocytosis. Microbiol. (United Kingdom). 162, 1185–1194

127. Hammel, M., Sfyroera, G., Pyrpassopoulos, S., Ricklin, D., Ramyar, K. X., Pop, M., Jin, Z., Lambris, J. D., and Geisbrecht, B. V. (2007) Characterization of Ehp, a secreted complement inhibitory protein from *Staphylococcus aureus*. J. Biol. Chem. 282, 30051–30061

128. Jongerius, I., Garcia, B. L., Geisbrecht, B. V., Van Strijp, J. a G., and Rooijakkers, S. H. M. (2010) Convertase inhibitory properties of staphylococcal extracellular complement-binding protein. J. Biol. Chem. 285, 14973–14979

129. Jongerius, I., Von Kockritz-Blickwede, M., Horsburgh, M. J., Ruyken, M., Nizet, V., and Rooijakkers, S. H. M. (2012) *Staphylococcus aureus* virulence is enhanced by secreted factors that block innate immune defenses. J. Innate Immun. 4, 301–311

130. Sharp, J. a., Echague, C. G., Hair, P. S., Ward, M. D., Nyalwidhe, J. O., Geoghegan, J. a., Foster, T. J., and Cunnion, K. M. (2012) *Staphylococcus aureus* surface protein SdrE binds complement regulator factor H as an immune evasion tactic. PLoS One. 10.1371/journal.pone.0038407

131. Zhang, Y., Wu, M., Hang, T., Wang, C., Yang, Y., Pan, W., Zang, J., Zhang, M., and Zhang, X. (2017) *Staphylococcus aureus* SdrE captures complement factor H's C-terminus via a novel "close, dock, lock and latch" mechanism for complement evasion. Biochem. J. 474, 1619–1631

132. Hair, P. S., Ward, M. D., Semmes, O. J., Foster, T. J., and Cunnion, K. M. (2008) *Staphylococcus aureus* Clumping Factor A Binds to Complement Regulator Factor I and Increases Factor I Cleavage of C3b. J. Infect. Dis. 198, 125–133

133. Hair, P. S., Echague, C. G., Sholl, A. M., Watkins, J. a., Geoghegan, J. a., Foster, T. J., and Cunnion, K. M. (2010) Clumping factor A interaction with complement factor I increases C3b cleavage on the bacterial surface of *Staphylococcus aureus* and decreases complement-mediated phagocytosis. Infect. Immun. 78, 1717–1727

134. Woehl, J. L., Stapels, D. a. C., Garcia, B. L., Ramyar, K. X., Keightley, A., Ruyken, M., Syriga, M., Sfyroera, G., Weber, A. B., Zolkiewski, M., Ricklin, D., Lambris, J. D., Rooijakkers, S. H. M., and Geisbrecht, B. V. (2014) The Extracellular Adherence Protein from *Staphylococcus aureus* Inhibits the Classical and Lectin Pathways of Complement by Blocking Formation of the C3 Proconvertase. J. Immunol. 193, 6161–6171

135. Rooijakkers, S. H. M., Van Wamel, W. J. B., Ruyken, M., Van Kessel, K. P. M., and Van Strijp, J. a G. (2005) Anti-opsonic properties of staphylokinase. Microbes Infect. 7, 476–484

136. Langley, R., Wines, B., Willoughby, N., Basu, I., Proft, T., and Fraser, J. D. (2005) The Staphylococcal Superantigen-Like Protein 7 Binds IgA and Complement C5 and Inhibits IgA-Fc RI Binding and Serum Killing of Bacteria. J. Immunol. 174, 2926–2933

137. Laursen, N. S., Gordon, N., Hermans, S., Lorenz, N., Jackson, N., Wines, B., Spillner, E., Christensen, J. B., Jensen, M., Fredslund, F., Bjerre, M., Sottrup-Jensen, L., Fraser, J. D., and Andersen, G. R. (2010) Structural basis for inhibition of complement C5 by the SSL7 protein from *Staphylococcus aureus*. Proc. Natl. Acad. Sci. U. S. A. 107, 3681–6

138. Bestebroer, J., Aerts, P. C., Rooijakkers, S. H. M., Pandey, M. K., Köhl, J., Van Strijp, J. a G., and De Haas, C. J. C. (2010) Functional basis for complement evasion by staphylococcal superantigen-like 7. Cell. Microbiol. 12, 1506–1516

139. Kang, M., Ko, Y. P., Liang, X., Ross, C. L., Liu, Q., Murray, B. E., and Höök, M. (2013) Collagen-binding microbial surface components recognizing adhesive matrix molecule (MSCRAMM) of gram-positive bacteria inhibit complement activation via the classical pathway. J. Biol. Chem. 288, 20520–20531

140. Brinkmann, V., Reichard, U., Goosmann, C., Fauler, B., Uhlemann, Y., Weiss, D. S., Weinrauch, Y., and Zychlinsky, A. (2004) Neutrophil Extracellular Traps Kill Bacteria. Science (80-.). 303, 1532–1535

141. Metzler, K. D., Goosmann, C., Lubojemska, A., Zychlinsky, A., and Papayannopoulos, V. (2014) A myeloperoxidase-containing complex regulates neutrophil elastase release and actin dynamics during NETosis. Cell Rep. 8, 883–96

142. Von Köckritz-Blickwede, M., and Nizet, V. (2009) Innate immunity turned inside-out: Antimicrobial defense by phagocyte extracellular traps. J. Mol. Med. 87, 775–783

143. McDonald, B., Urrutia, R., Yipp, B. G., Jenne, C. N., and Kubes, P. (2012) Intravascular neutrophil extracellular traps capture bacteria from the bloodstream during sepsis. Cell Host Microbe. 12, 324–333

144. Berends, E. T. M., Horswill, A. R., Haste, N. M., Monestier, M., Nizet, V., and Von Köckritz-Blickwede, M. (2010) Nuclease expression by *Staphylococcus aureus* facilitates escape from neutrophil extracellular traps. J. Innate Immun. 2, 576–586

145. Thammavongsa, V., Missiakas, D. M., and Schneewind, O. (2013) *Staphylococcus aureus* Degrades Neutrophil Extracellular Traps to Promote Immune Cell Death. Science (80-.). 342, 863–866

146. Manda-Handzlik, A., and Demkow, U. (2015) Neutrophils: The role of oxidative and nitrosative stress in health and disease. Adv. Exp. Med. Biol. 857, 51–60

147. Borregaard, N., and Cowland, J. B. (1997) Granules of the human neutrophilic polymorphonuclear leukocyte. Blood. 89, 3503–21

148. Egesten, A., Breton-Gorius, J., Guichard, J., Gullberg, U., and Olsson, I. (1994) The heterogeneity of azurophil granules in neutrophil promyelocytes: immunogold localization of myeloperoxidase, cathepsin G, elastase, proteinase 3, and bactericidal/permeability increasing protein. Blood. 83, 2985–94

149. Levy, O. (2004) Antimicrobial proteins and peptides: anti-infective molecules of mammalian leukocytes. J. Leukoc. Biol. 76, 909–925

150. Turner, J., Cho, Y., Dinh, N. N., Waring, A. J., and Lehrer, R. I. (1998) Activities of LL-37, a cathelin-associated antimicrobial peptide of human neutrophils. Antimicrob. Agents Chemother. 42, 2206–2214

151. Noore, J., Noore, A., and Li, B. (2013) Cationic antimicrobial peptide ll-37 is effective against both extraand intracellular *staphylococcus aureus*. Antimicrob. Agents Chemother. 57, 1283–1290

152. Wimley, W. C., Selsted, M. E., and White, S. H. (1994) Interactions between human defensins and lipid bilayers: Evidence for formation of multimeric pores. Protein Sci. 3, 1362–1373

153. Pham, C. T. N. (2006) Neutrophil serine proteases: specific regulators of inflammation. Nat. Rev. Immunol. 6, 541–550

154. Reeves, E. P., Lu, H., Jacobs, H. L., Messina, C. G. M., Bolsover, S., Gabella, G., Potma, E. O., Warley, A., Roes, J., and Segal, A. W. (2002) Killing activity of neutrophils is mediated through activation of proteases by K+ flux. Nature. 416, 291–297

155. Corbin, B. D., Seeley, E. H., Raab, A., Feldmann, J., Miller, M. R., Torres, V. J., Anderson, K. L., Dattilo, B. M., Anderson, K. L., Dunman, P. M., Gerads, R., Caprioli, R., Nacken, W., Chazin, W. J., and Skaar, E. P. (2008) Bacterial Growth in Tissue Abscesses. Science (80-.). 319, 962–966

156. Stříž, I., and Trebichavský, I. (2004) Calprotectin - A pleiotropic molecule in acute and chronic inflammation. Physiol. Res. 53, 245–253

157. Schindler, M., Sharon, N., Assaf, Y., and Chipman, D. M. (1977) Mechanism of Lysozyme Catalysis: Role of Ground-State Strain in Subsite D in Hen Egg-White and Human Lysozymes. Biochemistry. 16, 423–431

158. Selsted, M. E., and Martinez, R. J. (1978) Lysozyme: primary bactericidin in human plasma serum active against Bacillus subtilis. Infect. Immun. 20, 782–791

159. Babior, B. M., Lambeth, J. D., and Nauseef, W. (2002) The neutrophil NADPH oxidase. Arch. Biochem. Biophys. 397, 342–344

160. Kettle, A. J., Anderson, R. F., Hampton, M. B., and Winterbourn, C. C. (2007) Reactions of superoxide with myeloperoxidase. Biochemistry. 46, 4888–4897

161. Klebanoff, S. J., Kettle, A. J., Rosen, H., Winterbourn, C. C., and Nauseef, W. M. (2013) Myeloperoxidase: a front-line defender against phagocytosed microorganisms. J. Leukoc. Biol. 93, 185–98

162. Klebanoff, S. J. (2005) Myeloperoxidase: friend and foe. J. Leukoc. Biol. 77, 598–625

163. Liu, G. Y., Essex, A., Buchanan, J. T., Datta, V., Hoffman, H. M., Bastian, J. F., Fierer, J., and Nizet, V. (2005) *Staphylococcus aureus* golden pigment impairs neutrophil killing and promotes virulence through its antioxidant activity. J. Exp. Med. 202, 209–15

164. Liu, C.-I., Liu, G. Y., Song, Y., Yin, F., Hensler, M. E., Jeng, W.-Y., Nizet, V., Wang, A. H.-J., and Oldfield, E. (2008) A cholesterol biosynthesis inhibitor blocks *Staphylococcus aureus* virulence. Science. 319, 1391–4

165. Song, Y., Liu, C. I., Lin, F. Y., Joo, H. N., Hensler, M., Liu, Y. L., Jeng, W. Y., Low, J., Liu, G. Y., Nizet, V., Wang, A. H. J., and Oldfield, E. (2009) Inhibition of staphyloxanthin virulence factor biosynthesis in *Staphylococcus aureus*: *In vitro*, *in vivo*, and crystallographic results. J. Med. Chem. 52, 3869–3880

166. Karavolos, M. H. (2003) Role and regulation of the superoxide dismutases of *Staphylococcus aureus*.

Microbiology. 149, 2749–2758

167. Valderas, M. W., and Hart, M. E. (2001) Identification and Characterization of a Second Superoxide Dismutase Gene (sodM) from *Staphylococcus aureus*. J. Bacteriol. 183, 3399–3407

168. Mandell, G. L. (1975) Catalase, superoxide dismutase, and virulence of *Staphylococcus aureus*. *In vitro* and *in vivo* studies with emphasis on staphylococcal-leukocyte interaction. J. Clin. Invest. 55, 561–566

169. Horsburgh, M. J., Clements, M. O., Crossley, H., Ingham, E., and Foster, S. J. (2001) PerR controls oxidative stress resistance and iron storage proteins and is required for virulence in *Staphylococcus aureus*. Infect. Immun. 69, 3744–3754

170. Cosgrove, K., Coutts, G., Jonsson, I.-M., Tarkowski, a., Kokai-Kun, J. F., Mond, J. J., and Foster, S. J. (2007) Catalase (KatA) and Alkyl Hydroperoxide Reductase (AhpC) Have Compensatory Roles in Peroxide Stress Resistance and Are Required for Survival, Persistence, and Nasal Colonization in *Staphylococcus aureus*. J. Bacteriol. 189, 1025–1035

171. Guerra, F. E., Addison, C. B., de Jong, N. W. M., Azzolino, J., Pallister, K. B., van Strijp, J. A. G., and Voyich, J. M. (2016) *Staphylococcus aureus* SaeR/S-regulated factors reduce human neutrophil reactive oxygen species production. J. Leukoc. Biol. 100, 1–6

172. De Jong, N. W. M., Ramyar, K. X., Guerra, F. E., Nijland, R., Fevre, C., Voyich, J. M., McCarthy, A. J., Garcia, B. L., van Kessel, K. P. M., van Strijp, J. A. G., Geisbrecht, B. V., and Haas, P.-J. a. (2017) Immune evasion by a staphylococcal inhibitor of myeloperoxidase. Proc. Natl. Acad. Sci. 10.1073/pnas.1707032114

173. Richardson, A. R., Dunman, P. M., and Fang, F. C. (2006) The nitrosative stress response of *Staphylococcus aureus* is required for resistance to innate immunity. Mol. Microbiol. 61, 927–939

174. Richardson, A. R., Libby, S. J., and Fang, F. C. (2008) A Nitric Oxide-Inducible Lactate Dehydrogenase Enables *Staphylococcus aureus* to Resist Innate Immunity. Science (80-.). 319, 1672–1676

175. Peschel, a, Otto, M., Jack, R. W., Kalbacher, H., Jung, G., and Götz, F. (1999) Inactivation of the dlt operon in *Staphylococcus aureus* confers sensitivity to defensins, protegrins, and other antimicrobial peptides. J. Biol. Chem. 274, 8405–8410

176. Collins, L. V., Kristian, S. a, Weidenmaier, C., Faigle, M., Van Kessel, K. P. M., Van Strijp, J. a G., Götz, F., Neumeister, B., and Peschel, A. (2002) *Staphylococcus aureus* strains lacking D-alanine modifications of teichoic acids are highly susceptible to human neutrophil killing and are virulence attenuated in mice. J. Infect. Dis. 186, 214–9

177. Peschel, B. A., Jack, R. W., Otto, M., Collins, L. V., Staubitz, P., Nicholson, G., Kalbacher, H., Nieuwenhuizen, W. F., Jung, G., Tarkowski, A., Kessel, K. P. M. Van, Strijp, J. A. G. Van, Peschel, A., Jack, R. W., Otto, M., Collins, L. V., Staubitz, P., Nicholson, G., Kalbacher, H., Nieuwenhuizen, W. F., Jung, G., Tarkowski, A., van Kessel, K. P. M., and van Strijp, J. a. G. (2001) *Staphylococcus aureus* Resistance to Human Defensins and Evasion of Neutrophil Killing via the Novel Virulence Factor Mprf Is Based on Modification of Membrane Lipids with l-Lysine. J. Exp. Med. 193, 1067–1076

178. Oku, Y., Kurokawa, K., Ichihashi, N., and Sekimizu, K. (2004) Characterization of the *Staphylococcus aureus* mprF gene, involved in lysinylation of phosphatidylglycerol. Microbiology. 150, 45–51

179. Sieprawska-Lupa, M., Mydel, P., Krawczyk, K., Wójcik, K., Puklo, M., Lupa, B., Suder, P., Silberring, J., Reed, M., Pohl, J., Shafer, W., McAleese, F., Foster, T., Travis, J., and Potempa, J. (2004) Degradation of Human Antimicrobial Peptide LL-37 by *Staphylococcus aureus* -Derived Proteinases. Antimicrob. Agents Chemother. 48, 4673–4679

180. Bera, A., Herbert, S., Jakob, A., Vollmer, W., and Götz, F. (2005) Why are pathogenic staphylococci so lysozyme resistant? The peptidoglycan O-acetyltransferase OatA is the major determinant for lysozyme resistance of *Staphylococcus aureus*. Mol. Microbiol. 55, 778–787

181. Herbert, S., Bera, A., Nerz, C., Kraus, D., Peschel, A., Goerke, C., Meehl, M., Cheung, A., and Götz, F. (2007) Molecular basis of resistance to muramidase and cationic antimicrobial peptide activity of lysozyme in staphylococci. PLoS Pathog. 3, e102

182. Stapels, D. a, Ramyar, K. X., Bischoff, M., von Kockritz-Blickwede, M., Milder, F. J., Ruyken, M., Eisenbeis, J., McWhorter, W. J., Herrmann, M., van Kessel, K. P., Geisbrecht, B. V, and Rooijakkers, S. H. (2014) *Staphylococcus aureus* secretes a unique class of neutrophil serine protease inhibitors. Proc Natl Acad Sci U S A. 111, 13187–13192

183. Stapels, D. a. C., Woehl, J. L., Milder, F. J., Tromp, A. T., van Batenburg, A. a., de Graaf, W. C., Broll, S.

C., White, N. M., Rooijakkers, S. H. M., and Geisbrecht, B. V. (2017) Evidence for multiple modes of neutrophil serine protease recognition by the EAP family of Staphylococcal innate immune evasion proteins. Protein Sci. 00, 1–14

184. Stapels, D. a C., Kuipers, a., Von Köckritz-Blickwede, M., Ruyken, M., Tromp, a. T., Horsburgh, M. J., de Haas, C. J. C., Van Strijp, J. a G., Van Kessel, K. P. M., and Rooijakkers, S. H. M. (2016) *Staphylococcus aureus* protects its immune-evasion proteins against degradation by neutrophil serine proteases. Cell. Microbiol. 18, 536–545

185. Jin, T., Bokarewa, M., Foster, T., Mitchell, J., Higgins, J., and Tarkowski, A. (2004) *Staphylococcus aureus* resists human defensins by production of staphylokinase, a novel bacterial evasion mechanism. J. Immunol. 172, 1169–1176

186. Wilke, G. a., and Wardenburg, J. B. (2010) Role of a disintegrin and metalloprotease 10 in *Staphylococcus aureus* α-hemolysin-mediated cellular injury. Proc. Natl. Acad. Sci. 107, 13473–13478

187. Powers, M. E., Kim, H. K., Wang, Y., and Wardenburg, J. B. (2012) ADAM10 mediates vascular injury induced by *staphylococcus aureus* α-hemolysin. J. Infect. Dis. 206, 352–356

188. Inoshima, I., Inoshima, N., Wilke, G. a, Powers, M. E., Frank, K. M., Wang, Y., and Wardenburg, J. B. (2011) A *Staphylococcus aureus* pore-forming toxin subverts the activity of ADAM10 to cause lethal infection in mice. Nat. Med. 17, 1310–1314

189. Valeva, A., Walev, I., Pinkernell, M., Walker, B., Bayley, H., Palmer, M., and Bhakdi, S. (1997) Transmembrane β-barrel of staphylococcal α-toxin forms in sensitive but not in resistant cells. Proc.Natl.Acad.Sci.U.S A. 94, 11607–11611

190. Jayasinghe, L., and Bayley, H. (2005) The leukocidin pore: evidence for an octamer with four LukF subunits and four LukS subunits alternating around a central axis. Protein Sci. 14, 2550–61

191. Koop, G., Vrieling, M., Storisteanu, D. M. L., Lok, L. S. C., Monie, T., van Wigcheren, G., Raisen, C., Ba, X., Gleadall, N., Hadjirin, N., Timmerman, A. J., Wagenaar, J. A., Klunder, H. M., Fitzgerald, J. R., Zadoks, R., Paterson, G. K., Torres, C., Waller, A. S., Loeffler, A., Loncaric, I., Hoet, A. E., Bergström, K., De Martino, L., Pomba, C., de Lencastre, H., Ben Slama, K., Gharsa, H., Richardson, E. J., Chilvers, E. R., de Haas, C., van Kessel, K., van Strijp, J. A. G., Harrison, E. M., and Holmes, M. A. (2017) Identification of LukPQ, a novel, equid-adapted leukocidin of *Staphylococcus aureus*. Sci. Rep. 7, 40660

192. Vrieling, M., Koymans, K. J., Heesterbeek, D. a, Aerts, P. C., Rutten, V. P., de Haas, C. J., van Kessel, K. P., Koets, a P., Nijland, R., and van Strijp, J. a (2015) Bovine *Staphylococcus aureus* Secretes the Leukocidin LukMF' To Kill Migrating Neutrophils through CCR1. MBio. 6, e00335

193. Alonzo, F., and Torres, V. J. (2014) The Bicomponent Pore-Forming Leucocidins of *Staphylococcus aureus*. Microbiol. Mol. Biol. Rev. 78, 199–230

194. Spaan, A. N., van Strijp, J. a. G., and Torres, V. J. (2017) Leukocidins: staphylococcal bi-component pore-forming toxins find their receptors. Nat. Rev. Microbiol. 15, 435–447

195. Spaan, A. N., Reyes-Robles, T., Badiou, C., Cochet, S., Boguslawski, K. M., Yoong, P., Day, C. J., De Haas, C. J. C., Van Kessel, K. P. M., Vandenesch, F., Jennings, M. P., Le Van Kim, C., Colin, Y., Van Strijp, J. a. G., Henry, T., and Torres, V. J. (2015) *Staphylococcus aureus* Targets the Duffy Antigen Receptor for Chemokines (DARC) to Lyse Erythrocytes. Cell Host Microbe. 18, 363–370

196. DuMont, A. L., Yoong, P., Surewaard, B. G. J., Benson, M. a., Nijland, R., Strijp, J. a G. Van, and Torres, V. J. (2013) *Staphylococcus aureus* elaborates leukocidin AB to mediate escape from within human neutrophils. Infect. Immun. 81, 1830–1841

197. Naimi, T. S., LeDell, K. H., Como-Sabetti, K., Borchardt, S. M., Boxrud, D. J., Etienne, J., Johnson, S. K., Vandenesch, F., Fridkin, S., O'Boyle, C., Danila, R. N., and Lynfield, R. (2003) Comparison of community- and health care-associated methicillin-resistant *Staphylococcus aureus* infection. JAMA. 290, 2976–84

198. Wang, R., Braughton, K. R., Kretschmer, D., Bach, T.-H. L., Queck, S. Y., Li, M., Kennedy, A. D., Dorward, D. W., Klebanoff, S. J., Peschel, A., DeLeo, F. R., and Otto, M. (2007) Identification of novel cytolytic peptides as key virulence determinants for community-associated MRSA. Nat. Med. 13, 1510–1514

199. Surewaard, B. G. J., Nijland, R., Spaan, A. N., Kruijtzer, J. a W., de Haas, C. J. C., and van Strijp, J. a G. (2012) Inactivation of staphylococcal phenol soluble modulins by serum lipoprotein particles. PLoS Pathog. 8, e1002606

200. Surewaard, B. G. J., de Haas, C. J. C., Vervoort, F., Rigby, K. M., DeLeo, F. R., Otto, M., van Strijp, J. a G.,

and Nijland, R. (2013) Staphylococcal alpha-phenol soluble modulins contribute to neutrophil lysis after phagocytosis. Cell. Microbiol. 15, 1427–37

201. Lina, G., Bohach, G. a, Nair, S. P., Hiramatsu, K., Jouvin-Marche, E., and Mariuzza, R. (2004) Standard nomenclature for the superantigens expressed by Staphylococcus. J. Infect. Dis. 189, 2334–2336

202. Fraser, J. D., and Proft, T. (2008) The bacterial superantigen and superantigen-like proteins. Immunol. Rev. 225, 226–243

203. Thwaites, G. E., and Gant, V. (2011) Are bloodstream leukocytes Trojan Horses for the metastasis of *Staphylococcus aureus*? Nat. Rev. Microbiol. 9, 215–22

Chapter 2

Fluorescent reporters for markerless genomic integration in *Staphylococcus aureus*

Nienke W. M. de Jong[1], Thijs van der Horst[1], Jos A. G. van Strijp[1] & Reindert Nijland[1,2]

[1] Department of Medical Microbiology, University Medical Center Utrecht, Utrecht University, Utrecht, the Netherlands

[2] Laboratory of Phytopathology, Wageningen University, Wageningen, The Netherlands

Sci Rep. 2017 Mar 7;7:43889. doi: 10.1038/srep43889

ABSTRACT

We present integration vectors for *Staphylococcus aureus* encoding the fluorescent reporters mAmetrine, CFP, sGFP, YFP, mCherry and mKate. The expression is driven either from the *sarA*-P1 promoter or from any other promoter of choice. The reporter can be inserted markerless in the chromosome of a wide range of *S. aureus* strains. The integration site chosen does not disrupt any open reading frame, provides good expression, and has no detectable effect on the strains physiology. As an intermediate construct, we present a set of replicating plasmids containing the same fluorescent reporters. Also in these reporter plasmids the *sarA*-P1 promoter can be replaced by any other promoter of interest for expression studies. Cassettes from the replication plasmids can be readily swapped with the integration vector. With these constructs it becomes possible to monitor reporters of separate fluorescent wavelengths simultaneously.

INTRODUCTION

Staphylococcus aureus is one of the most problematic pathogens for human health, able to cause skin and soft tissue infections, as well as serious invasive diseases such as sepsis, endocarditis, osteomyelitis, toxic shock syndrome and pneumonia (1). Tools to analyse host-pathogen interaction and gene expressions in *S. aureus* are still in short supply. In the last years several very useful constructs have been made which aid in the study of *S. aureus* using fluorescent proteins, using either replicating plasmids (2, 3), or integrating the reporter into the genome with the aid of a selectable resistance marker (4). Also plasmid systems to integrate the fluorescent reporters at the locus of the original genes has been described, using the presence of a *bursa aurealis* transposon in the genome of the target strains created for and available through the Nebraska Transposon Mutant Library (5). However, as this system requires the previous insertion of the transposon, it is not readily applicable to other strains of *S. aureus*.

The use of fluorescence reporters is clear in the field of microscopy and flow cytometry analysis. However, also in plate readers with the capability to measure fluorescence both growth (constitutive promoter) as well as specific promoter activity can be measured, such as demonstrated in (6).

In this study, we build upon the constructs already available to the *S. aureus* research community (2–4). We created constitutively expressed fluorescent reporters CFP, GFP, YFP and multiple red variants (DsRED, mCherry, mKate2). Further, we introduce a new fluorescent reporter already in use in eukaryotic systems but so far absent from prokaryotic toolboxes, mAmetrine (7). This latter protein is excited at a much shorter wavelength, but fluoresces at a wavelength similar to GFP. The expression of these reporters is controlled by the *sarA*-P1 promoter and the expression cassette is integrated in the genome of the *S. aureus* strains by homologous recombination. As an intermediate, but similarly useful tool, we produced replicating plasmids containing all mentioned reporter genes, and wherein the *sarA*-P1 promoter, which is flanked by restriction sites, can be replaced by any other promoter of interest for expression studies. With these constructs it becomes possible to study multiple promoter activities in different fluorescent colours. For example, it is possible to transform a GFP containing plasmid under control of a promoter of your interest, in bacteria constitutively expressing mAmetrine or CFP from its chromosomal location, and analyse promoter activity compared to bacterial growth in conditions where OD cannot be measured reliably due to the turbidity of the medium used or in (confocal) microscopy when non-fluorescent cells are very difficult to spot.

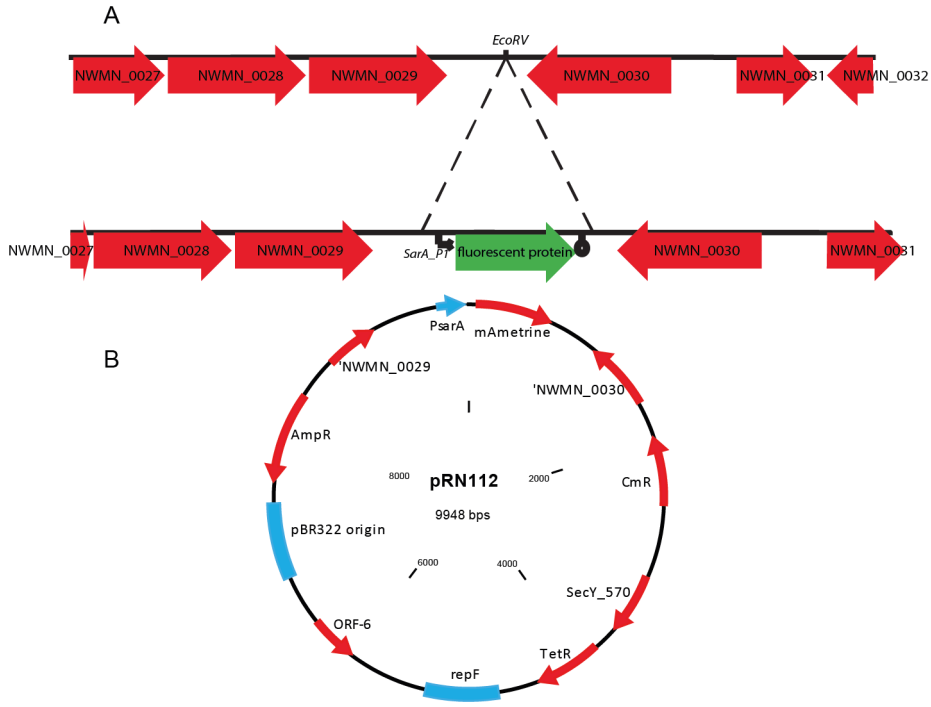

Figure 1: Genomic region of *S. aureus* strain Newman where the fluorescent contrusts were integrated. (**A**) Schematic overview of the insertion site for the fluorescent protein expression construct in the chromosome of *S. aureus* Newman (NC_009641.1). The construct is introduced by a double cross over event between the genes NWMN0029 and NWMN0030. (**B**) plasmid pRN1112 used for integration by double cross over of PsarA_P1-mAmetrineA construct in the chromosome of *S. aureus* strains. CmR = chloramphenicol resistance gene; TetR: Tetracycline resistance gene; AmpR = Ampicillin resistance gene.

RESULTS AND DISCUSSION

Plasmids containing expression cassettes of various fluorescent proteins

pCM29 was chosen as starting vector for building all other reporter plasmids, since it is a stable plasmid with replicates both in *E. coli* and *S. aureus* and contains sGFP under the control of *sarA*-P1 promoter (8). By exchanging sGFP with DsRED, mCherry, mKate2, CFP, YFP and mAmetrine we created pTH1, pRN10, pRN11, pTH2, pTH3 and pRN12 respectively with the same backbone as pCM29. In these plasmids multiple unique restriction sites are present flanking both sides of the *sarA*-P1 promoter, allowing for easy exchange of this promoter with any other promoter to study its expression. In their present form with the *sarA*-P1 promoter these plasmids give a very strong fluorescent signal, and it is possible to precisely separate the cells expressing each of the four different fluorescent proteins in one sample (**Figure 3**). The fluorescent signal from the DsRed construct was sometimes strong, but unfortunately the expression of this specific fluorescent protein appeared unstable compared to the other

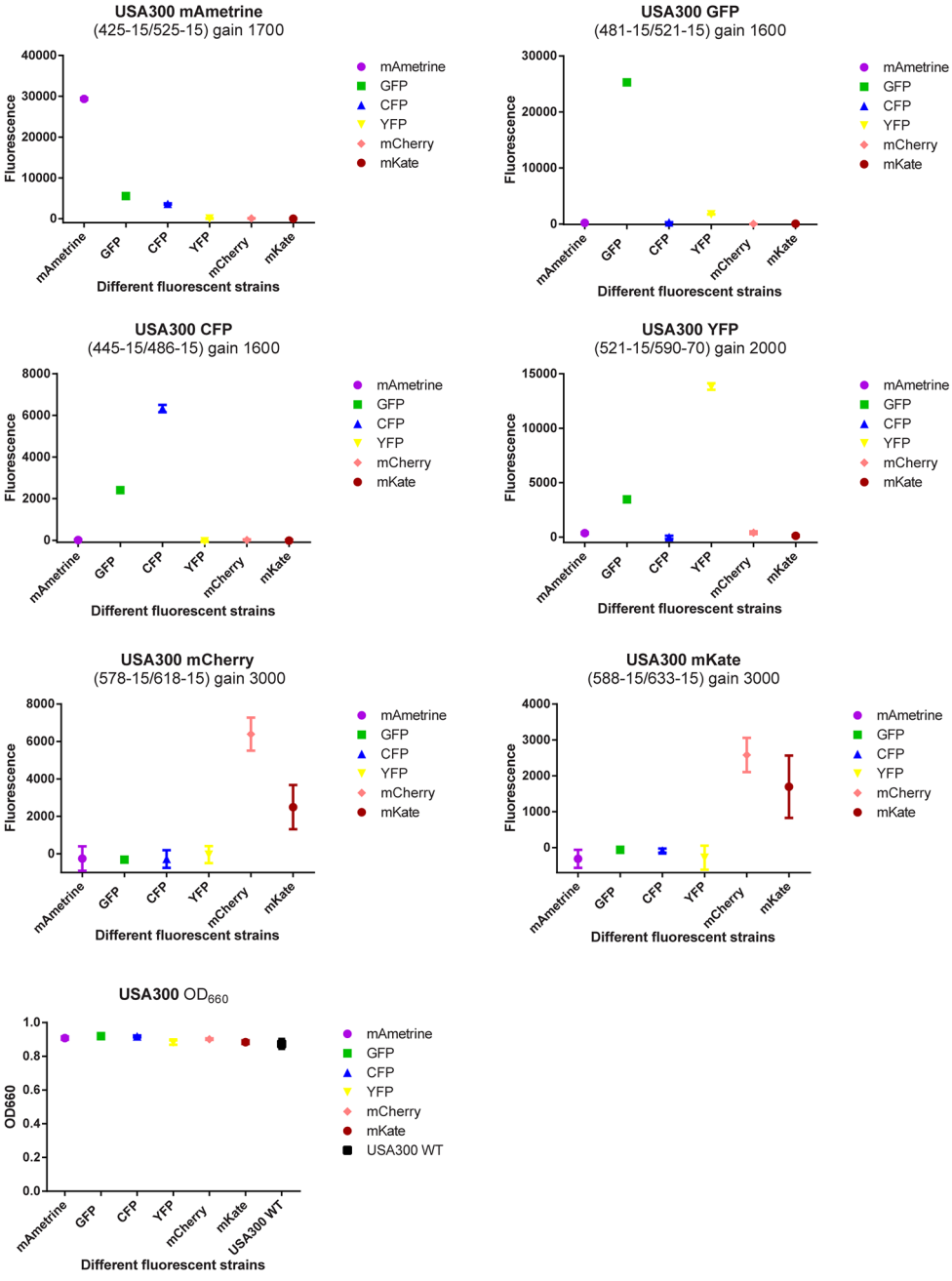

Figure 2: Spectral separation and intensity of all fluorescent constructs obtained by integration in the chromosome of *S. aureus* strains USA300. Data points show mean +/- SD is shown of 4 technical replicates.

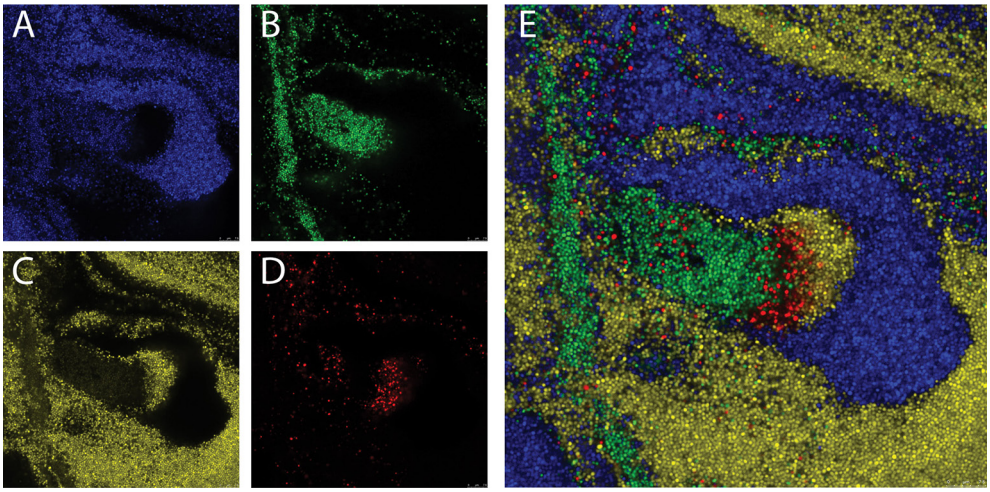

Figure 3: Simultaneous imaging of a mix of 4 separate *S. aureus* strains expressing fluorescent proteins from replicative plasmids using confocal microscopy. Acquisition settings: **A**: CFP: excitation laser 458nm, detection 465-502nm; **B**: GFP: excitation laser 476nm, detection 500-510nm; **C**: YFP: excitation laser 514nm, detection 525-600nm; **D**: DsRed: excitation laser 543nm, detection 598-709nm. **E**: Composite image of A-D.

fluorescent proteins, and a large population of cells rapidly lost DsRed expression after continued subculturing (not shown).

mAmetrine excitation and emission spectra

To determine the excitation and emission spectra of mAmetrine when expressed in the cytosol of *S. aureus*, we measured these spectra (**Figure 4**). A maximum excitation of mAmetrine was observed at 422nm, and a maximum emission at 525nm, similar to the reported values for mAmetrine in the literature (7). As *S. aureus* shows autofluorescence, particularly when excited with blue light, this correction of the spectra using a non-fluorescent strain resulted in

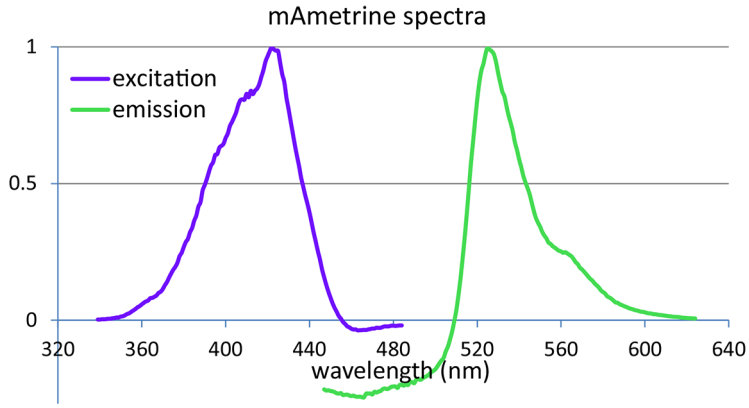

Figure 4: Excitation and emission spectra for mAmetrine when expressed in the cytosol of *S. aureus* USA300.

negative numbers for the emission spectrum below 510nm.

Selection of site for markerless genomic integration

The stable integration of a reporter gene in the bacterial genome has several benefits over expression from a replicating plasmid. However, integration also has some drawbacks, notable a lower signal due to its single presence per copy of the chromosome and possible pleiotropic effects on the disrupted genes. To reduce these drawbacks as much as possible, our integration site was selected based on the following criteria: to minimize downstream effects of the integration, the reporter cassette should not be integrated inside an operon or in a promoter sequence. Preferably it should be integrated at the 3` end of both open reading frames between which it will be located. Furthermore, the locus should be relatively close to the chromosomal origin of replication. In exponentially growing cells, chromosome division is an almost continuous process resulting in a higher copy number of genes close to the origin of replication compared to genes close to the terminus (9). It is therefore advantageous to integrate a reporter construct close to the origin as this will result in more copies of the construct and therefore a brighter signal. To minimize the impact of integration on the adjacent genomic regions, we selected a region with two open reading frames that are transcribed in opposing directions, their stop codons facing each other. The reporters are then integrated into their shared downstream region, in such a way that no nucleotides are replaced, but simply the reporter cassette is added, as such influencing only the spacing between the two open reading frames.

The site chosen to integrate the reporter cassette is located between genes NWMN_0029 and NWMN_0030 (*S. aureus* Newman; NC_009641.1). There is 666bp spacing between the two open reading frames, and the presence of an endogenous EcoRV recognition site in the region between genes 29 and 30 (EcoRV site 167bp down 29; 499bp down 30) in Newman which was not present in the cloning vector pJB38 was of practical benefit (**Figure 1**). Gene NWMN_0029 is annotated as a hypothetical protein similar to a pyridine nucleotide-disulfide oxidoreductase, and gene NWMN_0030 is annotated as a tRNA-dihydrouridine synthase.

Finally, the region chosen was highly conserved in the sequenced *S. aureus* strains. In a Blast search against *S. aureus* genomes available at Genbank, the selected region of the Newman chromosome was shown to be identical in USA300, NCTC8325, COL, and has 1 basepair difference in strain RN4220. The lowest similarity encountered of the fragment used for homologous recombination was 99.5% (1794/1803), present in strains MSSA476 and MW2. In the later strain integration was not more problematic than with strain Newman. Note that in the different *S. aureus* strains the gene names and numbers differ. For USA300 the genes are not designated gene numbers 29 and 30, instead gene NWMN_0029 is identical to SAUSA300_0087 (due to the integration of SSC-mec and ACME upstream of the selected site). **Supplemental Table 1** lists the corresponding location of the integration site in frequently used *S. aureus* strains.

When going through the genome of *S. aureus* strain Newman another region showed to be adhering the criteria set above, and could be useful for making double labelled strains or stable integration of other genes of interest. This is the genomic region between genes NWMN_0048/NWMN_RS00280 and NWMN_0049/NWMN_RS00285 (63771 bp-64264 bp). The reason not to select this region here was because it is slightly less conserved across most *S. aureus* strains compared to the 29_30 region. It was 100% homologous to strains Newman, Col, USA300, NCTC 8325, there was a little gap in this region in strains MSSA476 and MW2, and a homology below 95% in N315, Mu50.

Remark on the selected genomic integration site

Recently all bacterial genomes, including those of most *S. aureus* strains, were re-annotated at NCBI, and their locus tags have changed (10, 11), see also **Supplemental Table 1**. In this new annotation, a very small open reading frame is annotated between genes 29 and 30. This open reading frame is annotated to encode USP (universal stress protein). The sequence is starting with an unusual start codon (TTG) and is very short (102 bp). Upon close inspection of the sequence, both a potential RBS (GGAGGTA) is present 17 bp upstream of the start codon, and also a potential promoter binding site (-35 TTTACA, -10 AATTAAAAT), BPROM (12) is predicted 66bp upstream of the TTG start codon. The EcoRV site used to insert the fluorescent sequences is 36 bp upstream of the start of the -35 site of this predicted promoter. As a result, the location chosen between the opposing genes NWMN_0029 and NWMN_0030 no longer confirms to all criteria set out above. The insertion site is now situated between genes 30 and the USP-gene, which are in a similar orientation, although not likely to be in an operon. The NARSA transposon insertion database (13) shows no insertion in homologs of genes 29 (SAUSA300_0087/ SAUSA300_RS00450) and SAUSA300_RS00455 (although 29 homolog is not shown in the NARSA database as its sequence contains a premature stop codon in and is therefore annotated as a pseudogene). Insertions were abundantly present in the homolog of gene 30 (SAUSA300_0089/SAUSA300_RS00460). Nevertheless, the relative ease of making insertions and double cross over events indicates that our insertion does not have a strong effect on the fitness of the strain, and also growth is comparable between the control and fluorescent strains (**Figure 5**).

Markerless genomic integration of genes encoding fluorescent proteins

pJB38 is a plasmid with a temperature sensitive replicon for *S. aureus*, which can be used for chromosomal integration (5). By adding the NWMN29-NWMN30 sequence, pJB38-NWMN29-30 was created as a backbone for targeted integration in the *S. aureus* genome. Markerless insertion of the constructed fluorescent expression cassettes mAmetrine, CFP, sGFP, YFP, mCherry, mKate was efficient, both in stains Newman, MW2 and USA300. Furthermore, the sGFP cassette (pTH100) was successfully inserted in strain SH1000 (Personal communication François Vandenesch). Unfortunately, the DsRED construct was difficult to obtain, and when a clone with the construct integrated in the chromosome was eventually isolated it rapidly

lost DsRED expression, likely due to secondary mutations. This again indicated, as seen with the replicative plasmid, that DsRED was a problematic fluorescent protein to express in the *S. aureus* strains used. As an alternative we have created both mCherry and mKate constructs, whose excitation and emission spectra are both at a longer wavelength compared to DsRed, allowing for improved separation of multiple fluorophores in the same sample.

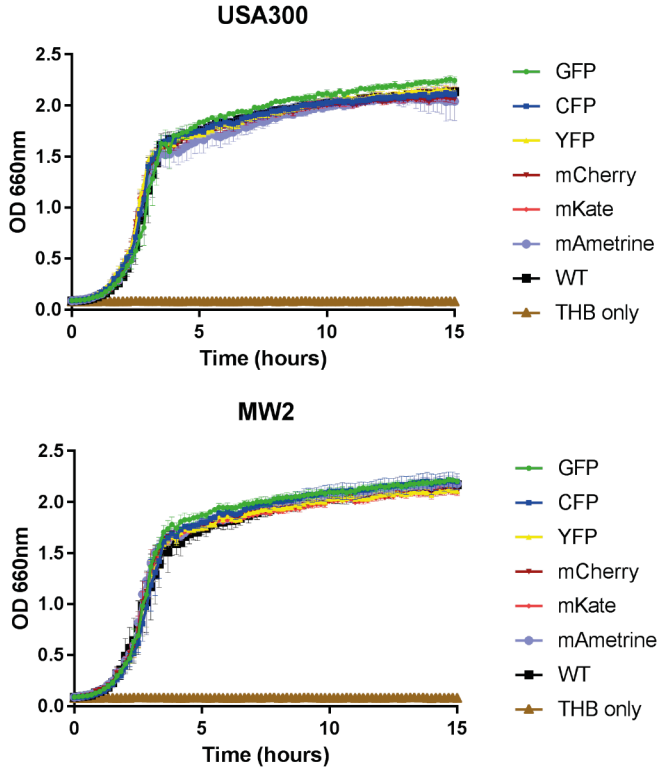

Figure 5: Growth of *S. aureus* strains USA300 and MW2 with chromosomal integration of different fluorescent markers. No effect on growth dynamics of the genomic integration of the various fluorescent constructs is visible.

Stability of the reporters and influence on growth rate

To test whether the newly integrated reporters influenced the growth of *S. aureus*, we have grown both the WT strain and the reporter containing strains in a microplate reader. As is clear from **Figure 5**, no differences in growth were detected for both MW2 and USA300. Fluorescence could be detected for all fluorescent proteins using the appropriate excitation and emission setting (**Table 2**, **Figure 2**, **Supplemental Figure 1**), and during exponential growth a correlation was present between OD_{660} and fluorescence measurements, with the most similarity between optical density and fluorescence signal for GFP, CFP and YFP. The mAmetrine signal also followed the growth curve, but the mKate and mCherry signals are lagging, likely due to lower folding kinetics of these fluorescent proteins (14). Once cells reach stationary phase the OD_{660} obviously plateaus, but the fluorescence signal continues to accumulate, indicating that the activity of the *SarA*-P1 promoter continues into stationary phase.

Our results demonstrate that for the constructed reporter strains measuring fluorescence is a suitable alternative to measuring OD if turbidity due to the presence of eukaryotic cells such as neutrophils will prevent correct OD measurements. Depending on the type of fluorescent protein chosen the signal should be corrected based on the known maturation characteristics of the protein.

Potential applications of the developed tools

The constructs described here have a broad spectrum of applications in biological research. By using different fluorescent proteins for the specific promoter activity and the genomic integrated reporter, you can differentiate between bacterial growth and promoter activity. This setup will give novel information in a quick and dynamic way. This can be done with any promoter of *S. aureus*, which will greatly enhance research on this harmful bacterium. Alternatively, in a co-infection experiment, one could use different fluorescent chromosomal encoded markers in each strain, which after the experiment can readily be quantified using flow cytometry or, after plating, simply counting the number of blue, green and red fluorescent colonies using a fluorescence imager such as a LAS4010.

The plasmid backbone used for all reporter expression plasmids (from pCM29) contains the open reading frame encoding the Rep-1 protein for rolling circle replication in Gram-positive hosts (8). As such, this plasmid enables replication in several other Gram-positive bacteria in addition to *S. aureus*. We have tested *Bacillus subtilis* and *Paenibacillus sp.* Both organisms become brightly fluorescent when transformed with the pCM29 plasmid (data not shown), demonstrating that the collection of replicative plasmids described here is also able to drive high expression of fluorescent proteins from the *sarA*-P1 promoter in other Firmicutes.

ACKNOWLEDGEMENTS

We would like to thank Alexander Horswill for providing plasmid pCM29. Tim Foster and Ian Monk for E.coli strain DC10B, Ken Bayles and Jeffrey Bose for plasmids pJB38 and pKTE1, Jan Liese for plasmids pJL76, pJL77 and pPagr-mCherry, and Jan-Willem Veening and Morten Kjos for *S. pneumonia*e strain MK119.

AUTHOR CONTRIBUTIONS

R.N. designed research, N.d.J., T.v.d.H. and R.N. performed research, N.d.J., T.v.d.H., J.v.S. and R.N. analysed data and wrote the paper.

COMPETING INTERESTS

The authors declare no competing financial interests.

MATERIALS & METHODS

General procedures, plasmids, bacterial strains and media

All plasmids and strains used in this study are listed in **Table 1**. All plasmids were transformed into competent *E. coli* DC10B or *E. coli* Top10F'. Correct plasmids isolated from *E. coli* DC10B were directly transformed to *S. aureus* Newman, MW2 and USA300 strains by electroporation as described (15). If the plasmid was isolated from *E. coli* Top10 F' it was first introduced in *S. aureus* RN4220, re-isolated and subsequently introduced in the target *S. aureus* strain. *E. coli* was grown in LB broth or agar. *S. aureus* was grown in Todd-Hewitt agar or broth. When growing in liquid cultures, both E.coli and *S. aureus* were grown in 50ml tubes with maximum 10 ml of growth medium, shaken at 300rpm at 37°C. Ampicillin concentrations for *E. coli* were 100 µg/ml and chloramphenicol concentrations for *S. aureus* were 10 µg/ml. All restriction enzymes were purchased from New England Biolabs and were used according to the manufacturer's instructions. PCR was performed using Phusion DNA polymerase (Finnzymes) or PWO polymerase (Roche) for cloning, and using Taq-ready mix (Fermentas) for colony checking. Primers were obtained from Integrated DNA Technologies (IDT, Leuven, Belgium) and sequencing reactions were performed using BigDye Terminator V3.1 (Life Technologies) and analysed at the Central Sequence Facility at UMC Utrecht, or at Macrogen (Macrogen Easy-seq). PCR purifications were performed using a QIAquick PCR Purification Kit (Qiagen). Ligations were performed using a T4 DNA Ligase (Roche Applied Science) according to the manufacturer's instructions. Initial fluorescence expression was analysed using an ImageQuant LAS4010 (GE Health Care) or Leica TSC SP5 inverted microscope equipped with a HCX PL APO 40/0.85 objective (Leica Microsystems), with the correct excitation and emissions spectra for the different fluorescent colours (**Table 2**).

Design of *S. aureus* codon optimized mAmetrine coding sequence

The fluorescent protein mAmetrine has a very large stokes-shift (7), with an excitation maximum at 423nm and emission maximum at 525nm. The original coding sequence available in the literature had a high GC-content and is used in eukaryotes, and we assumed this to be less compatible with expression in low GC Gram-positive bacteria such as *S. aureus*. Therefore, its codon usage was optimized using the software Gene Designer 2.0 (DNA 2.0, USA) and *S. aureus* MW2 genome sequence as a reference for codon usage. A G-block of 750bp containing the newly designed coding sequence with a GC-content of 29% and upstream RBS and spacing to start of the reporter gene identical to pCM29 was ordered from IDT (IDT, Leuven, Belgium). Additional restriction sites were added by PCR (primers in **Table 3**), and this PCR product was cloned into a KpnI, EcoRI digested pCM29 as described below. The nucleotide sequence of the codon optimized mAmetrine gene is deposited at GenBank: KX759016.

DsRED, mKate2, mCherry, YFP & CFP and fluorescent reporters in plasmid pCM29

DsRed.T3(DNT), mKate2, mCherry, YFP (venus) and CFP (Cerulean) coding genes were amplified by PCR from several templates (templates and primers are presented in **Table 3**). For amplification of mCherry and mKate2 the forward primer was designed to include XmaI, KpnI and Bsu36I restriction sites, a RBS, and spacing to start of the gene encoding the reporter protein identical to the one present in pCM29 (**Table 3**). For mKate2 genomic DNA of *S. pneumonia*e strain MK119 (16) was used as a template. This strain contains a *S. pneumonia*e codon optimized gene encoding mKate2 C-terminally fused to a histone protein. To create a single gene also the ATG start codon

Table 1: Strains and plasmids used in this study

Strain/plasmid	Genotype/properties	**Reference**
E. coli		
DC10B	cloning strain, *dcm*-	(19)
Top10F'	cloning strain	Invitrogen
S. aureus		
RN4220	ST8; CC8; chemically mutagenized derivative of 8325-4, transformable with *E. coli* DNA	(20)
Newman	WT, NC_009641.1	
Newman-mAmetrine	integration of sarA_P1-mAmetrine-Term downstream gene NWMN_0029	This study
Newman-CFP	Integration of sarA_P1-CFP-Term downstream gene NWMN_0029	This study
Newman-sGFP	Integration of sarA_P1-sGFP-Term downstream gene NWMN_0029	This study
Newman-YFP	Integration of sarA_P1-YFP-Term downstream gene NWMN_0029	This study
Newman-mCherry	Integration of sarA_P1-mCherry-Term downstream gene NWMN_0029	This study
Newman-mKate2	Integration of sarA_P1-sKate2-Term downstream gene NWMN_0029	This study
MW2	WT, NC_003923.1	
MW2-CFP	Integration of sarA_P1-CFP-Term downstream gene MW0058	This study
MW2-mAmetrine	Integration of sarA_P1-mAmetrine-Term downstream gene MW0058	This study
MW2-sGFP	Integration of sarA_P1-sGFP-Term downstream gene MW0058	This study
MW2-YFP	Integration of sarA_P1-YFP-Term downstream gene MW0058	This study
MW2-mCherry	Integration of sarA_P1-mCherry-Term downstream gene MW0058	This study
MW2-mKate2	Integration of sarA_P1-sKate2-Term downstream gene MW0058	This study
USA300_FPR3757	WT strain, NC_007793.1	
USA300-mAmetrine	Integration of sarA_P1-mAmetrine-Term downstream pseudogene SAUSA300_0087	This study
USA300-CFP	Integration of sarA_P1-CFP-Term downstream pseudogene SAUSA300_0087	This study
USA300-sGFP	Integration of sarA_P1-sGFP-Term downstream pseudogene SAUSA300_0087	This study
USA300-YFP	Integration of sarA_P1-YFP-Term downstream pseudogene SAUSA300_0087	This study
USA300mCherry	Integration of sarA_P1-mCherry-Term downstream pseudogene SAUSA300_0087	This study
USA300-mKate2	Integration of sarA_P1-sKate2-Term downstream pseudogene SAUSA300_0087	This study
Plasmids		
pCM29	Plasmid for *sarA* P1- sGFP expression	(8)
pKTEI	Plasmid containing DsRed.T3(DNT)	(21)
pJL76	Plasmid containing CFP (Cerulean)	(3)
pJL77	Plasmid containing YFP (Venus)	(3)
pJL49	Plasmid containing Pagr-mCherry	(3)

pTH1	Plasmid for sarA P1- dsRED expression	This study
pTH2	Plasmid for sarA P1- CFP expression	This study
pTH3	Plasmid for sarA P1- YFP expression	This study
pRN10	Plasmid for sarA P1- mKate expression	This study
pRN11	Plasmid for sarA P1- mCherry expression	This study
pRN12	Plasmid for sarA P1- mAmetrine expression	This study
pJB38	Temperature sensitive plasmid for chromosomal integration	(5)
pJB38-NWMN29-30	pJB38 plasmid containing the Newman genetic region between genes 29 and 30	This study
pTH100	pJB38-NWMN29-30 + SarA_P1-sGFP-Term	This study
pTH101	pJB38-NWMN29-30 + SarA_P1-DsRed-Term	This study
pTH102	pJB38-NWMN29-30 + SarA_P1-CFP-Term	This study
pTH103	pJB38-NWMN29-30 + SarA_P1-YFP-Term	This study
pRN110	pJB38-NWMN29-30 + SarA_P1-mKate2-Term	This study
pRN111	pJB38-NWMN29-30 + SarA_P1-mCherry-Term	This study
pRN112	pJB28-NWMN29-30+ SarA_P1-mAmetrine-Term	This study

was added to the primer sequence (**Table 3**).

To create the mAmetrine, CFP, YFP, and DsRED expressing vectors, the pCM29 plasmid and PCR amplified reporter DNA were digested with KpnI and EcoRI. To create the mKate2 and mCherry constructs, pCM29 and PCR amplified reporter DNA were digested XmaI-EcoRI. After digestion, pCM29 was dephosphorylated, separated on an agarose gel, and the plasmid backbone was isolated from gel. The digested reporters were ligated into pCM29-backbone. The resulting plasmids were named pTH1 (DsRED), pTH2 (CFP), pTH3 (YFP), pRN10 (mKate2), pRN11 (mCherry), pRN12 (mAmetrine). All plasmids were transformed to competent *E. coli* DC10B and, after initial selection based on expected fluorescence spectrum of the colonies using the ImageQuant LAS4010 (GE Healthcare), checked for correct ligation and absence of mutations by restriction analysis and sequencing.

Creating integration plasmid pJB38-NWMN29-30

By PCR a chromosomal fragment of *S. aureus* Newman DNA (GenBank: AP009351.1) consisting of the region spanning from the nucleotides 40813-43668 containing the 3' part of NWMN_0029 and the 3' part of NWMN_0030 (NWMN29-30) was amplified using primers NWMN_0029-FW_EcoRI and NWMN_0030-RV_KpnI (**Table 3**). The amplified sequence was introduced into plasmid pJB38 by digesting pJB38 and the PCR product with EcoRI and KpnI followed by ligation. The plasmid was transformed in competent *E. coli* DC10B and analysed by restriction analysis and sequencing.

Addition of fluorescent reporters into pJB38-NWMN29-30

The fluorescent reporter expression cassettes present in the replicating shuttle vectors described above were amplified by PCR, and simultaneously a transcription terminator was added. The sequence encoding the transcription terminator was obtained from vector pMUTIN2 (17) and build into the primer pCM29_reporter_RV+term. pJB38-NWMN29-30 was digested with EcoRV (the EcoRV site is present in the Newman chromosomal DNA fragment) and dephosphorylated using shrimp alkaline phosphatase (SAP, Thermo Scientific). The PCR products were phosphorylated with polynucleotide kinase (PNK, NEB) and ligated into the plasmid. The plasmids were transformed in *E. coli* DC10B and initial selection was based on expected fluorescence spectrum of the colonies using the ImageQuant LAS4000. Fluorescent colonies were further analysed by plasmid isolation and restriction

Table 2: properties of fluorescent proteins constructed. All wavelength in nm. Em = emission; Ex= excitation; BP = bandpass filter; LP: longpass filter, * = bp 475-490nm; ** = bp 520-555nm; *** = bp 530-560nm.

Fluorescent protein	Excitation maximum	Emission maximum	LED excitation and filter used in imager	Filters cubes for epifluorescence microscopy	Detection settings in monochromator based plate reader	Detection settings in filter based plate reader: Ex filter/Em filter	Ref.
mAmetrine	423	525	N/A	A ex: BP340-380 dichroic 400 em LP425	425-15/525-15	420-10/520EM**	(7)
CFP (cerulean)	430	475	N/A	CFP ET ex: BP436/20 dichroic 455 em BP480/40	445-15/486-15	420-10/485EX*	(3)
sGFP	488	511	EpiRGB: Blue / 510DF10 GFP	GFP ET ex: BP470/40 dichroic 500 em BP525/50	481-15/524-15	485EX*/520EM**	(8)
YFP (venus)	515	528	EpiRGB: Blue / 510DF10 GFP	YFP ET ex: BP500/20 dichroic 515 em BP535/20	521-15/590-70	485EX*/520EM**	(3)
mCherry	587	610	EpiRGB: Green / 575DF20 Cy3	N21 ex: BP 515-560 dichroic 580 em LP590	578-15/618-15	544EX***/590-bp10	(3)
mCherry	588	633	EpiRGB: Green / 575DF20 Cy3	N21 ex: BP 515-560 dichroic 580 em LP590	588-15/633-15	544EX***/590-bp10	(16)

analysis. Plasmids containing the expression cassette in the desired orientation (expression cassette integrated in the direction of gene NWMN_0029) were checked by sequencing, and were designated pTH100 (sGFP); pTH101 (DsRed); pTH102 (CFP); pTH103 (YFP); pRN110 (mKate); pRN111 (mCherry) and pRN112 (mAmetrine). As an example, a map of plasmid pRN112 is given in **Figure 1B**. The new plasmids described here are available through Addgene, and we provide their properties and Addgene plasmids numbers in **Supplemental Table 2**.

Table 3. Overview of the DNA-templates and primers used in this study

Template	Primer	Orientation	Primer Sequence
pKTE1	DsRED-fw_kpnI++	FW	ATCCCCGGGTACCAGGAGGAAAAACATATG GACAACA
	DsRED-rv	RV	CGCGCCTGAATTCCTACAGGAACAGGTGGT
pJL76	CFP-YFP-fw_kpnI++	FW	ATCCCCGGGTACCTTAGGAGGATGATTATTT ATGAGTAAAG
	CFP-YFP-rv-EcoRI	RV	TGACGAATTCTTACTTGTACAGCTCGTCCAT
pJL49	mCherry-FW-KpnI++_ RBS	FW	ATCCCCGGGTACCTTAGGAGGATGTATACAT ATGGTGAGCAAGGGCGAGGAG
	mCherry+Term-rv_EcoRI	RV	TGACGAATTCGCCTGTCACTTTGCTTGATAT ATGAG
S. pneumoniae MK119 chromosomal DNA	mKate-FW_KpnI++_ RBS_ATG	FW	ATCCCCGGGTACCTTAGGAGGATGATTATTT ATGTCAGAACT-TATCAAGGAAAATATGCAC ATGAA
	mKate_rv-EcoRI	RV	TGACGAATTCTTAACGGTGTCCCAATTTACT AGG
750bp IDT-Gblock	mAmetrine gblock FW	FW	ATGTATCGAGCAAGATGCATCGGATCCCCG GGTACCTTAGGAGGATGATTATTTATGGTTT CAAAAG
	mAmetrine gblock RV	RV	ATAACAATTTCACACAGGAAACAGCTATGA CATGATTACGAATTCTTATTTATATAATTCAT CCATACCTGGTGTAAT
pCM29/other plasmids	pCM_PsarAfw-seq	FW	TTGCATGCCTGCAGGTCGACTCTA
	pCM29-reporter-RV-seq	RV	TTATGCTTCCGGCTCGTATGTTGTGTGG
S. aureus Newman chromosomal DNA	NWMN_0029-FW_EcoRI	FW	TCACGAATTCAGTGGCTACATTCGAACATAT CAA
	NWMN_0030-RV_KpnI	RV	GACTGGTACCGTAAGGGTTCCGGCTTAAT
All replicative reporter plasmids	pCM29_reporter_ RV+term	RV	ATATCGCGAGCTGCATAAAAAACGCCCGGC GGCAACCGAGCGTTCTGAATTAACACACA GGAAACAGCTATGACATGATTA
	pCM_reporterFW-nruI	FW	ATATCGCGATTGCATGCCTGCAGGTCGACTC TA
	NWMN29end_FW	FW	TATGTCACTTATCCTTTTGGAAATG
	NMWN30end_RV	RV	CATAATGTGTTGTAAACATTTTTTTTG
	pJB38-fw_seq	FW	AACCTATAAAAATAGGCGTATCA

Chromosomal integration of fluorescent reporters in *S. aureus*

The fluorescent protein expression cassettes were integrated markerless into the *S. aureus* chromosome between genes NWMN_0029 and NWMN_0030 (or homologs in the other strains, see **Figure 1A** and **Supplemental Table 1**) by homologous recombination as described previously (18) with some adaptations. Shortly, plasmids

pTH100, pTH101; pTH102; pTH103; pTH104, pRN110, pRN111 and pRN112 were introduced into the *S. aureus* strains Newman, MW2 and USA300 by electroporation and plated on TH agar containing chloramphenicol, and incubated overnight at 30°C. Fluorescent colonies were picked to a fresh plate and incubated at 45°C overnight to select for integration of the plasmid into the chromosome. Large colonies were picked (single-recombinants) and re-streaked on TH+Cm plates and grown at 45°C overnight. Single colonies were picked to Todd-Hewitt medium without antibiotics and incubated at 30°C, 250 rpm overnight. Cultures were diluted 1:1000, cultured during 7 hours (during day time), re-diluted, grown for 16 hours (overnight) etc. etc., resulting in 5-7 dilution-culturing cycles, to allow for double cross over events to occur. The final culture was plated on Todd-Hewitt agar containing 100ng/ml anhydrotetracycline and incubated O/N at 37°C to select for double cross over mutants. The anhydrotetracyclin induces the expression of the counter-selection marker present on the pJB38 derivative plasmids (5). Single colonies were plated on Todd-Hewitt plates with (AB+) and without (AB-) antibiotics and grown at 37°C. Colonies that were fluorescent and not able to grow on the AB+ plate (double-recombinants) were analysed by PCR for correct integration.

Measuring growth and fluorescence in a plate reader

Bacterial growth (optical density) and fluorescence were measured. Bacteria were diluted to an OD_{660} of 0.01 and 150µl was transferred to selected wells of a clear 96 well flat bottom polystyrene tissue culture plate (Greiner). The plate was incubated directly in a Fluostar Omega or Clariostar plate reader (BMG labtech) at 37°C with constant double orbital shaking (400 rpm) in between measurements. Both the optical density at 660nm and fluorescence of mAmetrine, CFP, GFP, YFP DsRED, mKate, mCherry were measured every 10 minutes for each well. The signal from 4 identical wells was averaged and corrected for blank wells containing only medium. Settings for the wavelengths measured using the Fluostar and Clariostar plate readers are given in **Table 2**, **Figure 2** and **Supplemental Figure 1**.

mAmetrine excitation and emission spectra measurement

The excitation and emission spectra were recorded using a BMG labtech Clariostar plate reader. 100µl of an overnight culture of *S. aureus* USA300 containing plasmid pRN12 were loaded in the wells of a flat bottom 96 well plate. Excitation was scanned using settings: excitation scan: 339.0 - 484.0; stepwidth 1.0nm, bandwidth 10nm; emission wavelength at 519nm, bandwidth 16nm. Emission was scanned using settings: excitation wavelength 401nm, bandwidth 16nm; Emission scan 447.0 - 624.0nm; stepwidth 1.0nm, bandwidth 8nm. To correct for autofluorescence, a similar overnight culture of wildtype *S. aureus* USA300 was taken along, and the spectra from this scan were used as blank.

Microscopy

Microscopic image acquisition of fluorescent bacteria was performed using a Leica TSC SP5 inverted microscope equipped with a HCX PL APO 40x0.85 CORR CS and HCX PL APO 63x/1.40-0.60 oil immersion (Leica Microsystems, The Netherlands). The microscope was encased in a dark environment chamber with temperature control. The cells and bacteria were monitored in brightfield, using wide field epifluorescence, or in confocal mode setting. Using the correct settings, it was possible to obtain an image where four fluorophores could be separately identified in one sample. The separate channels were combined using Leica LAS AF software.

REFERENCES

1. Lowy, F. D. (1998) *Staphylococcus aureus* infections. N. Engl. J. Med. 339, 520–532
2. Malone, C. L., Boles, B. R., Lauderdale, K. J., Thoendel, M., Kavanaugh, J. S., and Horswill, A. R. (2009) Fluorescent reporters for *Staphylococcus aureus*. J. Microbiol. Methods. 77, 251–260

3. Liese, J., Rooijakkers, S. H. M., van Strijp, J. A. G., Novick, R. P., and Dustin, M. L. (2013) Intravital two-photon microscopy of host-pathogen interactions in a mouse model of *Staphylococcus aureus* skin abscess formation. Cell. Microbiol. 15, 891–909

4. Pereira, P. M., Veiga, H., Jorge, A. M., and Pinho, M. G. (2010) Fluorescent reporters for studies of cellular localization of proteins in *Staphylococcus aureus*. Appl. Environ. Microbiol. 76, 4346–4353

5. Bose, J. L., Fey, P. D., and Bayles, K. W. (2013) Genetic tools to enhance the study of gene function and regulation in *Staphylococcus aureus*. Appl. Environ. Microbiol. 79, 2218–2224

6. Surewaard, B. G. J., de Haas, C. J. C., Vervoort, F., Rigby, K. M., DeLeo, F. R., Otto, M., van Strijp, J. a G., and Nijland, R. (2013) Staphylococcal alpha-phenol soluble modulins contribute to neutrophil lysis after phagocytosis. Cell. Microbiol. 15, 1427–37

7. Ai, H. W., Hazelwood, K. L., Davidson, M. W., and Campbell, R. E. (2008) Fluorescent protein FRET pairs for ratiometric imaging of dual biosensors. Nat. Methods. 5, 401–403

8. Pang, Y. Y., Schwartz, J., Thoendel, M., Ackermann, L. W., Horswill, A. R., and Nauseef, W. M. (2010) Agr-dependent interactions of *Staphylococcus aureus* USA300 with human polymorphonuclear neutrophils. J. Innate Immun. 2, 546–559

9. Slager, J., and Veening, J. W. (2016) Hard-Wired Control of Bacterial Processes by Chromosomal Gene Location. Trends Microbiol. 24, 788–800

10. NCBI (2015) Prokaryotic RefSeq Genome Re-annotation Project. http://www.ncbi.nlm.nih.gov/refseq/about/prokaryotes/reannotation/

11. Tatusova, T., Ciufo, S., Fedorov, B., O'Neill, K., and Tolstoy, I. (2015) RefSeq microbial genomes database: new representation and annotation strategy (vol 42, pg 553, 2014). Nucleic Acids Res. 43, 3872

12. Solovyev, V., and Salamov, A. (2011) Automatic annotation of microbial genomes and metagenomic sequences. In metagenomics and its applications in agriculture, biomedicine and environmental studies (Ed. R.W. Li). Nov. Sci. Publ.

13. Fey, P. D., Endres, J. L., Yajjala, V. K., Widhelm, T. J., Boissy, R. J., Bose, J. L., and Bayles, K. W. (2013) A genetic resource for rapid and comprehensive phenotype screening of nonessential *Staphylococcus aureus* genes. MBio. 10.1128/mBio.00537-12

14. Day, R. N., and Davidson, M. W. (2009) The fluorescent protein palette: tools for cellular imaging. Chem. Soc. Rev. 38, 2887

15. Schenk, S., and Laddaga, R. A. (1992) Improved method for electroporation of *Staphylococcus aureus*. FEMS Microbiol. Lett. 94, 133–138

16. Kjos, M., and Veening, J. W. (2014) Tracking of chromosome dynamics in live *Streptococcus pneumoniae* reveals that transcription promotes chromosome segregation. Mol. Microbiol. 91, 1088–1105

17. Vagner, V., Dervyn, E., and Ehrlich, S. D. (1998) A vector for systematic gene inactivation in *Bacillus subtilis*. Microbiology. 144, 3097–104

18. Bae, T., and Schneewind, O. (2006) Allelic replacement in *Staphylococcus aureus* with inducible counter-selection. Plasmid. 55, 58–63

19. Monk, I. R., Shah, I. M., Xu, M., Tan, M. W., and Foster, T. J. (2012) Transforming the untransformable: Application of direct transformation to manipulate genetically *Staphylococcus aureus* and Staphylococcus epidermidis. MBio. 10.1128/mBio.00277-11

20. Kreiswirth, B. N., Löfdahl, S., Betley, M. J., O'reilly, M., Schlievert, P. M., Bergdoll, M. S., and Novick, R. P. (1983) The toxic shock syndrome exotoxin structural gene is not detectably transmitted by a prophage. Nature. 305, 709–712

21. Dunn, A. K., Millikan, D. S., Adin, D. M., Bose, J. L., and Stabb, E. V. (2006) New rfp- and pES213-derived tools for analyzing symbiotic Vibrio fischeri reveal patterns of infection and lux expression in situ. Appl. Environ. Microbiol. 72, 802–810

SUPPLEMENTAL DATA

Supplemental Table 1: Gene identifiers for commonly used *S. aureus* laboratory strains for 14 genes identical to *S. aureus* Newman gene 29.

***S. aureus* subsp. *aureus* strain:**	**NCBI Reference Sequence + location in chromosome**	**Locus tag NWMN_0029 homolog Re-annotated locus tag (14)**
Newman	NC_009641.1 (40821..42014)	42014) NWMN_0029 NWMN_RS00180
MW2	NC_003923.1 (67771..68964)	MW0058 MW_RS00305
USA300_FPR3757	NC_007793.1 (95560..96753)	SAUSA300_0087 SAUSA300_RS00450
COL	NC_002951.2 (74754..75947)	SACOL0065 SACOL_RS00335
NCTC 8325	NC_007795.1 (40821..42014)	SAOUHSC_00037 Not re-annotated?
N315	NC_002745.2 (93968..95161)	SA0084 SA_RS00575
MSSA476	NC_002953.3 (66478..67671)	SAS0058 SAS_RS00285

Supplemental Table 2: Availability of plasmids and cloning vectors

plasmid	**Genotype/properties**	**Plasmid + sequence available from**
pCM29	Plasmid for sarA P1- sGFP expression	Pang. *et al*. Journal of Innate Immunity 2, 546 (2010)
pTH1	Plasmid for sarA P1 dsRED expression	Addgene, #84451
pTH2	Plasmid for sarA P1 CFP expression	Addgene, #84452
pTH3	Plasmid for sarA P1 YFP expression	Addgene, #84453
pRN10	Plasmid for sarA P1 mKate expression	Addgene, #84454
pRN11	Plasmid for sarA P1 mCherry expression	Addgene, #84455
pRN12	Plasmid for sarA P1 mAmetrine expression	Addgene, #84456
pJB38	Temperature sensitive plasmid for chromosomal integration	BEI, https://www.beiresources.org/ http://app1.unmc.edu/fgx/Static/ pJB38.txt
pJB38-NWMN2930	pJB38 plasmid containing Newman gene region 29-30	Addgene, #84457
pTH100	pJB38-NWMN29-30 + SarA_P1-sGFP-Term	Addgene, #84458
pTH101	pJB38-NWMN29-30 + SarA_P1-DsRed-Term	Addgene, #84459
pTH102	pJB38-NWMN29-30 + SarA_P1-CFP-Term	Addgene, #84460
pTH103	pJB38-NWMN29-30 + SarA_P1-YFP-Term	Addgene, #84461
pRN110	pJB38-NWMN29-30 + SarA_P1-mKate2-Term	Addgene, #84462
pRN111	pJB38-NWMN29-30 + SarA_P1-mCherry-Term	Addgene, # 84463
pRN112	pJB28-NWMN29-30+ SarA_P1-mAmetrine-Term	Addgene, # 84464

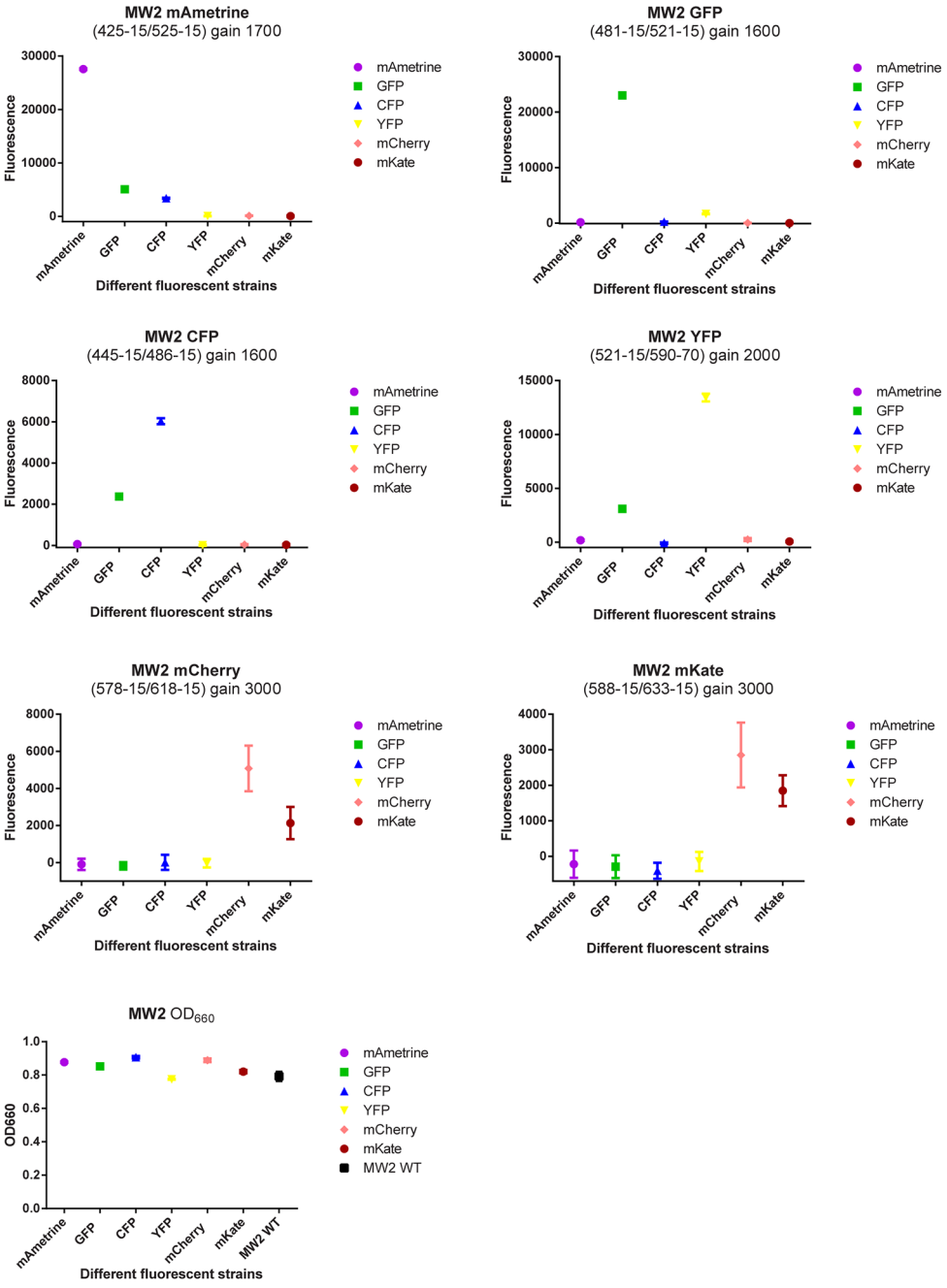

Supplemental Figure 1: Spectral separation and intensity of all fluorescent constructs obtained by integration in the chromosome of *S. aureus* strains MW2. Data points show mean +/- SD is shown of 4 technical replicates.

Chapter 3

Staphylococcus aureus SaeR/S-regulated factors reduce human neutrophil reactive oxygen species production

Fermin E. Guerra[1], Conrad B. Addison[2], Nienke W. M. de Jong[3], Joseph Azzolino[1], Kyler B. Pallister[1], Jos A. G. van Strijp[3], and Jovanka M. Voyich[1]

[1] Department of Microbiology and Immunology, Montana State University, Bozeman, Montana, USA

[2] School of Medicine, University of Washington, Seattle, Washington, USA

[3] Department of Medical Microbiology, University Medical Center Utrecht, Utrecht University, Utrecht, the Netherlands

J Leukoc Biol. 2016 Nov;100(5):1005-1010. DOI:10.1189/jlb.4VMAB0316-100RR

ABSTRACT

Neutrophils are the first line of defense after a pathogen has breached the epithelial barriers, and unimpaired neutrophil functions are essential to clear infections. *Staphylococcus aureus* is a prevalent human pathogen that is able to withstand neutrophil killing, yet the mechanisms used by *S. aureus* to inhibit neutrophil clearance remain incompletely defined. The production of reactive oxygen species (ROS) is a vital neutrophil antimicrobial mechanism. Herein, we test the hypothesis that *S. aureus* uses the SaeR/S two-component gene regulatory system to produce virulence factors that reduce neutrophil ROS production. With the use of ROS probes, the temporal and overall production of neutrophil ROS was assessed during exposure to the clinically relevant *S. aureus* USA300 (strain LAC) and its isogenic mutant LACΔ*saeR/S*. Our results demonstrated that SaeR/S-regulated factors do not inhibit neutrophil superoxide (O_2^-) production. However, subsequent neutrophil ROS production was significantly reduced during exposure to LAC compared with LACΔ*saeR/S*. In addition, neutrophil H_2O_2 production was reduced significantly by SaeR/S-regulated factors by a mechanism independent of catalase. Consequently, the reduction in neutrophil H_2O_2 resulted in decreased production of the highly antimicrobial agent hypochlorous acid/hypochlorite anion (HOCl/$^-$OCl). These findings suggest a new evasion strategy used by *S. aureus* to diminish a vital neutrophil antimicrobial mechanism.

INTRODUCTION

PMNs (leukocytes or neutrophils) are the most abundant WBC in the human body and the first line of defense during bacterial infection (1). Following migration to the site of infection and phagocytosis, neutrophils expose pathogens to an abundance of microbicidal components, including cationic peptides, proteases, and potent ROS (2, 3). Assembly and activation of the NADPH oxidase system result in the production of O_2^- from molecular O_2, followed by dismutation to H_2O_2 and to the formation of the highly bactericidal agent HOCl/$^-$OCl, catalyzed by the enzyme MPO (4–6).The production of neutrophil ROS is highly effective at killing many pathogens, including the Gram-positive pathogen *S. aureus* (7, 8). Microbicidal capacity of ROS against *S. aureus* is exemplified further by the observed increase in susceptibility to infections in individuals with genetic defects in any of the 5 structural components of the NADPH oxidase complex, resulting in chronic granulomatous disease (9, 10). Collectively, neutrophil microbicidal systems are very efficient at killing ingested bacteria and limiting inflammation.

Despite the neutrophil's capacity to contain most bacterial pathogens, its antimicrobial mechanisms are not fully effective in killing *S. aureus*, and bacterial survival following neutrophil phagocytosis has been proposed as a virulence strategy used by this bacterium (11, 12). This is best exemplified by the epidemic of CA-MRSA that began in the late 1990s (13). CA-MRSA can cause uncomplicated skin and soft-tissue infections, as well as invasive, life-threatening illnesses in otherwise healthy individuals (13–15), and its emergence has fostered research investigating the ability of *S. aureus* to survive after neutrophil phagocytosis.

Survival of *S. aureus* following neutrophil phagocytosis is dependent on the concerted effort of multiple virulence factors (11, 12, 16–18). The *S. aureus* SaeR/S two-component system regulates virulence genes essential for evasion of neutrophil killing (12, 19, 20). In brief, the *sae* locus consists of 4 open reading frames (*saePQRS*). *SaeS* and *saeR* code for the two-component module of the SaeR/S system, where SaeS is the histidine kinase, and SaeR is the cognate response regulator. SaeR/S-regulated genes are up-regulated in response to neutrophil-derived components, including human a-defensin-1 and H_2O_2 (19, 21, 22). Studies using isogenic *saeR/S* deletion mutants have shown that neutrophil lysis is reduced, and *S. aureus* has significantly reduced survival following neutrophil phagocytosis in the absence of SaeR/S (11, 12). SaeR also controls the expression of secreted virulence factors, including those that contribute to neutrophil lysis, such as leukocidin G/H (*lukG/H* also known as *lukA/B*), γ hemolysins (*hlgA, B, C*), and Panton- Valentine leukocidin (*lukF/S-PV*) (12, 23). Additionally, SaeR regulated factors influence neutrophil cell fate contributing to pathogen survival (22).

In this study, we investigate further the role of *S. aureus* SaeR/S in modulating neutrophil function by examining its influence on ROS production. Our results demonstrate that SaeR/S-regulated factors decrease neutrophil-derived H_2O_2 and HOCl production by a mechanism independent of catalase activity.

RESULTS AND DISCUSSION

SaeR/S-regulated factors decrease human neutrophil ROS production

Previous studies have shown that human neutrophils fail to kill *S. aureus* completely after phagocytosis, and SaeR/S-regulated factors are at least partially responsible for reduced bactericidal activity (11, 12). However, the mechanisms affected by SaeR/S-regulated factors leading to reduced neutrophil staphylococcal killing have yet to be elucidated fully. To this

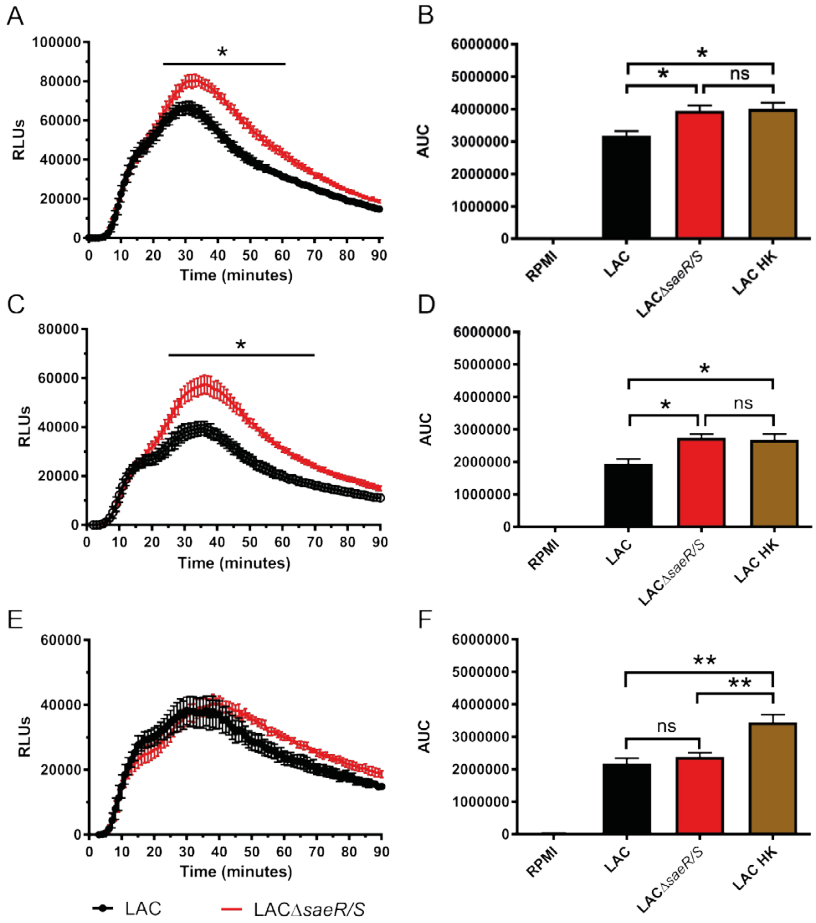

Figure 1: SaeR/S-regulated factors decrease intracellular ROS. Human PMNs were preloaded with luminol, as described in Materials and Methods, and exposed to LAC, LAC*Δ saeR/S*, or RPMI, and chemiluminescence was measured. (**A**) Time-dependent neutrophil intracellular ROS production following exposure to *S. aureus* LAC or LAC*Δ saeR/S*. (**B**) Total relative neutrophil ROS production determined by calculating the area under the curve (AUC) from **A**. (**C**) Time-dependent neutrophil intracellular ROS production following exposure to S. aureus LAC or LAC*Δ saeR/S* in the presence of exogenous SOD. (**D**) Total relative neutrophil ROS production determined by calculating the area under the curve from **C**. (**E**) Timedependent neutrophil intracellular ROS production following exposure to *S. aureus* LAC or LAC*Δ saeR/S* in the presence of exogenous catalase. (**F**) Total relative neutrophil ROS production determined by calculating the area under the curve from E. Data represent 5 separate experiments, using 5 different neutrophil donors; $^{*}P \leq 0.05$, $^{**}P \leq 0.01$, as determined by two-way ANOVA (**A**, **C**, and **E**) and one-way ANOVA (**B**, **D**, and **F**). RLUs, Relative luminescence units.

end, neutrophil ROS production in response to WT *S. aureus* strain LAC and its isogenic Δ*saeR/S* mutant strain (LACΔ*saeR/S*) was analyzed using probes to measure different ROS. First, intracellular neutrophil ROS production was measured with luminol. Whereas there were no significant differences in the time to maximum neutrophil ROS production, total neutrophil ROS production was reduced significantly in response to the *S. aureus* LAC compared with LACΔ*saeR/S* (**Figures 1A and B**). To determine if extracellular ROS contributed to abundance of intracellular ROS, neutrophils were exposed to LAC or LACΔ*saeR/S*, including SOD or catalase. As expected and in congruence with published findings, the addition of exogenous SOD reduced total neutrophil ROS production in response to LAC and LACΔ*saeR/S* (**Figure 1C**) (24, 25). In the presence of SOD, significant differences remained in total neutrophil intracellular ROS production during exposure to LAC and LACΔ*saeR/S* (**Figure 1D).** The addition of exogenous catalase also reduced total neutrophil intracellular ROS production in response to LAC and LACΔ*saeR/S* compared with untreated neutrophils exposed to bacteria (**Figure 1E**). However, neutrophils produced similar amounts of intracellular ROS in response to LAC and LACΔ*saeR/S* in the presence of exogenous catalase (**Figure 1F**). Collectively, these results suggest that *S. aureus* SaeR/S-regulated factors reduce intracellular ROS production. Additionally, neutrophils exposed to LAC HK produced similar amounts of intracellular ROS as those exposed to LACΔ*saeR/S* (**Figures 1B and D**), confirming that reduction of neutrophil ROS by *S. aureus* is an active process that requires a viable organism and SaeR/S. Importantly, the neutralization of extracellular H_2O_2 with exogenous catalase eliminated differences in intracellular neutrophil ROS production in response to LAC and LACΔ*saeR/S*. These results suggest that *S. aureus* SaeR/S-regulated factors reduce the production of neutrophil-derived H_2O_2, leading to a reduction in overall ROS production. Of note, neutrophil propidium iodide uptake was not significantly different between neutrophils exposed to LAC or LACΔ*saeR/S* after 90 min, confirming that differences in ROS production were not a result of differences in neutrophil membrane damage (data not shown). As differences in uptake of LAC and LACΔ*saeR/S* could influence ROS abundance, we assessed neutrophil phagocytosis using fluorescence microscopy. There were no differences in neutrophil ingestion of WT LAC compared with the LACΔ*saeR/S* mutant (**Supplemental Figure 1**), which is in agreement with previous findings (12).

SaeR/S-regulated factors reduce the production of neutrophil-derived H_2O_2

Luminol measures overall intracellular ROS production. As our results showed that extracellular ROS played a significant role in enhancing intracellular neutrophil ROS production (**Figure 1A–F**) and suggested that SaeR/S-regulated factors reduce the production of neutrophil-derived H_2O_2, we used isoluminol and Amplex Red probes to measure specifically O_2^- and H_2O_2, respectively. Cell-impermeable isoluminol was used to measure neutrophil extracellular O_2^- production in response to LAC and LACΔ*saeR/S*. We hypothesized that neutrophil O_2^- production would not be reduced by SaeR/S-regulated factors, as significant differences remained in overall neutrophil intracellular ROS production during exposure to LAC and LACΔ*saeR/S* in the presence of exogenous SOD (**Figure 1C and D**). The neutrophil O_2^- burst

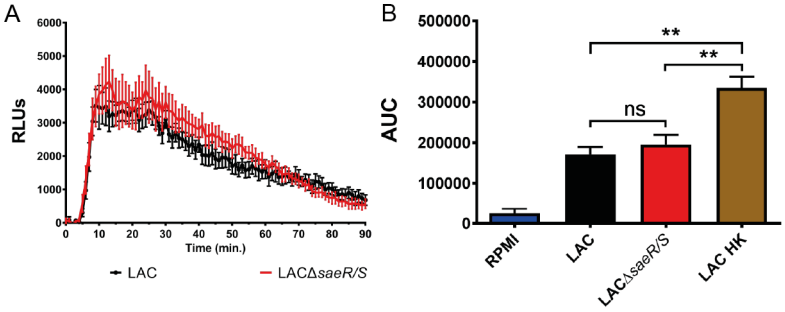

Figure 2: Human neutrophil extracellular O_2^- production following exposure to WT *S. aureus* LAC and LACΔ*saeR/S* using isoluminol. (**A**) Time-dependent neutrophil extracellular O_2^- production following exposure to *S. aureus* LAC or LACΔ*saeR/S*. (**B**) Total relative neutrophil O_2^- production determined by calculating the area under the curve from **A**. Data represent 4 separate experiments, using 4 different neutrophil donors; **P ≤ 0.01, as determined by two-way ANOVA (**A**) and one-way ANOVA (**B**).

occurred within 10 min after recording luminescence (**Figure 2A**). Consistent with results shown in **Figure 1C and D**, there were no significant differences in neutrophil O_2^- production during exposure to LAC or LACΔ*saeR/S* (**Figure 2B**). This suggests that activation and assembly of the NADPH oxidase complex are not affected by SaeR/S-regulated factors. Exposure to LAC

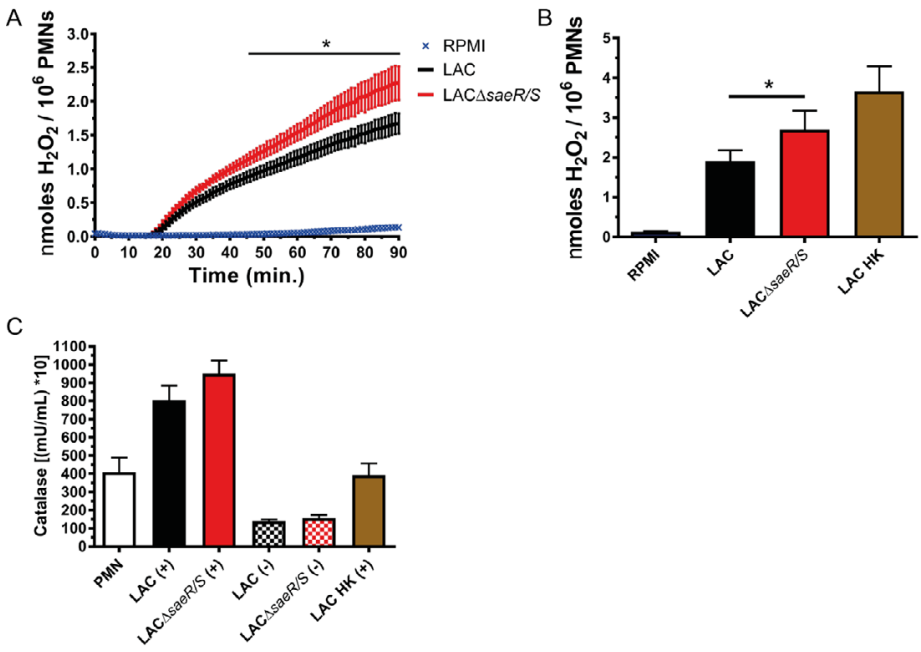

Figure 3: Human neutrophil extracellular H_2O_2 production is significantly reduced by SaeR/S-regulated *S. aureus* factors. (**A**) Time-dependent neutrophil extracellular H_2O_2 production was measured using Amplex Red, following exposure *S. aureus* LAC or LACΔ*saeR/S* or RPMI as a control. (**B**) Neutrophil-derived extracellular H_2O_2 production calculated from an H_2O_2 standard curve. (**C**) Secreted catalase following *S. aureus* exposure to human neutrophils. Bacteria exposed (+) or not exposed (-) to neutrophils. Data represent 4 separate experiments (**A** and **C**) and 5 separate experiments (**B**), with *P ≤ 0.05, as determined by two-way ANOVA (**A**) and paired *t* test (**B**).

HK did result in significantly increased O_2^- production compared with LAC and LAC*ΔsaeR/S*. This is expected, as *S. aureus* produces SOD to neutralize O_2^- via sodA and sodM, but these genes are not regulated by SaeR/S (12, 23, 26, 27).

As the measurement of neutrophil intracellular ROS with luminol in the presence of catalase suggested that SaeR/ S-regulated factors reduce production of extracellular H_2O_2 (**Figures 1C and D**), we used the H_2O_2-specific probe Amplex Red to measure neutrophil extracellular H_2O_2 production in response to *S. aureus* LAC and LAC*ΔsaeR/S*. Detectable neutrophil-derived H_2O_2 was observed within 20 min of exposure to LAC and LAC*ΔsaeR/S* (**Figure 3A**). Significant differences in extracellular H_2O_2 production between neutrophils exposed to LAC and LAC*ΔsaeR/S* were observed, starting at 43 min. In addition, there were significant increases in molar amounts of H_2O_2 produced by neutrophils in response to LAC*ΔsaeR/S* versus LAC at the end of the 90 min assay (**Figure 3B**). Differences in extracellular H_2O_2 production by neutrophils confirmed results showing overall reduction in ROS—and no significant differences between neutrophils exposed to LAC and LAC*ΔsaeR/S*—when the cell-impermeable catalase was present (**Figures 1E and F**). Importantly, there were no differences in the secreted catalase that could degrade extracellular H_2O_2 (**Figure 3C**), confirming that SaeR/S does not regulate catalase following neutrophil phagocytosis.

SaeR/S-regulated factors reduce the production of neutrophil-derived HOCl

HOCl is present in neutrophil phagosomes and is highly bactericidal. H_2O_2 is a precursor to the production of MPO catalysed HOCl. Therefore, we measured intracellular HOCl production using the cell-permeable R19-S probe to assess how SaeR/S-regulated factors affect HOCl production (**Figure 4A**). Consistent with our results showing that SaeR/S reduced H_2O_2 production, SaeR/S-regulated factors significantly decreased neutrophil HOCl production (**Figures 4B and C**). Production of neutrophil H_2O_2 and HOCl was detected at ~ 20 min, with the maximum H_2O_2 burst occurring earlier than the HOCl burst (**Supplemental Figure 2**).

The formation of H_2O_2 from O_2^- can occur spontaneously or is catalyzed by SOD or MPO (28, 29). Based on our observations, we propose that unidentified SaeR/S-regulated factor(s) interfere with the enzymatic reactions catalyzed by MPO to produce H_2O_2 and HOCl. Inasmuch as there are no differences in secreted catalase between neutrophils exposed to *S. aureus* LAC and LAC*ΔsaeR/S* (**Figure 3C**), we propose that the significant decrease in H_2O_2 produced by neutrophils exposed to LAC compared with LAC*ΔsaeR/S* is a result of SaeR/S-regulated factors inhibiting the SOD activity of MPO to produce H_2O_2. In addition, SaeR/S-regulated factors may interfere with the chlorination activity of MPO, resulting in decreased production of HOCl. Ongoing studies are determining if decreased HOCl production is a direct result of lower H_2O_2 production or if SaeR/S-regulated factors directly interfere with both the dismutase and chlorination activity of MPO.

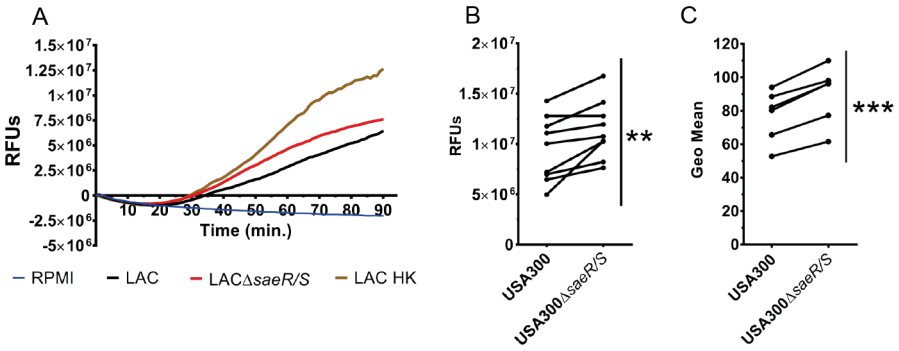

Figure 4: Human neutrophil intracellular hypochlorite production is reduced significantly by SaeR/S-regulated *S. aureus* factors. HOCl production was measured in human neutrophils using R19-S, following exposure to WT *S. aureus* LAC or LAC*ΔsaeR/S*. (**A**) Representative plot of time-dependent neutrophil intracellular HOCl production following exposure to *S. aureus* LAC or LAC*ΔsaeR/S* or LAC HK or RPMI as a control. (**B**) Relative neutrophil-derived HOCl production at the end of the 90 min assay from **A**. (**C**) Relative neutrophil-derived intracellular HOCl measured by flow cytometry. Data represent 9 separate experiments (**B**) and 6 separate experiments (**C**); **P ≤ 0.01, ***P ≤ 0.001, as determined by paired *t* test (**B** and **C**). RFUs, Relative fluorescence units.

WT *S. aureus* LAC and LAC*ΔsaeR/S* are equally susceptible to reagent HOCl

S. aureus SaeR/S-regulated factors significantly decreased neutrophil-derived HOCl production in response to WT LAC versus LAC*ΔsaeR/S* (**Figure 4**). To determine if the WT and mutant were differentially susceptible to HOCl, we exposed LAC and LAC*ΔsaeR/S* to varied concentrations of HOCl. As shown in **Figure 5**, LAC and LAC*ΔsaeR/S* were equally susceptible to HOCl exposure. HOCl concentrations below 5 μM did not kill *S. aureus*. However, there was a precipitous decrease in *S. aureus* survival following exposure between 5 and 15 μM HOCl. These data are in agreement with previously published findings (30). Future studies will investigate the physiologically relevant question as to whether reduction in ROS makes WT *S. aureus* more resistant to neutrophil killing reflective of clinical syndromes, demonstrating the importance

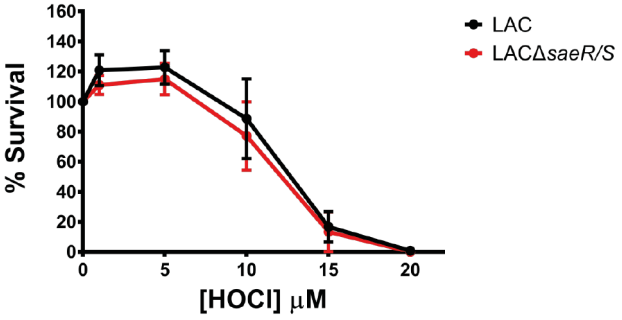

Figure 5: *S. aureus* LAC and LAC*ΔsaeR/S* are equally susceptible to killing by HOCl. Bacteria (1 x 10^7) were exposed to different concentrations of HOCl for 30 min at 37°C. Subsequently, bacteria were serially diluted and plated on trypticase soy agar plates, and CFUs were enumerated following overnight incubation at 37°C. Data represent 5 separate experiments.

of ROS in controlling *S. aureus* (9, 10). It is possible that a SaeR/S-mediated reduction in ROS makes the ROS amount insufficient to kill *S. aureus*, as *in vitro* studies have demonstrated a fine line between ROS amounts that are effective versus amounts that the pathogen can tolerate (**Figure 5** and ref. (19)).

The importance of detoxifying ROS is demonstrated by the many mechanisms used by *S. aureus* that include scavenging and neutralizing ROS, such as O_2^- and H_2O_2, with SODs (SodA and SodM) and catalase (KatA), respectively (31, 32). In addition, the iron-regulated surface-determinant proteins IsdA and IsdB have been implicated in increasing *S. aureus* resistance to killing by H_2O_2 (22), as well as methionine sulfoxide reductases to reduce oxidized methionine residues following oxidative stress that increase *S. aureus* resistance to ROS (33). Unlike previously described mechanisms to neutralize ROS, our data suggest that *S. aureus* can directly inhibit H_2O_2 and HOCl production, resulting in increased *S. aureus* survival. Future studies will focus on identifying specific SaeR/S-regulated factors that inhibit neutrophil ROS production.

AUTHORSHIP

F.E.G. contributed to project design and experimental procedures, analyzed data, provided the figure presentation, and wrote the manuscript. C.B.A., J.A., N.W.M.d.J., K.B.P., and J.v.S. contributed to project design and experimental procedures. J.M.V. provided oversight and contributed to project design, data analysis, figure presentation, and manuscript writing.

ACKNOWLEDGMENTS

This work was supported by the U.S. National Institutes of Health (Grants NIH-R01A1090046, NIH-PAR98-072, and NIH-RR020185 for a fellowship award to F.E.G.), as well as funds from the Montana University System Research Initiative (51040-MUSRI2015-03) and Montana State University Agriculture Experiment Station and an equipment grant from Murdoch Charitable Trust.

DISCLOSURES

The authors have declared that there are no conflicts of interest.

MATERIALS & METHODS

Bacterial strains and culture

WT *S. aureus* pulsed-field gel electrophoresis-type USA300 (strain LAC) (34) and its previously generated isogenic *saeR/S* mutant strain (LACΔ*saeR/S*) (23) were grown in tryptic soy broth containing 0.5% glucose and harvested at midexponential growth, as described previously (11, 22, 23).

Neutrophil and ROS assays

Human neutrophils were isolated from heparinized venous blood of healthy volunteer donors in accordance with a protocol approved by the Institutional Review Board for Human Subjects at Montana State University. Human neutrophils were isolated as described previously (11, 12). For all ROS assays, 1 x 10^6 neutrophils (loaded with various probes, described below) were exposed to 1 x 10^7 bacteria (10:1 bacteria:PMN ratio) in 96-well serum-coated plates in duplicate. Neutrophils were also exposed to LAC HK (5 min at 99°C), 500 ng/ml PMA, or RPMI, and phagocytosis was synchronized (11). All measurements were done using a SpectraMax Paradigm Multi-Mode Microplate Reader (Molecular Devices, Sunnyvale, CA, USA).

Luminol. Neutrophil-derived ROS detection by the oxidation of cellpermeable luminol, resulting in chemiluminescence, was measured as described previously (35). Neutrophils were stained with 100 mM luminol for 15 min in the dark at 4°C. Chemiluminescence was measured in 1 min intervals. The final concentrations of SOD and catalase were 50 and 2000 U/ml, respectively.

Isoluminol. Neutrophil-derived O_2^- production by the oxidation of cellimpermeable isoluminol, resulting in chemiluminescence, was measured as described previously (35). Neutrophils were stained with 100 mM isoluminol for 15 min in the dark at 4°C. Chemiluminescence was measured in 1 min intervals.

Amplex Red. Neutrophil-derived extracellular H_2O_2 production was measured using the Amplex Red Hydrogen Peroxide/Peroxidase Kit (Thermo Fisher Scientific, Waltham, MA, USA), following the manufacturer's instructions. Amplex Red oxidation was measured in 1 min intervals with 535/595 nm excitation/emission wavelengths.

Secreted catalase. The Amplex Red Catalase Assay Kit (Thermo Fisher Scientific) was used following the manufacturer's suggested protocol. Supernatants from PMN and/or bacterial incubations were collected following 90 min exposure at 37°C and sterile filtered with 0.22 mm syringe filters.

R19-S. Neutrophil-derived HOCl production was measured using R19-S (FutureChem, Seoul, South Korea) (36, 37). Oxidation of R19-S was measured in 1 min intervals with 485/535 nm excitation/emission wavelengths. Alternatively, neutrophil intracellular HOCl production at 90 min was measured by flow cytometry with a BD FACSCalibur (BD Biosciences, San Jose, CA, USA) using 488/530 nm emission/excitation wavelengths.

Neutrophil phagocytosis assay

Phagocytosis of *S. aureus* by human neutrophils was determined with fluorescence microscopy, as described previously (11). FITC-labeled bacteria were added (10:1 bacteria:neutrophil ratio), and phagocytosis was synchronized as above. To counterstain uningested bacteria, samples were stained with anti-FITC conjugated to Alexa Fluor 594 (Thermo Fisher Scientific), and mounted coverslips were evaluated using fluorescence microscopy. The number of *S. aureus* bound and/or ingested was evaluated in 25 or 50 neutrophils per experiment from separate fields of view, and percent phagocytosis was calculated as (number of ingested bacteria per cell/total number of PMN-associated bacteria per cell, bound or ingested) x 100.

HOCl killing

A mixture of HOCl/$^-$OCl was generated by mixing 10 ml commercially available Clorox, 5 ml DPBS, and 160 ml 36.5–38.0% hydrochloric acid. After overnight incubation in the dark, the concentration of HOCl/$^-$OCl was calculated using Beer's Law (38). The average pH of the solution was 7.51 6 0.09, similar to the acid dissociation

constant for HOCl/$^-$OCl (pKa = 7.44) (38, 39). Bacteria (1 x 10^7), resuspended in DPBS, were mixed with HOCl/$^-$OCl, diluted in DPBS to desired working concentrations and incubated at 37°C for 30 min. Bacteria were enumerated following overnight incubation at 37°C. Bacterial survival was calculated relative to bacterial concentration following exposure to DPBS only. Statistical procedures Statistical analyses were performed using GraphPad Prism version 6.0a (GraphPad Software, La Jolla, CA, USA) with t tests and ANOVA as indicated, and error bars represent the SEM.

REFERENCES

1. Amulic, B., Cazalet, C., Hayes, G. L., Metzler, K. D., and Zychlinsky, A. (2012) Neutrophil function: from mechanisms to disease. Annu. Rev. Immunol. 30, 459–89
2. Nordenfelt, P., and Tapper, H. (2011) Phagosome dynamics during phagocytosis by neutrophils. J. Leukoc. Biol. 90, 271–84
3. Hurst, J. K. (2012) What really happens in the neutrophil phagosome? Free Radic. Biol. Med. 53, 508–520
4. DeLeo, F. R., and Quinn, M. T. (1996) Assembly of the phagocyte NADPH oxidase: molecular interaction of oxidase proteins. J. Leukoc. Biol. 60, 677–91
5. DeLeo, F. R., Allen, L. A., Apicella, M., and Nauseef, W. M. (1999) NADPH oxidase activation and assembly during phagocytosis. J. Immunol. 163, 6732–40
6. Winterbourn, C. C., and Kettle, A. J. (2013) Redox Reactions and Microbial Killing in the Neutrophil Phagosome. Antioxid. Redox Signal. 18, 642–660
7. Hampton, M. B., and Winterbourn, C. C. (1995) Modification of neutrophil oxidant production with diphenyleneiodonium and its effect on bacterial killing. Free Radic. Biol. Med. 18, 633–639
8. Hampton, M. B., Kettle, A. J., and Winterbourn, C. C. (1996) Involvement of superoxide and myeloperoxidase in oxygen-dependent killing of *Staphylococcus aureus* by neutrophils. Infect. Immun. 64, 3512–3517
9. Lekstrom-Himes, J. A., and Gallin, J. I. (2000) Immunodeficiency Diseases Caused by Defects in Phagocytes. N. Engl. J. Med. 343, 1703–1714
10. Roos, D., and de Boer, M. (2014) Molecular diagnosis of chronic granulomatous disease. Clin. Exp. Immunol. 175, 139–149
11. Voyich, J. M., Braughton, K. R., Sturdevant, D. E., Whitney, A. R., Saïd-Salim, B., Porcella, S. F., Long, R. D., Dorward, D. W., Gardner, D. J., Kreiswirth, B. N., Musser, J. M., and DeLeo, F. R. (2005) Insights into mechanisms used by *Staphylococcus aureus* to avoid destruction by human neutrophils. J. Immunol. 175, 3907–3919
12. Voyich, J. M., Vuong, C., DeWald, M., Nygaard, T. K., Kocianova, S., Griffith, S., Jones, J., Iverson, C., Sturdevant, D. E., Braughton, K. R., Whitney, A. R., Otto, M., and DeLeo, F. R. (2009) The SaeR/S gene regulatory system is essential for innate immune evasion by *Staphylococcus aureus*. J. Infect. Dis. 199, 1698–706
13. DeLeo, F. R., and Chambers, H. F. (2009) Reemergence of antibiotic-resistant *Staphylococcus aureus* in the genomics era. J. Clin. Invest. 119, 2464–2474
14. Miller, L. G., Perdreau-Remington, F., Rieg, G., Mehdi, S., Perlroth, J., Bayer, A. S., Tang, A. W., Phung, T. O., and Spellberg, B. (2005) Necrotizing fasciitis caused by community-associated methicillin-resistant *Staphylococcus aureus* in Los Angeles. N. Engl. J. Med. 352, 1445–53
15. Kreisel, K. M., Stine, O. C., Johnson, J. K., Perencevich, E. N., Shardell, M. D., Lesse, A. J., Gordin, F. M., Climo, M. W., and Roghmann, M. C. (2011) USA300 methicillin-resistant *Staphylococcus aureus* bacteremia and the risk of severe sepsis: Is USA300 methicillin-resistant *Staphylococcus aureus* associated with more severe infections? Diagn. Microbiol. Infect. Dis. 70, 285–290
16. Genestier, A. L., Michallet, M. C., Prévost, G., Bellot, G., Chalabreysse, L., Peyrol, S., Thivolet, F., Etienne, J., Lina, G., Vallette, F. M., Vandenesch, F., and Genestier, L. (2005) *Staphylococcus aureus* Panton-Valentine leukocidin directly targets mitochondria and induces Bax-independent apoptosis of human neutrophils.

J. Clin. Invest. 115, 3117–3127

17. Wardenburg, J. B., Bae, T., Otto, M., DeLeo, F. R., and Schneewind, O. (2007) Poring over pores: α-hemolysin and Panton-Valentine leukocidin in *Staphylococcus aureus* pneumonia. Nat. Med. 13, 1405–1406
18. Wang, R., Braughton, K. R., Kretschmer, D., Bach, T.-H. L., Queck, S. Y., Li, M., Kennedy, A. D., Dorward, D. W., Klebanoff, S. J., Peschel, A., DeLeo, F. R., and Otto, M. (2007) Identification of novel cytolytic peptides as key virulence determinants for community-associated MRSA. Nat. Med. 13, 1510–1514
19. Flack, C. E., Zurek, O. W., Meishery, D. D., Pallister, K. B., Malone, C. L., Horswill, A. R., and Voyich, J. M. (2014) Differential regulation of staphylococcal virulence by the sensor kinase SaeS in response to neutrophil-derived stimuli. Proc. Natl. Acad. Sci. 111, E2037–E2045
20. Zurek, O. W., Pallister, K. B., and Voyich, J. M. (2015) *Staphylococcus aureus* Inhibits Neutrophil-derived IL-8 to Promote Cell Death. J. Infect. Dis. 212, 934–938
21. Palazzolo-Ballance, a. M., Reniere, M. L., Braughton, K. R., Sturdevant, D. E., Otto, M., Kreiswirth, B. N., Skaar, E. P., and DeLeo, F. R. (2007) Neutrophil Microbicides Induce a Pathogen Survival Response in Community-Associated Methicillin-Resistant *Staphylococcus aureus*. J. Immunol. 180, 500–509
22. Zurek, O. W., Nygaard, T. K., Watkins, R. L., Pallister, K. B., Torres, V. J., Horswill, A. R., and Voyich, J. M. (2014) The role of innate immunity in promoting SaeR/S-mediated virulence in *staphylococcus aureus*. J. Innate Immun. 6, 21–30
23. Nygaard, T. K., Pallister, K. B., Ruzevich, P., Griffith, S., Vuong, C., and Voyich, J. M. (2010) SaeR binds a consensus sequence within virulence gene promoters to advance USA300 pathogenesis. J Infect Dis. 201, 241–254
24. Ohno, Y., and Gallin, J. I. (1985) Diffusion of extracellular hydrogen peroxide into intracellular compartments of human neutrophils: Studies utilizing the inactivation of myeloperoxidase by hydrogen peroxide and azide. J. Biol. Chem. 260, 8438–8446
25. Gerber, C. E., Bruchelt, G., Falk, U. B., Kimpfler, A., Hauschild, O., Kuçi, S., Bächi, T., Niethammer, D., and Schubert, R. (2001) Reconstitution of bactericidal activity in chronic granulomatous disease cells by glucose-oxidase-containing liposomes. Blood. 98, 3097–3105
26. Rogasch, K., Rühmling, V., Pané-Farré, J., Höper, D., Weinberg, C., Fuchs, S., Schmudde, M., Bröker, B. M., Wolz, C., Hecker, M., and Engelmann, S. (2006) Influence of the two-component system SaeRS on global gene expression in two different *Staphylococcus aureus* strains. J. Bacteriol. 188, 7742–58
27. Sun, F., Li, C., Jeong, D., Sohn, C., He, C., and Bae, T. (2010) In the *Staphylococcus aureus* two-component system sae, the response regulator SaeR binds to a direct repeat sequence and DNA binding requires phosphorylation by the sensor kinase SaeS. J. Bacteriol. 192, 2111–27
28. McCord, J. M., and Fridovich, I. (1969) Superoxide dismutase. An enzymic function for erythrocuprein (hemocuprein). J. Biol. Chem. 244, 6049–6055
29. Kettle, A. J., Anderson, R. F., Hampton, M. B., and Winterbourn, C. C. (2007) Reactions of superoxide with myeloperoxidase. Biochemistry. 46, 4888–4897
30. Chapman, A. L. P., Hampton, M. B., Senthilmohan, R., Winterbourn, C. C., and Kettle, A. J. (2002) Chlorination of bacterial and neutrophil proteins during phagocytosis and killing of *Staphylococcus aureus*. J. Biol. Chem. 277, 9757–9762
31. Horsburgh, M. J., Clements, M. O., Crossley, H., Ingham, E., and Foster, S. J. (2001) PerR controls oxidative stress resistance and iron storage proteins and is required for virulence in *Staphylococcus aureus*. Infect. Immun. 69, 3744–3754
32. Karavolos, M. H. (2003) Role and regulation of the superoxide dismutases of *Staphylococcus aureus*. Microbiology. 149, 2749–2758
33. Singh, V. K., Vaish, M., Johansson, T. R., Baum, K. R., Ring, R. P., Singh, S., Shukla, S. K., and Moskovitz, J. (2015) Significance of four methionine sulfoxide reductases in *Staphylococcus aureus*. PLoS One. 10.1371/journal.pone.0117594
34. Diep, B. A., Gill, S. R., Chang, R. F., Phan, T. H. Van, Chen, J. H., Davidson, M. G., Lin, F., Lin, J., Carleton, H. A., Mongodin, E. F., Sensabaugh, G. F., and Perdreau-Remington, F. (2006) Complete genome sequence of USA300, an epidemic clone of community-acquired meticillin-resistant *Staphylococcus aureus*. Lancet. 367, 731–739

35. Bylund, J., Björnsdottir, H., Sundqvist, M., Karlsson, A., and Dahlgren, C. (2014) Measurement of respiratory burst products, released or retained, during activation of professional phagocytes. Methods Mol. Biol. 1124, 321–338

36. Chen, X., Lee, K.-A., Ha, E.-M., Lee, K. M., Seo, Y. Y., Choi, H. K., Kim, H. N., Kim, M. J., Cho, C.-S., Lee, S. Y., Lee, W.-J., and Yoon, J. (2011) A specific and sensitive method for detection of hypochlorous acid for the imaging of microbe-induced HOCl production. Chem. Commun. 47, 4373

37. Ng, H. P., Zhou, Y., Song, K., Hodges, C. A., Drumm, M. L., and Wang, G. (2014) Neutrophil-mediated phagocytic host defense defect in myeloid Cftr-inactivated mice. PLoS One. 10.1371/journal.pone.0106813

38. Morris, J. C. (1966) The Acid Ionization Constant of HOCl from 5 to 35°. J. Phys. Chem. 70, 3798–3805

39. Kettle, A. J., Albrett, A. M., Chapman, A. L., Dickerhof, N., Forbes, L. V, Khalilova, I., and Turner, R. (2014) Measuring chlorine bleach in biology and medicine. Biochim. Biophys. Acta. 1840, 781–93

SUPPLEMENTAL DATA

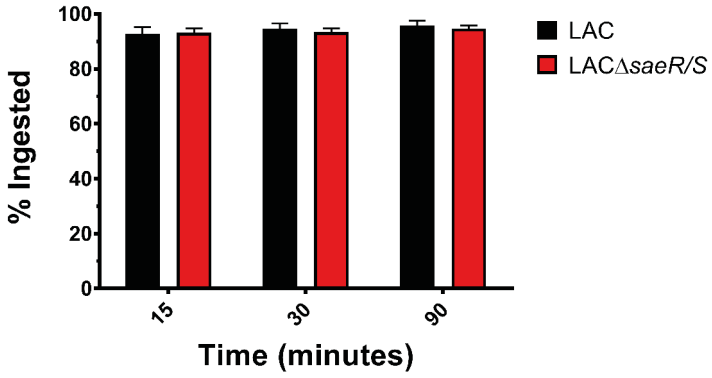

Supplemental Figure 1: Phagocytosis by human neutrophils is not influenced by SaeR/S-regulated factors. Percentage of LAC and LAC*Δ saeR/S* strains ingested by human PMNs was calculated using the equation: [(number of ingested bacteria per cell / total number of PMN-associated bacteria, bound or ingested)*100]. Results are from 3 separate donors.

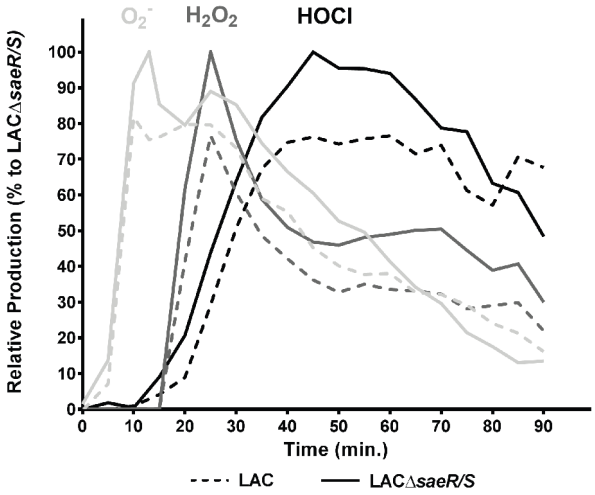

Supplemental Figure 2: ROS production by *S. aureus* LAC or LAC*Δsae*R/S during exposure to human neutrophils. Superoxide (O_2^-), hydrogen peroxide (H_2O_2) and hypohclorous acid (HOCl) production by human neutrophils was measured isoluminol, Amplex® Red, and R19-S, respectively. Results are shown as the average change over time in 5-minute intervals for each ROS measured and normalized to neutrophils exposed to LAC*Δ saeR/S*.

Chapter 4

Immune evasion by a staphylococcal inhibitor of myeloperoxidase

Nienke W. M. de Jong[1], Kasra X. Ramyar[2], Fermin E. Guerra[3], Reindert Nijland[1,4], Cindy Fevre[1], Jovanka M. Voyich[3], Alex J. McCarthy[1], Brandon L. Garcia[2], Kok P. M. van Kessel[1], Jos A. G. van Strijp[1], Brian V. Geisbrecht[2,#] and Pieter-Jan A. Haas[1,#]

[1] Department of Medical Microbiology, University Medical Center Utrecht, Utrecht University, Utrecht, the Netherlands

[2] Department of Biochemistry and Molecular Biophysics, Kansas State University, Manhattan, KS 66506

[3] Department of Microbiology and Immunology, Montana State University, Bozeman, MT 59717

[4] Laboratory of Phytopathology, Wageningen University, 6708 PB Wageningen, The Netherlands

[#] shared supervision

Proc Natl Acad Sci U S A. 2017 Aug 29;114(35):9439-9444. doi: 10.1073/pnas.1707032114

ABSTRACT

Staphylococcus aureus is highly adapted to its host and has evolved many strategies to resist opsonization and phagocytosis. Even after uptake by neutrophils, *S. aureus* shows resistance to killing, which suggests the presence of phagosomal immune evasion molecules. With the aid of secretome phage display, we identified a highly conserved protein that specifically binds and inhibits human myeloperoxidase (MPO), a major player in the oxidative defence of neutrophils. We have named this protein 'Staphylococcal Peroxidase INhibitor (SPIN)'. To gain insight into inhibition of MPO by SPIN, we solved the co-crystal structure of SPIN bound to a recombinant form of human MPO at 2.4 Å resolution. This structure reveals that SPIN acts as a molecular plug that prevents $H2_2O_2$ substrate access to the MPO active site. In subsequent experiments, we observed that SPIN expression increases inside the neutrophil phagosome, where MPO is located, when compared to outside the neutrophil. Moreover, bacteria with a deleted gene encoding SPIN showed decreased survival compared to WT bacteria after phagocytosis by neutrophils. Together, our results demonstrate that *S. aureus* secretes a unique proteinaceous MPO inhibitor to enhance survival by interfering with MPO-mediated killing.

SIGNIFICANCE

Staphylococcus aureus secretes numerous proteins to evade our innate immune system, for example to evade opsonization and phagocytosis by neutrophils. Here we describe the discovery that *S. aureus* has evolved a protein (SPIN) that specifically binds and inhibits the human myeloperoxidase enzyme (MPO). MPO is located inside the granules of neutrophils and is important in the oxidative burst against pathogens. We identify the molecular mode of action of SPIN inhibiting MPO, illustrate this with the co-crystal structure, and show that SPIN is important for bacterial survival by MPO-dependent killing. Our study shows that *S. aureus* fights back after it is engulfed by neutrophils, which will help our understanding of the complex nature of *S. aureus* infections.

INTRODUCTION

The bacterium *Staphylococcus aureus* is a rising threat to human health. Thirty percent of healthy adults are colonized with this bacterium, resulting in an increased risk for infections ranging from abscesses to endocarditis (1). Neutrophils play a prominent role in fighting staphylococcal infections (2), as their intracellular granules contain numerous antimicrobial proteins and components for generating bactericidal Reactive Oxygen Species (ROS). After *S. aureus* is phagocytosed, neutrophils' azurophilic granules fuse with the phagosome and release their contents (3). The five essential components of NADPH oxidase then assemble in the phagosomal membrane and become active (4). Active NADPH oxidase produces superoxide from O2, which converts to hydrogen peroxide (H_2O_2) either spontaneously or by the action of superoxide dismutase (SOD). Myeloperoxidase (MPO) catalyses the reaction of H_2O_2 with chloride to generate hypochlorous acid (HOCl), which is a major effector in the oxidative defence of neutrophils (5). MPO also forms radicals by oxidizing a wide range of substrates, such as tyrosine, nitrite, and phenols (6).

While the pathogen is taken up rapidly by phagocytes, mainly neutrophils and macrophages, not all bacteria are killed and these phagocytes can therefore act as so called 'Trojan Horses' and distribute a pathogen away from the initial site of infection (7). To counteract the manifold antimicrobial defences of neutrophils, *S. aureus* has evolved specific evasion molecules to inhibit intracellular killing (8). For example, the golden pigment staphyloxanthin serves as an antioxidant and is known to protect *S. aureus* against ROS (9). Catalase is yet another enzyme important for resistance against oxidative stress. This enzyme converts H_2O_2 into H_2O and O_2 and is considered to be a virulence factor. *S. aureus* also expresses an alkyl hydroperoxide reductase (ahpC) that contributes catalase-like activity. Whereas AhpC is believed to detoxify endogenously produced hydrogen peroxide, catalase appears more important for protection against external oxidative stress (10). Finally, *S. aureus* produces specific evasion proteins that disrupt phagosomal membranes, such as phenol-soluble modulins, hemolysin-alpha, and leukocidin AB (8). Together, these evasion molecules are believed to contribute to bacterial survival following phagocytosis.

Proteomic studies have shown that between 100-200 proteins are secreted from *S. aureus*, many with an unknown function(s) (11). Consequently, known evasion molecules are likely to represent only a small fraction of the total repertoire. Therefore we recently developed a phage display approach (12) as a non-biased high throughput method to screen for new potential staphylococcal immune evasion molecules. Since *S. aureus* can survive within the phagosome, but also because recent work suggests that SaeR/S regulated factors exist that inhibit neutrophil ROS production (13), we screened this staphylococcal phage library against several intracellular proteins of neutrophils.

Through this approach, we identified the hypothetical protein NWMN_0402 as a novel

evasion factor. We have named this protein Staphylococcal Peroxidase INhibitor (SPIN), as it is able to bind and inhibit MPO. Here, we characterize SPIN and detail the structural basis for MPO inhibition by SPIN. We further show that the production of SPIN is upregulated after phagocytosis of *S. aureus* by human neutrophils and that SPIN protects *S. aureus* from MPO-mediated killing.

RESULTS

Identification of SPIN

We designed a secretome phage display strategy to screen for unidentified evasion molecules that target neutrophil granule proteins as described earlier (12, 14). Isolated DNA of *S. aureus* strain Newman was randomly sheared and the resulting fragments where cloned in the pDJ01 phagemid vector for specific display of secretome proteins. Phage were produced upon addition of the VCSM13 helper phage. Screening was performed against total degranulate from TNF-primed, fMLF-stimulated neutrophils. After four rounds of selection, 48 clones were sequenced. The major hit was enriched in 36 clones and corresponded to the hypothetical open reading frame NWMN_0402 (accession number BAF66674 strain Newman) (**Supplemental Figure 1A**). We named this protein Staphylococcal Peroxidase INhibitor (SPIN) due to its ability to inhibit MPO, as described in *SPIN binds and inhibits MPO*.

The gene encoding SPIN, denoted as *spn*, is located on genomic island α, also known as νSaα. This island is found in all *S. aureus* genomes and contains a cluster of genes encoding known evasion molecules, most notably the staphylococcal superantigen-like (ssl) proteins (8). *spn* is located downstream of the ssl cluster with the coding sequence orientated in the reverse direction (**Supplemental Figure 1B**). The genes in νSaα are often variable and each *S. aureus* lineage has a unique combination of gene variant (15). However, *spn* is located in the conserved region of νSaα (**Supplemental Figure 1C**). It was present in 83 of 84 clinical strains isolated from ICU patients as well as in all completed *S. aureus* genomes included in our analysis (15).

The amino acid sequence of SPIN is highly conserved amongst almost all *S. aureus* clonal lineages, both human and animal associated strains, with 92.4% of residues conserved (**Supplemental Figure 1D**). Only two strains of clonal complex (CC)5 lineage, Mu3 and Mu50, encoded a truncated version of SPIN, lacking 35 amino acids at the C-terminus. To determine if SPIN is produced *in vivo* during colonization or infection of the human host, sera from 20 healthy individuals were tested for the presence of antibodies against SPIN. These sera showed substantial amounts of antibody, and elicited values comparable to CHIPS (**Supplemental Figure 1E**). CHIPS is a known *S. aureus* immune evasion molecule (16) that yielded an MFI value in a previous multiplex assay indicative of high IgG levels whereas the superantigens (e.g. SEI) did not (17). As SPIN is highly conserved in *S. aureus* strains, has a high prevalence and is

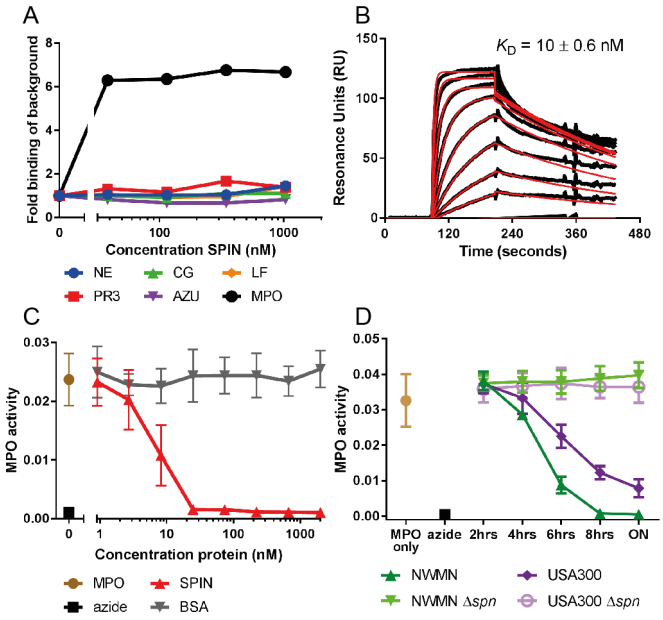

Figure 1: SPIN binds and inhibits MPO. (**A**) An ELISA-type binding assay of C-His SPIN to all candidate proteins. Abbreviations: NE, neutrophil elastase; PR3, proteinase 3; CG, Cathepsin G; AZU, azurocidin; LF, lactoferrin; MPO, myeloperoxidase. (**B**) Characterization of SPIN binding to MPO by SPR, where SPIN was injected over a surface of native MPO. (**C** and **D**) Recombinant SPIN and *S. aureus* supernatant inhibit MPO in a dose dependent manner. ON is overnight culture. Bars express SD with N=3 for **B**-**D**.

expressed *in vivo*, we further investigated this protein as a potential evasion molecule acting on one of the granular proteins of neutrophils.

SPIN binds and inhibits MPO

Since we identified SPIN as a potential evasion protein, recombinant SPIN was coupled to CNBr-activated sepharose beads and used for affinity chromatography to probe neutrophil degranulate for its binding partner. Eluted proteins were visualized by silver stained PAGE and identified by mass spectrometry. Although elastase, proteinase 3, cathepsin G, azurocidin, lactoferrin, and MPO were all identified as potential binding partners, a subsequent SPIN capture ELISA against these potential targets only showed evidence for SPIN binding to MPO (**Figure 1A**). Next, we used conventional surface plasmon resonance (SPR) (**Figure 1B**) as well as AlphaScreen equilibrium competitive binding assays (**Supplemental Figure 2**) to validate our ELISA result. Both SPR and AlphaScreen were consistent with low nanomolar affinity binding between SPIN and MPO, and yielded comparable K_D values of 10 ± 0.6 nM and 2.0 ± 0.07 nM, respectively.

Since SPIN forms a high-affinity complex with MPO, we hypothesized that SPIN disrupts MPO function. Indeed, a colorimetric MPO activity assay demonstrated that SPIN inhibits MPO in a dose dependent manner (**Figure 1C**) with an apparent IC50 of ~7 nM. Subsequently, we investigated whether SPIN was secreted as a functional protein in staphylococcal culture

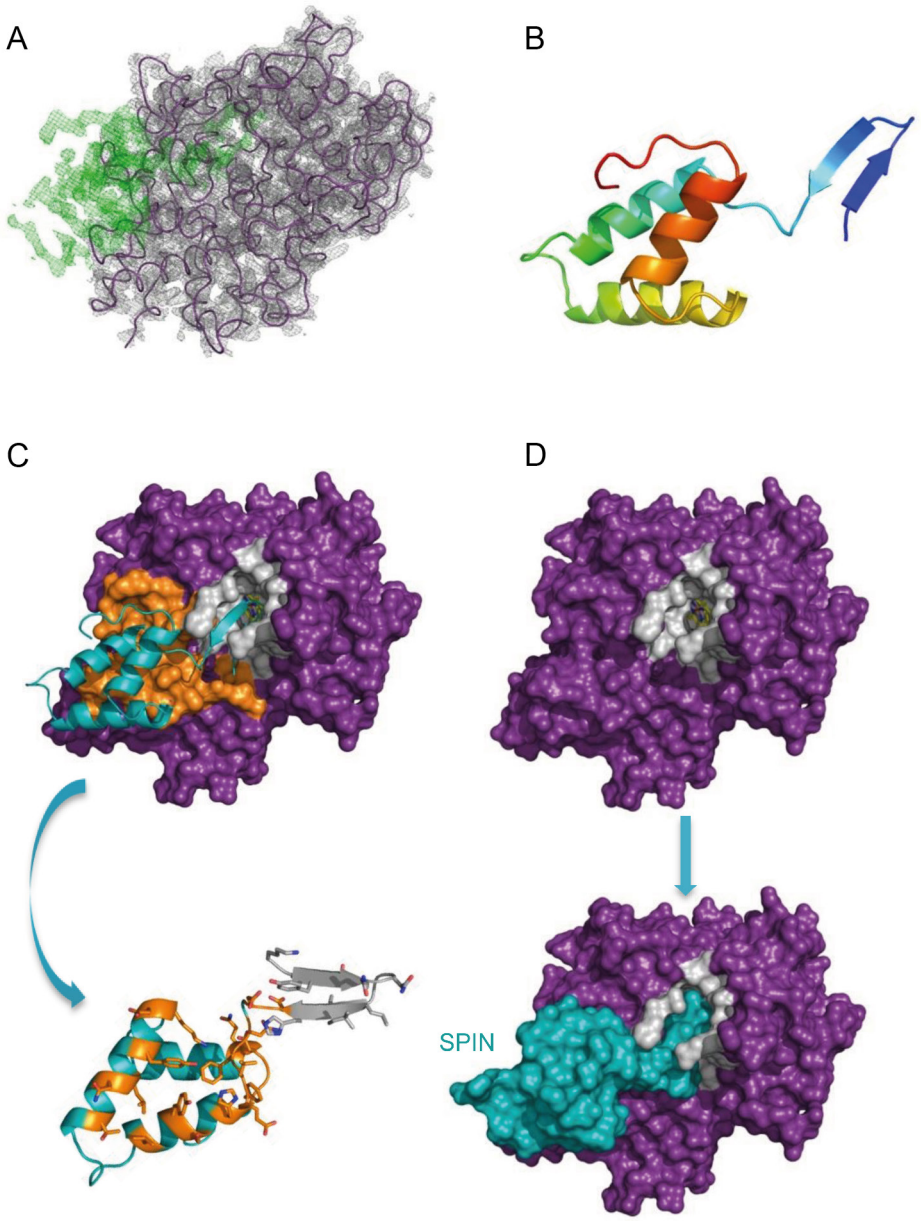

Figure 2: Structural Basis for Inhibition of MPO by SPIN. (**A**) 2.4 Å resolution electron density maps calculated after initial placement of an MPO model (Rfree = 28%). 2Fo-Fc density contoured at 1.5 σ (grey cage) is shown for the MPO model (purple wire), while Fo-Fc density contoured at 3.0 σ (green cage) is attributable to SPIN. (**B**) Structure SPIN polypeptide as a ribbon diagram. N-terminus of the protein is indicated in indigo, the C-terminus in red. The orientation of SPIN has been maintained across panels **A** and **B** for clarity. (**C**) Representation of the final model for the SPIN/MPO complex. Top panel, SPIN is shown as a cyan ribbon while MPO is depicted as a molecular surface. Residues comprising the first SPIN binding interface are coloured orange, while residues lining the MPO active site channel are coloured grey. Bottom panel, SPIN is drawn with the residues found at the first

interface coloured orange, while residues interacting with the MPO active site channel are coloured grey. The sidechains of interfacing residues are depicted in ball-and-stick convention. Note the orientation of SPIN in the bottom panel is flipped 180° in the viewing plane relative to the top panel. (**D**) Surface representations provide insight into the physical basis for MPO inhibition by SPIN. Top panel, MPO is shown as a molecular surface with the residues lining the active site channel in grey. Bottom panel, SPIN is drawn as a cyan molecular surface according to its position in the final model of the SPIN/MPO complex. The location of the reactive site heme from native human MPO (33) is shown as a coloured ball-and-stick. Note that the SPIN β-hairpin appears to completely occlude access of small molecules to the reactive site heme.

supernatant. Both wild type (WT) strains Newman and USA300 accumulated increasing levels of MPO inhibitory activity in conditioned culture medium over time. Moreover, we also found that strain Newman supernatant showed higher degree of inhibition when compared to USA300. To determine whether this MPO inhibitory activity was due to the SPIN protein, we generated isogenic knock-outs (KOs) of the *spn* gene in both Newman and USA300 backgrounds. Conditioned culture medium from both KOs was completely devoid of MPO inhibitory activity (**Figure 1D**).

We also performed a titration analysis on samples of conditioned culture supernatant from WT *S. aureus* strains Newman and USA300 (**Supplemental Figures 3A and 3B**). The IC50 of these samples was 0.12% and 0.30% supernatant for Newman and USA300, respectively. By comparing this to the IC50 from recombinant SPIN (**Figure 1C**), the amount of SPIN present in the overnight supernatant could be estimated. This appeared to be 5.9 μM for Newman and 2.4 μM for USA300. Interestingly, the supernatant from Mu50 strain, which contains a truncated version of *spn* (**Supplemental Figure 1D**), showed no detectable MPO inhibitory activity in its supernatant (**Supplemental Figure 3C**) indicating a non-functional SPIN-variant. The slight inhibitory effect observed at low dilutions of the conditioned media is due to the inhibitory colour of THB broth itself (**Supplemental Figure 3C**).

Structural basis for MPO inhibition by SPIN

SPIN shares no significant sequence homology to other characterized proteins. Thus, we sought structural information to better understand the physical basis for SPIN binding to and inhibition of MPO. We succeeded in crystallizing a complex of SPIN bound to a recombinant form of MPO, collected X-ray diffraction data to 2.4 Å Bragg limiting resolution, and solved the structure by molecular replacement (Table S1). Electron density maps calculated after the initial placement of a model for human MPO revealed a strong, contiguous feature in the crystallographic model that could not be explained by the presence of MPO (**Figure 2A**). A model of the SPIN polypeptide was completed through a combination of automated chain tracing and manual building, and the structure of the complex was refined to final Rwork /Rfree values of 18.4% and 24.1%, respectively (**Supplemental Table 1**). The SPIN protein consists of the common α-helix bundle fold found in other staphylococcal evasion proteins, with a unique addition of a prominent ß-hairpin at its N-terminus (**Figure 2B**). As there are no biochemical features that would promote stability of this β-hairpin in the absence of ligand (e.g. a disulfide bond), we suspect that this region of SPIN is disordered in the unbound state.

The interaction between SPIN and MPO buries 1633 Å from the bacterial inhibitor and is comprised of two conceptually distinct interfaces (**Figure 2C**). The first interface lies at the side of the peroxidase active site entrance, and accounts for 726 Å2 (~45%) buried in the complex. Sixteen of the twenty SPIN residues that contact this site are found on either the first or second helix of the inhibitor. The sidechains of five such residues form either hydrogen bonds or salt-bridges with groups donated by MPO, and likely help impart specificity for this enzyme. The second interface accounts for 907 Å2 (~55%) of the area buried in the complex, and is derived exclusively from residues within the SPIN β-hairpin. All positions in this region of SPIN form extensive contacts with residues that line the MPO active site channel. We find the Gly residue in the β-hairpin turn particularly noteworthy, since it not only allows the second strand to complete the hairpin but also dictates the extent to which this hairpin can penetrate the MPO

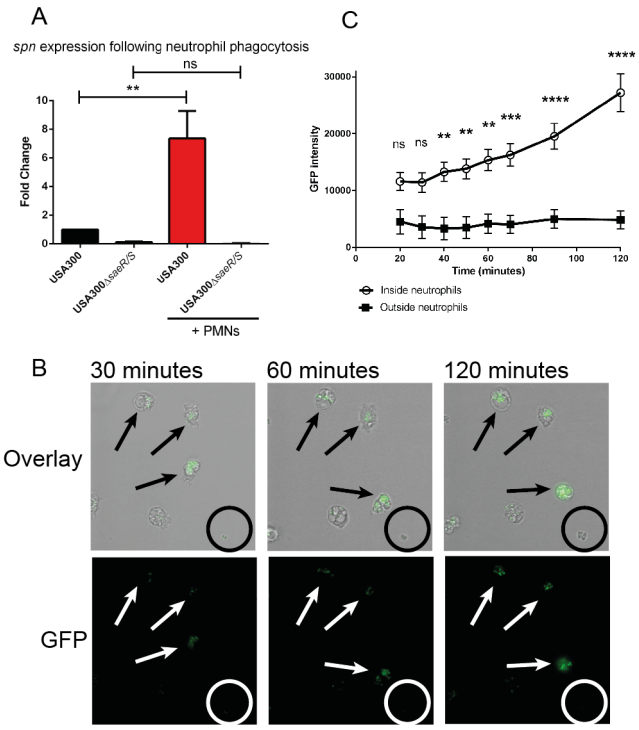

Figure 3: Production of SPIN is upregulated after phagocytosis inside neutrophils. (**A**) Analysis of *spn* expression following exposure to human neutrophils. Bars express SD with N=3. Statistical significance was determined using one-way ANOVA. (**B**) Time-lapse analysis of SPIN expression shown as GFP fluorescence promoter-reporter USA300 in a fibrin-thrombin matrix gel. An overlay of brightfield and GFP (top row) and GFP alone (bottom row) is shown. The time indicates the duration after start of phagocytosis. Arrows indicate bacteria inside neutrophils and the circle indicates a colony of bacteria growing outside neutrophils. One representative experiment is shown of three independent experiments. (**C**) Quantification of total GFP signal from neutrophil-resident or free bacteria. Three different experiments with 44 neutrophils and 26 colonies growing outside neutrophils were analysed. Bars express SEM. Significance was determined by two-way ANOVA with Bonferroni post-test correction for multiple comparison. ** $p \leq 0.01$, *** $p \leq 0.001$, **** $p \leq 0.0001$.

active site. The overall effect of this structural feature allows SPIN to act as a molecular plug and thereby prevent access of the H_2O_2 substrate to the reactive heme located deep within the MPO active site channel (**Figure 2D**).

Production of SPIN by *S. aureus* is upregulated after phagocytosis by neutrophils

To better understand the biological context of SPIN production by *S. aureus*, we compared *spn* gene expression and promoter activity in planktonically-grown bacteria with bacteria that had been phagocytosed by neutrophils. We used strain USA300, since SPIN is constitutively expressed at low levels by strain Newman. *spn* gene expression over time was monitored using qPCR, either with or without phagocytosis. We observed a highly significant, eight-fold increase in *spn*-expression following phagocytosis when compared to samples without neutrophils (**Figure 3A**). This outcome is comparable to our earlier microarray study where enhanced *spn* expression was detected after exposure to azurophilic granule proteins (18). Importantly, we did not detect a similar change in *spn* expression when we used bacteria lacking SaeR/S, which regulates production of multiple evasion factors (19). As a control, we found no significant change in *agrA* expression under any of these conditions (**Supplemental Figure 4**) (20).

Next, we used GFP promoter-reporter USA300 bacteria in a fibrin-thrombin matrix gel to immobilize cells. Time-lapse imaging of the bacteria revealed upregulation of the *spn* promoter-driven GFP signal following phagocytosis by neutrophils (arrows, **Figure 3B**). In contrast, the *spn* promoter appeared inactive in those bacteria that had not been phagocytosed (circle, **Figure 3B**); this observation correlates with *spn* promoter activity for THB-grown bacteria, which showed activity only after 2 hours of growth (**Supplemental Figure 5**). We further quantified the total GFP signal for either free or neutrophil-resident bacteria for 2 hours, beginning at 20 minutes. We found that GFP intensity increased more than two-fold over time for phagocytosed, but not free-living bacteria (**Figure 3C**).

Production of SPIN promotes survival against neutrophil-derived ROS

Since SPIN inhibits MPO and is upregulated following phagocytosis, we next investigated the relevance of SPIN to *S. aureus* evasion of neutrophil killing mechanisms. First we used an artificial system that mimics phagosomal ROS production using glucose oxidase (GO), which forms H_2O_2 in the presence of glucose. We evaluated bacterial survival after the addition of MPO and NaCl, which generates the bactericidal reagent HOCl (**Figure 4A and 4B**). Excessive quantities of GO result in bactericidal concentrations of H_2O_2, which makes it impossible to evaluate MPO mediated killing. In limiting concentrations of GO, increasing MPO concentrations led to killing of *S. aureus* Newman (left panel) and USA300 (right panel). Addition of SPIN restored the survival of bacteria (**Figure 4A**). Moreover, adding increasing concentrations of SPIN (**Figure 4B**) resulted in a dose-dependent rescue from HOCl killing for both Newman (left panel) and USA300 (right panel). This demonstrates clearly that the presence of SPIN is important for evasion of MPO-generated HOCl.

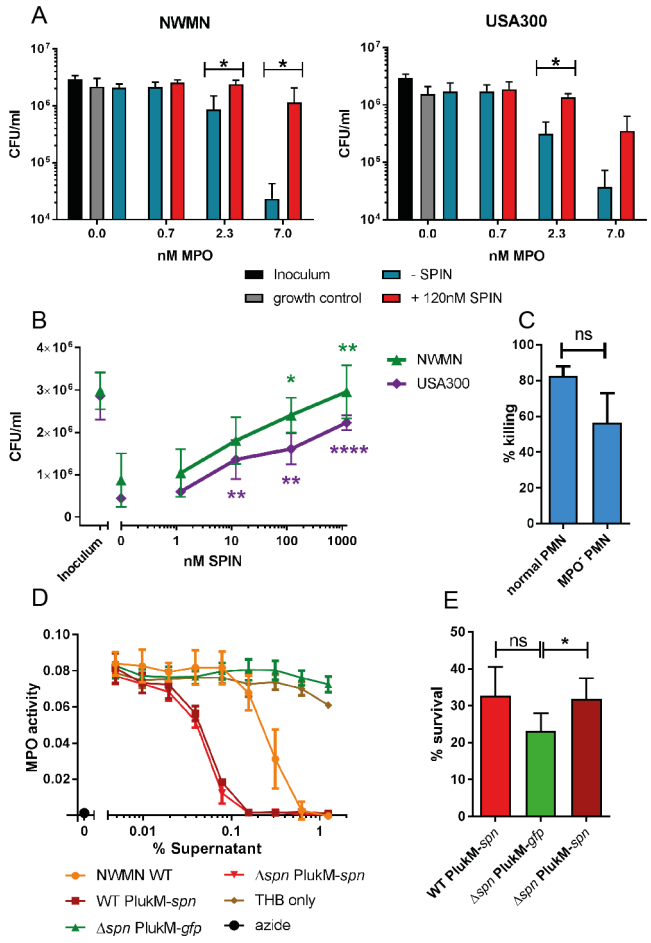

Figure 4: SPIN is important for evasion of MPO-dependent neutrophil killing. (**A**) *S. aureus* strains Newman (left graph) and USA300 (right graph) were killed in a dose dependent manner by adding 0.7-7.0 nM MPO in a coupled glucose oxidase-MPO system. Addition of 120 nM SPIN prevented ROS killing. Statistical significance was determined by two-way ANOVA with Bonferroni post-test correction for multiple comparison. (**B**) SPIN provides dose dependent protection from HOCl-mediated killing for strains Newman and USA300 relative to 0 nM SPIN. Statistical significance was determined by one-way ANOVA. (**C**) Differential bacterial survival of Newman WT from neutrophils with active or membrane permeable AZM198-inactivated MPO. (**D**) Supernatants of overnight culture of strains WT PlukM-*spn*, Δ*spn* PlukM-*spn*, Δ*spn* PlukM-*gfp* were diluted, tested for MPO activity, and compared to Newman WT. Bars express SD with N=3 (**A - D**). (**E**) Effect of *S. aureus* survival from isolated neutrophils after 60 minutes of phagocytosis. Statistical analysis determined by paired student *t*-test for **C** and **E**. Bars express SEM with N=6. * $p \leq 0.05$, ** $p \leq 0.01$, **** $p \leq 0.0001$, ns (non-significant).

SPIN is neither able to bind nor inhibit mouse, horse, cow, or rabbit MPOs, hampering the development of an *in vivo* animal model system (**Supplemental Figure 6)**. We therefore set out to investigate how the presence or absence of the *spn* gene influences *S. aureus* survival following phagocytosis by human neutrophils. First, the contribution of MPO to staphylococcal killing by neutrophils was investigated using the membrane permeable MPO inhibitor

AZM198 (21). Incubation of intact neutrophils with this inhibitor prior to washing and lysis was equally as effective as direct treatment of lysates, indicating that AZM198 is membrane permeable and completely inhibits MPO (**Supplemental Figure 7**). We quantified bacterial killing by neutrophils with and without AZM198 pre-treatment, and observed a difference of 26% between neutrophils with active and inactive MPO. This illustrates the modest extent of MPO-dependent staphylococcal killing by neutrophils in our experiments (**Figure 4C**).

Given the contribution of MPO in killing of phagocytosed *S. aureus*, we employed the strong lukM promoter (22) and used the Newman strain to increase intra-phagosomal SPIN production (WT PlukM-*spn*), thereby ensuring maximal levels of MPO inhibition in our bactericidal assays (**Figure 4D**). We used the same plasmid to complement the isogenic *spn* KO (Δ*spn* PlukM-*spn*) and prepared a strain of the *spn* KO expressing GFP from the same plasmid (PlukM-*gfp*) to serve as a negative control. Supernatants from overnight cultures of these strains were compared to Newman WT for their ability to inhibit MPO (**Figure 4D**). As predicted, the amount of SPIN produced in the WT PlukM-*spn* and Δ*spn* PlukM-*spn* was increased approximately five-fold relative to Newman WT, as judged by IC_{50} values. Importantly, these strains grew with similar kinetics in THB (**Supplemental Figure 8A**) and showed comparable phagocytosis by neutrophils at both 15 and 60 minute time points (**Supplemental Figure 8B and 8C**). Therefore, we used these three strains to detect differences in bacterial survival at 60 minutes following phagocytosis (**Figure 4E**). Indeed, we observed a *spn*-dependent, significant difference in killing between the negative control strain Δ*spn* and the complemented strain that overexpressed *spn*. Although the difference between the Δ*spn* strain and the overexpressing WT strain was not statistically significant, it nevertheless showed a trend toward increased survival similar to the complemented strain. Taken together, these data show that SPIN is an important component to *S. aureus* survival of the oxidative killing mechanisms deployed within the neutrophil phagosome.

DISCUSSION

Here we describe SPIN as a novel component of the *S. aureus* immune evasion arsenal that impairs bacterial killing by neutrophils. The phagocytosed bacteria must confront the numerous anti-bacterial systems within the phagosome. Considering this as a potentially important site for execution of an immune evasion strategy, we set out to identify any heretofore unknown *S. aureus* proteins that inhibit components within neutrophil granules. By employing an innovative phage display approach that is limited to *S. aureus* secreted proteins (**Supplemental Figure 1**), we discovered that SPIN binds MPO with low nanomolar affinity and inhibits its activity (**Figure 1**). Thus, together with the recently characterized neutrophil serine protease inhibitors, Eap, EapH1, and EapH2 (23), SPIN constitutes part of an elaborate staphylococcal innate immune evasion program that specifically targets the anti-bacterial enzymes stored within the azurophilic granules of neutrophils.

From experiments using promoter-GFP reporter bacteria, we observed that the promoter of *spn* is stimulated following uptake of *S. aureus* by neutrophils when compared to bacteria outside neutrophils or in the first two hours growing in THB (**Figure 3B, 3C, and Supplemental Figure 5**). Thus, SPIN is specifically upregulated intracellularly, where MPO is located. A similar result was also observed when looking at mRNA levels (**Figure 3A**), where the production of SPIN was increased over eight-fold 30 minutes after phagocytosis. Moreover, there was no upregulation observed when bacteria lacking the SaeR/S two-component regulatory system were used. The SaeR/S system plays an important role in neutrophil evasion (19) and regulates factors that reduce neutrophil ROS (13). SaeR/S is upregulated comparably to *spn* (approximately 3-10 fold 30 minutes after phagocytosis) (20) and the promoter of SPIN contains the binding consensus sequence of SaeR (24). At least two of the 11 ssl genes (*ssl5* and *ssl8*) are regulated via the Sae system (25), and are located directly upstream of the *spn* gene. Thus, we propose that SPIN is largely regulated via the SaeR/S regulon and likely contributes to the SaeR/S-dependent reduction of neutrophil ROS (13).

By using a simplified system consisting of an enzymatic H_2O_2 generating system and Cl^- as a substrate for MPO, we found that SPIN had a clear dose-dependent and statistically significant effect on *S. aureus* survival (**Figure 4A and 4B**). However, in the complex and necessarily redundant process of bacterial killing within neutrophils, a multitude of oxygen radicals, proteases and other enzymes must work in concert to ensure effective elimination of *S. aureus* cells. Although the contribution of MPO and its main product, HOCl, to *S. aureus* killing has been studied since the early 1970s (5), we and others believe this process remains incompletely understood (26). For example, it was previously believed that MPO is the main component for killing *S. aureus*, because neutrophils from MPO deficient patients showed a log difference in bacterial survival after phagocytosis (5). Using the potent and cell-permeable MPO inhibitor, AZM198, we found that while untreated neutrophils kill 82±5% of bacteria, MPO-depleted neutrophils are still able to kill 56±16% (Fig. 4C). Thus, under the specific test conditions in our assays, roughly one fourth of the staphylococcal killing is due to MPO. Nevertheless, when a strain of *S. aureus* overexpressing *spn* was compared with a *spn*-deleted counterpart (**Figure 4D**) (22), we observed a statistically significant difference in bacterial survival dependent on SPIN (**Figure 4E**). This not only confirms the relevance of SPIN-mediated inhibition of MPO in the physiological context, it also provides a starting point for re-analysis of previous studies where the presence of SPIN may have adversely affected data interpretation.

SPIN consists of a three α-helix bundle fold, which is commonly found among *S. aureus* innate immune evasion proteins, including Efb, Ecb (also called Ehp), Sbi, and SCINs (27). The triple helix motif is a thermodynamically stable structure which can accommodate high sequence diversity and adapt to binding a wide variety of targets (28). However, this simple structural motif is typically modified by an N-terminal extension that imparts specific function to the protein in question (27). Indeed, this appears to be the case for SPIN as well, as is suggested by the co-crystal structure of SPIN/MPO (**Figure 2**). To our knowledge, SPIN is the first example

of a pathogen-derived protein whose role is to specifically bind and inhibit MPO. SPIN is not the only known inhibitor of MPO, however, as it has previously been shown that the host serum protein ceruloplasmin (CP) binds MPO with a K_D of ~30 nM (29) and also blocks MPO activity (30). Examination of the crystal structure of CP bound to MPO (31) indicates that the mechanism through which CP inhibits MPO is conceptually distinct from that of SPIN. Indeed, even though the MPO active site appears to remain partly solvent accessible in the CP/MPO complex, CP attenuates MPO activity by disturbing essential transitions between the redox states of the peroxidase catalytic heme (32). In contrast, our structure of SPIN/MPO shows that SPIN forms a molecular plug that is likely to completely occlude access of substrates to the MPO active site (**Figure 2**). Separately, while CP and SPIN share partial overlap in their binding sites on MPO and recognize their target with similar affinities, they display no obvious homology to one another at the sequence or structural levels. This suggests that the MPO-inhibitory capacity of SPIN has arisen through independent evolutionary processes from that of CP.

In conclusion, we identified a new evasion protein called SPIN which is able to bind and inhibit human MPO. By solving the co-crystal structure of SPIN/MPO, we demonstrate the molecular mechanism of inhibition, via insertion of an N-terminal hairpin into the active site of MPO to block substrate access. We further show the expression of SPIN is upregulated inside the neutrophil, where MPO is located, and that its presence helps in evading MPO-mediated killing. Various proteins secreted by *S. aureus* are known to be human specific, which leads to restrictions in investigating this pathogen in animal models (8, 16). This seems to account for SPIN as well since it inhibits only human MPO and not MPO of other animals we have tested (**Supplemental Figure 6**). By adding this evasion molecule to the arsenal of previously identified evasion molecules, we can better understand the elaborate mechanism by which *S. aureus* evades killing through a multifaceted strategy that acts within the phagosomal compartment.

ACKNOWLEDGMENTS

We want to thank Franke A. Quee, Lindert Benedictus, Ruben Shrestha, Ping Li, and Kyler B. Pallister for experiments and statistical analysis. This research was supported by grants from the National Institutes of Health (AI111203 and GM121511) to B.V.G., (Grants NIH-R01AI1090046, NIH-PAR98-072) to J.M.V., and (NIH-RR020185 for a fellowship award) to F.E.G. and a ZonMw Grant 205200004 from the Netherlands Organization for Health Research and Development (to J.A.G.S.). X-ray diffraction data were collected at Southeast Regional Collaborative Access Team (SER-CAT) 22-BM beamline at the Advanced Photon Source, Argonne National Laboratory. Supporting institutions may be found at www.ser-cat.org/members.html. Use of the Advanced Photon Source was supported by the U. S. Department of Energy, Office of Science, Office of Basic Energy Sciences, under Contract No. W-31-109-Eng-38.

AUTHOR CONTRIBUTIONS

R.N., C.F., J.M.V., B.L.G., K.P.M.v.K., J.A.G.v.S., B.V.G., and P.J.A.H. designed research; N.W.M.d.J., K.X.R., F.E.G., A.J.M., B.L.G., and B.V.G. performed research; C.F., K.P.M.v.K., and P.J.A.H. were involved in the discovery of the protein and its function; and N.W.M.d.J., K.X.R., K.P.M.v.K., J.A.G.v.S., B.V.G., and P.J.A.H. wrote the paper.

COMPETING FINANCIAL INTEREST

The authors declare no competing financial interests.

MATERIALS & METHODS

Bacterial strains and constructs
The bacterial strains and constructs used in this study are described in detail in *SI Materials and Methods*.

Expression and purification of SPIN
SPIN was subsequently produced in *Escherichia coli* and purified according to *SI Materials and Methods*. Primers used in this study are listed in **Supplemental Table 2**.

Binding studies
Detailed procedures about ELISAs, SPR and Alphascreen assay are described in *SI Materials and Methods*.

MPO activity assay
SPIN activity was determined by measuring the MPO activity via the redox indicator o-Dianisidine. For detailed procedures, see *SI Materials and Methods*.

Crystallization, structure determination, refinement, and analysis
A description of crystal cell constants, diffraction data quality, and properties of the final model for the SPIN/MPO complex can be found in **Supplemental Table 1**. See *SI Materials and Methods* for detailed information about the SPIN/MPO crystal structure.

Analysis of *spn* and *agrA* expression following exposure to human neutrophils
Gene expression was assessed using TaqMan® RNA-to-CT™ 1-Step Kit (Life Technologies). For detailed procedures, see *SI Materials and Methods*.

Time-lapse microscopy and phagocytosis assay
Detailed information about time-lapse microscopy of promoter reporter USA300 bacteria and phagocytosis is described in *SI Materials and Methods*.

Bactericidal assays. Bactericidal assays with MPO and GO or neutrophils is described in detail in *SI Materials and Methods*.

Graphical and statistical analyses. MPO activity analyses and statistical analyses were performed with Graphpad Prism version 6. Statistical significance was calculated using ANOVA and Student's *t* test.

REFERENCES

1. Lowy, F. D. (1998) Staphylococcus aureus infections. N. Engl. J. Med. 339, 520–532
2. Rigby, K. M., and DeLeo, F. R. (2012) Neutrophils in innate host defense against Staphylococcus aureus infections. Semin. Immunopathol. 34, 237–59
3. Faurschou, M., and Borregaard, N. (2003) Neutrophil granules and secretory vesicles in inflammation. Microbes Infect. 5, 1317–1327
4. Babior, B. M., Lambeth, J. D., and Nauseef, W. (2002) The neutrophil NADPH oxidase. Arch. Biochem. Biophys. 397, 342–344
5. Klebanoff, S. J. (1972) Role of myeloperoxidase-mediated antimicrobial systems in intact leukocytes. J. Reticuloendothel. Soc. 12, 170–196
6. Kettle, A. J., and Winterbourn, C. C. (1997) Myeloperoxidase: A key regulator of neutrophil oxidant production. Redox Rep. 3, 3–15
7. Thwaites, G. E., and Gant, V. (2011) Are bloodstream leukocytes Trojan Horses for the metastasis of Staphylococcus aureus? Nat. Rev. Microbiol. 9, 215–22
8. Spaan, A. N., Surewaard, B. G. J., Nijland, R., and van Strijp, J. a G. (2013) Neutrophils versus Staphylococcus aureus: a biological tug of war. Annu. Rev. Microbiol. 67, 629–50
9. Liu, G. Y., Essex, A., Buchanan, J. T., Datta, V., Hoffman, H. M., Bastian, J. F., Fierer, J., and Nizet, V. (2005) Staphylococcus aureus golden pigment impairs neutrophil killing and promotes virulence through its antioxidant activity. J. Exp. Med. 202, 209–15
10. Cosgrove, K., Coutts, G., Jonsson, I.-M., Tarkowski, a., Kokai-Kun, J. F., Mond, J. J., and Foster, S. J. (2007) Catalase (KatA) and Alkyl Hydroperoxide Reductase (AhpC) Have Compensatory Roles in Peroxide Stress Resistance and Are Required for Survival, Persistence, and Nasal Colonization in Staphylococcus aureus. J. Bacteriol. 189, 1025–1035
11. Kusch, H., and Engelmann, S. (2014) Secrets of the secretome in Staphylococcus aureus. Int. J. Med. Microbiol. 304, 133–141
12. Fevre, C., Bestebroer, J., Mebius, M. M., de Haas, C. J. C., van Strijp, J. a G., Fitzgerald, J. R., and Haas, P. J. A. (2014) Staphylococcus aureus proteins SSL6 and SEIX interact with neutrophil receptors as identified using secretome phage display. Cell. Microbiol. 16, 1646–1665
13. Guerra, F. E., Addison, C. B., de Jong, N. W. M., Azzolino, J., Pallister, K. B., van Strijp, J. A. G., and Voyich, J. M. (2016) Staphylococcus aureus SaeR/S-regulated factors reduce human neutrophil reactive oxygen species production. J. Leukoc. Biol. 100, 1–6
14. Fevre, C., Scheepmaker, L., and Haas, P. (2017) Identifying Bacterial Immune Evasion Proteins Using Phage Display. in Methods in molecular biology (Clifton, N.J.), pp. 43–61, 1535, 43–61
15. McCarthy, A. J., and Lindsay, J. a (2013) Staphylococcus aureus innate immune evasion is lineage-specific: a bioinfomatics study. Infect. Genet. Evol. 19, 7–14
16. De Haas, C. J. C., Veldkamp, K. E., Peschel, A., Weerkamp, F., Wamel, W. J. B. Van, Heezius, E. C. J. M., Poppelier, M. J. J. G., Kessel, K. P. M. Van, and Van Strijp, J. a G. (2004) Chemotaxis Inhibitory Protein of Staphylococcus aureus , a Bacterial Antiinflammatory Agent. J. Exp. Med. J. Exp. Med. 03687900, 687–695
17. Verkaik, N. J., de Vogel, C. P., Boelens, H. a, Grumann, D., Hoogenboezem, T., Vink, C., Hooijkaas, H., Foster, T. J., Verbrugh, H. a, van Belkum, A., and van Wamel, W. J. B. (2009) Anti-Staphylococcal Humoral Immune Response in Persistent Nasal Carriers and Noncarriers of Staphylococcus aureus. J. Infect. Dis. 199, 625–632
18. Palazzolo-Ballance, a. M., Reniere, M. L., Braughton, K. R., Sturdevant, D. E., Otto, M., Kreiswirth, B. N., Skaar, E. P., and DeLeo, F. R. (2007) Neutrophil Microbicides Induce a Pathogen Survival Response in

Community-Associated Methicillin-Resistant Staphylococcus aureus. J. Immunol. 180, 500–509

19. Voyich, J. M., Vuong, C., DeWald, M., Nygaard, T. K., Kocianova, S., Griffith, S., Jones, J., Iverson, C., Sturdevant, D. E., Braughton, K. R., Whitney, A. R., Otto, M., and DeLeo, F. R. (2009) The SaeR/S gene regulatory system is essential for innate immune evasion by Staphylococcus aureus. J. Infect. Dis. 199, 1698–706

20. Voyich, J. M., Braughton, K. R., Sturdevant, D. E., Whitney, A. R., Saïd-Salim, B., Porcella, S. F., Long, R. D., Dorward, D. W., Gardner, D. J., Kreiswirth, B. N., Musser, J. M., and DeLeo, F. R. (2005) Insights into mechanisms used by Staphylococcus aureus to avoid destruction by human neutrophils. J. Immunol. 175, 3907–3919

21. Björnsdottir, H., Welin, A., Michaëlsson, E., Osla, V., Berg, S., Christenson, K., Sundqvist, M., Dahlgren, C., Karlsson, A., and Bylund, J. (2015) Neutrophil NET formation is regulated from the inside by myeloperoxidase-processed reactive oxygen species. Free Radic. Biol. Med. 89, 1024–1035

22. Vrieling, M., Koymans, K. J., Heesterbeek, D. a, Aerts, P. C., Rutten, V. P., de Haas, C. J., van Kessel, K. P., Koets, a P., Nijland, R., and van Strijp, J. a (2015) Bovine Staphylococcus aureus Secretes the Leukocidin LukMF' To Kill Migrating Neutrophils through CCR1. MBio. 6, e00335

23. Stapels, D. a, Ramyar, K. X., Bischoff, M., von Kockritz-Blickwede, M., Milder, F. J., Ruyken, M., Eisenbeis, J., McWhorter, W. J., Herrmann, M., van Kessel, K. P., Geisbrecht, B. V, and Rooijakkers, S. H. (2014) Staphylococcus aureus secretes a unique class of neutrophil serine protease inhibitors. Proc Natl Acad Sci U S A. 111, 13187–13192

24. Nygaard, T. K., Pallister, K. B., Ruzevich, P., Griffith, S., Vuong, C., and Voyich, J. M. (2010) SaeR binds a consensus sequence within virulence gene promoters to advance USA300 pathogenesis. J Infect Dis. 201, 241–254

25. Pantrangi, M., Singh, V. K., Wolz, C., and Shukla, S. K. (2010) Staphylococcal superantigen-like genes, ssl5 and ssl8, are positively regulated by Sae and negatively by Agr in the Newman strain. FEMS Microbiol. Lett. 308, 175–84

26. Klebanoff, S. J., Kettle, A. J., Rosen, H., Winterbourn, C. C., and Nauseef, W. M. (2013) Myeloperoxidase: a front-line defender against phagocytosed microorganisms. J. Leukoc. Biol. 93, 185–98

27. Serruto, D., Rappuoli, R., Scarselli, M., Gros, P., and van Strijp, J. a G. (2010) Molecular mechanisms of complement evasion: learning from staphylococci and meningococci. Nat. Rev. Microbiol. 8, 393–399

28. Koymans, K. J., Vrieling, M., Gorham, R. D., and van Strijp, J. A. G. (2016) Staphylococcal Immune Evasion Proteins: Structure, Function, and Host Adaptation. Curr. Top. Microbiol. Immunol. 6, 23–27

29. Bakhautdin, B., Goksoy Bakhautdin, E., and Fox, P. L. (2014) Ceruloplasmin has two nearly identical sites that bind myeloperoxidase. Biochem. Biophys. Res. Commun. 453, 722–727

30. Segelmark, M., Persson, B., Hellmark, T., and Wieslander, J. (1997) Binding and inhibition of myeloperoxidase (MPO): a major function of ceruloplasmin? Clin. Exp. Immunol. 108, 167–174

31. Samygina, V. R., Sokolov, A. V., Bourenkov, G., Petoukhov, M. V., Pulina, M. O., Zakharova, E. T., Vasilyev, V. B., Bartunik, H., and Svergun, D. I. (2013) Ceruloplasmin: Macromolecular Assemblies with Iron-Containing Acute Phase Proteins. PLoS One. 10.1371/journal.pone.0067145

32. Chapman, A. L. P., Mocatta, T. J., Shiva, S., Seidel, A., Chen, B., Khalilova, I., Paumann-Page, M. E., Jameson, G. N. L., Winterbourn, C. C., and Kettle, A. J. (2013) Ceruloplasmin is an endogenous inhibitor of myeloperoxidase. J. Biol. Chem. 288, 6465–6477

33. Fiedler, T. J. (2000) X-ray Crystal Structure and Characterization of Halide-binding Sites of Human Myeloperoxidase at 1.8 A Resolution. J. Biol. Chem. 275, 11964–11971

34. Van den Berg, S., Bonarius, H. P. J., van Kessel, K. P. M., Elsinga, G. S., Kooi, N., Westra, H., Bosma, T., van der Kooi-Pol, M. M., Koedijk, D. G. a M., Groen, H., van Dijl, J. M. A., Buist, G., and Bakker-Woudenberg, I. a J. M. (2015) A human monoclonal antibody targeting the conserved staphylococcal antigen IsaA protects mice against Staphylococcus aureus bacteremia. Int. J. Med. Microbiol. 305, 55–64

35. Waterhouse, A. M., Procter, J. B., Martin, D. M. a, Clamp, M., and Barton, G. J. (2009) Jalview Version 2-A multiple sequence alignment editor and analysis workbench. Bioinformatics. 25, 1189–1191

36. Carver, T. J., Rutherford, K. M., Berriman, M., Rajandream, M. A., Barrell, B. G., and Parkhill, J. (2005) ACT: The Artemis comparison tool. Bioinformatics. 21, 3422–3423

37. Bose, J. L., Fey, P. D., and Bayles, K. W. (2013) Genetic tools to enhance the study of gene function and regulation in Staphylococcus aureus. Appl. Environ. Microbiol. 79, 2218–2224

38. Pang, Y. Y., Schwartz, J., Thoendel, M., Ackermann, L. W., Horswill, A. R., and Nauseef, W. M. (2010) Agr-dependent interactions of Staphylococcus aureus USA300 with human polymorphonuclear neutrophils. J. Innate Immun. 2, 546–559

39. Van Kessel, K. P. M., Van Strijp, J. A. G., and Verhoef, J. (1991) Inactivation of recombinant human tumor necrosis factor-a by proteolytic enzymes released from stimulated human neutreophils. J. Immunol. 147, 3862–3868

40. Rooijakkers, S. H. M., Van Wamel, W. J. B., Ruyken, M., Van Kessel, K. P. M., and Van Strijp, J. a G. (2005) Anti-opsonic properties of staphylokinase. Microbes Infect. 7, 476–484

41. R. Bosse, C. Illy, D. C. (2002) Application note. Principles of AlphaScreen. PerkinElmer Life Sci. Boston, MA

42. Otwinowski, Z., and Minor, W. (1997) Processing of X-ray diffraction data collected in oscillation mode. Methods Enzymol. 276, 307–326

43. Zwart, P. H., Afonine, P. V., Grosse-Kunstleve, R. W., Hung, L.-W., Ioerger, T. R., McCoy, A. J., McKee, E., Moriarty, N. W., Read, R. J., Sacchettini, J. C., Sauter, N. K., Storoni, L. C., Terwilliger, T. C., and Adams, P. D. (2008) Automated Structure Solution with the PHENIX Suite, pp. 419–435, 10.1007/978-1-60327-058-8_28

44. Afonine, P. V., Mustyakimov, M., Grosse-Kunstleve, R. W., Moriarty, N. W., Langan, P., and Adams, P. D. (2010) Joint X-ray and neutron refinement with phenix.refine. Acta Crystallogr. Sect. D Biol. Crystallogr. 66, 1153–1163

45. Emsley, P., Lohkamp, B., Scott, W. G., and Cowtan, K. (2010) Features and development of Coot. Acta Crystallogr. Sect. D Biol. Crystallogr. 66, 486–501

46. Krissinel, E., and Henrick, K. (2007) Inference of Macromolecular Assemblies from Crystalline State. J. Mol. Biol. 372, 774–797

47. Voyich, J. M., Sturdevant, D. E., and DeLeo, F. R. (2008) Analysis of Staphylococcus aureus gene expression during PMN phagocytosis. Methods Mol. Biol. 431, 109–22

48. Denys, G. a., Grover, P., O'Hanley, P., and Stephens, J. T. (2011) In vitro antibacterial activity of E-101 solution, a novel myeloperoxidase-mediated antimicrobial, against Gram-positive and Gram-negative pathogens. J. Antimicrob. Chemother. 66, 335–342

49. Bestebroer, J., Poppelier, M. J. J. G., Ulfman, L. H., Lenting, P. J., Denis, C. V., Van Kessel, K. P. M., Van Strijp, J. a G., and De Haas, C. J. C. (2007) Staphylococcal superantigen-like 5 binds PSGL-1 and inhibits P-selectin-mediated neutrophil rolling. Blood. 109, 2936–2943

SUPPLEMENTAL DATA

SI Materials and Methods

Bacterial strains and constructs. In this study the *S. aureus* strains USA300, MU50 (34), and Newman (Tim Foster, Dublin, Ireland) were used. The genomes of 88 isolates representing 25 clonal complexes were analysed for the presence of the *spn* gene (15) in Jalview (35). The presence of the *spn* gene from 84 *S. aureus* clinical strains isolated from University Medical Center Utrecht patients was checked by PCR. The Artemis Comparison Tool was used to compare the genomic region GIα (36). The KO of *spn* in the Newman strain was generated by cloning ~1000 bp upstream and ~1000 bp downstream of the gene into the temperature-sensitive vector pJB38 as described before (37). Deletion of the *spn* gene in the KO was confirmed by sequencing. The promoter reporter construct was modified from pCM29 vector (38) where the *sarA* P1 promoter was changed to the *spn* promoter region and this vector was electroporated into USA300 strain. The super-producing SPIN strain was generated by fusing the promoter region of *lukM* (22) upstream of *spn* in pCM29 vector. This vector was electroporated in Newman WT and for complementation in the Δ*spn* Newman. In order to compare the super-producing SPIN strain and the super-producing complemented strain, the same vector was electroporated in Δ*spn* Newman, where the *spn*-open reading frame was replaced by GFP, resulting in the strain Δ*spn* PlukM-*gfp*.

Identification, expression and purification of SPIN. SPIN was identified by using secretome phage display. The library used was identical to the described (12) staphylococcal library, Briefly, isolated DNA from *S. aureus* strain Newman was randomly sheared into fragments ranging 0.3-3 kb in size. These fragments were cloned into the pDJ01 phagemid vector for specific display of secreted proteins. Constructs were transformed into TG1 *E. coli* yielding $7.2x10^7$ clones. The VCSM13 helper phage was used to create a *S. aureus* secretome phage library. This library was used to identify *S. aureus* proteins interacting with neutrophil degranulate. Panning was performed on coated total neutrophil degranulate obtained by stimulating TNF-α (10 ng/ml) and cytochalasin B (5 µg/ml) treated neutrophils (3 x 107 cells/ml) at 37°C with 1 µM fMLP as described before (39). After four rounds of selection 48 colonies were sequenced and 3 different phage clones containing SPIN were identified in 36 colonies. The primary phage identified ORF (hypothetical protein NWMN_0402) was cloned and expressed (see below) and 2.5 mg of C-His SPIN was coupled to 1 ml of CNBr-activated Sepharose 4B (GE Healthcare) according to manufacturer instructions with a couplings percentage of 56% and loaded on an empty Tricorn 5/50 column (GE Healthcare). Neutrophil degranulate was treated with 1 mM EDTA (Merck) and 5 mM DFP (Sigma-Aldrich) to inhibit metalloproteases and serine proteases, respectively. This degranulate was subsequently loaded on the SPIN column, washed with PBS and eluted with 0.1 M glycine buffer pH 2.7 (Serva) on an AKTA Explorer (GE Healthcare). The protein content of complete degranulate and eluate after affinity chromatography were analysed by SDS PAGE and silver stain. A protein species eluted from the SPIN-column was cut from the SDS PAGE gel and analysed by MALDI MS/MS (Alphalyse).

The *spn* gene, without the signal sequence (cleavage site between ADA-KV), of *S. aureus* strain Newman (hypothetical protein NWMN_0402) was used to make recombinant SPIN. PCR products were amplified using Phusion polymerase (Thermo Scientific) and ligated with NotI and BamHI restriction sites in the modified expression vector pRSETB (Invitrogen Life Technologies), containing a cleavable N-terminal 6xHis tag (N-His SPIN) or a non cleavable C-terminal 6xHis tag (C-His SPIN), leaving three alanines between SPIN and the C-His tag. Expression was performed in Escherichia coli Rosetta-gami(DE3)pLysS (Novagen; Merck Biosciences). The bacterial pellets were lysed with 10 µg/ml lysozyme and three freeze-thaw sonication cycles in 20 mM sodium phosphate (pH 7.8). After centrifugation, the His-tagged proteins were purified using nickel affinity chromatography (HiTrap chelating, HP, GE Healthcare) with an imidazole gradient (10-250 mM) (Sigma-Aldrich). The cleavable N-His SPIN was cleaved with enterokinase (Invitrogen) and subsequently untagged SPIN was obtained after a second nickel column passage. Purified C-His SPIN and untagged SPIN were stored in PBS at -20°C.

Binding studies. ELISAs were performed to show binding of C-His SPIN to MPO (Elastin products company), neutrophil elastase (NE), Proteinase 3 (PR3) (Elastin products company), Cathepsin G (Biocentrum), Azurocidin

(ITK Diagnostics), Lactoferrin (Sigma-Aldrich). The granule proteins were coated at 250 ng/well in PBS on Nunc maxisorp plate and after blocking with 4% (w/v) bovine serum albumin (BSA) (Serva) in PBST (or TBST for MPO), a concentration range of 0-1000 nM C-His SPIN was added. Bound His6 protein was detected by monoclonal His mouse antibody (Hytest) and peroxidase-conjugated goat anti-mouse IgG (Biorad) and visualized using tetramethylbenzidine for binding to other granular proteins. Alkaline phosphatase-conjugated goat anti-mouse IgG (Novex life technologies) and visualization by using para-Nitrophenylphosphate (pNPP) was used for MPO detection.

Direct binding of WT SPIN to native MPO was assessed by SPR using a Biacore 3000 instrument (GE Healthcare) at 25°C. A running buffer of 20 mM Hepes (pH 7.4), 140 mM NaCl, and 0.005% (v/v) Tween-20 and a flowrate of 20 µl min-1 was used for all experiments. A native MPO biosensor was created by immobilizing MPO on a CM5 sensor chip (GE Healthcare) using standard amine coupling chemistry to a final immobilization density of 3,330 RU. A reference surface was generated by activation and subsequent quenching of a separate flow cell. A variable concentration series of SPIN (0-1000 nM) was injected in triplicate over the MPO surface for 2 min and allowed to dissociate for 4 min. Regeneration of the MPO surface to baseline was achieved by three injections of glycine (pH 10.0) for 3 min. Kinetic analysis of each reference subtracted injection series was performed using BIAEvaluation software v4.1.1 (GE Healthcare) using a 1:1 (Langmuir) binding model and fitting R_{max} locally.

Anti-SPIN IgG antibodies were determined in Normal Human Serum (NHS) from 20 healthy donors as described (40), using Nunc maxisorp microtiter plates (Thermo Scientific) coated with 250 ng recombinant SPIN, CHIPS, or SEI in PBS. The titers were determined as logarithmic value of the dilution factor that gave an OD_{450} of 0.2 after subtraction of the background.

The AlphaScreen assay (PerkinElmer) (41) was used to determine the binding interaction between SPIN and MPO in PBS + 1 mg/ml BSA buffer. Human MPO, final concentration 0.6 nM, C-His SPIN, final concentration 1 nM, and untagged (shown as unlabelled) SPIN, final concentration ranging from 0-1000 nM, were mixed together and incubated at room temperature for 1 hour. Next, rabbit IgG against MPO (Dako) was added in a final concentration of 0.6 nM and incubation was continued for another hour. Finally Protein A donor beads and anti-His acceptor beads, each at a final concentration of 20 µg/ml were added and incubated in the dark for one hour. Binding was then measured in a CLARIOstar microplate reader (BMG Labtech). The K_D was calculated after fitting nonlinear regression, one-site specific binding using Graphpad Prism version 6.

MPO activity assay. The redox indicator o-Dianisidine was used at OD_{450} to measure MPO activity in the presence of H_2O_2. 0.2 U/ml MPO isolated from human sputum (Elastin Products Company), 18 µg/ml human rMPO (R&D Systems), or 18.8 µg/ml mouse rMPO (R&D Systems) were incubated with several dilutions of supernatant from different *S. aureus* strains, or with purified protein for 1 hour at 37°C in 96-well plates. Supernatant of WT and Δ*spn* strains from Newman and USA300 were taken at different time points and diluted 16-fold in PBS. THB and 0.3 mM azide were used as controls. A substrate mixture composed of 45 mM phosphate buffer pH 6.0, 0.5 mM H_2O_2, and 15 µg of o-Dianisidine dihydrochloride (tablet from Sigma-Aldrich) was used. OD_{450} nm was measured continuously every 45 seconds for 1 hour at 37°C using a Fluostar Omega microplate reader. The slope before saturation was calculated via Prism 6 and set as 'MPO activity'. 10 µM AZM198 (a kind gift from Innovative Medicines and Early Development Cardiovascular and Metabolic Diseases, AstraZeneca) was added for 1 hour at room temperature to $2x10^6$ neutrophils and washed afterwards to test the intracellular effect on intact cells. To prepare lysates, neutrophils were lysed with 0.1% (v/v) Triton-X100 in PBS, centrifuged for 5 min at 10,000 x g and cell-free supernatant was tested for MPO activity. As a positive control for AZM198, 10 µM of the inhibitor was added to the cell-free supernatant after lysis.

Crystallization, structure determination, refinement, and analysis. A sample of untagged SPIN bound to recombinant human MPO (R&D Systems) was prepared by mixing stoichiometric amounts of each protein and concentrating to 5 mg/ml total protein in a buffer of 5 mM tris (pH 7.4), 50 mM NaCl. Crystals of the SPIN/MPO complex were obtained by vapor diffusion of hanging drops at 20℃. Drops were established by mixing 1 µl complex with 1 µl of precipitant solution (0.2 M triammonium citrate (pH 7.0), 20% (w/v) peg-3350), and incubating over

500 µl precipitant solution. Rhomboid shaped crystals generally appeared within 2-3 days, although microseeding was occasionally necessary to facilitate nucleation of crystals. Single crystals were harvested and cryopreserved in precipitant solution supplemented with an additional 10% (v/v) peg-400. Monochromatic X-ray diffraction data were collected at 1.0 Å wavelength using beamline 22-BM of the Advanced Photon Source (Argonne National Laboratory). Diffraction data were integrated, scaled, and reduced using the HKL2000 software suite (42). Crystals grew in the space group C2 and contained a single copy of the complex in the asymmetric unit. Structure solution and refinement were carried out by individual programs as implemented in the PHENIX software package (43). Initial phases were obtained by molecular replacement using a single copy of native human MPO as a search model (PDB ID Code 1CXP(33)). Following an initial round of refinement, a model for the SPIN polypeptide was completed by a combination of automated chain tracing using PHENIX.AUTOBUILD (44) and manual building into electron density maps using COOT (45). The final model was completed upon iterative cycles of manual rebuilding and refinement using PHENIX.REFINE. The recombinant MPO preparation used here is characterized by a lower occupancy of the heme prosthetic group when compared to MPO isolated from human sources; this resulted in weak electron density for the heme in the co-crystal structure, and prevented inclusion of heme in the final model. Refined coordinates and structure factors have been deposited in the Protein Data Bank, Research Collaboratory for Structural Bioinformatics, Rutgers University (http://www.rcsb.org/) under accession number 5UZU. A description of crystal cell constants, diffraction data quality, and properties of the final model for the SPIN/MPO complex can be found in **Supplemental Table 1**. All structural analyses, including calculation of buried surface areas and identification of potential hydrogen bonds, were performed using the EBI-PISA server (http://www.ebi.ac.uk/pdbe/prot_int/pistart.html (46)). Representations of protein structures and electron density maps were generated by PyMol (http://www.pymol.org/).

Analysis of *spn* and *agrA* expression following exposure to human neutrophils. Overnight bacterial cultures grown in tryptic soy broth (TSB) were diluted 1:100 in fresh TSB and grown to OD_{600} = 1.5. Bacteria were washed in DPBS and re-suspended in RPMI supplemented with 5 mM HEPES. Human neutrophils were purified from human venous blood, as previously described (20). Informed consent was obtained from all subjects, in accordance with the Declaration of Helsinki. Approval from the medical ethics committee of the University Medical Center Utrecht was attained (METC-protocol 07-125/C approved on 1 March 2010). Human neutrophils ($1x10^7$) were exposed to strain USA300 ($1x10^8$) in human serum-coated 24-well plates and phagocytosis was synchronized by centrifugation as described elsewhere (47). After 30 minutes of incubation at 37°C in 5% (v/v) CO_2, RNA was extracted using RNeasy Mini Kit (Qiagen) (47). Gene expression was assessed using TaqMan® RNA-to-CT™ 1-Step Kit (Life Technologies) and amplification was measured using a 7500 Fast Real-Time PCR System (Applied Biosystems). gyrB expression was used as the endogenous control.

Time-lapse microscopy and phagocytosis assay. USA300 bacteria were electroporated with modified pCM29 GFP plasmid, where the promoter *SarA* was changed to the SPIN promoter from strain Newman. The promoter regions of USA300 and Newman are 100% identical. These bacteria were phagocytized by neutrophils (10 bacteria : 1 neutrophil with 10% NHS) for 10 minutes at 37°C and monitored by time-lapse microscopy every 10 minutes for 2 hours. After that time point bacteria started to proliferate and therefore showed an increase in GFP signal. The experiment was performed in a fibrin-thrombin matrix as previously described (22) with a Leica TSC SP5 inverted microscope equipped with a HCX PL APO 40 ¥ 0.85 objective (Leica Microsystems, the Netherlands). Total GFP was quantified by defining individual regions of interest (ROI) from single neutrophils or bacterial colonies outside neutrophils after background subtraction (ROI outside cells) using ImageJ.

Phagocytosis assays were performed using FITC (Sigma-Aldrich) labelled bacteria and phagocytosis by isolated neutrophils in the presence of varying concentrations of sera. The percentage of FITC positive neutrophils was calculated after 15 minutes and 60 minutes of phagocytosis by FACS as described elsewhere (40).

Bactericidal assays with MPO and GO. This experiment was adapted from Denys et al., 2010 (48). In short, bacteria were grown to logarithmic phase (OD_{660} ~ 0.5) from an overnight culture, washed twice and resuspended to OD_{660} ~ 0.5 in sterile Hanks' Balanced Salt Solution (HBSS). 100µl of bacteria were diluted into 10 ml of substrate solution containing 300 mM glucose (Merck) in HBSS. 50 µl of this bacterial stock solution was diluted 1:1 (v/v)

with an enzyme solution containing 4 ng/ml GO (from Aspergillus, Sigma-Aldrich), and MPO concentrations ranging from 0-7 nM with or without the addition of 120 nM recombinant SPIN. Further experiments were performed by titrating SPIN (ranging from 0-1200 nM) with 2.3 nM MPO. The enzyme/bacteria mixture was incubated for 1 hour at 37°C and peroxidase activity was stopped by addition of 1 mg/ml catalase from bovine liver (Sigma-Aldrich). Samples were serially diluted in PBS and plated onto Todd Hewitt Agar (THA) plates. Colony forming units (CFU) were counted the next day after overnight incubation at 37°C.

Bactericidal assays by neutrophils. Neutrophils were purified from healthy volunteers by Ficoll/Histopaque centrifugation as described before (49). Bacteria were grown to logarithmic phase (OD_{660} ~ 0.5) from an overnight culture in THB, washed twice and diluted in HBSS supplemented with 0.05% (w/v) human serum albumin (HSA, Sanquin). To inhibit MPO activity, 10 μM AZM198 was added for 1 hour at room temperature with gentle shaking, after which neutrophils were washed once in HBSS + 0.05% (w/v) HSA. Per condition, 8.5x105 neutrophils with $1.70x10^4$ bacteria ($8.5x10^5$ neutrophils with $5.1x10^5$ bacteria for AZM198 experiment) and 5% (w/v) NHS, were added in sterile siliconized tubes and incubated various times with shaking in a 5% (v/v) CO_2 incubator. After 60 minutes of incubation, the neutrophils were lysed for 5 minutes with ice cold 0.3% (w/v) saponin (Sigma-Aldrich) in water. Samples were then serially diluted in PBS and plated onto THA plates in duplicate. CFUs were counted after overnight incubation at 37°C, and percentage survival was calculated and compared to inoculum.

Growth curves. Bacteria were grown overnight in Todd Hewitt-Broth (THB), diluted 1:100 the next morning and grown until they reached logarithmic phase. The bacteria were diluted again to OD_{660} 0.01 and placed in 96-wells flat bottom plates in 150 μl volume, 4 wells per strain. Absorbance at OD_{660} was measured in a plate reader (Fluostar Omega, BMG Labtech) every 10 minutes at 37°C with 600 RPM intermittent shaking.

SI FIGURES & TABLES

Supplemental Figure 1: Identification of SPIN as a potential staphylococcal evasion protein. (**A**) Output from phages of secretome phage display after four rounds of selection against granular proteins of neutrophils showed enrichment of hypothetical open reading frame NWMN_0402. (**B**) Gene distribution of *S. aureus* genomic island α. The *spn* gene is located in the middle, downstream of the *staphylococcal superantigen-like* (*ssl*) cluster with the coding sequence orientated in the reverse direction. Proteins indicated in grey have an unknown function. (**C**) Genomic region of Giα (also known as νSaα) is compared between *S. aureus* strains Newman (clonal complex (CC)8), MW2 (CC1), N315 (CC5), 5096 (CC22) and MRSA252 (CC30) using the Artemis Comparison Tool. Red blocks are indicative of homology between strains. GIα, SPIN (NWMN_0402) and the proteins encoded by genes in GIα are indicated at the top of the figure; these genes encode SSL proteins, type I restriction-modification system modification (HsdM) and specificity (HsdS) subunits and lipoproteins. (**D**) Amino acid sequence alignment of SPIN with signal sequence from Newman strain to 88 isolates, clustered by their clonal complex. The clonal complexes are both of human and animal origin (CC130, CC151, CC398, CC425, CC1173 are animal associated and indicated in blue). The Cleavage site that yields the mature protein is located between ADA-KV, and is indicated by a black line. Red indicates homology and the secondary structure of SPIN is indicated on top. (**E**) Anti-SPIN titers were determined from 20 healthy laboratory workers and compared to anti-CHIPS and anti-SEI titers by ELISA. Five donors for anti-SEI titers were below the detection limit. The values represent the logarithmic of the dilution factor that gave an OD_{450} of 0.2 after subtraction of the background. Each dot represents one individual in one experiment. Graph is representative of two trials.

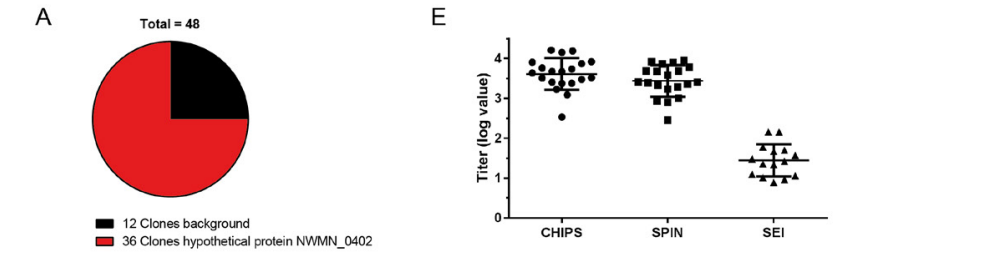
A
Total = 48
12 Clones background
36 Clones hypothetical protein NWMN_0402
E
Titer (log value)
CHIPS
SPIN
SEI

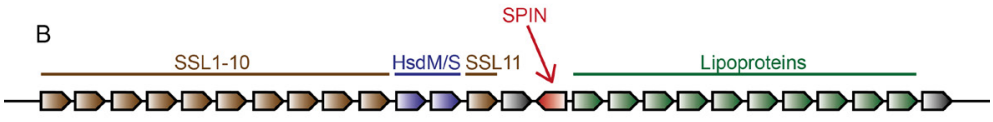
B
SPIN
SSL1-10
HsdM/S SSL11
Lipoproteins

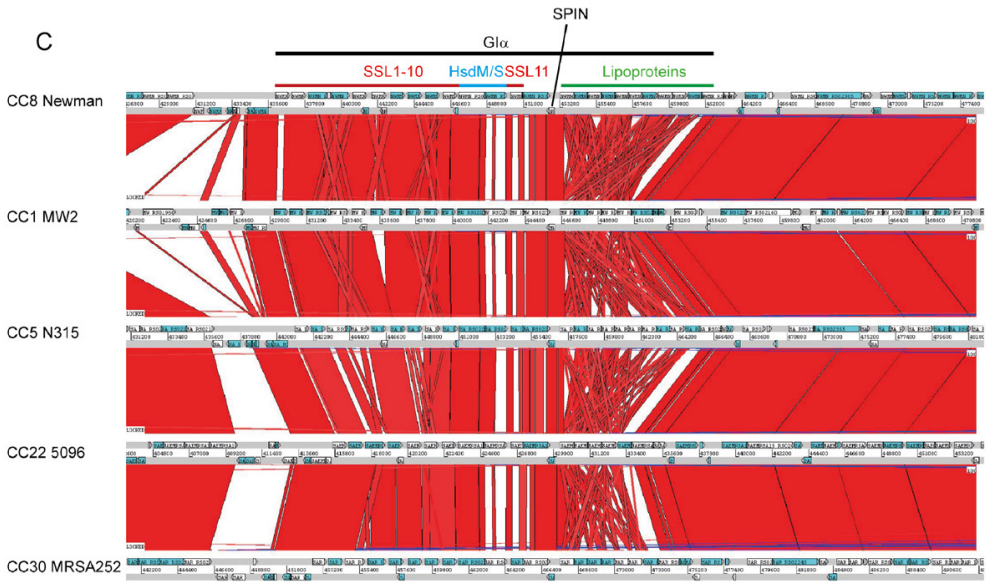
C
SPIN
Glα
SSL1-10
HsdM/SSSL11
Lipoproteins
CC8 Newman
CC1 MW2
CC5 N315
CC22 5096
CC30 MRSA252

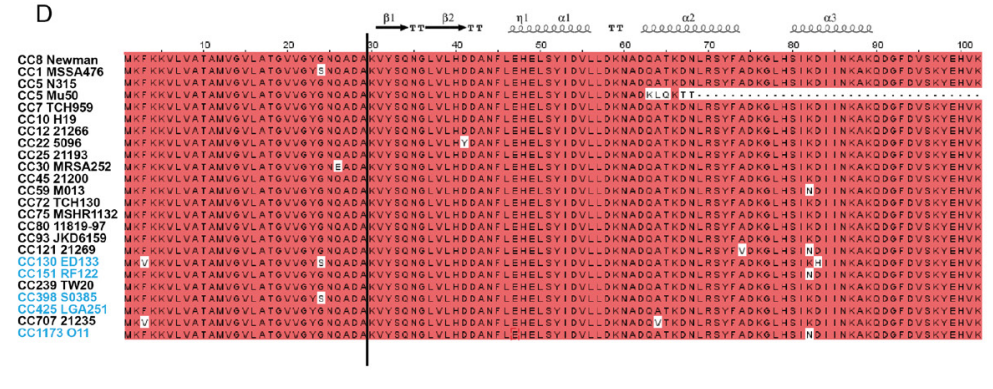
D
CC8 Newman
CC1 MSSA476
CC5 N315
CC5 Mu50
CC7 TCH959
CC10 H19
CC12 21266
CC22 5096
CC25 21193
CC30 MRSA252
CC45 21200
CC59 M013
CC72 TCH130
CC75 MSHR1132
CC80 11819-97
CC93 JKD6159
CC121 21269
CC130 ED133
CC151 RF122
CC239 TW20
CC398 S0385
CC425 LGA251
CC707 21235
CC1173 O11

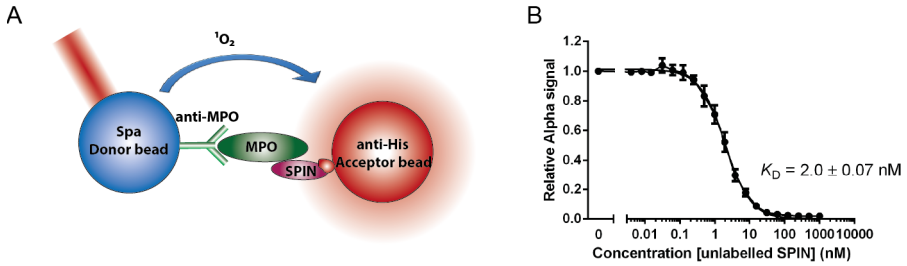

Supplemental Figure 2: Determining K_D of SPIN to MPO by AlphaScreen equilibrium competitive binding assay. An Alpha equilibrium binding signal was observed by capturing MPO via antibodies to Protein-A donor beads and using C-His SPIN bound to anti-His acceptor beads (**A**). A concentration series of untagged SPIN was used to compete for MPO binding and a K_D of 2 ± 0.07 nM was derived from non-linear curve-fitting (**B**).

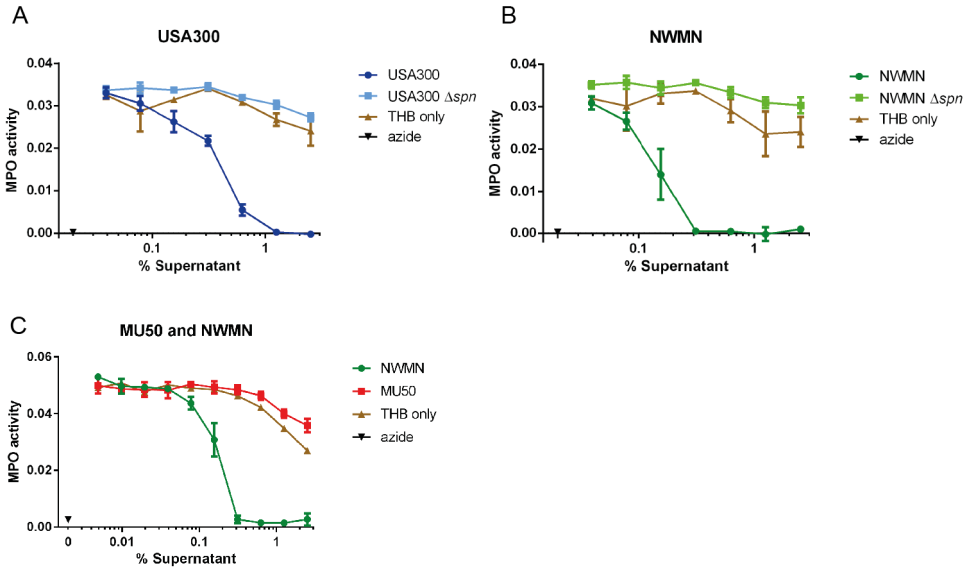

Supplemental Figure 3: MPO activity from overnight culture supernatant of different *S. aureus* strains. (**A and B**) Supernatant from USA300 (**A**) or Newman (**B**) overnight culture was diluted and pre-incubated with native MPO. WT strains show inhibition of MPO whereas the KO strains (Δ*spn*) do not. (**C**) Truncated SPIN of MU50 doesn't inhibit MPO. MPO activity from supernatant of MU50 is on the THB control line. The lines of THB, Mu50, and both KOs show background inhibition at high concentration due to the colour of the undiluted THB. Sodium azide is used as a positive control for complete MPO inhibition. Bars express SD with N=3.

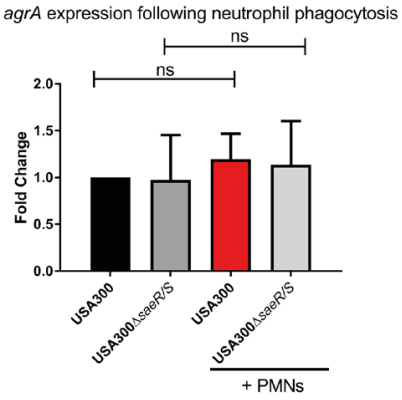

Supplemental Figure 4: Analysis of agrA expression following exposure to human neutrophils. Bars express SD with N=3. Statistical significance was determined using one-way ANOVA.

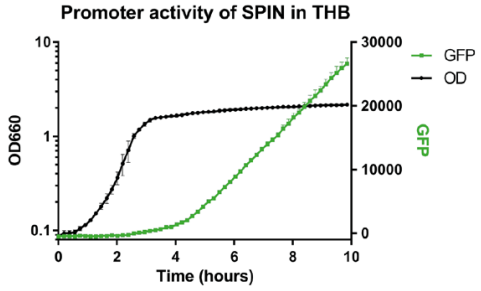

Supplemental Figure 5: Promoter expression of SPIN after 2 hours in THB culture. Bacteria were grown overnight in THB where GFP fluorescence and absorbance at OD_{660} was both measured in 10 minutes intervals, GFP signal was subtracted from the background of USA300 WT strain. The promoter of SPIN is activated after 2 hours, when bacteria are within the late exponential phase. Data are representative of three independent experiments with duplicate measurements.

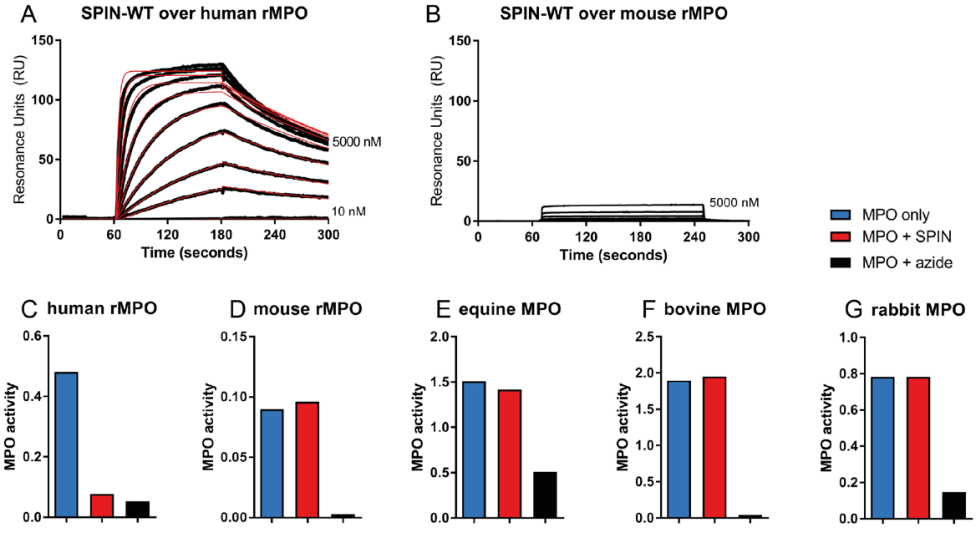

Supplemental Figure 6: SPIN does not inhibit murine, bovine, equine, or rabbit MPO. (**A and B**) Direct binding of SPIN to human recombinant MPO (rMPO) (**A**) and mouse rMPO (**B**) determined by SPR. SPIN is able to bind to human rMPO, but not to mouse rMPO. (**C**) SPIN inhibits human rMPO. 'MPO only' shows MPO activity, adding 1 µg/ml SPIN inhibits the activity of MPO similar to azide control. (**D**) SPIN cannot inhibit mouse rMPO. Adding 50 µg/ml SPIN does not change the activity. Azide is able to completely inhibit the activity of the mouse rMPO. (**E-G**) SPIN cannot inhibit bovine, equine, and rabbit MPO. Neutrophils from cow, horse, and rabbit were lysed and incubated with 10 µg/ml SPIN (cow and horse) or 9 µg/ml SPIN (rabbit).

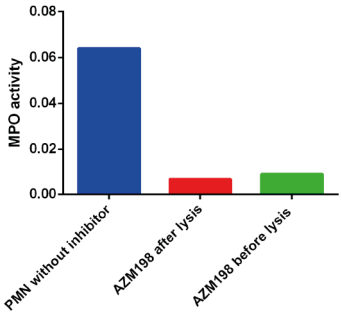

Supplemental Figure 7: MPO inhibitor AZM198 is able to cross neutrophil membrane and inhibit intracellular MPO. PMN lysate without the inhibitor shows MPO activity. PMNs incubated with 10 µM inhibitor for 1 hour at room temperature, washed and then lysed, are devoid of MPO activity. The activity was comparable to samples which were incubated with the inhibitor after lysis. Thus the MPO inhibitor AZM198 crosses the neutrophil membrane and is suitable to use for bactericidal assays to test the MPO-dependent killing of bacteria.

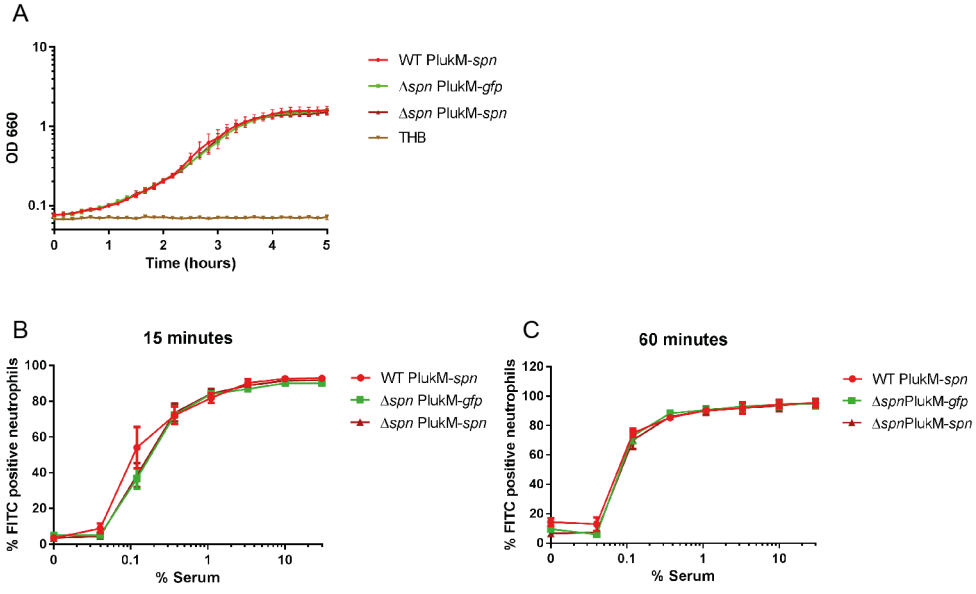

Supplemental Figure 8: No difference in growth or phagocytosis between mutant strains WT PlukM-*spn*, Δ*spn* PlukM-*gfp*, and Δ*spn* PlukM-*spn*. (**A**) Newman mutants show growth with similar kinetics in THB. Absorbance at OD_{660} was measured every 10 minutes. (**B and C**) No difference in phagocytosis of WT PlukM-*spn*, Δ*spn* PlukM-gfp, and Δ*spn* PlukM-*spn* by neutrophils. The three Newman strains were labelled with FITC, washed and treated with indicated dilutions of NHS. The percentage FITC positive neutrophils was measured after 15 or 60 minutes of phagocytosis by FACS. All strains were phagocytosed by neutrophils at comparable levels. Bars express SD with N=3 for **A-C**.

Supplemental Table 1: Data collection and refinement statistics (molecular replacement)

	SPIN/MPO
Data collection	
Space group	C 1 2 1
Cell dimensions	
a, *b*, *c*, Å	129.03 92.94 80.39
α, β, γ, °	90 120.14, 90
Resolution, Å	43.34-2.40 (2.49-2.40)
R_{pim}	0.056 (0.357)
$I/\sigma I$	14.1 (2.0)
Completeness, %	99.8 (98.3)
Redundancy	7.5 (6.4)
Refinement	
Resolution, Å	43.34-2.40
No. reflections	31,961
R_{work} / R_{free}	18.4/24.1
No. atoms	
Protein	5,171
Ligand/ion	85
Water	169
B-factors	
Protein	49.59
Ligand/ion	39.34
Water	45.03
Rmsd	
Bond lengths, Å	0.004
Bond angles, °	0.605

Supplemental Table 2: Primers used in this study

Primer	Sequence
spn_NotI_stopcodon_fwd	5′-ATATGCGGCCGCTTATTTTACGTGTTCATATTTTG-3′
spn_NotI_fwd	5′-ATATGCGGCCGCTTTTACGTGTTCATATTTTG-3′
spn_enterokinase_BamHI_rvs	5′-CGGGATCCGACGATGACGACAAGAAAGTTTATTCTCAAAATGGAC-3′
spn_BamHI_rvs	5′-CGGGATCCAAAGTTTATTCTCAAAATGGAC-3′
PSPIN_XbaI_fwd	5′-ATCGTCTAGAATTCTCTTTTACGTTACCAAAATATACATATAC-3′
PSPIN_KpnI_rvs	5′-ATTAAGGTACCTAACTCCATCATAACACTGAATATTAAGAAAAT-3′
KO_Gibson_EcoRI_UP_fwd	5′-GAGGCCCTTTCGTCTTCAAGAATTCCCTACAGAACTGCCTTTCAG-3′
KO_Gibson_KpnI_DN_rvs	5′-GACTCTAGAGGATCCCCGGGTACCAAAAGATGGACATCACCAAG-3′
KO_UP_rvs	5′-GCATTATTGAATATCTATCACTCCTCTAAAAATTG-3′
KO_DN_fwd	5′-AGAGGAGTGATAGATATTCAATAATGCTTTGTAAC-3′
pLukM_spn_rvs	5′-GCTACTAAAACCTTTTTAAATTTCATAGTTTCACTTTCTTTCTCTTTATA-3′
pLukM_spn_fwd	5′-TATAAAGAGAAAGAAAGTGAAACTATGAAATTTAAAAAGGTTTTAGTAGC-3′
pCM29_pLukM_fwd	5′-CATGCCTGCAGGTCGACTCTAGAAAACGCGCAGTTAATAAAAAG-3′
spn_pCM29_rvs	5′-GAAACAGCTATGACATGATTACGAATTCTTATTTTACGTGTTCATATTTTG-3′
spn_qPCR_fwd	5′-GATGATGCAAACTTCTTAGAACATGAATTAAGT-3′
spn_qPCR_rvs	5′-GTCCTTTATCGGCGAAGTATGATCT-3′
spn_qPCR_probe	5′-CTTGGTCAGCATTCTT-3′
agrA_qPCR_fwd	5′-GTTACGAGTCACAGTGAACTTACCT-3′
agrA_qPCR_rvs	5′-CGAGTTCTTAATTCAGCTGGATCATCT-3′
agrA_qPCR_probe	5′-CATCGCTGCAACTTT-3′
gyrB_qPCR_fwd	5′-CGCACGTACAGTGGTTGAAAA-3′
gyrB_qPCR_rvs	5′-CGTGTTACTTCACGCGCTT-3′
gyrB_qPCR_probe	5′-ACGTGCCGCCATAATA-3′

Restriction sites are underlined.

Chapter 5

A Structurally Dynamic N-terminal Region Drives Function of the Staphylococcal Peroxidase Inhibitor (SPIN)

Nienke W. M. de Jong[1,*], Nicoleta T. Ploscariu[2,*], Kasra X. Ramyar[2], Brandon L. Garcia[2], Alvaro I. Herrera[2], Om Prakash[2], Benjamin B. Katz[2], Kevin G. Leidal[3], William M. Nauseef[3,†], Kok P. M. van Kessel[1], Jos A. G. van Strijp[1], and Brian V. Geisbrecht[2]

[1] Department of Medical Microbiology, University Medical Center Utrecht, Utrecht University, Utrecht, the Netherlands

[2]Dept. of Biochemistry & Molecular Biophysics, Kansas State University, Manhattan, KS 66506, USA

[3] Inflammation Program, Department of Internal Medicine, Roy J. and Lucille A. Carver College of Medicine University of Iowa

[†]Veterans Administration Medical Center, Iowa City, IA 52240

* equal contribution

J Biol Chem. 2018 Jan 5. pii: jbc.RA117.000134. doi: 10.1074/jbc.RA117.000134

ABSTRACT

The heme-containing enzyme myeloperoxidase (MPO) is critical for optimal antimicrobial activity of human neutrophils. We recently discovered that the bacterium *Staphylococcus aureus* expresses a novel immune evasion protein, called SPIN, that binds tightly to MPO, inhibits MPO activity, and contributes to bacterial survival following phagocytosis. A co-crystal structure of SPIN bound to MPO suggested that SPIN blocks substrate access to the catalytic heme by inserting an N-terminal β-hairpin into the MPO active site channel. Here, we describe a series of experiments that more completely define the structure/function relationships of SPIN. Whereas the SPIN N-terminus adopts a β-hairpin confirmation upon binding to MPO, solution NMR studies presented here are consistent with this region of SPIN being dynamically structured in the unbound state. Curiously, while the N-terminal β-hairpin of SPIN accounts for ~55% of the buried surface area in the SPIN/MPO complex, its deletion did not significantly change the affinity of SPIN for MPO but did eliminate the ability of SPIN to inhibit MPO. The flexible nature of the SPIN N-terminus rendered it susceptible to proteolytic degradation by a series of chymotrypsin-like proteases found within neutrophil granules, thereby abrogating SPIN activity. Degradation of SPIN was prevented by the *S. aureus* immune evasion protein Eap, which acts as a selective inhibitor of neutrophil serine proteases. Together, these studies provide insight into MPO inhibition by SPIN and suggest possible functional synergy between two distinct classes of *S. aureus* immune evasion proteins.

INTRODUCTION

Neutrophils are the most abundant white blood cells in human circulation and key players in the first line defense against invading bacteria (1). Upon activation, neutrophils phagocytose pathogens whereby their various intracellular granules fuse with the maturing phagosome (2,3). Neutrophils' azurophilic granules (sometimes referred to as primary granules) contain high concentrations of antibacterial peptides and proteins/enzymes. The most abundant component of azurophilic granules is the enzyme myeloperoxidase (MPO). In the presence of halides, MPO converts hydrogen peroxide (H_2O_2) into bactericidal hypohalous acids, such as HOCl and HOBr (4). Azurophilic granules also contain high concentrations of chymotrypsin-like proteases (NSPs), which can directly attack certain bacterial cells and/or the secreted and surface-retained proteins these cells produce (5-7). Although the activites of MPO and NSPs are typically viewed as independent entities, some studies have indicated that these two systems have synergistic effects with one another inside the phagosome (8). Thus, the concerted action of MPO and NSPs forms a foundation of neutrophil-mediated defense against potentially infectious bacteria.

Invading pathogens are subjected to a nearly instantaneous assault by their host's innate immune system. As a consequence, there is heavy selective pressure for these organisms to evolve the molecular wherewithal that provides for escape from the innate immune response. While extensive study of various pathogens has cataloged an array of these so-called immune evasion strategies, the Gram-positive bacterium *Staphylococcus aureus* appears to be particularly adept at attempting to block the events that lead to its opsonization with complement components and subsequent phagocytosis by neutrophils (9-12). Recent work has shown that a portion of those *S. aureus* cells that undergo phagocytosis survive, leading to speculation that these leukocytes might serve as "Trojan Horses" for bacterial dissemination *in vivo* (13). For this to be the case, we believe that *S. aureus* is engaged in an elaborate immune evasion program that acts intracellularly, and likely within the maturing phagosome. Indeed, our discovery of *S. aureus* extracellular adherence proteins (EAPs) as highly selective NSP inhibitors that promote virulence is consistent with this hypothesis (14).

We recently deployed a phage display strategy to identify secreted *S. aureus* proteins that interact with putative evasion targets found within neutrophils (15). Since MPO is the most abundant component of azurophilic granules (4,16), it represented an promising initial candidate for this approach. We succeded in identifying a novel protein of 8.4 kDa that binds and inhibits human MPO and named it SPIN, for Staphylococcal Peroxidase INhibitor (17). Gene expression studies revealed that spn transcription is upregulated following phagocytosis of *S. aureus* cells by neutrophils, suggesting that the SPIN protein operates primarily within the phagosomal compartment (17). Through subsequent studies, we found that SPIN protects *S. aureus* from MPO-mediated killing and thereby established SPIN as a novel immune evasion

protein of *S. aureus* (17).

SPIN shows no sequence similarity to other characterized proteins, which initially prevented understanding of its effects on MPO. To circumvent this limitation, we solved a 2.4 Å resolution crystal structure of SPIN bound to a recombinant form of human MPO (i.e. rMPO) (17). This structure suggested that SPIN acts by occluding the exchange of substrate, product, and bulk solvent with the reactive heme that lies the within the MPO active site. While a majority of the SPIN protein adopts a three α-helical bundle fold (**Supplemental Figure 1**), inspection of the crystal structure suggested that this helical bundle might not be responsible per se for inhibiting MPO. Instead, an approximately 10-residue extension at the SPIN N-terminus assumes a β-hairpin structure which almost completely occupies the MPO active site channel (17). Further examination of the SPIN structure suggested that this N-terminal β-hairpin might not be intrinsically stable in the absence of its MPO ligand, however, as it lacks features such as disulfide bonds, etc., that would constrain these two short β-strands into their MPO-bound conformation.

In this report, we present the outcome of a series of experiments designed to assess the structure/function relationships of SPIN. We initially carried out a solution NMR study to characterize the SPIN N-terminus in the absence of MPO. We then prepared and characterized a panel of deletion and site-directed mutants of SPIN to define the contributions of its two discrete regions in MPO binding and inhibition. Together, our results suggest that the SPIN N-terminus is dynamically structured in the absence of MPO, but is absolutely required to inhibit MPO activity even though it contributes only modestly to binding. Intriguingly, we found that the SPIN N-terminus is suspectible to site-specific proteolysis by NSPs, but protected in the presence of an *S. aureus* EAP protein. This suggests that functional synergy may exist between these two distinct classes of intracellularly-acting innate immune evasion proteins. Collectively, our data provide insights into SPIN structure/function relationships, and deepen our appreciation of the biomolecular events that underlie *S. aureus* innate immune evasion.

RESULTS

The N-terminal Region of SPIN is Dynamically Structured in the Absence of MPO

Although we previously solved a 2.4 Å resolution crystal structure of SPIN bound to rMPO, our attempts to crystallize SPIN on its own were unsuccessful. We therefore explored solution NMR spectroscopy as an alternative approach to obtain insight into the structure of SPIN in its unbound state. Since the ^{1}H-^{15}N HSQC spectrum of isotopically-enriched SPIN exhibited excellent dispersion (**Supplemental Figure 2**), we collected a standard suite of two- and three-dimensional NMR spectra to permit assignment of the SPIN backbone resonances (18). Initially, 97% of the resonances identified in the ^{1}H-^{15}N HSQC spectrum collected at 700

MHz were assigned, leaving only those arising from Phe[48] and Leu[49] unaccounted for. These chemical shift assignments have been deposited in the BioMagResBank (accession number 27069), and are described elsewhere (18).

We used the TALOS-N platform to calculate the secondary structure of SPIN on the basis of backbone chemical shift values (19), and additionally determined both the longitudinal (R_1) and transverse (R_2) relaxation rates for the backbone resonances assigned in the ^{1}H-^{15}N HSQC spectrum (**Figures 1A-C**). Since the relaxation data were recorded on an 500 MHz spectrometer, we collected an additional ^{1}H-^{15}N HSQC spectrum at this lower field strength; due to the decreased resolution at 500 MHz, the resonances of Gln[37] and Glu[50] were no longer detected. From these data, we inferred that the four unassigned residues from the SPIN backbone (i.e. Gln[37], Phe[48], Leu[49], and Glu[50]) are all located within an apparently flexible region that comprises the N-terminus up to the start of the first α-helix (i.e. His[51]-Asp[61]). For internally rigid proteins, the values of R_1 and R_2 are expected to have homogeneous values. However, we found that the N-terminal residues of SPIN displayed higher and lower values for R_1 and R_2, respectively, when compared to the entire protein on average. For these parameters, deviation from the average is often associated with sites that present backbone flexibility and undergo fast internal dynamics (20). In the case of SPIN, the overall average value for R_1 was 2.49±0.58 with a value of 2.90±0.78 for the N-terminal region, while R_2 rates overall averaged 8.97±1.29 with a value of 7.64±1.33 in the N-terminal region. Similarly, the overall average value of R_2/R_1 was 3.72±0.73, while residues in the N-terminal region averaged 2.76±0.59.

To gain further insight into the solution structure of SPIN, we also collected three-dimensional HCCONH, CCCONH, HCCH-TOCSY, ^{15}N HSQC-TOCSY and ^{15}N-edited NOESY spectra to facilitate sidechain assignments. These efforts resulted in assignment of 95% of the $^{13}C\alpha$ resonances and 92% of the $^{13}C\beta$ resonances for SPIN (18). We compared the chemical shift index (CSI) values for these SPIN resonances to the BMRB statistical database values for CSI (**Figures 1D-E**). For these parameters, residues that approach a neutral CSI value are associated with a random-coil like structure (21); residues within α-helical structure have positive values for Cα and negative values for Cβ, while residues within β-strands are characterized by negative values for Cα and positive values for Cβ (21). Significantly, the CSI variance for residues in the SPIN N-terminal region was markedly lower than that of the protein overall, and was consistent with the absence of regular secondary structure.

Finally, we used the CS-Rosetta server to calculate an ensemble of 40,000 three-dimensional structural models compatible with the SPIN chemical shift data. Comparison of the entire ensemble versus the lowest-energy structure gave an RMSD of 1.13±0.32 Å. When we carried out similar calculations using an option where flexible regions were truncated automatically (i.e. residues 33-53), the RMSD of the ensemble relative to the lowest-energy structure was 0.80±0.16 Å. Superposition of this lowest-energy model onto the structure of MPO-bound SPIN (17) yielded an RMSD of 1.47 Å for all backbone atoms, and demonstrated otherwise

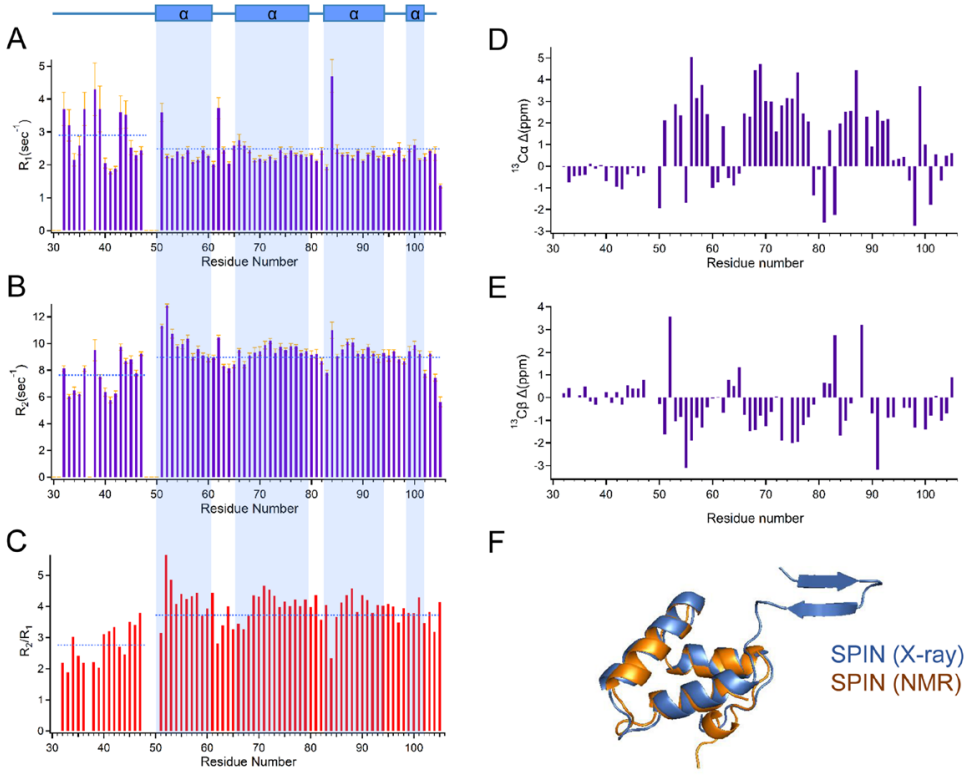

Figure 1: The N-terminal Region of SPIN is Dynamically Structured in the Absence of Ligand. NMR spectroscopy was used to characterize the solution structure of SPIN in the absence of MPO. A series of solution dyanmics studies were performed following assignment of the resonances identified in a ^{1}H-^{15}N HSQC spectrum of isotopically-enriched SPIN. A summary of ^{15}N (**A**) longitudinal (R_1) relaxation time constants, (**B**) transverse (R_2) relaxation time constants, and (**C**) R_2/R_1 values are presented as a measure of site-specific rotational diffusion motion. The highlighted regions (light blue) illustrate the TALOS-N prediction of SPIN secondary structure in the free form based upon NMR chemical shift data, as represented above the top of panel in rectangular boxes (alpha helical regions). The mean value for each parameter (R_1, R_2, or R_2/R_1) for residues within either the N-terminal region or the protein overall is represented a dashed blue line. Chemical Shift Index variance plots for (**D**) Cα and (**E**) Cβ resonances, respectively. The values were calculated as the difference between the experimentally determined chemical shift and BMRB statistical chemical shift values for residues found in unstructured regions. (**F**) Three-dimensional superposition of MPO-bound SPIN and a chemical shift-derived model for SPIN in the solution state. The model in blue represents the bound form of SPIN as determined by the SPIN/rMPO crystal structure, while the model in orange represents the structure of SPIN calculated by the Chemical Shift Rosetta server derived from solution NMR measurements.

good agreement between structural data obtained for the α-helical bundle region SPIN in solution versus the crystalline form (**Figure 1F**). In summary, while SPIN in the bound state displays a β-hairpin structure at its N-terminus, our studies presented here strongly suggest that this region is dynamic and has a random coil character prior to MPO binding.

The N-terminal Region of SPIN is Dispensable for MPO Binding

The crystal structure of SPIN bound to rMPO buries approximately 1600 Å^2 of SPIN surface area (17), as judged by the EBI-PISA server (22). Although the SPIN/rMPO interface is contiguous on the SPIN surface, it is useful for purposes of analysis to consider it comprised of two distinct binding sites (17). The first site accounts for ~45% of the buried SPIN surface area and is derived from residues within the α-helical bundle; the second binding site accounts for the remaining ~55% of buried SPIN surface area and arises from residues within the N-terminal β-hairpin (17). The number of potential hydrogen bonds and salt bridges at the SPIN/rMPO interace is distributed roughly equally across these two binding sites, although the α-helical bundle appears to contribute more hydrogen bonds and the β-hairpin seems to predominate in salt bridges. Given the inconclusive nature of this interface analysis, we determined that structural information alone could not be used to establish which binding site was more important to forming and/or maintaining the SPIN/MPO interaction. However, since the N-terminal β-hairpin of SPIN does not appear to form until after MPO binding has occurred (**Figure 1**), we hypothesized that the α-helical bundle site might be of primary importance in initially binding to MPO.

To test this hypothesis, we prepared and characterized both a deletion and site-directed mutant that altered the SPIN N-terminus (**Supplemental Figures 1 and 2**). The deletion mutant removed the entire N-terminal region, and consisted of residues Ala^{46}-Lys^{105} inclusive (i.e. SPIN$^{46\text{-}105}$). The site-directed mutant was prepared to assess the contributions of His^{43}, Asp^{44}, and Asp^{45}, and exchanged each of these residues for Ala in the full-length SPIN background (i.e. SPIN$^{43\text{-}45\rightarrow AAA}$). These residues are essentially invariant across SPIN sequences from non-aureus *Staphylococcus spp.* and also form polar interactions with MPO sidechains in the SPIN/rMPO co-crystal structure (17).

Table 1: Surface Plasmon Resonance Assessment of SPIN Proteins Binding to Various Forms of MPO

Analyte	Surface	K_D (nM)	k_{on} ($M^{-1}s^{-1}$)	error k_{on} ($M^{-1}s^{-1}$)	k_{off} (s^{-1})	error k_{off} (s^{-1})	χ^2
SPIN	Native MPO	9.3	$5.37*10^5$	$3.5*10^3$	$4.99*10^{-3}$	$3.0*10^{-5}$	0.148
SPIN	Human rMPO	11.8	$4.46*10^5$	$1.5*10^3$	$5.24e*10^{-3}$	$1.5*10^{-5}$	0.128
SPIN$^{46\text{-}105}$	Native MPO	29.8	$6.19*10^5$	$2.3*10^3$	$1.85*10^{-2}$	$3.0*10^{-5}$	0.102
SPIN$^{46\text{-}105}$	Human rMPO	35.1	$4.30*10^5$	$1.2*10^3$	$1.51*10^{-2}$	$2.0*10^{-5}$	0.067
SPIN$^{43\text{-}45\rightarrow AAA}$	Native MPO	31.4	$5.27*10^5$	$3.3*10^3$	$1.65*10^{-2}$	$1.0*10^{-4}$	0.170
SPIN$^{43\text{-}45\rightarrow AAA}$	Human rMPO	32.6	$4.88*10^5$	$1.2*10^3$	$1.59*10^{-2}$	$1.8*10^{-5}$	0.043

We examined the ability of these SPIN mutants to bind both native MPO and recombinant human MPO (rMPO) using a surface plasmon resonance approach (**Figure 2A-C**). We found that SPIN$^{46\text{-}105}$ is approximately 3.2-fold weakened in its affinity for native human MPO relative to full-length SPIN (**Table 1**). Similarly, SPIN$^{43\text{-}45\rightarrow AAA}$ is 3.4-fold diminished in its affinity for native human MPO (**Table 1**). For both mutants, the decreased affinity for MPO was associated

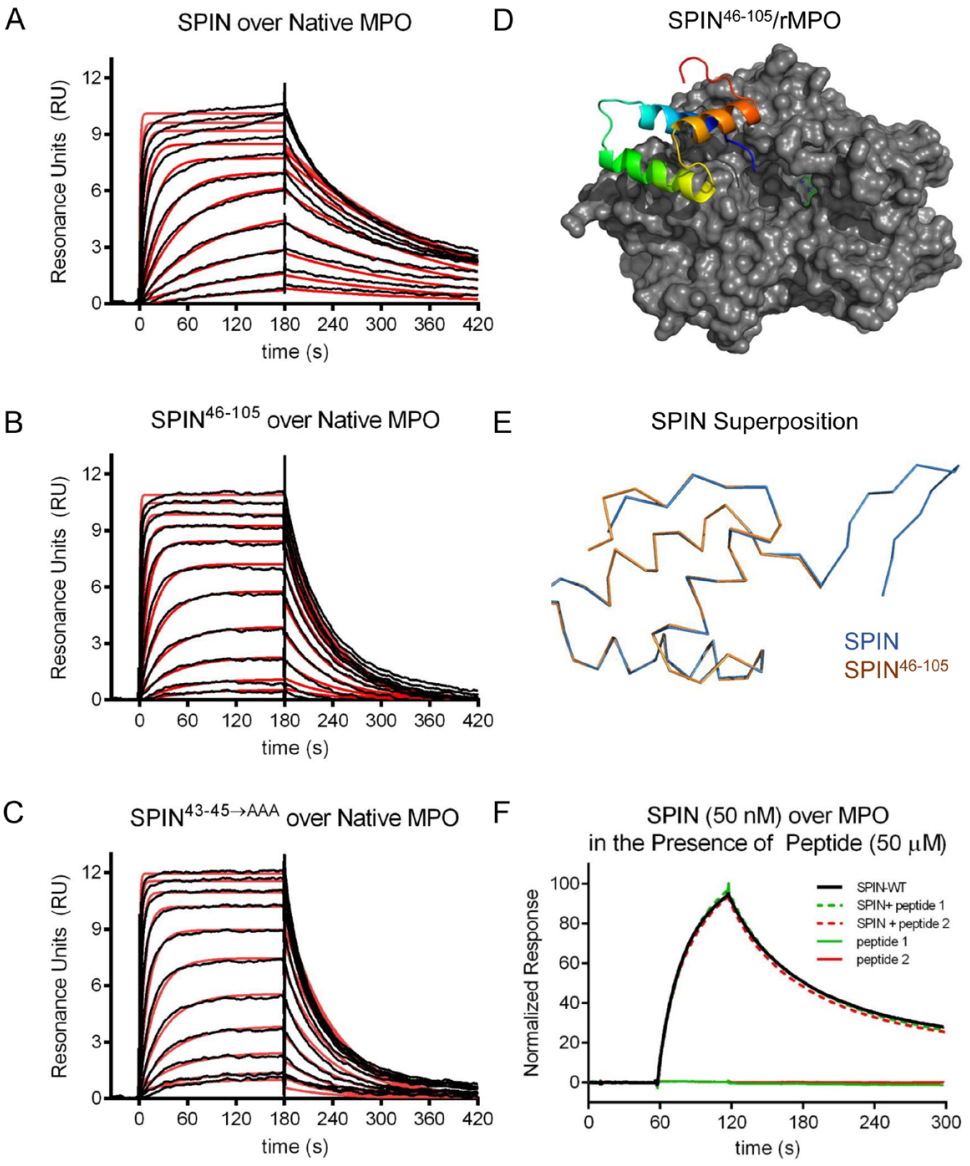

Figure 2: The N-terminal region of SPIN is dispensable for binding to MPO. The ability of SPIN proteins and SPIN-derived peptides to bind MPO was examined using a combination of biochemical and structural methods. A two-fold dilution series of SPIN proteins ranging from 1.35 to 2000 nM was injected over a biosensor surface of prepared from randomly immobilized MPO. Representative sensorgram series are shown for native MPO binding to (**A**) full-length SPIN, (**B**) SPIN$^{46\text{-}105}$, and (**C**) SPIN$^{43\text{-}45\rightarrow AAA}$. Additional curve fitting and analysis parameters are presented in **Table 1**. (**D**) Representation of a 2.3 Å resolution co-crystal structure of SPIN$^{46\text{-}105}$ bound to a recombinant form of human MPO. SPIN$^{46\text{-}105}$ is depicted as a ribbon diagram and is colored with its N-terminus in blue and its C-terminus in red, while MPO is rendered as a grey surface. The location of the MPO active site heme is indicated by a green ball-and-stick for the purposes of reference. (**E**) Superposition of the MPO-bound forms of SPIN$^{46\text{-}105}$ and full-length SPIN, as judged by X-ray crystallography. Proteins are depicted as wire diagrams,

where the N-terminal β-hairpin of full-length SPIN is shown at the top right of the panel. (**F**) The MPO binding properties of two different synthetic peptides corresponding to SPIN N-terminal region were assessed by SPR. Peptide binding was investigated using both a direct binding approach (single injection at 50 μM) and through a competition format where peptides were co-injected along with SPIN (50 nM). Neither approach showed any evidence for binding between these peptides and MPO. A representative sensorgram series is shown.

with an enhanced dissociation rate of the complex relative to wild-type SPIN. Nevertheless, these mutants still bind MPO with low nanomolar K_D values near 30 nM, and retain the potent MPO-binding capacity intrinsic to wild-type SPIN (17). This latter feature is reflected in a 2.3 Å resolution crystal structure of $SPIN^{46-105}$ bound to rMPO, which we solved and refined to Rwork/Rfree values of 17.9 and 22.9%, respectively (**Figure 2D and Supplemental Table 1**). In this regard, the structure of $SPIN^{46-105}$/rMPO is largely indistinguishable from SPIN/rMPO, as the Cα positions from the two models superimpose upon one another with an RMSD of 0.16 Å (**Figure 2E**).

Our studies with these SPIN mutants indicated that the N-terminal region of SPIN is dispensable for MPO binding. However, to examine this issue through an alternative approach, we synthesized two short peptides designed to mimic the SPIN N-terminus (**Supplemental Figure 1**). The first such peptide corresponded to the 13 N-terminal-most residues of SPIN (i.e. SPIN-p1), flanked by two Ser residues. The second contained the same residues as the first, plus a pair of Cys at the respective termini (i.e. SPIN-p2) that were oxidized to constrain the peptide into the β-hairpin conformation adopted by this region in the SPIN/rMPO crystal structure (17). Due to the small size of these peptides, we examined their MPO binding properties through both conventional SPR methods as well as a competition-based assay wherein wild-type SPIN would be impeded from binding to the immobilized MPO surface. We found that neither SPIN-p1 nor SPIN-p2 gave evidence for direct or competitive binding to MPO at concentrations up to 50 μM (**Figure 2F**). Thus, the experiments with these synthetic peptides were consistent with our mutagenesis and crystallographic studies in defining the α-helical region as the primary MPO binding site of SPIN.

The N-terminal Region of SPIN is Necessary, but Not Sufficient for Inhibition of MPO

Whereas the SPIN N-terminus could be removed from the protein with only an ~3-fold loss of affinity for MPO, the SPIN/rMPO crystal structure suggests that this region of SPIN likely makes important contributions to inhibition of MPO (17). Moreover, while the α-helical region of SPIN is responsible for MPO binding (**Figure 2 and Table 1**), it remained unknown if this portion of SPIN retained any MPO inhibitory capacity on its own. To investigate these questions, we characterized our SPIN mutants using an MPO activity assay wherein H_2O_2 reduction was linked to oxidation of o-dianisidine (17). Since previous analysis of our SPIN mutants showed that they have affinities within the 9-35 nM range for MPO (**Table 1**), we used a single concentration for each potential inhibitor (i.e. 74 nM) sufficiently higher than the K_D to ensure high occupancy of the respective complexes. Whereas full-length SPIN significantly inhibited MPO activity under these conditions, we found that $SPIN^{46-105}$ failed to inhibit MPO

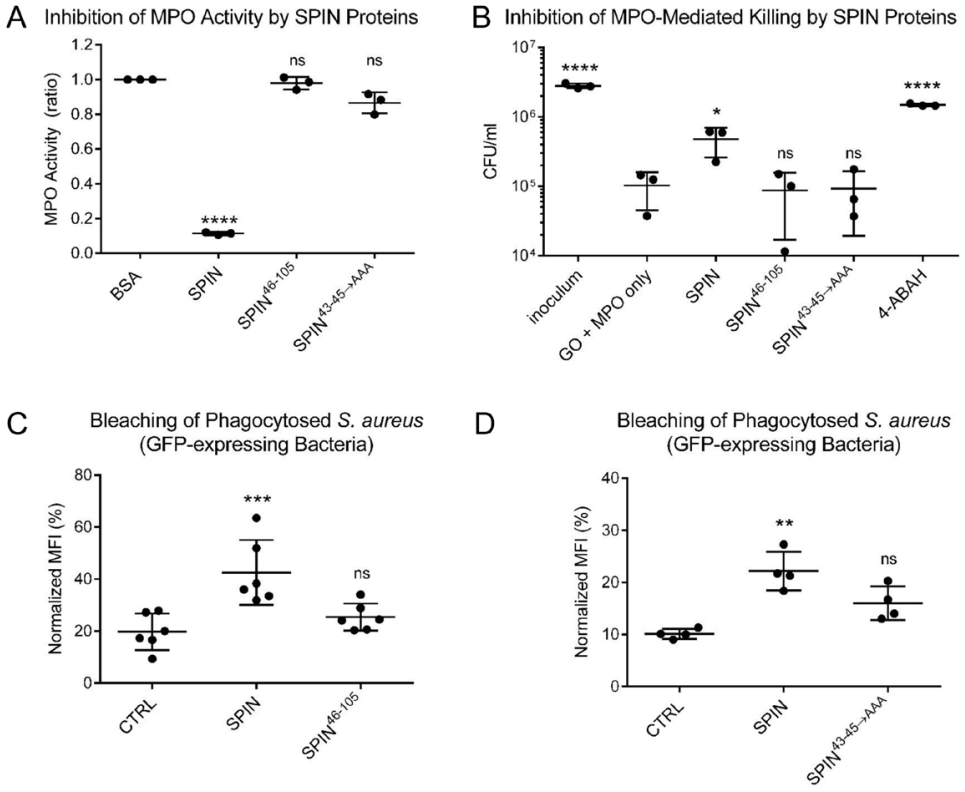

Figure 3: The N-terminal region of SPIN is necessary, but not sufficient for inhibition of MPO. The functional consequences of deletion or mutation within the SPIN N-terminal region were assessed using two independent assay formats. (**A**) The effect of SPIN proteins on MPO activity was investigated using a spectrophotometric assay. Various SPIN proteins (74 nM final concentration) were incubated with MPO for 1 h prior to addition of a substrate mixture. Peroxidase activity was then measured at OD_{450} nm relative to a negative control. Although full-length SPIN inhibits MPO activity, loss of either the entire N-terminus ($SPIN^{46-105}$) or positions 43-45 ($SPIN^{43-45\rightarrow AAA}$) rendered SPIN inactive. Significance relative to the negative control was determined by one-way ANOVA with Dunnett post-test correction for multiple comparison. Bars express SD with N=3. (**B**) The influence of SPIN proteins on a coupled glucose oxidase-MPO system that kills *S. aureus* strain Newman was also investigated. Whereas addition of full-length SPIN protects *S. aureus* from MPO-dependent killing, neither $SPIN^{46-105}$ nor $SPIN^{43-45\rightarrow AAA}$ retained this property, as judged by recovery of CFU counts compared to 'GO+MPO only'. As a control, the MPO inhibitor 4-aminobenzoic acid hydrazide (4-ABAH) also led to *S. aureus* survival. Significance relative to 'GO+MPO only' (a negative control for inhibition) was determined by one-way ANOVA with Dunnett post-test correction for multiple comparison. Bars express SD with N=3. (**C**) *S. aureus* cells constitutively expressing a cytosolic form of GFP were opsonized by human serum and incubated with 50 µM SPIN, 50 µM $SPIN^{46-105}$, or buffer alone (ctrl). The mixture of opsonized bacteria was added to freshly isolated human neutrophils to allow for phagocytosis to occur. The geometric mean of MFI for each sample was determined by flow cytometry at 2 hrs following inception of phagocytosis and normalized to the signal for DPI-treated neutrophils at time zero. Whereas full-length SPIN significantly protected the GFP-expressing *S. aureus* cells from MPO-mediated bleaching, $SPIN^{46-105}$ gave only a slight, though not significant protection against bleaching relative to control. Levels of significance relative to buffer control were determined by one-way ANOVA with Dunnett post-test correction for multiple comparison. Bars express SD with N=6. (**D**) An analogous experiment to that shown in panel **C**, except that the properties of 50 µM SPIN, 50 µM $SPIN^{43-45\rightarrow AAA}$, or buffer alone (ctrl) were compared.

SPIN$^{43\text{-}45\rightarrow AAA}$ gave only a slight, though not significant protection against bleaching relative to control. Levels of significance relative to buffer control were determined by one-way ANOVA with Dunnett post-test correction for multiple comparison. Bars express SD with N=4. Since SPIN$^{46\text{-}105}$ and SPIN$^{43\text{-}45\rightarrow AAA}$ do not inhibit MPO in activity (panel **A**) or killing assays (panel **B**), the signal observed in panels **C** and **D** likely reflects competition between the inactive SPIN protein and GFP for reaction with HOCl generated in the phagosome, thereby blocking bleaching of GFP indirectly. Experiments in panels **C** and **D** are presented separatedly due to variability in the assay, as they were conducted with neutrophils isolated at different times from different donors. * $p \leq 0.05$, ** $p \leq 0.01$, *** $p \leq 0.001$, **** $p \leq 0.0001$, ns (non-significant).

when compared to the negative control, BSA (**Figure 3A**). Intriguingly, SPIN$^{43\text{-}45\rightarrow AAA}$ also failed to block MPO activity, even though it binds MPO with a K_D ~30 nM and has a full length N-terminal region (**Supplemental Figure 1**).

As an independent test of SPIN function, we examined the effects of our mutants in an *in vitro* assay designed to replicate HOCl-dependent killing of bacteria within the phagosomal compartment (17,23). In this model, the enzyme glucose oxidase (GO) is employed as a surrogate H_2O_2-generating system for MPO in lieu of the multipartite NADPH-oxidase that assembles within the phagosomal membrane. Whereas full-length SPIN added in trans increased bacterial survival, neither SPIN$^{46\text{-}105}$ nor SPIN$^{43\text{-}45\rightarrow AAA}$ had any significant influence on the killing of *S. aureus* via bactericidal levels of HOCl generated by MPO (**Figure 3B**). By contrast, the MPO inhibitor 4-ABAH restored the survival of the bacteria to normal levels. A similar trend was also seen in a neutrophil bleaching assay, which measures the loss of fluorescence by GFP-expressing *S. aureus* cells following phagocytosis (24). Here, full-length SPIN added in trans significantly preserved the bacterially-derived GFP signal, while neither SPIN$^{46\text{-}105}$ (**Figure 3C**) nor SPIN$^{43\text{-}45\rightarrow AAA}$ (**Figure 3D**) added at an identical concentration were significantly more effective than buffer control. The slight reduction in bleaching observed for both SPIN$^{46\text{-}105}$ and SPIN$^{43\text{-}45\rightarrow AAA}$ likely resulted from these proteins acting competitively as a target for HOCl, rather than as inhibitors of MPO activity per se (**Figure 3A, C-D**). Together, these results established that the N-terminal region of SPIN is necessary, but not sufficient for blocking MPO activity even though it makes only relatively minor contributions to MPO binding.

The N-terminal Region of SPIN is a Target for Degradation by NSPs

The phagosomal compartment matures in a step-wise fashion following uptake of opsonized bacteria. Early on in this process, azurophilic granules fuse with the phagosome whereby their contents are released into its lumen. This results in the accumulation of high levels of antimicrobial enzymes in the phagosome, with concentrations of MPO estimated to approach 1 mM (25). Concentrations in this range have also been proposed for NSPs (7,26-28), which render the maturing phagosomal compartment not only highly oxidizing, but exceptionally digestive in character. In light of this, the dynamically-structured nature of the SPIN N-terminal region suggested that it might be susceptible to proteolysis. As an initial test of this hypothesis, we treated full-length SPIN with the relatively non-specific protease, subtilisin. Indeed, characterization of the reaction products by SDS-PAGE and MALDI-TOF mass spectrometry

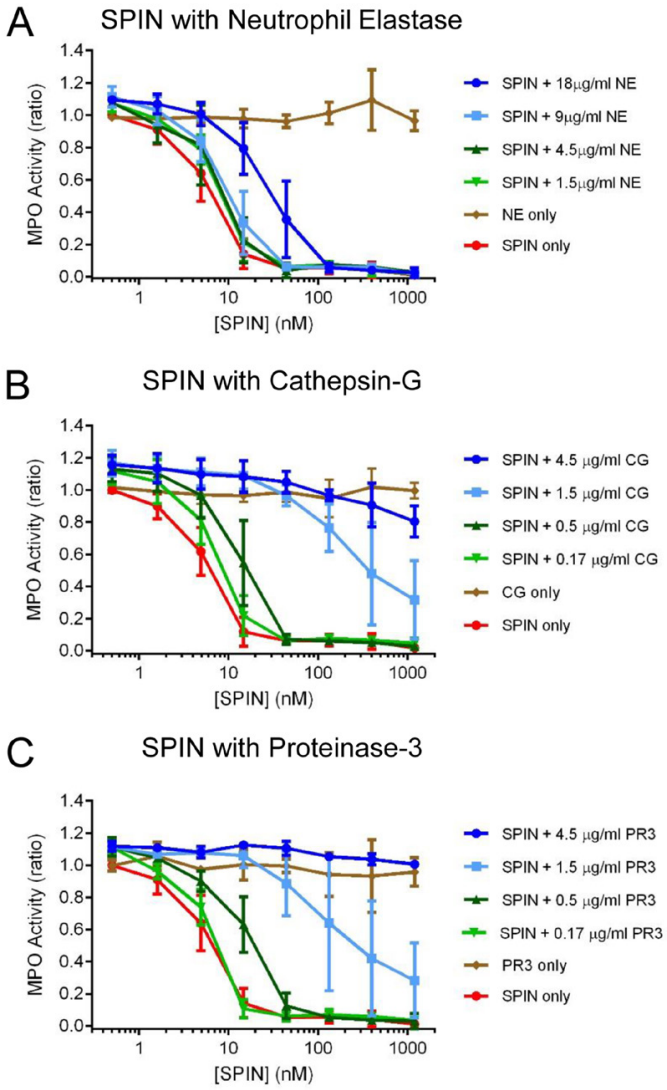

Figure 4: The N-terminal Region of SPIN is Subject to Proteolysis by NSPs. The influence of three proteases found in neutrophil azurophilic granules on SPIN activity was investigated using a spectrophotometric assay. Four different concentrations of (**A**) NE, (**B**) CG, and (**C**) PR3 were incubated with purified SPIN for 1 h after which proteolysis was stopped by adding PMSF. The reaction contents were serially diluted and incubated with MPO for 1 h further, prior to addition of a substrate mixture. Peroxidase activity was then measured at OD_{450} nm relative to a negative control for each set of samples. Significantly, preincubation with all three NSPs examined resulted in dose-dependent loss of SPIN activity, although this effect was far more pronounced for CG and PR3 when compared to NE. Subsequent characterization of the NSP digestion products of SPIN revealed that loss of activity was due to specific cleavage of the functionally essential SPIN N-terminal region (**Supplemental Figures 4 and 5**). Bars express SD with N=3, and legends are inset.

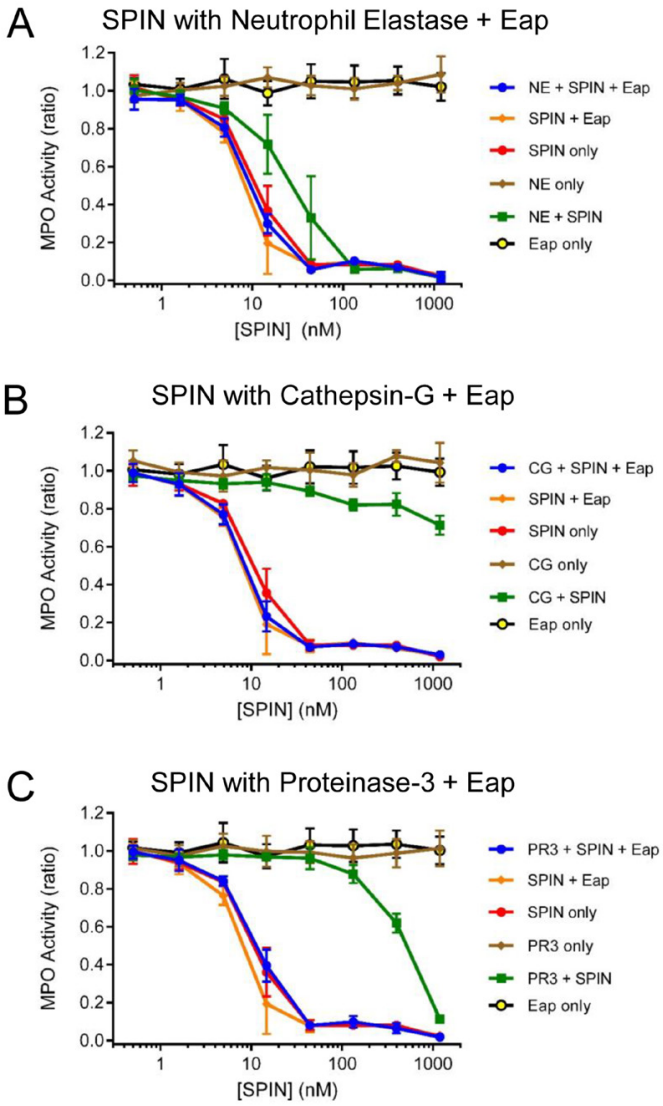

Figure 5: *S. aureus* Eap Protects the N-terminus of SPIN from Degradation by NSPs. The consequences of including the *S. aureus* derived NSP inhibitor, Eap (14), in the SPIN/NSP proteolysis reactions were assessed using an assay format identical to that presented in **Figure 4**. The presence of Eap protected the N-terminus of SPIN from proteolysis by (**A**) 18 µg/ml NE, (**B**) 4.5 µg/ml CG, and (**C**) 4.5 µg/ml PR3. Importantly, while SPIN on its own inhibited MPO activity, the addition of Eap was required to fully-restore SPIN function in the presence the NSPs. Bars express SD with N=3, and legends are inset.

revealed that the ten N-terminal residues of SPIN were removed following a 30 min exposure to catalytic levels of enzyme (**Supplemental Figure 3**).

To examine the protease sensitivity of SPIN under more biologically relevant conditions, we tested whether the three canonical NSPs Neutrophil Elastase (NE), Cathepsin G (CG),

and Proteinase-3 (PR3) might also degrade the SPIN N-terminus. Moreover, because this region of SPIN is required for SPIN to inhibit MPO (**Figure 3**), we investigated the functional consequences of such proteolysis using an MPO activity assay. We found that an excess of NE had to be incubated with SPIN to restore MPO activity to appreciable levels (**Figure 4A**); this was due to incomplete cleavage by NE and residual full-length SPIN present in the reaction (**Supplemental Figure 4**). By contrast, we observed that incubation of SPIN with either CG (**Figure 4B**) or PR3 (**Figure 4C**) each resulted in loss of MPO-inhibitory activity in a dose-dependent manner. Significantly, analysis of the SPIN cleavage products after CG and PR3 treatment not only showed clear evidence of proteolysis in the SPIN N-terminal region (**Supplemental Figures 4 and 5**), it was also consistent with the established cleavage preference for these NSPs (5).

We previously showed that production of SPIN is upregulated following phagocytosis of *S. aureus* cells (17). A similar increase in expression has also been reported for the genes encoding Eap and EapH1 upon exposure of *S. aureus* to crude neutrophil degranulate (29). Since both Eap and EapH1 act as specific inhibitors of NSPs (14), we wondered whether these staphylococcal innate immune evasion proteins might rescue SPIN from deleterious proteolysis by NSPs. To test this possibility, we repeated the assays described above both in the absence and presence of saturating levels of recombinant Eap (14). Consistent with the previously described NSP-inhibitory function of Eap (14), as well as prior results shown here (**Figure 4**), we found that Eap protected SPIN from degradation by all three canonical NSPs (**Figure 5**). Together, these results show that the N-terminal region of SPIN is subject to proteolysis by NSPs, but can be protected from such degradation through the action of the *S. aureus* NSP inhibitor, Eap.

DISCUSSION

The last decade has witnessed tremendous growth in our understanding of staphylococcal innate immune evasion. In many respects, a majority of the functional, mechanistic, and structural details have been elucidated for those *S. aureus* secreted proteins that disrupt complement initiation and amplification, neutrophil recruitment, and the initial steps of phagocytosis (9-12). While the topic of intracellularly-acting immune evasion proteins has received considerably less attention, it is no less relevant; in fact, the ability of *S. aureus* cells to resist killing within the neutrophil phagosome suggests that additional evasion molecules remain to be undiscovered (12). Recent work from our groups has led to identification of distinct *S. aureus* proteins that block function of NSPs (14) and MPO (17), which are key antimicrobial enzyme systems of neutrophils that act primarily within the phagosome (3,12). Herein, we have further defined the structure/function relationships of the novel MPO inhibitor, SPIN (17) (**Figures 1-3**). We have also provided evidence which suggests a potential functional synergy between SPIN and the EAP family of NSP inhibitors (14) (**Figures 4 and 5**). Together, this

work significantly furthers our understanding of an only recently discovered aspect *S. aureus* immune escape.

Our previous crystal structure of SPIN/rMPO identified two MPO-binding sites within the SPIN protein (17). While the relative contributions of each potential site to MPO binding could not be parsed directly from the structure, the biochemical data we present here have largely resolved this ambiguity. We found that loss of the SPIN N-terminal region has a minimal overall effect on its MPO-binding properties, as the K_D of 29.8 nM for SPIN$^{46-105}$/MPO compares favorably to that of 9.3 nM for SPIN/MPO (**Figure 2 and Table 1**). Still, it is noteworthy that the observed 3.2-fold decrease in MPO affinity of SPIN$^{46-105}$ relative to its full-length counterpart is attributable almost entirely to a faster dissociation rate constant for its complex (3.7-fold enhancement (**Table 1**)). This result might be expected if the apparent interaction site involving the SPIN N-terminal region only forms after an initial binding event has occurred via the SPIN α-helical bundle. Consistent with this premise, synthetic peptides corresponding to both linear and constrained forms of the SPIN N-terminal region failed to bind MPO, even at concentrations some three orders of magnitude above the K_D for SPIN/MPO (**Figure 2 and Table 1**). These data, along with successful determination of a co-crystal structure of SPIN$^{46-105}$ bound to rMPO argue that the primary MPO-binding site of SPIN lies within its α-helical bundle domain.

Although the α-helical bundle is responsible for driving SPIN binding to MPO, we found that the SPIN N-terminal region is absolutely required for inhibiting MPO activity (**Figure 3**). SPIN$^{46-105}$ binds MPO with relatively high affinity (**Figure 2 and Table 1**), yet has no inhibitory capacity on its own (**Figure 3**). This result appears to eliminate the possibility that SPIN binding inhibits MPO via perturbation of its heme redox chemistry, as has been described for the endogenous MPO inhibitor, ceruloplasmin (30). In light of the data currently available, we favor a two-step steric/competitive model for SPIN action, whereby the initial MPO binding event is driven by the α-helical bundle region then the inhibitory β-hairpin folds and inserts into MPO active site. In this manner, SPIN acts as a molecular plug, as suggested by our initial SPIN/rMPO crystal structure (17).

While deletion of the N-terminus yielded a SPIN protein that could not inhibit MPO, simply having these residues in the context of full-length SPIN was not sufficient to manifest inhibition on its own (**Figure 3**). Our studies investigating residues His^{43}-Asp^{45} were particularly helpful in addressing this issue, as loss of these conserved sidechains caused only a 3.4-fold loss of affinity for MPO, yet rendered the SPIN$^{43-45\rightarrow AAA}$ mutant incapable of inhibiting MPO (**Figure 3**). Examination of the SPIN/rMPO (17) structure reveals that both His43 and Asp44 form salt bridges with Asp^{379} and Arg^{271} of rMPO, respectively. Since these residues do not seem to contribute significantly to MPO binding (**Figure 2 and Table 1**), we suggest that His^{43}-Asp^{45} might help guide insertion of the inhibitory N-terminal β-hairpin into the MPO active site channel.

It seems that SPIN faces a rather precarious existence inside the phagosomal compartment. While SPIN is absolutely dependent on its N-terminus for function (**Figure 3**), this region of the protein is dynamic in the absence of its binding partner (**Figure 1**) and sensitive to proteolysis by NSPs in a manner that yields biologically inactive SPIN fragments (**Figure 4, Supplemental Figures 4 and 5**). Although the high concentration of MPO within the maturing phagosome would appear to promote stability of SPIN by effectively chaperoning its N-terminus, the abundance of NSPs in the same environment suggests that a significant portion of SPIN molecules could be cleaved soon after secretion. In light of this, our observation that *S. aureus* Eap preserves SPIN function by inhibiting CG, NE, and PR3 is a potentially significant finding (**Figure 5**). All three *S. aureus* EAP domain-containing proteins act as tightly binding, non-covalent inhibitors of NSPs (14), and they have been shown to protect against NSP-mediated cleavage of key staphylococcal virulence factors *in vitro* and *in vivo* (31). Although that previous study examined virulence proteins that act in the extracellular environment (31), our results here suggest that EAP domains can serve a similarly protective role for SPIN, and perhaps other molecules whose primary sites of action lie within the phagosomal compartment. While these results highlight the potential for functional synergy among various *S. aureus* immune evasion proteins, much work remains to be done if we are to truly understand the complex relationships of these proteins with one another. In this regard, long-standing evidence describing functional synergy between MPO and NSPs (8) serves as an important reminder that the numerous biochemical events inside the phagosome are best considered as part of an overall process, rather than reactions in isolation.

ACKNOWLEDGEMENTS

This work was supported by a ZonMw Grant 205200004 from the Netherlands Organization for Health Research and Development (to J.A.G.v.S.) and US National Institutes of Health Grants AI111203 and GM121511 (to B.V.G.) and AI116546 (W.M.N). The Nauseef lab was supported also by a Merit Review award and use of facilities at the Iowa City Department of Veterans Affairs (VA) Medical Center, Iowa City, IA 52246. X-ray diffraction data were collected at Southeast Regional Collaborative Access Team (SER-CAT) 22-BM beamline at the Advanced Photon Source, Argonne National Laboratory. A list of supporting institutions may be found at www.ser-cat.org/members.html. Use of the Advanced Photon Source was supported by the U.S. Department of Energy, Office of Science, Office of Basic Energy Sciences, under Contract No. W-31-109-Eng-38.

FOOTNOTES

* Authors N.W.M.d.J. and N.T.P. made equal contributions to this study.

#The refined coordinates and structure factors have been deposited in the RCSB Protein Data Bank under the accession code 6AZP.

CONFLICT OF INTEREST

The authors declare that they have no conflicts of interest with the contents of this article.

AUTHOR CONTRIBUTIONS

N. W. d. J., N. T. P., K. X. R., B. L. G., A. I. H., O. P., W. N., K. v. K., J. v. S., and B.V.G. conceptualization; N. W. d. J., N. T. P., K. X. R., B. L. G., A. I. H., O. P., B. B. K., K. G. L., W. N., K. v. K., J. v. S., and B. V. G. formal analysis; N. W. d. J., N. T. P., K. X. R., B. L. G., A. I. H., B. B. K., K. G. L., and K. v. K. investigation; N. W. d. J., N. T. P., B. L. G., K. v. K., J. v. S., and B. V. G. visualization; N. W. d. J., N. T. P., K. X. R., B. L. G., A. I. H., O. P., B. B. K., K. G. L., K. v. K., and B. V. G. methodology; N. W. d. J., N. T. P., J. v. S., and B. V. G. writing-original draft; N. W. d. J., N. T. P., J. v. S., and B. V. G. writing-review and editing; N. T. P., K. X. R., B. L. G., A. I. H., O. P., K. G. L., W. N., K. v. K., J.v.S., and B. V. G. data curation; N. T. P., K. X. R., B. L. G., A. I. H., O. P., and B. V. G. validation; K. X. R., B. L. G., O. P., W. N., K. v. K., J. v. S., and B. V. G. supervision; O. P., W. N., J. v. S., and B. V. G. resources; W. N., J. v. S., and B. V. G. funding acquisition; B. V. G. project administration.

MATERIALS & METHODS

Human Neutrophil Protein Preparations

Forms of human myeloperoxidase (MPO) were purchased from various commercial sources. For structural studies, a recombinant form of MPO bearing a C-terminal 10-His tag (catalog #3174-MP-250) was obtained from R&D Systems (Minneapolis, MN). For biochemical and functional analyses, native MPO isolated from purlent human sputum (catalog #MY862) was obtained from Elastin Products Corp. (Owensville, MO). The neutrophil serine proteinases Neutrophil Elastase (catalog #SE563), Cathepsin G (catalog #SG623), and Proteinase-3 (catalog #ML734) were likewise isolated from purulent human sputum and obtained from Elastin Products Corp. (Owensville, MO). All materials were reconstituted and handled according to manufacturer's suggestions unless otherwise noted.

Recombinant Protein Expression and Purification

A codon-optimized form of the *S. aureus* SPIN open reading frame from strain Newman that lacks the N-terminal signal sequence was synthesized using gBlocks Gene Fragments (Integrated DNA Technologies, USA). This coding fragment was subcloned into the SalI and EcoRI sites of a modified form of the prokaryotic expression vector, pT7HMT (32). All other expression vectors for site-directed mutants of SPIN were derived from this parental plasmid, and were constructed using standard mutagenic PCR approaches. Each plasmid was verified by DNA sequencing prior to use.

All recombinant SPIN proteins were expressed as N-terminally his-tagged precursors and prepared according to standard techniques. Briefly, recombinant strains of *E. coli* BL21(DE3) bearing a plasmid of interest were grown in 1 L of selective Terrific Broth at 37 ºC, prior to inducing protein expression with 1 mM IPTG at 18 ºC overnight. Cells from the induced culture were harvested by centrifugation, resuspended, lysed by microfluidization, and processed for Ni-NTA affinity chromatography as previously described (33). Following initial purification, the recombinant SPIN proteins were digested with TEV protease to remove the affinity tag as described elsewhere (32). Final purification was achieved by gel-filtration chromatography in a buffer of PBS (pH 7.4) using a Superdex 75 26/60 column connected to an AKTA FPLC system (GE Life Sciences).

Uniformly ^{15}N and $^{15}N/^{13}C$ double-labeled SPIN proteins were prepared for NMR spectroscopy studies. Both forms of wild-type SPIN were expressed in *E. coli* BL21(DE3) cells grown in minimal medium (M9) enriched with $^{15}NH^4Cl$ and ^{13}C-glucose as described before (34).

Samples of recombinant Eap (*S. aureus* strain Mu50) were expressed and purified from *E. coli* strain BL21(DE3) as previously described (35).

Synthetic Peptide Mimics of the SPIN N-terminus

Peptides SKVYSQNGLVLHDDS (i.e. SPIN-p1) and CKVYSQNGLVLHDDC (i.e. SPIN-p2) were synthesized at >90% purity by GenScript (Piscataway, NJ). Peptide SPIN-p2 was chemically oxidized to form a disulfide bond between its two cysteine residues. The identity of each product was confirmed by MALDI-TOF prior to use. Peptide stock solutions were prepared at 5 mM in ddH_2O.

Solution NMR Spectroscopy

All NMR measurements were performed at 25 ºC on either a Varian 500VNMR (499.84 MHz for ^1H frequency) or a Bruker Avance (700.11 MHz for ^1H frequency) spectrometer, both of which were equipped with cryogenic probes. The ^1H chemical shifts were referenced to the external standard 2,2-dimethyl-2-silapentane-5-sulphonic acid (DSS) at 25 °C and the ^{13}C and ^{15}N chemical shifts were referenced indirectly from DSS. The purified, isotopically-enriched SPIN proteins were dissolved at 0.75-1.0 mM final concentration in 50 mM sodium phosphate (pH 6.5) supplemented with 5% (v/v) D_2O as a lock solvent prior to spectral collection.

Backbone and sidechain resonances for SPIN were assigned through standard double and triple resonance spectra. Triple-resonance NMR spectra corresponding to HNCA, HN(CO)CA, HNCACB, CBCA(CO)NH, and HNCO were recorded on uniformly $^{15}N/^{13}C$ labelled SPIN samples to facilitate backbone assignment. Two-dimensional ^{13}C HSQC and three-dimensional HCCONH, CCCONH, HCCH-TOCSY, ^{15}N HSQC-TOCSY (tm=80 ms) and ^{15}N-edited NOESY (tm =100 ms) spectra were recorded for sidechain assignment. NMR data were processed using NMRPipe (35), while spectra were analyzed and visualized using CARA (http://www.nmr.ch/) (36). The chemical shift assignments have been deposited in the BioMagResBank (www.bmrb.wisc.edu/) under the accession number 27069, and described in more detail elsewhere (18).

Longitudinal (R_1) and transverse (R_2) relaxation time constants for ^{15}N amide atoms were determined using the steady-state, inversion-recovery and Carr-Purcell-Meiboom-Gill methods respectively (37,38). For R_1 determination, 15N-HSQC spectra with the following relaxation delays were collected: 0.03, 0.05, 0.07, 0.12, 0.15, 0.23, 0.35, 0.80, 1.00, 1.20, 15.0, and 1.80 s. For R_2 determination, ^{15}N-HSQC spectra with the following delays were collected: 0.03, 0.05, 0.07, 0.13, 0.15, 0.17, 0.19, 0.21, and 0.23 s. The R_1 and R_2 time constants were calculated by measuring the intensity of the peak corresponding to each assigned ^1H-^{15}N pair from the ^{15}N-HSQC spectra and fitting the resulting decay as function of time delay (t) to a two-parameter exponential decay described by I(t)=Ioe-tR, where I(t) is the intensity of the peak as a function of relaxation delay time t. Io is the normalized peak

intensity at t=0. All such calculations were performed using the Rate Analysis feature of NMRView 9.2 (One Moon Scientific, Westfield, NJ) (39).

The experimentally-derived chemical shift values for SPIN resonances were used to determine solution structural features of SPIN in the absence of MPO. The secondary structure of SPIN was predicted using the TALOS-N platform (18,19). Likewise, the CS-Rosetta Server (Rosetta v3.8, CS-Rosetta Toolbox v3.3) was used to generate 40,000 independent models for three-dimensional structure of SPIN (40,41) consistent with the chemical shift data. This approach was used because the NMR spectra collected on SPIN were not sufficient to permit experimental determination of its structure.

Surface Plasmon Resonance

Direct binding of SPIN proteins to various forms of MPO was assessed by SPR using a Biacore T-200 instrument (GE Healthcare) at 25 °C (17). All experiments used a running buffer of HBS-T (20 mM HEPES (pH 7.4), 140 mM NaCl, and 0.005% (v/v) Tween-20) and a flowrate of 20 µl min-1. Experimental biosensors were created on CMD 200M sensor chips (XanTec Bioanalytics GmbH; Dusselorf, Germany) by coupling native human MPO (1183 RU) and rMPO (1718 RU) to separate flow cells using random amine chemistry, while a reference surface was prepared by activation followed by immediate inactivation with ethanolamine. A concentration series of each SPIN protein was injected over the surfaces for 3 min and allowed to dissociate for 4 min. Regeneration to baseline was achieved by three consecutive 30 s injections of 100 mM glycine (pH 10.0). Kinetic analysis of each reference subtracted injection series was performed using Biacore T-200 Evaluation Software v3.0 (GE Healthcare) using a 1:1 binding model and fitting Rmax locally.

The ability of SPIN peptides to compete with SPIN/MPO complex formation was assessed using an SPR-based competition assay. All experiments were performed on a Biacore T-200 at 25°C using a flowrate of 30 µl min-1 in HBS-T running buffer. Injections were performed for 1 min and dissociation was monitored for 3 min at which point baseline regeneration was achieved as described above. SPIN (50 nM) or SPIN peptides (50 µM) were injected either alone or as a mixture (i.e. SPIN + peptide) over the MPO surface and the response was monitored. Residual response of SPIN during co-injections was calculated by subtracting the response of the peptide-only injections. Sensorgram overlays were prepared using Biacore T-200 Evaluation Software and GraphPad Prism.

Crystallization, Structure Determination, Refinement, and Analysis

A sample of SPIN$^{46\text{-}105}$ bound to recombinant human MPO (R&D Systems) was prepared by mixing stoichiometric amounts of each protein and concentrating to 5 mg/ml total protein in a buffer of 5 mM tris (pH 7.4), 50 mM NaCl. Crystals were obtained as initially described for the SPIN/rMPO complex (17). Single crystals were harvested and cryopreserved in precipitant solution supplemented with an additional 10% (v/v) peg-400.

X-ray diffraction data were collected at 1.0 Å wavelength using beamline 22-BM of the Advanced Photon Source (Argonne National Laboratory). The reflections were processed using the HKL-2000 package (42), and the structure was solved by molecular replacement using the refined coordinates of full-length SPIN/rMPO (PDB entry 5UZU) as a search model (17) and PHASER (43) as implemented within the PHENIX software suite (44,45). The final model was constructed by both automated and manual rebuilding, followed by refinement using PHENIX.REFINE (44,45). 94.26% of the modeled polypeptide residues lie in favored regions of the Ramachandran plot, with only 1.26% of residues found in areas classified as outliers. A quantitative description of the cell constants, diffraction data quality, and properties of the final model for the SPIN$^{46\text{-}105}$/rMPO complex can be found in **Supplemental Table 1**.

The rMPO used for these structural studies binds SPIN similarly to native human MPO (**Table 1**), but has a lower

occupancy of the heme prosthetic group when compared to MPO produced by human neutrophils. This resulted in weak electron density for the heme in the SPIN$^{46-105}$/rMPO co-crystal structure, and precluded inclusion of heme in the final crystallographic model. When necessary, the location of the heme prothesthic group was inferred from the coordinates of halide-bound, native human MPO (PDB entry 1CXP) (46). All structural analyses, including calculation of buried surface areas and identification of potential hydrogen bonds, were performed using EBI-PISA (http://www.ebi.ac.uk/pdbe/prot_int/pistart.html). Representations of protein structures were generated by PyMol (http://www.pymol.org/).

MPO Activity Assays

MPO activity in the presence of H_2O_2 as a substrate and o-dianisidine as a redox indicator was monitored at 450 nm (17). Briefly, either 0.2 U/ml MPO isolated from human sputum (Elastin Products Company) was incubated with 74 nM of various SPIN proteins for 1 h at 37 °C in 96-well plates to allow protein-protein interactions to form. A substrate mixture comprised of 45 mM phosphate buffer (pH 6.0), 0.5 mM H_2O_2, and 15 µg of o-dianisidine dihydrochloride (Sigma-Aldrich catalog #D9154) was then added. The OD450 nm was measured continuously every 45 seconds for 1 h at 37 °C using a FLUOstar Omega microplate reader. The slope of each trial before saturation was calculated via GraphPad Prism 6 and defined as MPO activity. BSA was used as a negative control for inhibition.

The influence of NSPs on MPO inhibition by SPIN was also examined through a similar approach. Specifically, full-length SPIN was pre-incubated for 1 h at 37 °C with either 18 µg/ml NE, 4.5 µg/ml CG, or 4.5 µg/ml PR3 after which 1 mM PMSF was added to stop protease activity. The SPIN digestion reaction was then serially diluted and assayed for MPO activity as described above. Where indicated, NSPs were also pre-incubated for 5 min at room temperature with 37.5 µg/ml Eap prior to adding this mixture to full-length SPIN.

MPO Bactericidal Assay

S. aureus cells were grown to logarithmic phase (OD_{660} ~0.5) in Todd Hewitt Broth (THB), washed twice, and resuspended to an OD_{660} ~0.5 in sterile Hanks Balanced Salt Solution (HBSS). 100 µl of bacterial suspension were diluted into 10 ml of substrate solution containing 300 mM glucose in HBSS. 50 µl of this mixture were diluted with an equal part of enzyme solution containing 4 ng/ml Glucose Oxidase from Aspergillus (Sigma-Aldrich), and 2.3 nM MPO with or without the addition of 40 nM SPIN proteins. 4-aminobenzoic acid hydrazide (4-ABAH) was included in a separate sample at a final concentration of 500 µM and served as a control for MPO-inhibited conditions. The enzyme/bacteria mixture was incubated for 1 hour at 37 °C and peroxidase activity was stopped by addition of 10 mg/ml catalase from bovine liver (Sigma-Aldrich). Samples were serially diluted in PBS and plated onto Todd Hewitt Agar (THA) plates. The final number of colony forming units (CFU) were counted the next day following an overnight incubation at 37°C.

Photobleaching of GFP-expressing *S. aureus* by Neutrophils

The capacity of SPIN proteins inhibit MPO activity within neutrophil phagosomes was examined. Human neutrophils were isolated from venous blood, as described previously (47). Written consent was obtained from each volunteer in accordance with both the Declaration of Helsinki and a protocol approved by the Institutional Review Board for Human Subjects at the University of Iowa. Isolated neutrophils were then fed opsonized cells of S.aureus strain USA300 expressing superfolded GFP (MOI 1:1) as previously described (24), either in the absence or presence of 50 µM SPIN proteins. Samples identical to these except for the presence of 10 µM diphenyleneiodonium (DPI) were run in parallel and were included to inhibit NADPH oxidase-dependent bleaching of GFP (48). After 10 min of phagocytosis, undigested bacteria were removed, and neutrophils laden with S.aureus were incubated at 37 °C for 0 or 120 minutes. Samples were analyzed by flow cytometry for loss of GFP fluorescence, as previously reported (24). The mean fluorescence intensity (MFI) for each sample was

calculated as the geometric mean of the GFP-positive population multiplied by the percent of cells gated. The percent MFI was normalized to values obtained for DPI-treated neutrophils.

REFERENCES

1. Nauseef, W. M. (2007) How Human Neutrophils Kills and Degrade Microbes: an Integrated View. Immunol. Rev. 219, 88-102
2. Faurschou, M., and Borregaard, N. (2003) Neutrophil Granules and Secretory Vesicles in Inflammation. Microbes Infect. 5, 1317-1327
3. Amulic, B., Cazalet, C., Hayes, G. L., Metzler, K. D., and Zychlinsky, A. (2012) Neutrophil Function: From Mechanisms to Disease. Annu. Rev. Immunol. 30, 459-489
4. Nauseef, W. M. (2014) Myeloperoxidase in Human Neutrophil Host Defense. Cell Microbiol. 16, 1146-1155
5. Korkmaz, B., Horwitz, M. S., Jenne, D. E., and Gauthier, F. (2010) Neutrophil Elastase, Proteinase 3, and Cathepsin G as Therapeutic Targets in Human Disease. Pharmacol. Rev. 62, 726-759
6. Pham, C. T. N. (2006) Neutrophil Serine Proteases: Specific Regulators of Inflammation. Nat. Rev. Immunol. 6, 541-550
7. Stapels, D. A., Geisbrecht, B. V., and Rooijakkers, S. H. (2015) Neutrophil Serine Proteases in Antibacterial Defense. Curr. Opin. Microbiol. 23C, 42-48
8. Odeberg, H., and Olsson, I. (1976) Microbicidal Mechanisms of Human Granulocytes: Synergisitc Effects of Granulocyte Elastase and Myeloperoxidase or Chymotrypsin-Like Cationic Protein. Infect. Immun. 14, 1276-1283
9. Garcia, B. L., Zwarthoff, S. A., Rooijakkers, S. H. M., and Geisbrecht, B. V. (2016) Novel Evasion Mechanisms of the Classical Complement Pathway. J. Immunol. 197, 2051-2060
10. Kim, H. K., Thammavongsa, V., Schneewind, O., and Missiakas, D. (2012) Recurrent Infections and Immune Evasion Strategies of *Staphylococcus aureus*. Curr. Opin. Microbiol. 15, 92-99
11. Lambris, J. D., Ricklin, D., and Geisbrecht, B. V. (2008) Complement Evasion by Human Pathogens. Nat. Rev. Microbiol. 6, 132-142
12. Spaan, A. N., Surewaard, B. G. J., Nijland, R., and van Strijp, J. A. G. (2013) Neutrophils versus *Staphylococcus aureus*: a Biological Tug of War. Annu. Rev. Microbiol. 67, 629-650
13. Thwaites, G. E., and Gant, V. (2011) Are Bloodstream Leukocytes Trojan Horses for the Metastasis of *Staphylococcus aureus*? Pathogens 9, 215-222
14. Stapels, D. A. C., Ramyar, K. X., Bischoff, M., von Koeckritz-Blickwede, M., Milder, F. J., Ruyken, M., Eisenbeis, J., McWhorter, W. J., Herrmann, M., van Kessel, K. P., Geisbrecht, B. V., and Rooijakkers, S. H. M. (2014) *Staphylococcus aureus* Secretes a Novel Class of Neutrophil-Serine-Protease Inhibitors that Promote Bacterial Infection. Proc. Natl. Acad. Sci. U.S.A. 111, 13187-13192
15. Fevre, C., Bestebroer, J., Mebius, M. M., De Haas, C. J., van Strijp, J. A. G., Fitzgerald, J. R., and Haas, P.-J. A. (2014) *Staphylococcus aureus* Proteins SSL6 and SEIX Interact with Neutrophil Receptors as Identified Using Secretome Phage Display. Cell. Microbiol. 16, 1646-1665
16. Schultz, J., and Kaminker, K. (1962) Myeloperoxidase of the Leucocyte of Normal Human Blood. I. Content and Localization. Arch. Biochem. Biophys. 96, 465-467
17. de Jong, N. W. M., Ramyar, K. X., Guerra, F. E., Nijland, R., Fevre, C., Voyich, J. M., McCarthy, A. J., Garcia, B. L., van Kessel, K. P. M., van Strijp, J. A. G., Geisbrecht, B. V., and Haas, P. A. (2017) Immune Evasion by a Staphylococcal Inhibitor of Myeloperoxidase. Proc. Natl. Acad. Sci. U.S.A. 114, 9439-9444
18. Ploscariu, N. T., Herrera, A. I., Jayanthi, S., Kumar, T. K. S., Geisbrecht, B. V., and Prakash, O. (2017) Backbone and Side-Chain 1H, 15N, and 13C Resonance Assignments of a Novel Staphylococcal Inhibitor of Myeloperoxidase. Biomol. NMR Assign. 11, 285-288

19. Shen, Y., and Bax, A. (2013) Protein Backbone and Sidechain Torsion Angles Predicted from NMR Chemical Shifts using Artificial Neural Networks. J. Biomol. NMR 56, 227-241

20. Kleckner, I. R., and Foster, M. P. (2011) An Introduction to NMR-Based Approaches for Measuring Protein Dynamics. Biochim. Biophys. Acta 1814, 942-968

21. Wishart, D. S., Sykes, B. D., and Richards, F. M. (1991) Relationship Between Nuclear Magentic Resonance Chemical Shift and Protein Secondary Structure. J. Mol. Biol. 222, 311-333

22. Krissinel, E., and Henrick, K. (2007) Inference of Macromolecular Assemblies from Crystalline State. J. Mol. Biol. 372, 774-797

23. Denys, G. A., Grover, P., O'Hanley, P., and Stephens, J. T. J. (2011) *In vitro* Antibacterial Activity of E-101 Solution, a Novel Myeloperoxidase-Mediated Antimicrobial, Against Gram-Positive and Gram-Negative Pathogens. J. Antimicrob. Chemother. 66, 335-342

24. Schwartz, J., Leidal, K. G., Femling, J. K., Weiss, J. P., and Nauseef, W. M. (2009) Neutrophil Bleaching of GFP-expressing Staphylococci: Probing the Intraphagosomal Fate of Individual Bacteria. J. Immunol. 183, 2632-2641

25. Winterbourn, C. C., Hampton, M. B., Livesey, J. H., and Kettle, A. J. (2006) Modeling the Reactions of Superoxide and Myeloperoxidase in the Neutrophil Phagosome. J. Biol. Chem. 281, 39860-39869

26. Reeves, E. P., Lu, H., Jacobs, H. L., Messina, C. G., Bolsover, S., Gabella, G., Potma, E. O., Warley, A., Roes, J., and Segal, A. W. (2002) Killing Activity of Neutrophils is Mediated Through Activation of Proteases by K+ Flux. Nature 416, 291-297

27. Campbell, E. J., Campbell, M. A., and Owen, C. A. (2000) Bioactive Proteinase 3 on the Cell Surface of Human Neutrophils: Quantification, Catalytic Activity, and Susceptibility to Inhibition. J. Immunol. 165, 3366-3374

28. Campbell, E. J., Silverman, E. K., and Campbell, M. A. (1989) Elastase and Cathepsin G of Human Monocytes. Quantificaiton of Cellular Content, Release in Response to Stimuli, and Heterogeneity in Elastase-Mediated Proteolytic Activity. J. Immunol. 143, 2961-2968

29. Palazzolo-Ballance, A. M., Reniere, M. L., Braughton, K. R., Sturdevant, D. E., Otto, M., Kreiswirth, B. N., Skaar, E. P., and Deleo, F. R. (2008) Neutrophil Microbicides Induce a Pathogen Survival Response in Community-Associated Methicillin-Resistant *Staphylococcus aureus*. J. Immunol. 180, 500-509

30. Chapman, A. L., Mocatta, T. J., Shiva, S., Seidel, A., Chen, B., Khalilova, I., Paumann-Page, M. E., Jameson, G. N., Winterbourn, C. C., and Kettle, A. J. (2013) Ceruloplasmin is an Endogenous Inhibitor of Myeloperoxidase. J. Biol. Chem. 288, 6465-6477

31. Stapels, D. A., Kuipers, A., von Koeckritz-Blickwede, M., Ruyken, M., Tromp, A. T., Horsburgh, M. J., de Haas, C. J., van Strijp, J. A., van Kessel, K. P., and Rooijakkers, S. H. (2016) *Staphylococcus aureus* Protects its Immune-Evasion Proteins Against Degradation by Neutrophil Serine Proteases. Cell Microbiol. 18, 536-545

32. Geisbrecht, B. V., Bouyain, S., and Pop, M. (2006) An Optimized System for the Expression and Purification of Secreted Bacterial Proteins. Prot. Expr. Purif. 46, 23-32

33. Barta, M. L., Skaff, D. A., McWhorter, W. J., Herdendorf, T. J., Miziorko, H. M., and Geisbrecht, B. V. (2011) Crystal structures of Staphylococcus epidermidis mevalonate diphosphate decarboxylase bound to inhibitory analogs reveal new insight into substrate binding and catalysis. J. Biol. Chem. 286, 23900-23910

34. Woehl, J., Takahashi, D., Herrera, A., Geisbrecht, B. V., and Prakash, O. (2016) Backbone and Side-Chain 1H, 15N, and 13C Resonance Assingments of *Staphylococcus aureus* Extracellular Adherence Protein Domain 4. Biomol. NMR Assign. 10, 301-305

35. Delaglio, F., Grzesiek, S., Vuister, G. W., Zhu, G., Pfeifer, J., and Bax, A. . (1995) NMRPipe: a multidimensional spectral processing system based on UNIX pipes. J. Biomol. NMR 6, 277-293

36. Keller, R. (2004) The Computer Aided Resonance Assignment Tutorial,

37. Farrow, N. A., Muhandiram, R., Singer, A. U., Pascal, S. M., Kay, C. M., Gish, G., Shoelson, S. E., Pawson, T., Forman-Kay, J. D., and Kay, L. E. (1994) Backbone Dynamics of a Free and a Phosphopeptide-Complexed Src Homology 2 Domain Studied by 15N NMR Relaxation. Biochemistry 33, 5984-6003

38. Kay, L. E., Nicholson, L. K., Delaglio, F., Bax, A., and Torchia, D. A. (1992) Pulse Sequences for the Removal of

the Effects of Cross Correlation Between Dipolar and Chemical-Shift Anisotropy Relaxation Mechanisms on the Measurement of Heteronuclear T1 and T2 Values in Proteins. J. Magn. Reson. 97, 359-375

39. Johnson, B. A., and Blevins, R. A. . (1994) NMRView: A computer program for the visualization and analysis of NMR data. J. Biomol. NMR 4, 603-614

40. Lange, O. F., Rossi, P., Sgourakis, N. G., Song, Y., Lee, H.-W., Aramini, J. M., Ertekin, A., Xiao, R., Acton, T. B., Montelione, G. T., and Baker, D. (2012) Determination of Solution Structures of Protein up to 40 kDa using CS-Rosetta with Sparse NMR Data from Deuterated Samples. Proc. Natl. Acad. Sci. U.S.A. 109, 10873-10878

41. Shen, Y., Bryan, P. N., He, Y., Orban, J., Baker, D., and Bax, A. (2010) De Novo Structure Generation using Chemical Shifts for Proteins with High-Sequence Identity but Different Folds. Protein Sci. 19, 349-356

42. Otwinowski, Z., and Minor, W. (1997) Processing of X-ray Diffraction Data Collected in Oscillation Mode. Methods Enzymol. 276, 307-326

43. McCoy, A. J., Grosse-Kunstleve, R. W., Adams, P. D., Winn, M. D., Storoni, L. C., and Read, R. J. (2007) Phaser Crystallographic Software. J. Appl. Cryst. 40, 658-674

44. Adams, P. D., Grosse-Kunstleve, R. W., Hung, L.-W., Ioerger, T. R., McCoy, A. J., Moriarty, N. W., Read, R. J., Sacchettini, J. C., Sauter, N. K., and Terwilliger, T. C. (2002) PHENIX: Building New Software for Automated Crystallographic Structure Determination. Acta Cryst. D58, 1948-1954

45. Adams, P. D., Afonine, P. V., Bunkoczi, G., Chen, V. B., Davis, I. W., Echols, N., Headd, J. J., Hung, L. W., Kapral, G. J., Grosse-Kunstleve, R. W., McCoy, A. J., Moriarty, M. W., Oeffner, R., Read, R. J., Richardson, D. C., Richardson, J. S., Terwilliger, T. C., and Zwart, P. H. (2010) PHENIX: a Comprehensive Python-Based System for Macromolecular Structure Solution. Acta. Cryst. D Biol. Crystallogr. 66, 213-221

46. Fiedler, T. J., Davey, C. A., and Fenna, R. E. (2000) X-ray Crystal Structure and Characterization of Halide-Binding Sites of Human Myeloperoxidase at 1.8 A Resolution. J. Biol. Chem. 275, 11964-11971

47. Nauseef, W. M. (2014) Isolation of Human Neutrophils from Venous Blood. Methods Mol. Biol. 1124, 13-18

48. Greenlee-Wacker, M. C., Rigby, K. M., Kobayashi, S. D., Porter, A. R., Deleo, F. R., and Nauseef, W. M. (2014) Phagocytosis of *Staphylococcus aureus* by Human Neutrophils Prevents Efferocytosis and Induces Programmed Necrosis. J. Immunol. 192, 4709-4717

SUPPLEMENTAL DATA

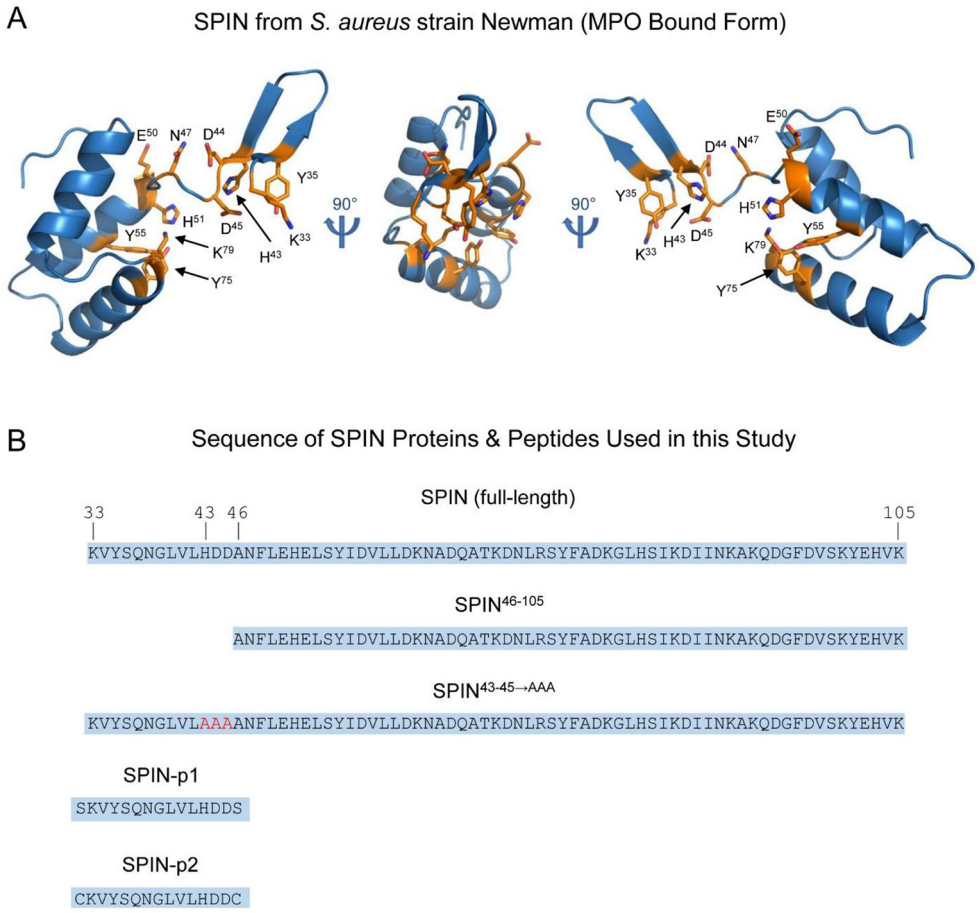

Supplemental Figure 1: Structure of *S. aureus* SPIN and Sequences of SPIN Proteins Used in this Study. (**A**) Three different views of the MPO-bound *S. aureus* SPIN structure (PDB entry 5UZU). The SPIN protein is drawn as a blue ribbon. Residues whose sidechains participate in either hydrogen bonds or salt bridges with MPO are drawn in stick convention, with carbon atoms colored orange, nitrogen in dark blue, and oxygen in red. The labels of these residues reflect the values shown in panel **B** below. (**B**) The sequences of recombinant proteins and synthetic peptides used in this study are presented above. The full-length SPIN sequence from *S. aureus* strain Newman is shown at the top. Numbering reflects those residues found in the matured polypeptide following removal of the secretion signal sequence. Letters shown in red typeface indicate the positions altered by site-direction mutations.

Supplemental Table 1: X-ray Diffraction Data Collection and Refinement Statistics

	SPIN$^{46-105}$/rMPO
Data collection	
Space group	C 1 2 1
Cell dimensions	
a, *b*, *c*, Å	128.85 92.88 80.46
α, β, γ, °	90.00 119.91 90.00
Resolution (Å)	38.96-2.29 (2.38-2.29)
R_{pim}	0.063 (0.414)
I/ σ*I*	12.0 (2.2)
Completeness (%)	99.0 (98.3)
Redundancy	7.7 (7.1)
Refinement	
Resolution, Å	38.96-2.29
No. reflections	36,470
R_{work} / R_{free}	17.9/22.9
No. atoms	
Protein	5082
Ligand/ion	68
Water	282
B-factors	
Protein	41.95
Ligand/ion	62.87
Water	38.18
R.m.s. deviations	
Bond lengths (Å)	0.011
Bond angles (°)	1.136

* Values in parentheses are for highest-resolution shell.

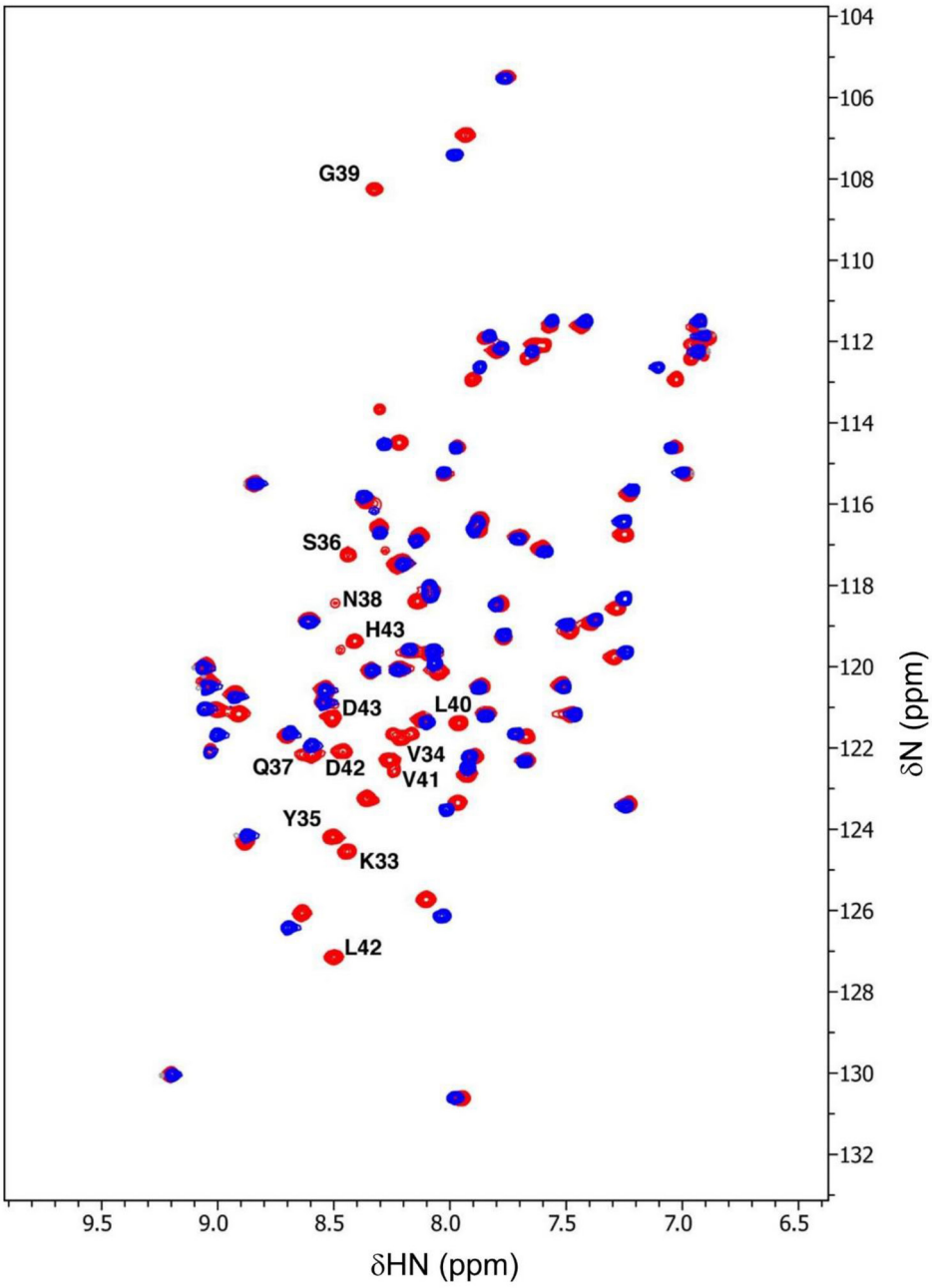

Supplemental Figure 2: Comparison of $^{1}H^{15}N$-HSQC Spectra of ^{15}N-labeled full-length SPIN (red) and SPIN$^{46-105}$ (blue) recorded at 25^{0}C on a Varian 500VNMR Spectrometer. The labels represent resonances corresponding to residues found within the N-terminal region of the SPIN protein.

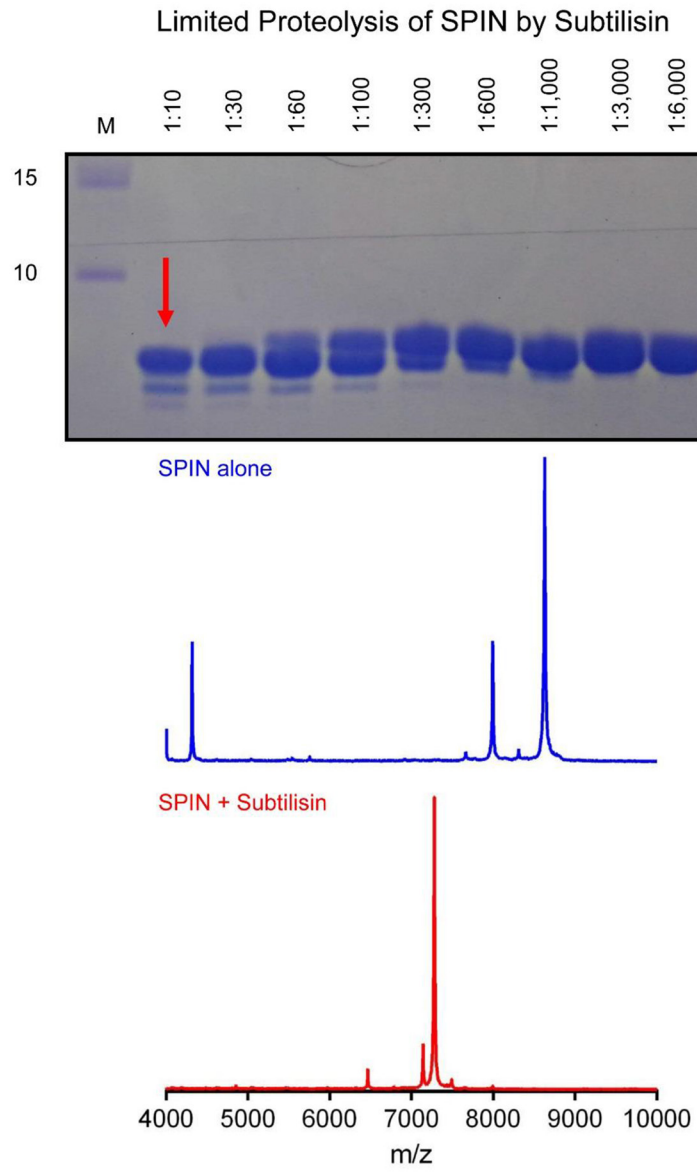

Supplemental Figure 3: Limited Proteolysis of SPIN by Subtilisin. Full-length SPIN (1 µg/µl) was subjected to limited proteolysis by Subtilisin for 30 min at room temperature. Serial dilutions of protease mass relative to the SPIN substrate were prepared as indicated, and the digestion products were separated by 16% Tris-Tricine PAGE. Whereas full-length SPIN showed a major species (m/z = 8,629) that matched the expected mass of the recombinant protein, the protease stable digestion product (red arrow in the top panel; m/z = 7,280) corresponded to SPIN residues 43-105 (7,279 Da expected).

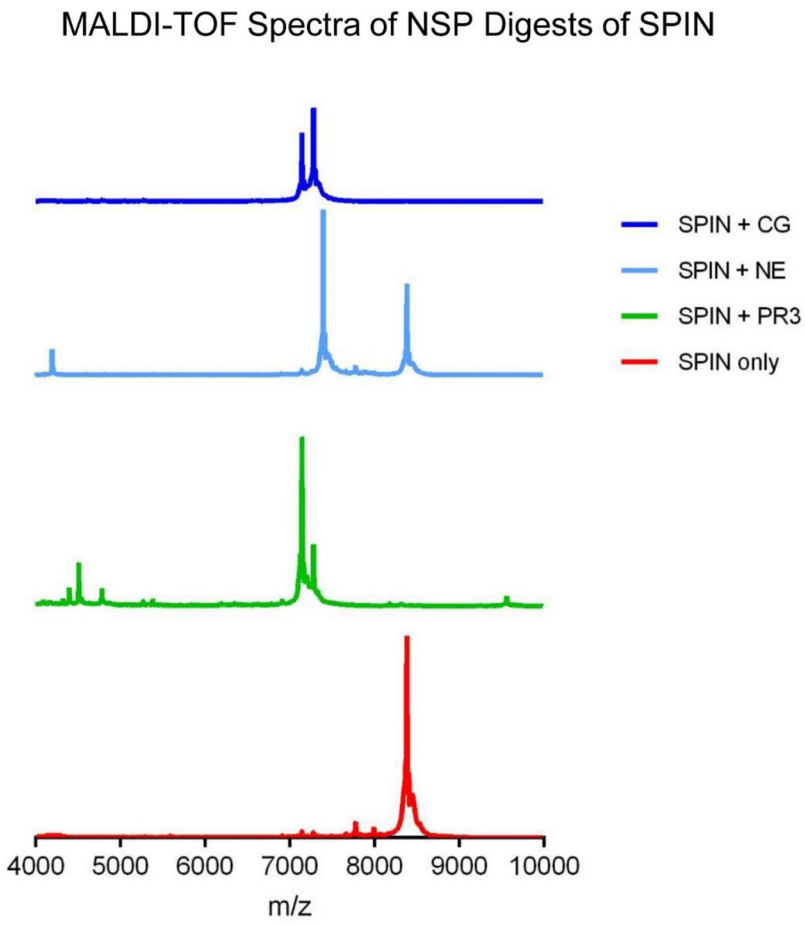

Supplemental Figure 4: MALDI-TOF Spectra of SPIN Following Digestion with Various NSPs. Purified SPIN was incubated for 1 h with 18 µg/ml NE, 4.5 µg/ml CG, or 4.5 µg/ml PR3 after which proteolytic activity was stopped by addition of PMSF. A portion of the NSP-treated SPIN samples were assayed for their MPO-inhibitory activity (**Figure 4**), while additional samples were examined for evidence of proteolytic digestion by MALDI-TOF mass spectrometry. Whereas the untreated SPIN protein showed no evidence of cleavage (m/z = 8,381), samples of SPIN treated with either CG (m/z = 7,278) or PR3 (m/z = 7,142) were characterized by well-defined smaller molecular weight species consistent with site-specific proteolysis. SPIN treated with NE appeared to result in incomplete digestion (m/z =7,392 and 8,381), however, which explained the residual MPO inhibitory activity found in this sample (**Figure 4A**).

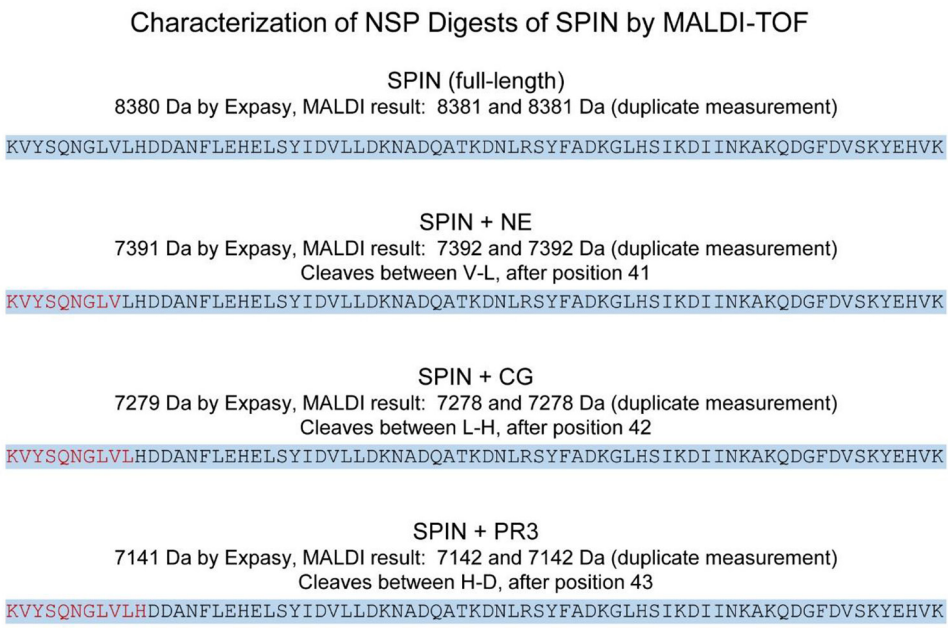

Supplemental Figure 5: Further Characterization of SPIN Cleavage Products Following Proteolysis by NSPs. The MALDI-TOF data presented in **Supplemental Figure 4** were compared to the sequence of SPIN to more fully characterize each digestion reaction. The main product of each SPIN digest was in good agreement with the known cleavage site preferences of NE, CG, and PR3. The identity of those residues removed upon digestion by each NSP is shown in red typeface. Together, these data indicate that the SPIN N-terminal region is cleaved by CG and PR3, and to a lesser extent, NE.

Chapter 6

Identification and Structural Characterization of a Novel Myeloperoxidase Inhibitor from *Staphylococcus delphini*

Nicoleta T. Ploscariu[1], Nienke W. M. de Jong[2], Kok. P. M. van Kessel[2], Jos A. G. van Strijp[2], and Brian V. Geisbrecht[1]

[1] Department of Biochemistry & Molecular Biophysics, Kansas State University, 141 Chalmers Hall, 1711 Claflin Road Manhattan, KS, USA 66506

[2] Department of Medical Microbiology, University Medical Center Utrecht, Utrecht University, Heidelberglaan 100 3584 CX Utrecht, The Netherlands

Manuscript under revision, Archives of Biochemistry and Biophysics

ABSTRACT

Staphylococcus aureus and related species are highly adapted to their hosts and have evolved numerous strategies to evade the immune system. *S. aureus* shows resistance to killing following uptake into the phagosome, which suggests that the bacterium evades intracellular killing mechanisms used by neutrophils. We recently discovered an *S. aureus* protein (SPIN for Staphylococcal Peroxidase INhibitor) that binds to and inhibits myeloperoxidase (MPO), a major player in the oxidative defense of neutrophils. To allow for comparative studies between multiple SPIN sequences, we identified a panel of homologs from species closely related to *S. aureus*. Characterization of these proteins revealed that SPIN molecules from *S. agnetis*, *S. delphini*, *S. schleiferi*, and *S. intermedius* all bind human MPO with nanomolar affinities, and that those from *S. delphini*, *S. schleiferi*, and *S. intermedius* inhibit human MPO in a dose-dependent manner. A 2.4 Å resolution co-crystal structure of SPIN-*delphini* bound to recombinant human MPO allowed us to identify conserved structural features of SPIN proteins, and to propose sequence-dependent physical explanations for why SPIN-*aureus* binds human MPO with higher affinity than SPIN-*delphini*. Together, these studies expand our understanding of MPO binding and inhibition by a recently identified component of the staphylococcal innate immune evasion arsenal.

HIGHLIGHTS

- *S. aureus* secretes a protein, SPIN, that potently inhibits human Myeloperoxidase
- A number of closely related staphylococci also encode SPIN homologs
- SPIN homologs vary in their binding to and inhibition of human Myeloperoxidase
- SPIN from *S. delphini* has been co-crystallized with recombinant human MPO
- Comparison of SPIN co-crystal structures explains differences in binding behavior

INTRODUCTION

Neutrophils are the most abundant white blood cells in human circulation and play a critical role in the acute phase of inflammation. Neutrophils serve as the first line of defense against invading bacteria (1, 2), and eliminate bacterial pathogens following phagocytosis. Efficient phagocytic killing is a complex process dependent upon the various antimicrobial proteins and peptides contained within neutrophils' subcellular granules (Reviewed in (1–5)). As the phagosomal compartment matures, an enzymatic system that leads to generation of diverse reactive oxidant species assembles within its membrane. Activity of the multipartite NADPH oxidase converts O_2 into O_2^-, which dismutates either directly or enzymatically into H_2O_2. Although H_2O_2 on its own is cytotoxic, it also serves as a substrate for the abundant heme-dependent granule enzyme, myeloperoxidase (MPO). MPO generates highly toxic and reactive oxidant species, most notably hypochlorous acid (HOCl). Neutrophil granules likewise contain high levels of antibacterial peptides and proteases, such as neutrophil elastase (NE), cathepsin G (CG), and proteinase-3 (PR3). While these proteases on their own are sufficient to kill certain bacteria (6–8), there is evidence to suggest that they function synergistically with MPO-derived oxidants to enhance killing of bacteria trapped within the phagosome (9). Thus, the abundant and overlapping anti-bacterial systems acting within the neutrophils' phagosomal compartment present a formidable innate defense against infection.

Staphylococcus aureus is a Gram-positive pathogenic bacterium that causes a broad range of infections in humans and animals (10). Along with closely related staphylococcal species, *S. aureus* has an increasingly negative impact worldwide due to a rapidly expanding incidence of antibiotic resistance as well as a generally enhanced capacity for virulence. Even though neutrophils play a central role in the overall response to *S. aureus* infection (11, 12), the bacterium has evolved a broad repertoire of strategies to resist both opsonisation and phagocytosis (13–16). Furthermore, *S. aureus* shows resistance to killing following uptake into the phagosome, which suggests that the bacterium can actively evade specific intracellular killing mechanisms used by neutrophils (13). In this regard, we identified a family of proteins secreted by *S. aureus* that bind non-covalently to and block function of the neutrophil granule proteases NE, CG, and PR3 (17). More recently, we discovered a previously uncharacterized protein, SPIN (for Staphylococcal Peroxidase INhibitor), that binds tightly to MPO and inhibits its enzymatic activity (18).

Since SPIN shares no sequence relationships to other known proteins, we have relied on structure-based approaches to better understand the molecular basis for its function. A co-crystal structure of *S. aureus* SPIN bound to a recombinant form of human MPO (rhMPO) indicated that this inhibitor acts as a molecular stopper to prevent exchange of substrates/products with the MPO active site (18). This structure also revealed that the ~8.3 kDa SPIN protein consists of two functionally distinct regions. Whereas the C-terminal 60 amino

acids adopt a compact three α-helical bundle fold, the N-terminal 13 residues comprise a unique β-hairpin motif (18). Subsequent studies showed that the α-helical bundle domain is responsible for driving interaction of SPIN with MPO, while the β-hairpin region makes only minor contributions to SPIN/MPO binding (19). This latter feature is consistent with solution NMR spectroscopy studies on SPIN, which demonstrated that the N-terminal β-hairpin is actually disordered in the absence of MPO (19, 20). Nevertheless, the N-terminal residues of SPIN are required for inhibiting MPO activity (19), since the β-hairpin they comprise inserts into the MPO active site cavity and blocks substrate/product exchange (18).

Although molecular level analysis of *S. aureus* SPIN (hereafter SPIN-*aureus*) has provided fundamental insights into the structure and function this novel MPO inhibitor, our current understanding is restricted to sequence/structure features specific to the SPIN-*aureus* protein. To circumvent this limitation, we sought to identify SPIN-*aureus* homologs in other staphylococcal species and characterize their interactions with and effects on human MPO. We report here the identification of eight SPIN homologs, three of which bind to and inhibit human MPO in a dose-dependent manner. We also present a 2.4 Å co-crystal structure of SPIN from *Staphylococcus delphini* (SPIN-*delphini*) bound to rhMPO. This work not only allows the first comparative analyses of SPIN proteins, it also broadens our appreciation of a unique class of MPO inhibitor that functions in staphylococcal evasion of neutrophil-mediated immunity.

RESULTS

Identification of SPIN homologs in a subset of staphylococcal species

The *spn* gene is nearly ubiquitous among both human and animal-derived clonal lineages of *S. aureus* (18). Furthermore, aside from *S. aureus* strains Mu3 and Mu50 which encode a substantially truncated and therefore inactive protein, there is little variability in the SPIN coding sequence between *S. aureus* strains (18). Although these previous studies indicated that SPIN is highly conserved among *S. aureus* strains, we wondered whether genes encoding SPIN homologs might be found in related staphylococcal species. To test this possibility, we used the BLASTP algorithm to query the NCBI non-redundant protein database for any uncharacterized molecules with sequence homology to SPIN-*aureus* from strain Newman. Indeed, we identified eight such proteins from closely related staphylococcal species that are documented pathogens of humans, livestock, and/or domestic companion animals. Since SPIN is targeted for secretion from the bacterial cell via an N-terminal signal peptide, we used the SignalP server (http://www.cbs.dtu.dk/services/SignalP/) to deduce the predicted matured sequences of the SPIN homologs (21). We then compared these sequences to one another and with SPIN-*aureus* using a combination of CLUSTAL OMEGA (22) and MultAlin (23) (**Table 1**).

We found agreement in our phylogenetic analysis of these novel SPIN-like sequences and

Table 1: Sequence identities among the SPIN sequences of various staphylococcal species.

SPIN	*sciuri*	*aureus*	*chromog*	*agnetis*	*hyicus*	*schleiferi*	*delphini*	*intermed*	*pseudint*
sciuri	100	-	-	-	-	-	-	-	-
aureus	38	100	-	-	-	-	-	-	-
chromog	35	48	100	-	-	-	-	-	-
agnetis	41	52	75	100	-	-	-	-	-
hyicus	38	46	69	85	100	-	-	-	-
schleiferi	29	56	61	59	51	100	-	-	-
delphini	33	53	58	54	48	69	100	-	-
intermed	39	57	53	50	47	59	74	100	-
pseudint	38	57	55	55	49	69	75	81	100

previous analyses that identified relationships between these staphylococcal species (24) (**Figure 1A**). For example, *S. hyicus* and *S. agnetis*, belong to the same clade of staphylococci (25). Comparison of SPIN-*hyicus* and SPIN-*agnetis* revealed less than 5 point accepted mutations (PAM) and ~85% sequence identity between these two proteins. A similar relationship was observed between *S. schleiferi* and established members of the *Staphylococcus intermedius* group (SIG) (i.e. *S. intermedius*, *S. pseudintermedius*, and *S. delphini*) (26). SPIN sequences within this cluster share no less than ~59% identity with one another (i.e. SPIN-*intermedius* v. SPIN-*schleiferi*), and also display the highest overall sequence identities with SPIN-*aureus* (~53-57%). By contrast, the distant phylogenetic relationship between *S. sciuri* and other staphylococci (27, 28) was also reflected in the relatively low sequence identity of SPIN-*sciuri* with the other SPIN sequences we analyzed here (~29-39% identity).

All published structure/function analyses thus far have been carried out using either natively-produced or recombinantly-expressed SPIN-*aureus* (18). In this regard, the overall sequence identity of the matured homologs to SPIN-*aureus* varies between 38-57% (**Figure 1A** and **Table 1**). Surprisingly, examination of a multiple sequence alignment revealed that only 10 of 73 positions (~14%) are invariant across the nine sequences analyzed (**Figures 1B-C**). Of

Table 2: Binding analysis of SPIN homologs to native human MPO as determined by SPR*.

SPIN	**k_a ($M^{-1}s^{-1}$) x 10^4**	**k_d (s^{-1}) x 10^{-3}**	**K_D (nM)**
aureus	20.10 ± 2.22	3.16 ± 0.04	15.9 ± 2.1
agnetis	5.64 ± 0.14	2.36 ± 0.10	41.8 ± 1.1
schleiferi	1.12 ± 0.14	2.52 ± 0.17	230 ± 42.1
delphini	1.08 ± 0.08	3.34 ± 0.17	310 ± 42.5
intermedius	0.35 ± 0.08	3.34 ± 0.12	984 ± 274

* Values represent the mean plus or minus the standard deviation obtained from replicate injections across three independent flow cells derivatized with native human MPO.

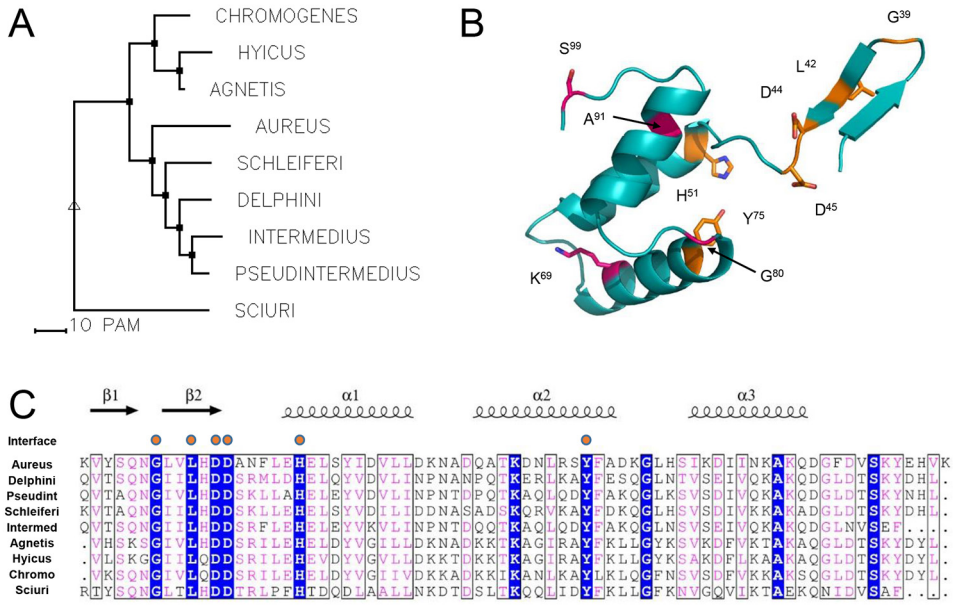

Figure 1: Analysis of sequence conservation across putative SPIN homologs. A group of hypothetical sequences homologous to SPIN-*aureus* was identified by BLAST searching in the NCBI non-redundant protein database. The predicted mature form of each protein following cleavage of the signal peptide was determined via the SignalP server (21). (**A**) Phylogenetic tree based upon the matured amino acid sequences of SPIN-*aureus* and eight other species of staphylococci. The tree is drawn to scale with branch lengths measured in the number of substitutions per site. (**B**) The structure of rhMPO-bound SPIN-*aureus* is shown as a ribbon diagram (PDB code 5UZU (18)). Residues invariant in all SPIN homologs and found at the SPIN/rhMPO interface are colored orange, while invariant residues that do not play a direct role in rhMPO contact are colored pink. Numbering reflects the sequence of matured SPIN-*aureus*. The N-terminal β-hairpin is shown at the top right of the image for purposes of orientation. (**C**) The sequences of putative SPIN homologs were aligned to that of SPIN-*aureus* using Clustal Omega (22), and displayed using EsPript (42). Invariant residues are shown in reverse blue typeface, while residues conserved in a majority of sequences and conservative substitutions are shown in purple typeface. The secondary structure of rhMPO-bound SPIN-*aureus* is displayed above the alignment. Residues invariant across all SPIN homologs and found at the SPIN/rhMPO interface are designated with an orange circle.

these, only six residues (G^{39}, L^{42}, D^{44}, D^{45}, H^{51}, and Y^{75} per SPIN-*aureus* numbering) were found at the SPIN-*aureus*/rhMPO interface, as judged by the co-crystal structure (18). Interestingly, four of these residues (G^{39}, L^{42}, D^{44}, and D^{45}) lie within the N-terminal region of the SPIN protein. Although this region of SPIN-*aureus* appears to make only minor contributions to SPIN binding of MPO, it is essential for inhibiting MPO enzymatic activity (19). Thus, the relatively low level of absolute identity within the known MPO-binding site of SPIN suggested that valuable insights might be gained from further structure/function studies on these SPIN homologs.

A subset of SPIN-*aureus* homologs bind to and inhibit the enzymatic activity of human MPO

Since genomic DNA was not readily available for all of these staphylococcal species, we designed

Table 3: X-ray Diffraction Data Collection and Refinement

	SPIN-*delphini*/rhMPO
Data Collection	
Space group	*P* 2_1 2_1 2_1
Cell dimensions	
a, b, c (Å)	84.63 90.67 125.66
Resolution (Å)	45.34-2.40 (2.49-2.40)*
Rpim	0.045 (0.382)
I / σI	15.5 (1.7)
Completeness (%)	99.7 (97.2)
Redundancy	13.5 (7.7)
Refinement	
Resolution (Å)	45.34-2.40
Number of Reflections	36,188
Rwork / Rfree	18.5/21.8
No. atoms	
Protein	5143
Ligand/ion	87
Solvent	105
Mean *B*-factors (Å^2)	
Protein	56.8
Ligand/ion	65.3
Solvent	50.9
R.M.S. deviations	
Bond lengths (Å)	0.015
Bond angles (°)	1.48

* Values in parentheses are for the highest-resolution shell.

synthetic coding sequences for each of the SPIN homologs, subcloned these fragments into a plasmid vector that directs expression of N-terminally his-tagged fusion proteins (29), and used these plasmids to produce highly purified forms of each putative SPIN. The integrity of each protein was confirmed by MALDI-TOF mass spectrometry. Unfortunately, the SPIN-*hyicus* protein appeared prone to degradation, and was thereby excluded from further analysis. We then examined the ability of each remaining SPIN protein to bind immobilized native human MPO by a surface plasmon resonance (SPR) approach. Injections of an increasing concentration of each recombinant SPIN gave clear evidence of binding for several of the homologs (**Figure 2**). SPIN-*chromogenes* and SPIN-*sciuri* appeared to bind human MPO much more weakly than the others and were not analyzed further (data not shown), while SPIN-pseud*intermedius* gave no evidence of binding whatsoever (**Figure 2**). The reference subtracted sensorgrams for all other series were analyzed using a kinetic model of 1:1 binding to derive association (k_a),

dissociation (k_d), and affinity constants (K_D) for each interaction (**Table 2**).

We previously reported that SPIN-*aureus* binds immobilized native human MPO with an apparent K_D of 10±0.6 nM (18). Replicate measurements performed during this present study yielded a similar value of 15.9±2.1 nM (**Table 2**), which indicated a high level of precision for

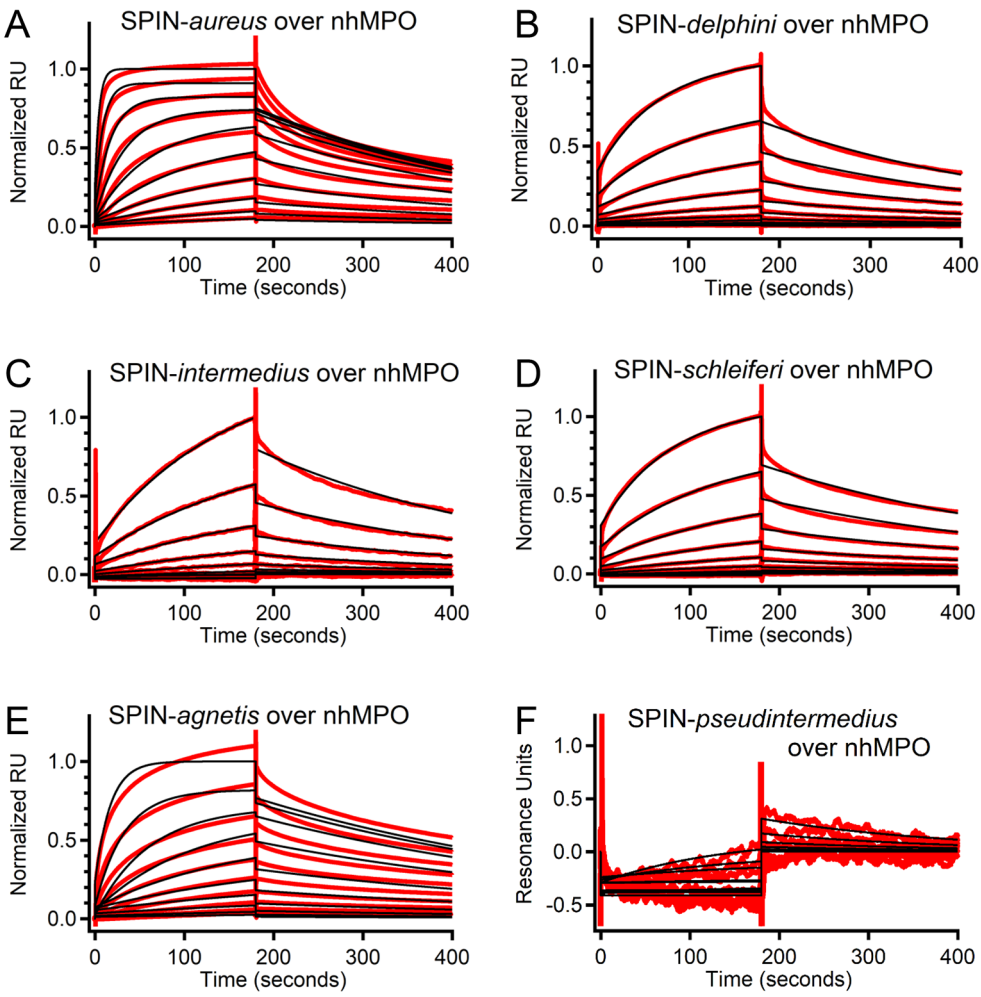

Figure 2: Characterization of SPIN homolog binding to native human MPO by surface plasmon resonance. A two-fold dilution series of recombinant SPIN-*aureus* and various homologs was injected over three separate flow-cells of native human MPO that had been randomly immobilized at different surface densities. The reference-subtracted sensorgrams for each injection series (black traces) were fit to a 1:1 binding model (red traces) and normalized to their respective maximal responses. Representative sensorgram series are shown for native MPO binding to (**A**) SPIN-*aureus*, (**B**) SPIN-*delphini*, (**C**) SPIN-*intermedius*, (**D**) SPIN-*schleiferi*, and (**E**) SPIN-*agnetis*. (**F**) Representative traces for injections of SPIN-*pseudintermedius* over native MPO surfaces. SPIN-pseud*intermedius* does not appear to bind significantly to native human MPO, since the observed response values were very low for this homolog. As a consequence, the data were not normalized. Comparatively weak binding to human MPO was observed for SPIN-chromogenes and SPIN-*sciuri*, so these are not presented here in the interest of space.

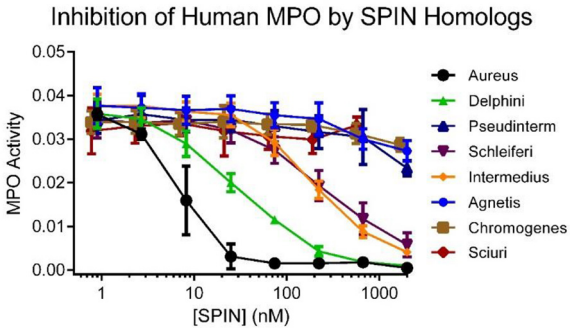

Figure 3: A subset of SPIN homologs inhibit the enzymatic activity of native human MPO. The enzymatic activity of native human MPO was investigated across a dilution series of various recombinant SPIN homologs. Initial reaction velocities were determined in triplicate at each concentration point prior to curve fitting and determination of IC_{50} values. Whereas SPIN-*delphini*, SPIN-*schleiferi* and SPIN-*intermedius* all inhibit MPO in a dose-dependent manner, SPIN-*agnetis* fails to do so even though it binds with low-nanomolar affinity to native MPO. SPIN-*aureus* is included as a control for inhibition (18). Bars express the mean plus or minus the standard deviation (n=3). A legend is inset.

the SPR interaction assay across several independent experiments. We found considerable variability in the interactions between human MPO and the SPIN homologs, however (**Figure 2** and **Table 2**). Although no SPIN homolog bound MPO as well as SPIN-*aureus*, SPIN-*agnetis* displayed the second highest affinity for MPO, as judged by its K_D of 41.8±1.1 nM. The affinity of the remaining homologs ranged from 230±42.1 nM for SPIN-*schleiferi* to 984±274 nM for SPIN-*intermedius*. These values represent approximately 14.5 and 61.9-fold decreases in affinity for human MPO, respectively, when compared to SPIN-*aureus*. We also noted that all of the SPIN homologs that bind human MPO had similar dissociation rate constants (k_d), which ranged from $2.36x10^{-3}$ to $3.34x10^{-3}$ s^{-1} as a group. Conversely, the association rate constants (k_a) for binding to MPO varied widely, from a high of 20.1x104 $M^{-1}s^{-1}$ for SPIN-*aureus* to a low of 0.354x104 $M^{-1}s^{-1}$ for SPIN-*intermedius*. Thus, nearly all of the differences in affinity for human MPO displayed by these SPIN homologs is attributable to variations in their association rate constants.

Our co-crystal structure of SPIN-*aureus*/rhMPO indicates that SPIN acts as a molecular plug to block solute exchange to and from the MPO active site (18). However, subsequent studies on a series of site-directed and deletion mutants of SPIN-*aureus* revealed that binding to MPO is necessary, but not sufficient for inhibiting its activity (19). We therefore sought additional information on whether the SPIN homologs that bound MPO in the SPR assay could also block MPO function in an enzymatic activity assay. We used a colorimetric activity assay to examine the ability of each SPIN to inhibit MPO function in vitro (**Figure 3**). Each SPIN homolog was added to the assay in triplicate across a dilution series that spanned three orders of magnitude. Consistent with our previous work, we found that SPIN-*aureus* significantly inhibited MPO activity under these conditions (IC_{50} ~8 nM) (18, 19). Conversely, we also found that all SPIN variants that failed to bind human MPO (i.e. SPIN-*sciuri*, SPIN-*chromogenes*, and

SPIN-pseud*intermedius*) also failed to inhibit its activity.

Out of the homologs that remained, we found that three retained a clear inhibitory capacity against human MPO. Whereas SPIN-*intermedius* and SPIN-*schleiferi* inhibited MPO with IC_{50} values of ~200 nM, SPIN-*delphini* displayed an approximately 6.7-fold more potent IC_{50} value of ~30 nM. These differences in IC_{50} values were somewhat unexpected, given that these three SPIN homologs are part of the same phylogenetic clade and share over 60% identity with one another (**Figure 1A** and **Table 1**). The most surprising results were obtained for SPIN-*agnetis*. This protein failed to significantly inhibit MPO at concentrations up to 2 μM, even though it binds human MPO with a K_D of 41.8 nM as judged by SPR (**Figure 2** and **Table 2**). In this regard, the functional properties of SPIN-*agnetis* most closely resemble those of a site-directed mutant in SPIN-*aureus* where the conserved sidechains of H^{43}, D^{44}, and D^{45} were simultaneously changed to alanine (19). This mutant also failed to inhibit MPO despite the fact that it binds MPO with a K_D near 30 nM.

The crystal structure of SPIN-*delphini* bound to recombinant human MPO at 2.4 Å resolution

We required additional structural information on rhMPO in complex with a tightly binding SPIN homolog in order to better understand the similarities and differences among these newly identified SPIN family members. We succeeded in growing single crystals of SPIN-*delphini* bound to rhMPO that diffracted synchrotron X-rays to 2.4 Å limiting resolution, and solved and refined this structure to Rwork/Rfree values of 18.5 and 21.8%, respectively (**Figure 4A** and **Table 3**). As expected, the structure of SPIN-*delphini*/rhMPO compares favorably to the structure of SPIN-*aureus*/rhMPO (**Figure 4B**), as the 539 Cα positions from the two coordinate sets that align with one another superimpose with an RMSD of 0.289 Å. When we compared only the structures of rhMPO-bound SPIN-*aureus* and SPIN-*delphini* to one another, the 61 Cα positions align with an RMSD of 0.812 Å (**Figure 4C**). This high level of structural identity was preserved throughout the entirety of the models, save for some minor deviations at the proteins' N and C-termini.

For reasons that remain unclear, our crystal structures of rhMPO bound to either full-length or an N-terminally deleted SPIN-*aureus* are characterized by low occupancy of the heme prosthetic group (18, 19). Absence of the heme was not required for SPIN binding though, as full-length and N-terminally deleted SPIN-*aureus* bind equally well to both rhMPO and native MPO that had been isolated from purulent human sputum (18, 19). Interestingly, examination of the Fo-Fc electron density map calculated after initial placement of the polypeptide models in the SPIN-*delphini*/rhMPO asymmetric unit revealed an obvious planar density at contour levels up to 3σ within the rhMPO active site (**Figure 4D**). Following model building and refinement, our final SPIN-*delphini*/rhMPO coordinates have full occupancy of the heme prosthetic group with a median B-factor of 57.6 $Å^2$. This value is consistent with the structure as a whole, whose all atom mean B-factor is 56.8 $Å^2$ (**Table 3**).

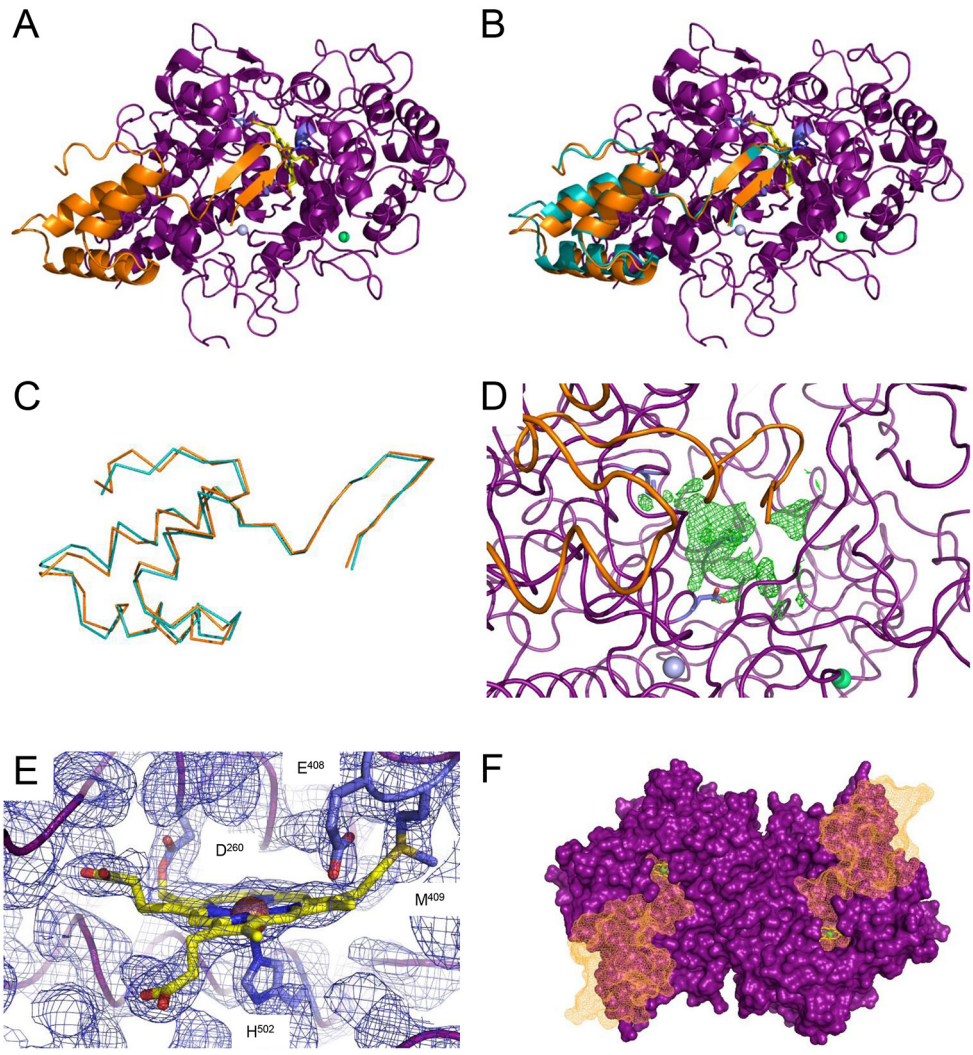

Figure 4: The structural basis for inhibition of MPO by SPIN-*delphini*. (**A**) A 2.4 Å co-crystal structure of rhMPO (purple) bound to SPIN-*delphini* (orange). Proteins are represented as ribbon diagrams, while the covalently bound heme prosthetic group is drawn in ball-and-stick convention with carbon atoms in yellow, nitrogen in blue, oxygen in red, and the iron ion as a red sphere. Ordered Ca^{2+} and Cl^- ions are drawn as light blue and green spheres, respectively. (**B**) Superposition of the SPIN-*aureus*/rhMPO co-crystal structure (PDB code 5UZU (18)) onto the SPIN-*delphini*/rhMPO structure as shown in panel **A**. SPIN-*aureus* is drawn as a cyan ribbon. (**C**) Superposition of rhMPO-bound forms of SPIN-*aureus* (cyan) and SPIN-*delphini* (orange). The proteins are drawn in wire convention with the N-terminal β-hairpin at the right-hand side of the image. (D) F_o-F_c electron density map (green mesh contoured at 2.5σ) within the rhMPO active site after initial structure solution by molecular replacement. The proteins chains are colored identically to the panels above for clarity, while the locations of the Ca^{2+} and Cl^- ions are included for reference. (**E**) Properties of the heme prosthetic group in the final model of SPIN-*delphini*/rhMPO. The heme is drawn as in panel **A**, while noteworthy rhMPO sidechains (labels insert) are drawn as stick models (carbon atoms light purple). Note the inclusion of three covalent bonds as described in the text. $2F_o$-F_c electron density (blue mesh contoured at 1.3σ) is shown as an indicator of model to map correlation.

(**F**) Visualization of the SPIN binding site on MPO in the context of the native human MPO dimer. Two copies of the SPIN-*delphini*/rhMPO structure were superimposed on native human MPO (PDB code 1CXP (30)). MPO is drawn in purple as a molecular surface, while SPIN-*delphini* is drawn as an orange, space-filling mesh. The heme is drawn as in panel **A**, with the exception that the iron ion is colored green to enhance contrast.

The final $2F_o$-F_c electron density maps were consistent with the existence of four covalent bonds between SPIN-*delphini* bound rhMPO and the heme group (**Figure 4E**). However, we included only three of these four covalent bonds in our final model: H^{502} to heme Fe at 2.51 Å, M^{409} to heme CBB at 1.95 Å, and D^{260} to heme CMD at 1.58 Å. The final covalent bond between E^{408} and heme CMB was visible as contiguous density within the $2F_o$-F_c map at levels up to 1.4 σ, but at 2.16 Å fell outside an acceptable bond length for this linkage (c.f. 1.55 Å for the corresponding bond in PDB entry 1CXP (30). We believe this discrepancy likely resulted from the lower positional certainty of coordinates at 2.4 Å resolution when compared to higher resolution structures, such as the 1.8 Å resolution structure of halide-bound native human MPO referenced above (30). These minor differences aside, the structure of SPIN-*delphini*/rhMPO presented here demonstrates that binding of SPIN family proteins is not mutually exclusive with high occupancy of the heme prosthetic group in rhMPO.

Native MPO exists as a ~150 kDa dimer comprised of two heavy and two light chains, respectively (19). Moreover, crystal structures of native MPO from both human (30) and canine (31) sources revealed the presence of dimers within the asymmetric unit. The crystals of SPIN-*aureus* bound to rhMPO contain only a single copy of each polypeptide in the asymmetric unit (18), however, and examination of the protein-protein interfaces created by crystallographic symmetry operators showed no dimeric features equivalent to those found in native MPO. Similarly, the crystals of SPIN-*delphini*/rhMPO likewise contain only a single copy of the complex within the asymmetric unit (**Figure 4A**), and there was no dimer equivalent to native MPO visible via crystallographic symmetry operations. Despite the fact that both SPIN-*aureus* and SPIN-*delphini* crystallized with rhMPO as binary complexes, we found that each of these structures is still compatible with the dimeric assembly found in native MPO (**Figure 4F**). Superposition of both sets of coordinates onto the structure of dimeric native MPO revealed no obvious steric clashes that would prevent binding of either SPIN to such an arrangement. In fact, this is consistent with analytical gel filtration chromatography studies that show clear evidence for binding of both SPINs to native human MPO (data not shown). Thus, the differences in oligomerization state observed in our structural studies most likely resulted from the rhMPO we used in this work, rather than reflecting bona fide consequences of SPIN binding to MPO.

Sequence-dependent structural differences between SPIN-*delphini* and SPIN-*aureus* offer an explanation for their differences in affinity for human MPO

Whereas SPIN-*delphini* and SPIN-*aureus* form complexes with rhMPO that closely resemble one another (**Figure 4B**), the affinities of these proteins for MPO differ by nearly 20-fold at

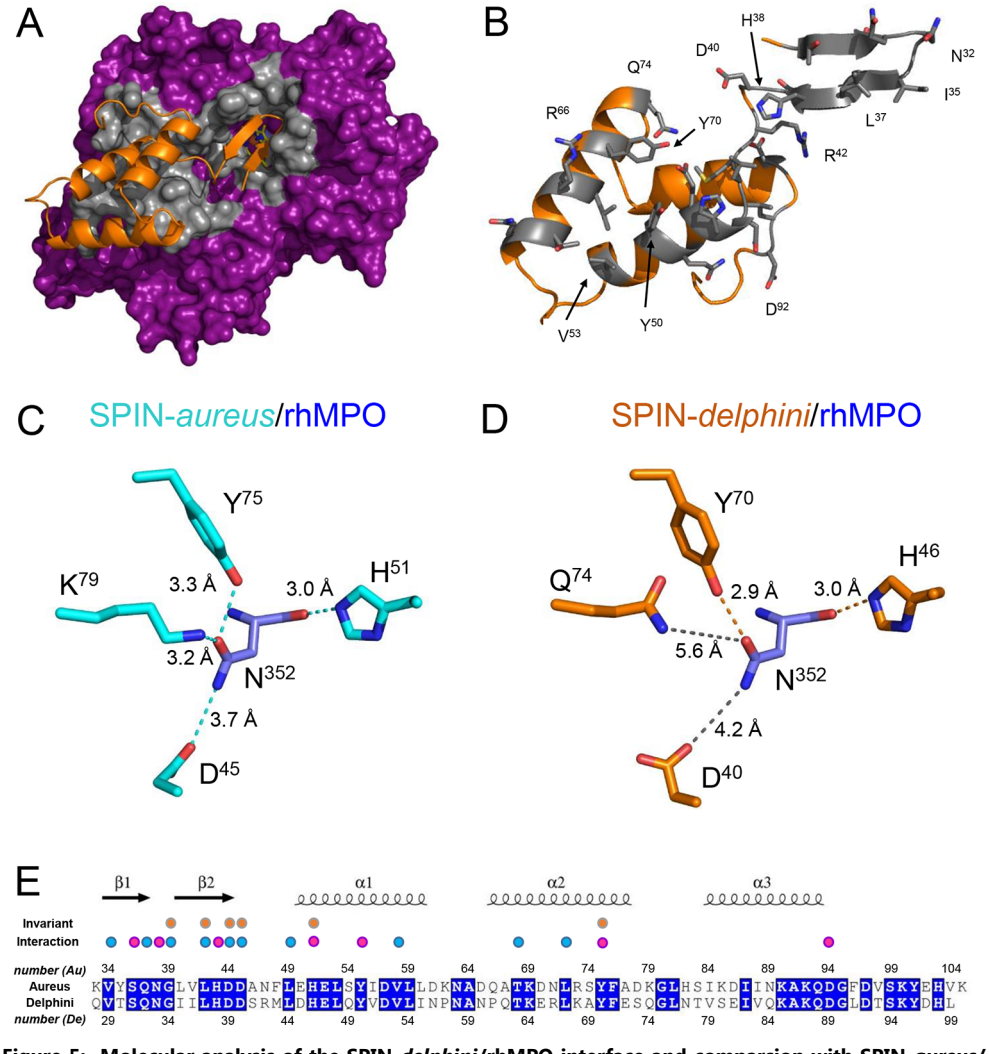

Figure 5: Molecular analysis of the SPIN-*delphini*/rhMPO interface and comparsion with SPIN-*aureus*/rhMPO. (**A**) Representation of the SPIN-*delphini*/rhMPO structure highlighting the residues comprising the SPIN-*delphini* binding site on rhMPO. SPIN-*delphini* is shown as an orange ribbon, while rhMPO is drawn as a molecular surface with non-interacting residues in purple and interfacing residues in grey. The heme prosthetic group is drawn as in **Figure 4** for reference. (**B**) The structure of SPIN-*delphini* drawn as an orange ribbon. Sidechains found at the rhMPO interface are drawn in stick convention with the carbon atoms colored grey. Selected sidechains are individually labeled. Note that this representation of SPIN-*delphini* is rotated approximately 180° in the plane of the page relative to panel **A**. (**C**) Polar interactions between SPIN-*aureus* sidechains (cyan) and N^{352} of rhMPO (blue). Likely interactions (cyan dashes) and their corresponding distances are labeled. (**D**) Polar interactions between SPIN-*delphini* sidechains (orange) and N^{352} of rhMPO (blue). Likely interactions (orange dashes) and their corresponding distances are labeled. Grey dashes represent interactions not formed due to excessive distance between donor and acceptor groups. (**E**) Sequence comparison between SPIN-*aureus* (numbering above) and SPIN-*delphini* (numbering below) with identical residues shown reverse blue typeface. The secondary structure of rhMPO-bound SPIN-*aureus* is displayed above the alignment. Identical residues found at the rhMPO interface of each complex that form non-polar interactions are indicated by a cyan circle, while those that form polar interactions are indicated by a magenta circle. Residues invariant across all SPIN homologs and found at the

SPIN/rhMPO interface are designated with an orange circle. Note the participation of invariant residues D^{45}, H^{51}, and Y^{75} (per SPIN-*aureus* numbering) in interactions with N^{352} of rhMPO, and how this varies in SPIN-*delphini* by comparing panels **C** and **D** above.

310 nM and 15.9 nM, respectively (**Table 1**). Since SPIN-*delphini* shares 53% identity with SPIN-*aureus*, we considered whether the differences in affinities observed by SPR were due to alterations of key sidechains found at the SPIN/rhMPO interfaces. We analyzed the SPIN-*delphini*/rhMPO complex using the PISA server (32) and used the output to construct both an interface map (**Figure 5A**) and a list of likely intermolecular interactions (**Table 4**). We then compared these data from SPIN-*delphini*/rhMPO to analogous results obtained for SPIN-*aureus*/rhMPO (18) (**Table 4**).

We determined that the total number of inhibitor-derived residues at the SPIN-*delphini*/rhMPO interface, 30, is nearly identical to that of SPIN-*aureus*/rhMPO, 31 (**Figures 5A-B**). Consistent with the overall identity between these two proteins, however, only 17 interfacing residues are identical between SPIN-*delphini* and SPIN-*aureus*. Given that even minor changes at the interface might result in altered surface compatibility between rhMPO and the two SPINs, we analyzed the surface complementarity of both structures using the program s.c. (33). Both SPIN-*delphini*/rhMPO and SPIN-*aureus*/rhMPO have similar overall s.c. coefficients of 0.715 and 0.704, respectively; these values are slightly lower than those of other high-affinity protein/protein interactions relevant to staphylococcal innate immune evasion, such as that of the neutrophil serine protease inhibitor, EapH1, bound to neutrophil elastase (s.c. = 0.77) (17). Nevertheless, since previous work had shown that the SPIN-*aureus*/MPO interaction primarily arises via the α-helical bundle region of the inhibitor (19), we recalculated the s.c. coefficients of these structures in the absence of the N-terminal β-hairpin motifs. This yielded an s.c. value of 0.715 for SPIN-*delphini*/rhMPO, but of 0.774 for SPIN-*aureus*/rhMPO. We considered the rather large difference between these two s.c. values as evidence that the α-helical bundle region SPIN-*aureus* is far better suited to packing tightly against rhMPO than is SPIN-*delphini*. Consistent with this prediction, SPIN-*delphini* buries only 1365 $Å^2$ of its surface area when bound to rhMPO. This value is only ~85% of that previously reported for SPIN-*aureus* (18).

We also found that the number of polar interactions (i.e. hydrogen bonds and salt bridges) formed with rhMPO is considerably smaller for SPIN-*delphini* than for SPIN-*aureus*. Of the 31 residues found at the interface between SPIN-*aureus* and rhMPO, 14 appeared to participate in one or more polar contacts with groups from rhMPO. By contrast, of the 30 residues found at the SPIN-*delphini*/rhMPO interface, only 11 were judged to form polar contacts with rhMPO. Whereas seven of these residues are identical between the two SPINs and deemed to form equivalent interactions (i.e. S^{31}, N^{33}, H^{38}, H^{46}, Y^{50}, Y^{70}, and D^{89} per SPIN-*delphini* numbering), the other conserved position (i.e. D^{40}) fails to form a hydrogen bond in the SPIN-*delphini*/rhMPO structure even though it does so in the SPIN-*aureus*/rhMPO structure. Furthermore, three other positions in SPIN-*delphini* (i.e. Q^{28}, T^{30}, and Q^{74}) represent non-conservative changes when compared to SPIN-*aureus* and thereby disrupt polar contacts.

Table 4: Comparative interface analysis of SPIN-*delphini*/rhMPO and SPIN-*aureus*/rhMPO

SPIN-*delphini*	Bond type	SPIN-*aureus*	Bond type	MPO residue
		33 LYS	HS	GLU346
29 **VAL**		34 **VAL**		
30 THR		35 TYR	H	GLU346
31 **SER**	H	36 **SER**	H	GLU268
32 **GLN**	H	37 **GLN**		THR265
33 **ASN**	H	38 **ASN**	H	GLU268
34 **GLY**		39 **GLY**		
35 ILE		40 LEU		
36 ILE		41 VAL		
37 **LEU**		42 **LEU**		
38 **HIS**	S	43 **HIS**	HS	ASP380
39 **ASP**		44 **ASP**	HS*	ARG272*
40 **ASP**		45 **ASP**	H	ASN352
42 ARG	H	47 ASN	H	ASN381
		47 ASN	H	HIS383
43 MET	H	48 PHE	H	ASN381
44 **LEU**		49 **LEU**		
45 ASP	S	50 GLU	HS	ARG368
46 **HIS**	H	51 **HIS**	H	ASN352
47 GLU				
49 GLN		54 SER		
50 **TYR**	H	55 **TYR**	H	MET356
		55 **TYR**	H	ARG354
53 **VAL**		58 **VAL**		
62 GLN				
63 **THR**		68 **THR**		
66 ARG		71 ASN		
67 **LEU**		72 **LEU**		
70 **TYR**	H	75 **TYR**	H	ASN352
		78 ASP		
74 GLN		79 LYS	H	ASN352
		93 GLN		
89 **ASP**	H	94 **ASP**	H	ASN381
		95 GLY		
91 LEU		96 PHE		
92 ASP				

Identical Positions in Bold Typeface
H: hydrogen bond
S: salt bridge
*ARG271 is found on apo-MPO only

residues at the interface with MPO
bond forming residues, only by SPIN-*delphini*
bond forming residues, only by SPIN-*aureus*
bond forming residues, by both SPIN proteins

Since only the Q^{74} from SPIN-*delphini* resides in the α-helical bundle, we surmised that this change from K^{79} in SPIN-*aureus* is likely the most significant alteration in terms of MPO binding. In that regard, we noted that the residues D^{45}, H^{51}, and K^{79} of SPIN-*aureus* (corresponding to SPIN-*delphini* D^{40}, H^{46}, and Q^{74}) are all involved in hydrogen bonding to groups from position N^{352} of rhMPO (**Figures 5C-D**). In the case of SPIN-*aureus* D^{45} versus SPIN-*delphini* D40, the observed distance between acceptor and donor is 3.7 Å in SPIN-*aureus*/rhMPO compared to 4.2 Å in SPIN-*delphini*/rhMPO. A similar situation is found for SPIN-*aureus* K^{79} versus SPIN-*delphini* Q74, where the observed distance to the N^{352} sidechain is 3.2 Å compared to 5.6 Å. Although both SPIN-*aureus* and SPIN-*delphini* utilize a conserved histidine sidechain (i.e. H^{51} and H^{46}, respectively) to form hydrogen bonds of ~3.0 Å distance to the backbone oxygen from N^{352} in rhMPO, disruption of the other interactions with the N^{352} sidechain as described above may be a contributing factor to the reduced affinity of SPIN-*delphini* for MPO. In summary, while SPIN-*delphini* maintains an ability to bind human MPO and inhibit its activity (**Figures 2-3**), the quantitative differences between SPIN-*delphini* and SPIN-*aureus* vis-à-vis affinity for and inhibition of MPO appear to be predicated on sequence/structure changes that affect both the overall shape and positioning of functional groups at the MPO binding site of these closely related proteins (**Figure 5E**).

DISCUSSION

Though neutrophils serve many essential roles in the innate immune response, the significance of their contributions in preventing bacterial infection is underscored by the manifold strategies *S. aureus* deploys to evade opsonophagocytosis and efficient intracellular killing by these leukocytes (13). In this regard, the recently identified inhibitor of MPO, SPIN, is one component of a multipartite *S. aureus* evasion program that acts within the maturing phagosome. Although investigations of SPIN-*aureus* have provided vital information on this novel protein (18, 19), the studies we present here are an important step toward a broader understanding of the structure/function relationships of the SPIN protein family. Herein, we have identified eight different SPIN homologs (**Figure 1**), shown that four homologs bind human MPO (**Figure 2**), and further demonstrated that three of these block enzymatic activity of human MPO (**Figure 3**). We have also determined a 2.4 Å co-crystal structure of SPIN-*delphini* bound to rhMPO (**Figure 4**), thus allowing the first comparative structural analyses between SPIN proteins in complex with rhMPO (**Figure 5**).

Our work has confirmed that functional SPIN proteins are distributed amongst several bacterial species closely related to *S. aureus*. However, this has also opened up avenues for further investigation. For example, whereas *S. aureus* is a known pathogen of both humans and livestock (e.g. dairy cattle), several staphylococcal species that encode a SPIN-like sequence (e.g. the *Staphylococcus intermedius* group (26)) are primarily veterinary pathogens. We have previously shown that SPIN-*aureus* exhibits a pronounced binding selectivity and inhibitory capacity toward MPO from known hosts of this organism (18); this feature is perhaps best illustrated by tight binding to and inhibition of human MPO by SPIN-*aureus*, but an apparent lack of interaction with or inhibition of murine MPO (18). Consequently, it seems reasonable that several of the SPIN homologs which failed to bind or inhibit human MPO (**Figures 2-3**) might instead display a similar selectivity for MPO proteins derived from their preferred hosts. While additional studies will be necessary to determine whether or not this is the case, an experimental approach similar to those we employed here would be well-suited to addressing this issue.

Separately, our comparative analysis of the SPIN-*aureus*/rhMPO and SPIN-*delphini*/rhMPO complexes has allowed for a more thorough understanding of SPIN/MPO interactions at the sequence/structure level. First, we found no substantially greater level of conservation of the residues at the SPIN/MPO interface (i.e. 17/30 or 17/31 = ~56%) when compared to the two proteins overall (53%) (**Figures 4-5** and **Table 1**). This result was somewhat surprising, given that SPIN-*delphini* still maintains a relatively robust interaction with human MPO (K_D = 310 nM) (**Figure 2** and **Table 2**). Second, and along these lines, we noted that the numerous changes in SPIN-*delphini* when compared to SPIN-*aureus* manifest themselves as a notably lower overall surface complementary for rhMPO and buried surface area within the SPIN-*delphini*/rhMPO

complex. This is particularly true within the α-helical bundle region of the SPIN protein, which drives interaction with MPO (19). Though it is difficult to infer or test experimentally which of these subtle changes was most detrimental to a highly optimized and cooperative system like a protein/protein interaction, we believe that the cumulative effects of these alterations must have impacted the observed affinity of the complexes (**Figure 2** and **Table 2**). Finally, we found that the SPIN-*delphini*/rhMPO interface contains a significantly smaller number of polar interactions than does SPIN-*aureus*/rhMPO (**Figure 5** and **Table 4**). While some of the differences are due to loss of specific sidechains (e.g. SPIN-*delphini* Q^{74} vs SPIN-*aureus* K^{79}), others are due to unfavorable distances in the SPIN-*delphini*/rhMPO structure as compared to SPIN-*aureus*/rhMPO (e.g. SPIN-*delphini* D^{40} vs SPIN-*aureus* D^{45}). It seems then that changes in both shape complementarity and presentation of key polar groups at the MPO interface are contributing factors to the distinct MPO-binding and inhibitory properties of SPIN-*aureus* and SPIN-*delphini*.

SPIN is not the only staphylococcal innate immune evasion protein that shows strong selectivity for a target molecule from a biologically-relevant host of *S. aureus* (18). Species selectivity has also been described for the *S. aureus* SCIN family of proteins (34), as SCINs block activity of the alternative complement pathway in humans but not mice (34, 35). The bi-component pore forming leukocidins of *S. aureus* and related staphylococci likewise show strong preference for interaction with cellular receptors from specific species, thereby explaining their differential effects on target leukocytes from various hosts (36). Unfortunately, our current understanding of this selectivity is limited primarily to qualitative descriptions of binding and function. While these considerations are clearly useful, we believe that there must also be specific structural and bio/physical-chemical features which underlie such marked host selectivity. This is likely to be true for not only *S. aureus* innate immune evasion proteins, but for any molecules involved in pathogen/host interactions in a much broader sense. Considering that multiple SPIN sequences are now available and that quantitative biochemical, functional, and comparative structural information on these SPINs bound to MPO from various host species can in theory be obtained, we suggest that the SPIN/MPO interaction can be developed into a valuable model system for understanding the structure/function principles that underlie host specific evolution of virulence proteins.

ACKNOWLEDGEMENTS

We acknowledge helpful discussions with Drs. Kasra X. Ramyar and Brandon L. Garcia during the course of this study. This work was supported by a ZonMw Grant 205200004 from the Netherlands Organization for Health Research and Development (to J.A.G.v.S.) and US National Institutes of Health Grants AI111203 and GM121511 (to B.V.G.). X-ray diffraction data were collected at Southeast Regional Collaborative Access Team (SER-CAT) 22-ID beamline at the Advanced Photon Source, Argonne National Laboratory. A list of supporting institutions

may be found at www.ser-cat.org/members.html/. Use of the Advanced Photon Source was supported by the U.S. Department of Energy, Office of Science, Office of Basic Energy Sciences, under Contract No. W-31-109-Eng-38.

FOOTNOTES

The refined coordinates and structure factors have been deposited in the RCSB Protein Data Bank under the accession code 6BMT.

CONFLICT OF INTEREST

The authors declare that they have no conflict of interest with the contents of this article.

MATERIALS & METHODS

Proteins

Two different forms of human myeloperoxidase were used during the course of this work. Native human myeloperoxidase (MPO) that had been chromatographically isolated from purulent sputum was obtained from Elastin Products Corp. (Owensville, MO; catalog # MY862) and was used for biochemical and functional analyses. A recombinant form of human MPO (rhMPO) bearing a C-terminal 10-His tag was purchased from R&D Systems (Minneapolis, MN; catalog # 3174-MP-250) and was used for structural studies. The lyophilized proteins were reconstituted and handled as suggested by the supplier.

SPIN from *S. aureus* strain Newman was expressed and purified as described previously (18). The sequences of the predicted mature form of various SPIN homologs were codon optimized for E. coli expression using the Sequence Manipulation Suite Reverse Translate tool (http://www.bioinformatics.org/sms2/rev_trans.html) (37). The corresponding DNA fragments were synthesized as gBlocks Gene Fragments (Integrated DNA Technologies; Coralville, IA, USA) with BamH1 and Not1 sites appended at the 5′ and 3′ ends, respectively. Each of the coding fragments were subcloned into the BamHI and Not1 sites of a modified form of the prokaryotic expression vector pT7HMT (29). The integrity of each insert was verified by DNA sequencing prior to transformation into E. coli BL21(DE3) cells for protein expression as previously described (18, 29). The vector pT7HMT encodes an N-terminal 6-His affinity tag that is used for Ni^{2+}-affinity chromatography purification of the protein, but which can be removed by digestion with Tobacco Etch Virus (TEV) protease (29). Following TEV cleavage, the recombinant form of each SPIN protein contains an artificial “GSTGS” amino acid sequence at its N-terminus. All SPIN proteins were analyzed by MALDI-TOF mass spectrometry for both purity and integrity prior to their usage in subsequent experiments.

Surface Plasmon Resonance

Direct binding studies of SPIN proteins to native human MPO were performed on a Biacore T-200 instrument (GE Healthcare). All experiments were carried at 25 ºC using a running buffer of 20 mM HEPES (pH 7.4), 140 mM NaCl, and 0.005% (v/v) Tween-20 and a flowrate of 30 µl/min. Experimental surfaces were created on CMD

200M sensor chips (XanTec Bioanalytics GmbH; Dusselorf, Germany) by coupling native human MPO on three separate flow cells via random amine chemistry. MPO was immobilized at different levels on each flow cell to allow for replicate measurements while ensuring that surface density did not substantially affect the interaction parameters; two flow cells had a relatively high level of MPO at 7155 and 7311 resonance units (RU), respectively, while a third flow cell was derivatized with 2829 RU of MPO. A reference surface was also prepared by activation followed by immediate inactivation with ethanolamine. A concentration series for each SPIN protein was injected over the flow cells for 3 min, followed by a 4 min dissociation phase. Regeneration to baseline was achieved by two consecutive 0.5 min injections of 0.1 M glycine (pH 10.0). Data processing was performed using Biacore T-200 Evaluation Software v3.0 (GE Healthcare). Each reference subtracted injection series was analyzed using a 1:1 binding model (Langmuir) and fitting Rmax locally. The fitted binding curves and were imported and graphed in Igor Pro (Wavemetrics) and the resonance units (RU) were normalized to the maximal response for each experimental series.

MPO Activity Assays

MPO activity was measured spectrophotometrically as previously described using H_2O_2 as a substrate and o-Dianisidine as a redox indicator (18). Each reaction contained 0.2 U/mL MPO isolated from human sputum, 0.5 mM H_2O_2, and 15 µg of o-Dianisidine dihydrochloride (tablet from Sigma-Aldrich) dissolved in 45 mM phosphate buffer (pH 6.0). The absorbance at 450 nm was measured every 45 s for 1 h at 37 °C using a FLUOstar Omega (BMG LABTECH) microplate reader. The slope before saturation was taken as a measure of MPO activity. For enzyme inhibition studies, the MPO protein was incubated for 1 h at 37 °C with a dilution series (2000 nM to 1 nM) of each SPIN protein prior to substrate addition.

Crystallization, Structure Determination and Refinement

A sample of the SPIN-*delphini*/rhMPO complex was prepared by mixing the purified monomers in an equimolar ratio. The sample was then concentrated to 5 mg/ml total protein and exchanged by ultrafiltration into a buffer of 5 mM tris (pH 7.4), 50 mM NaCl. Initial crystallization trials were carried out by vapor diffusion of hanging drops at 20 ºC using Hampton Research Crystal Screen I and II and various customized buffers. Crystals suitable for X-ray diffraction studies were grown over the course of 7-10 days from drops that contained 1 µL of complex mixed with 0.5 µL distilled water and 0.5 µL of a precipitant solution consisting of 0.1 M sodium acetate (pH 4.6), 25% (v/v) PEG 3350. The crystals were briefly soaked in a cryoprotectant solution of 0.1 M sodium acetate (pH 4.6), 25% (w/v) PEG 3350 and 10% (v/v) PEG 4000 prior to flash cooling in liquid N_2.

X-ray diffraction data were collected at beamline 22-ID of the Advanced Photon Source of Argonne National Laboratory. A total of 360 images were collected with an oscillation angle of 1º, an exposure time of 1 s, radiation of λ=1.000 Å, and a sample to detector distance of 300 mm. The reflections were indexed, integrated, and scaled using the HKL-2000 package (38). The structure was solved by molecular replacement using and the refined polypeptide coordinates of SPIN-*aureus*/rhMPO (PDB entry 5UZU) as a search model (18) and PHASER (39) as implemented in the PHENIX software suite (40, 41). The final model was constructed by an iterative combination of automated and manual rebuilding, followed by crystallographic refinement using PHENIX.REFINE (40, 41). 96.08% of the modeled polypeptide residues lie in favored regions of the Ramachandran plot, with only 0.31% in regions classified as outliers. In addition to the two polypeptides, the final model contains 105 ordered solvent molecules, a Ca^{2+} ion coordinated entirely by groups derived from rhMPO, a single Cl^- ion, and a covalently bound heme prosthetic group within the MPO active site. A more detailed description of the cell constants, diffraction data quality, and properties of the final model can be found in **Table 3**. All structural analyses, including calculation of buried surface areas and identification of potential hydrogen bonds and salt bridges, were performed using EBI-PISA (http://www.ebi.ac.uk/msd-srv/prot_int/cgi-bin/piserver). Representations of protein structures were generated by PyMol (http://www.pymol.org/).

REFERENCES

1. Nauseef, W. M. (2007) How human neutrophils kill and degrade microbes: An integrated view. Immunol. Rev. 219, 88–102
2. Nauseef, W. M., and Borregaard, N. (2014) Neutrophils at work. Nat. Immunol. 15, 602–611
3. Faurschou, M., and Borregaard, N. (2003) Neutrophil granules and secretory vesicles in inflammation. Microbes Infect. 5, 1317–1327
4. Nauseef, W. M. (2014) Myeloperoxidase in human neutrophil host defence. Cell. Microbiol. 16, 1146–1155
5. Amulic, B., Cazalet, C., Hayes, G. L., Metzler, K. D., and Zychlinsky, A. (2012) Neutrophil function: from mechanisms to disease. Annu. Rev. Immunol. 30, 459–89
6. Korkmaz, B., Horwitz, M., Jenne, D., and Gauthier, F. (2010) Neutrophil elastase, proteinase 3, and cathepsin G as therapeutic targets in human diseases. Pharmacol. Rev. 62, 726–759
7. Pham, C. T. N. (2006) Neutrophil serine proteases: specific regulators of inflammation. Nat. Rev. Immunol. 6, 541–550
8. Stapels, D. A. C., Geisbrecht, B. V., and Rooijakkers, S. H. M. (2015) Neutrophil serine proteases in antibacterial defense. Curr. Opin. Microbiol. 23, 42–28
9. Odeberg, H., and Olsson, I. (1976) Microbicidal mechanisms of human granulocytes: synergistic effects of granulocyte elastase and myeloperoxidase or chymotrypsin-like cationic protein. Infect. Immun. 14, 1276–1283
10. Lowy, F. D. (1998) *Staphylococcus aureus* infections. N. Engl. J. Med. 339, 520–532
11. Rigby, K. M., and DeLeo, F. R. (2012) Neutrophils in innate host defense against *Staphylococcus aureus* infections. Semin. Immunopathol. 34, 237–59
12. Lu, T., Porter, A. R., Kennedy, A. D., Kobayashi, S. D., and DeLeo, F. R. (2014) Phagocytosis and killing of *staphylococcus aureus* by human neutrophils. J. Innate Immun. 6, 639–649
13. Spaan, A. N., Surewaard, B. G. J., Nijland, R., and van Strijp, J. a G. (2013) Neutrophils versus *Staphylococcus aureus*: a biological tug of war. Annu. Rev. Microbiol. 67, 629–50
14. Garcia, B. L., Zwarthoff, S. A., Rooijakkers, S. H. M., and Geisbrecht, B. V. (2016) Novel Evasion Mechanisms of the Classical Complement Pathway. J. Immunol. 197, 2051–2060
15. Kim, H. K., Thammavongsa, V., Schneewind, O., and Missiakas, D. (2012) Recurrent infections and immune evasion strategies of *Staphylococcus aureus*. Curr. Opin. Microbiol. 15, 92–99
16. Lambris, J. D., Ricklin, D., and Geisbrecht, B. V. (2008) Complement evasion by human pathogens. Nat. Rev. Microbiol. 6, 132–142
17. Stapels, D. a, Ramyar, K. X., Bischoff, M., von Kockritz-Blickwede, M., Milder, F. J., Ruyken, M., Eisenbeis, J., McWhorter, W. J., Herrmann, M., van Kessel, K. P., Geisbrecht, B. V, and Rooijakkers, S. H. (2014) *Staphylococcus aureus* secretes a unique class of neutrophil serine protease inhibitors. Proc Natl Acad Sci U S A. 111, 13187–13192
18. De Jong, N. W. M., Ramyar, K. X., Guerra, F. E., Nijland, R., Fevre, C., Voyich, J. M., McCarthy, A. J., Garcia, B. L., van Kessel, K. P. M., van Strijp, J. A. G., Geisbrecht, B. V., and Haas, P.-J. a. (2017) Immune evasion by a staphylococcal inhibitor of myeloperoxidase. Proc. Natl. Acad. Sci. 10.1073/pnas.1707032114
19. De Jong, N. W. M., Ploscariu, N. T., Ramyar, K. X., Garcia, B. L., Herrera, A. I., Prakash, O., Katz, B. B., Leidal, K. G., Nauseef, W. M., van Kessel, K. P. M., van Strijp, J. a. G., and Geisbrecht, B. V. (2018) A Structurally Dynamic N-terminal Region Drives Function of the Staphylococcal Peroxidase Inhibitor (SPIN). J. Biol. Chem. 10.1074/jbc.RA117.000134
20. Ploscariu, N. T., Herrera, A. I., Jayanthi, S., Suresh Kumar, T. K., Geisbrecht, B. V., and Prakash, O. (2017) Backbone and side-chain 1H, 15N, and 13C resonance assignments of a novel Staphylococcal inhibitor of myeloperoxidase. Biomol. NMR Assign. 11, 285–288
21. Nielsen, H. (2017) Predicting Secretory Proteins with SignalP, pp. 59–73, 1611, 59–73
22. Sievers, F., Wilm, A., Dineen, D., Gibson, T. J., Karplus, K., Li, W., Lopez, R., McWilliam, H., Remmert, M., Söding, J., Thompson, J. D., and Higgins, D. G. (2011) Fast, scalable generation of high-quality protein

multiple sequence alignments using Clustal Omega. Mol. Syst. Biol. 10.1038/msb.2011.75

23. Corpet, F. (1988) Multiple sequence alignment with hierarchical clustering. Nucleic Acids Res. 16, 10881–90
24. Lamers, R. P., Muthukrishnan, G., Castoe, T. A., Tafur, S., Cole, A. M., and Parkinson, C. L. (2012) Phylogenetic relationships among Staphylococcus species and refinement of cluster groups based on multilocus data. BMC Evol. Biol. 10.1186/1471-2148-12-171
25. Taponen, S., Supré, K., Piessens, V., van Coillie, E., de Vliegher, S., and Koort, J. M. K. (2011) Staphylococcus *agnetis* sp. nov., a coagulasevariable species from bovine subclinical and mild clinical mastitis. Int. J. Syst. Evol. Microbiol. 62, 61–65
26. Sasaki, T., Kikuchi, K., Tanaka, Y., Takahashi, N., Kamata, S., and Hiramatsu, K. (2007) Reclassification of phenotypically identified *Staphylococcus intermedius* strains. J. Clin. Microbiol. 45, 2770–2778
27. Stepanović, S., Ježek, P., Vuković, D., Dakić, I., and Petráš, P. (2003) Isolation of Members of the Staphylococcus *sciuri* Group from Urine and Their Relationship to Urinary Tract Infections. J. Clin. Microbiol. 41, 5262–5264
28. Kloos, W. E., Schleifer, K. H., and Smith, R. F. (1976) Characterization of Staphylococcus *sciuri* sp.nov. and Its Subspecies. Int. J. Syst. Bacteriol. 26, 22–37
29. Geisbrecht, B. V., Bouyain, S., and Pop, M. (2006) An optimized system for expression and purification of secreted bacterial proteins. Protein Expr. Purif. 46, 23–32
30. Fiedler, T. J. (2000) X-ray Crystal Structure and Characterization of Halide-binding Sites of Human Myeloperoxidase at 1.8 A Resolution. J. Biol. Chem. 275, 11964–11971
31. Zeng, J., and Fenna, R. E. (1992) X-ray crystal structure of canine myeloperoxidase at 3 Å resolution. J. Mol. Biol. 226, 185–207
32. Shrake, A., and Rupley, J. A. (1973) Environment and exposure to solvent of protein atoms. Lysozyme and insulin. J. Mol. Biol. 10.1016/0022-2836(73)90011-9
33. Lawrence, M. C., and Colman, P. M. (1994) Shape complementarity at protein–protein interfaces. Biopolymers. 34, 933–940
34. Rooijakkers, S. H. M., Ruyken, M., Roos, A., Daha, M. R., Presanis, J. S., Sim, R. B., van Wamel, W. J. B., van Kessel, K. P. M., and van Strijp, J. A. G. (2005) Immune evasion by a staphylococcal complement inhibitor that acts on C3 convertases. Nat. Immunol. 6, 920–927
35. Jongerius, I., Köhl, J., Pandey, M. K., Ruyken, M., van Kessel, K. P. M., van Strijp, J. a. G., and Rooijakkers, S. H. M. (2007) Staphylococcal complement evasion by various convertase-blocking molecules. J. Exp. Med. 204, 2461–2471
36. Spaan, A. N., van Strijp, J. a. G., and Torres, V. J. (2017) Leukocidins: staphylococcal bi-component pore-forming toxins find their receptors. Nat. Rev. Microbiol. 15, 435–447
37. Stothard, P. (2000) The sequence manipulation suite: JavaScript programs for analyzing and formatting protein and DNA sequences. Biotechniques
38. Otwinowski, Z., and Minor, W. (1997) Processing of X-ray diffraction data collected in oscillation mode. Methods Enzymol. 276, 307–326
39. McCoy, A. J., Grosse-Kunstleve, R. W., Adams, P. D., Winn, M. D., Storoni, L. C., and Read, R. J. (2007) Phaser crystallographic software. J. Appl. Crystallogr. 40, 658–674
40. Adams, P. D., Grosse-Kunstleve, R. W., Hung, L.-W., Ioerger, T. R., McCoy, A. J., Moriarty, N. W., Read, R. J., Sacchettini, J. C., Sauter, N. K., and Terwilliger, T. C. (2002) PHENIX: building new software for automated crystallographic structure determination. Acta Crystallogr. Sect. D Biol. Crystallogr. 58, 1948–1954
41. Adams, P. D., Afonine, P. V., Bunkóczi, G., Chen, V. B., Davis, I. W., Echols, N., Headd, J. J., Hung, L. W., Kapral, G. J., Grosse-Kunstleve, R. W., McCoy, A. J., Moriarty, N. W., Oeffner, R., Read, R. J., Richardson, D. C., Richardson, J. S., Terwilliger, T. C., and Zwart, P. H. (2010) PHENIX: A comprehensive Python-based system for macromolecular structure solution. Acta Crystallogr. Sect. D Biol. Crystallogr. 66, 213–221
42. Robert, X., and Gouet, P. (2014) Deciphering key features in protein structures with the new ENDscript server. Nucleic Acids Res. 10.1093/nar/gku316

Chapter 7

Identification of a Staphylococcal Complement Inhibitor with broad host specificity in equid *S. aureus* strains

Nienke W. M. de Jong[1,*], Manouk Vrieling[1,2,*], Brandon L. Garcia[3], Gerrit Koop[4], Matt Brettmann[3], Piet C. Aerts[1], Maartje Ruyken[1], Jos A. G. van Strijp[1], Mark Holmes[5], Ewan M. Harrison[6], Brian V. Geisbrecht[3,#] and Suzan H. M. Rooijakkers[1,#]

[1] Dept. of Medical Microbiology, University Medical Center Utrecht, 3584 CX Utrecht, The Netherlands

[2] The Roslin Institute, University of Edinburgh, Easter Bush Campus, Midlothian EH25 9RG, UK

[3] Dept. of Biochemistry & Molecular Biophysics, Kansas State University, Manhattan, KS 66506, USA

[4] Dept. of Farm Animal Health, Faculty of Veterinary Medicine, Utrecht University, 3584 CL Utrecht, The Netherlands

[5] Department of Veterinary Medicine, University of Cambridge, Cambridge CB3 0ES, UK

[6] Department of Medicine, University of Cambridge, Addenbrooke's Hospital, Cambridge CB2 0QQ, UK

* equal contribution

shared supervision

J Biol Chem. 2018 Feb 5. pii: jbc.RA117.000599. doi: 10.1074/jbc.RA117.000599

ABSTRACT

Staphylococcus aureus is a versatile pathogen capable of causing a broad range of diseases in many different hosts. *S. aureus* can adapt to its host through modification of its genome, e.g. by acquisition and exchange of mobile genetic elements that encode host-specific virulence factors. Recently the prophage ΦSaeq1 was discovered in *S. aureus* strains from six different clonal lineages almost exclusively isolated from equids. Within this phage we discovered a novel variant of Staphylococcal Complement Inhibitor (SCIN), a secreted protein that interferes with activation of the human complement system, an important line of host defense. We here show that this equine variant of SCIN, eqSCIN, is a potent blocker of equine complement system activation and subsequent phagocytosis of bacteria by phagocytes. Mechanistic studies indicate that eqSCIN blocks equine complement activation by specific inhibition of the C3 convertase enzyme (C3bBb). Whereas SCIN-A from human *S. aureus* isolates exclusively inhibits human complement, eqSCIN represents the first animal-adapted SCIN variant that functions in a broader range of hosts (horses, humans and pigs). Binding analyses suggest that the human-specific activity of SCIN-A is related to amino acid differences on both sides of the SCIN-C3b interface. These data suggest that modification of this phage-encoded complement inhibitor plays a role in the host adaptation of *S. aureus* and are important to understand how this pathogen transfers between different hosts.

INTRODUCTION

The Gram-positive bacterium *Staphylococcus aureus* (*S. aureus*) has become a major risk for both human and animal health. While the bacterium harmlessly colonizes thirty percent of healthy adults, it can also cause severe infections ranging from abscesses to endocarditis, sepsis and toxic shock syndrome (1). Furthermore, *S. aureus* also colonizes and infects a broad range of animal species including cows, sheep, goats, poultry, rabbits and horses (2). For example, *S. aureus* is a major cause of intramammary infections in dairy cows and therefore a major economic burden for the dairy industry (3). In horses, *S. aureus* can cause both community-onset infections (joint, skin or soft tissue infections (4)) and severe surgical site infections in hospitalized horses.

Previous studies on human *S. aureus* isolates have shown that this pathogen is highly versatile and can successfully adapt to its host and various host tissues via production of specific virulence factors. For instance, *S. aureus* expresses both surface-attached and secreted proteins that allow the bacterium to adhere to various human tissues, directly kill host cells or block important immune mechanisms (5). Some of these factors are encoded by mobile genetic elements (MGEs) such as bacteriophages and pathogenicity islands, which allow more rapid acquisition and exchange of virulence genes between strains. In the past, our group was involved in the identification of a *S. aureus* bacteriophage that encodes four human-specific immune evasion molecules: the Staphylococcal Complement Inhibitor (SCIN, referred to as SCIN-A hereafter), Chemotaxis Inhibitory proteins of Staphylococci (CHIPS), Staphylokinase (SAK) and Staphylococcal Enterotoxin A (SEA). This prophage ϕSa3, which specifically inserts in the β-hemolysin gene, was only found in human *S. aureus* isolates (prevalence of 90% from a genetically diverse clinical *S. aureus* strain collection (6)) and encodes secreted proteins that solely block human immune functions. The fact that this phage (and its immune evasion cluster) is lost in animal-associated strains (7, 8) suggests that this cluster is important for *S. aureus* infection in humans (6). The gene with the highest prevalence on ϕSa3 is *scn,* which encodes SCIN, a 9.8 kDa alpha-helical molecule that specifically blocks activation of the human complement system (9).

Complement is a protein network in plasma that labels bacterial cells for phagocytosis by human immune cells. This labelling is achieved via specific activation of the complement reaction on the bacterial cell (via pattern recognition molecules) that subsequently drive formation of surface-bound protease complexes (C3 convertases) that cleave C3, the major complement protein in blood. Conversion of C3 into the reactive C3b fragment results in covalent surface deposition of C3b molecules that are recognized by complement receptors on phagocytic cells (10). The SCIN-A molecule, which is secreted by *S. aureus*, specifically binds and blocks C3 convertases via a unique inhibitory mechanism that is well-characterized via structural studies (11–13). Functional studies showed that SCIN-A is highly specific for human

complement, since it does not block complement activation in sera of other animals (mouse, rat, dog, sheep, guinea pig, goat, and cow) (9).

Here we identify a novel variant of SCIN that is present in *S. aureus* isolates from horses and encoded by an equid-specific prophage (termed ϕSaeq1). This equine SCIN molecule (eqSCIN) represents the first animal-adapted SCIN variant since it inhibits C3 convertases of horses and other animals. These data suggest that *S. aureus* can adapt to other hosts by modification of phage-encoded complement evasion proteins.

Results

eqSCIN is encoded on prophage ϕSaeq1

Recently, a 45 kb prophage ϕSaeq1 was discovered in *S. aureus* clonal complex (CC)133 isolates from horses and donkeys that encodes the equine-specific leukocidin LukPQ (14), a bi-component pore forming toxin consisting of LukP and LukQ subunits (**Figure 1A**). Interestingly, LukPQ has an enhanced ability to kill equine host cells as compared to related staphylococcal leukocidins located elsewhere in the genome. Sequence analysis of CC133 reference isolate 3711 revealed that ϕSaeq1 also encodes a novel variant of SCIN-A (termed eqSCIN) that shares 57.8% amino acid identity with ϕSa3-encoded SCIN-A (**Figure 1B**). The gene for eqSCIN (*scn-eq*) is located downstream of *lukQ* on the outer end of the prophage near the attL phage attachment site (**Figure 1A**). Previously, we found *lukPQ* and ϕSaeq1 to be associated with equid strains of *S. aureus*. Here, we set out to investigate the distribution of *scn-eq*. BLASTn analysis of our collection of sequenced isolates (14) revealed that *scn-eq* was present in 29 strains from 5 different clonal complexes (CC1, CC133, CC522, CC350, CC1660) isolated in geographically distinct locations (**Supplemental Table 1**). The majority of these strains were cultured from equid hosts, but the gene was also present in a few ruminant isolates. All isolates that harbored *scn-eq* also encoded *lukQ* and *lukP*, indicating that these virulence genes are prone to occur together. Even in isolates that do not encode a complete ϕSaeq1 prophage, as observed in two isolates from Brazilian buffalo (14), *scn-eq*, *lukQ* and *lukP* are found in close proximity of each other on the chromosome. The sequence identity of *scn-eq* was highly conserved (>95%) and only a few SNPs were observed, which were associated with clonal lineage (**Supplemental Table 1**). The *scn-eq* sequence of the CC1660 isolate showed the largest degree of variability and contained an insertion of nine base pairs, adding three amino acids (VKA) to the N-terminus of eqSCIN. Altogether, we here describe a novel phage-encoded variant of SCIN associated with equid *S. aureus* isolates. The *scn-eq* gene co-localizes with the *lukPQ* genes and was found in all isolates encoding this equine-specific leukocidin.

eqSCIN blocks complement activation in equine serum

To test whether eqSCIN indeed functions as a complement inhibitor, we first cloned and

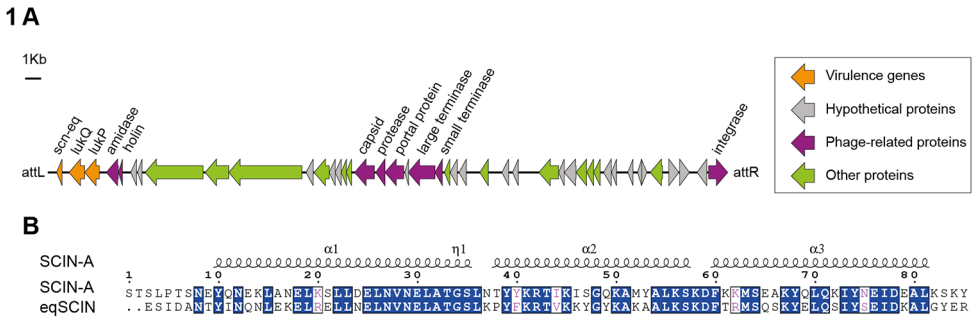

Figure 1: eqSCIN is a novel SCIN variant encoded by prophage ϕSaeq1. (**A**) Location of the *scn-eq* gene on prophage ϕSaeq1 of equine CC133 reference isolate 3711. (**B**) Amino acid alignment of eqSCIN (strain 3711) with SCIN-A (Newman) shows that these SCIN variants share 57.8% sequence identity. Conserved regions are highlighted.

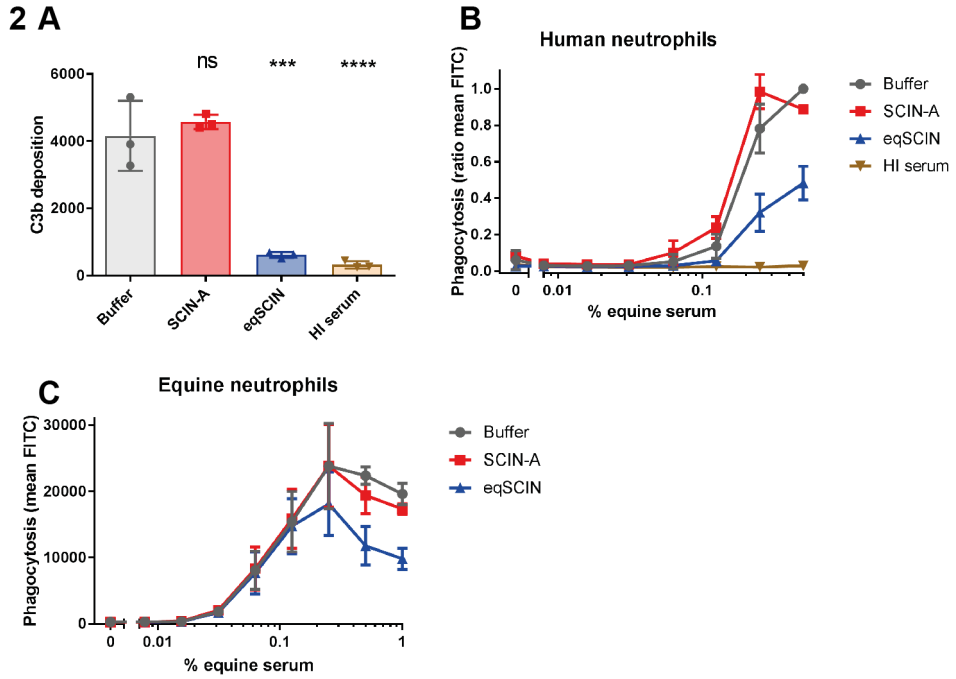

Figure 2: eqSCIN blocks complement activation in equine serum. (**A**) eqSCIN inhibits C3b deposition on *S. aureus* in equine serum. Twenty percent horse serum was incubated with 30 nM SCIN-A or 37 nM eqSCIN, after which C3b deposition on cells of *S. aureus* strain Wood was measured via staining with anti-human C3b antibodies and flow cytometry. The extent of C3b deposition is shown as the geometric mean fluorescence of all gated bacteria. HI = heat-inactivated serum. (**B and C**) eqSCIN inhibits phagocytosis of *S. aureus* strain Wood by human (**B**) and equine (**C**) neutrophils after opsonization with a concentration range of horse complement. Pre-incubation of serum with SCIN-A shows no effect on phagocytosis.
The amount of phagocytosis is shown as ratio of mean FITC with 0.5 % serum with buffer control set as 1 for **B** and mean FITC for **C**. Bars express SD with N=3. Significance relative to buffer control was determined by one-way ANOVA with Bonferroni post-test correction for multiple comparison. ns (non-significant), **** $p \leq 0.0001$.

expressed the *scn-eq* gene (without the signal sequence) in *E. coli* and purified the recombinant protein using nickel affinity chromatography. Then we analyzed whether eqSCIN could block complement activity in equine serum. Since reagents for functional complement analyses in equine sera are limited, we developed a C3b opsonization assay on *S. aureus* in equine serum using flow cytometry. *S. aureus* (commonly used lab strain Wood) was incubated with equine serum and deposition of C3b molecules onto staphylococci was determined via staining with anti-human C3b antibodies and flow cytometry. Representative flow plots of the assay are shown in **Supplemental Figure 1**. Western blotting was used to verify that polyclonal anti-human C3b antibodies cross-react with horse C3 (data not shown). In 20% equine serum, the antibodies detected C3b molecules on the bacterial surface, which was specific since no signal was observed in serum that was heat-treated at 56°C (to abrogate complement activity (15)). SCIN-A from human isolates effectively blocks C3b labelling in human sera (9, 16), but not in equine serum (**Figure 2A**). In contrast, eqSCIN strongly inhibited C3b labelling by equine serum.

We next studied whether eqSCIN could affect the phagocytosis of *S. aureus* by neutrophils, which are critical immune cells in the first line of defense against *S. aureus* (17). To this end, GFP-labelled *S. aureus* strain Wood was pre-incubated with equine serum as a complement source after which freshly isolated neutrophils were added for 15 minutes. We used human and equine neutrophils for our phagocytosis assays and showed that equine complement was competent for promoting phagocytosis by both human and equine neutrophils (Fig. 2B and 2C). Again, we used heat-inactivated (HI) serum as a control to show that bacterial phagocytosis was indeed complement-dependent. Previous studies have established that SCIN-A from human isolates potently inhibits phagocytosis in the presence of human serum (9). In concordance with the C3b deposition experiments, we likewise observed that this SCIN-A does not interfere with phagocytosis in the presence of equine serum. However, the eqSCIN variant inhibited phagocytosis in equine serum (**Figure 2B and 2C**). Altogether these data show that eqSCIN, in contrast to human SCIN-A, blocks complement activity in equine serum.

eqSCIN interferes with equine C3 convertases

Previous investigations from our groups showed that SCIN-A blocks C3b deposition via a specific interaction with the C3 convertase enzymes (11). In the alternative pathway (AP), the C3 convertase consists of a transiently stable complex between surface-attached C3b and protease Bb (C3bBb) (18). For C3 cleavage to occur in this context, C3bBb first forms a 1:1 complex with its C3 substrate, then Bb reorients itself into proximity with the scissile bond of C3 (by virtue of Bb binding a flexible domain of C3b). From structural studies of SCIN-A in complex with C3bBb (11), C3b and its C3c fragment (19), we now know that the SCIN-A molecule makes ~1,400 $Å^2$ of contact with both C3b and protease Bb. This bipartite interaction blocks movement of Bb toward its substrate thus rendering the enzymatic complex inactive.

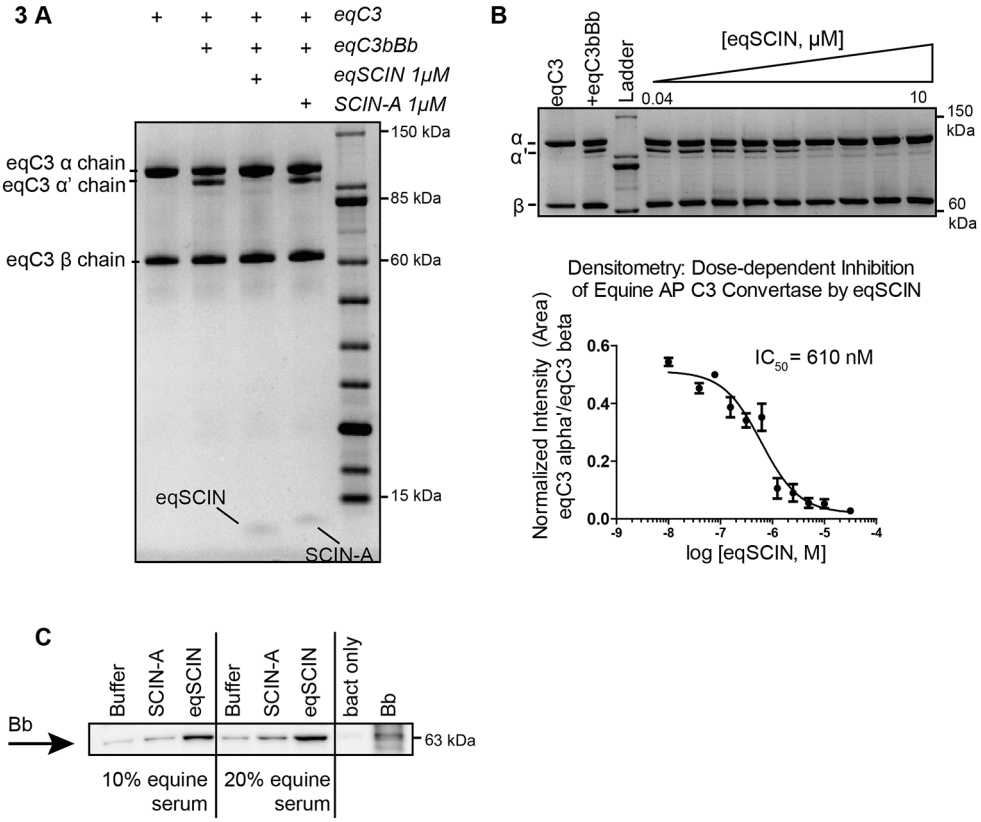

Figure 3: eqSCIN interferes with equine C3 convertases. (**A**) The ability of eqSCIN or SCIN-A to inhibit the fluid phase equine AP convertase was assessed. An equimolar solution of eqC3b and equine factor B was mixed with human factor D to form an equine AP convertase (eqC3bBb). Equine C3 was mixed in the presence or absence of 1 μM eqSCIN or SCIN-A for 1 hour at 37°C. The conversion of eqC3 α-chain to α' was monitored on a reducing SDS-PAGE gel. In the presence of 1 μM eqSCIN this conversion is inhibited, while in the presence of SCIN-A the reaction proceeds in a manner similar to buffer control. (**B**) A two-fold serial dilution of eqSCIN (0.04 to 10 μM) was incubated with eqC3bBb and the band corresponding to the eqC3 α'-chain was quantified by densitometry using ImageJ where the invariant eqC3 β-chain was used to normalize each lane. These data indicate that while eqSCIN inhibits equine AP convertases, SCIN-A does not. All assays were performed in duplicate and the half maximal inhibitory concentration (IC_{50}) was calculated using variable non-linear regression in GraphPad Prism 5. (**C**) eqSCIN stabilizes Bb on the surface of bacteria opsonized with 10% and 20% equine serum, SCIN-A does not. Buffer only and 1 μM SCIN-A showed background levels of Bb, whereas Bb stabilization was increased by adding 1 μM eqSCIN. One representative experiment is shown of three independent experiments.

To study whether eqSCIN blocks the equine AP C3 convertase in a similar manner, we first purified C3, C3b and factor B from equine plasma using a modified purification protocol for human complement components. We then developed an assay in which activity of equine AP C3 convertase could be measured using these purified components. In this system, C3 conversion was assessed by adding equine C3 (eqC3) as a substrate to equine AP C3 convertase (eqC3bBb) that had been produced by mixing a solution of equine C3b (eqC3b), equine factor B, and human factor D. Inhibition of equine C3 cleavage was seen with eqSCIN,

whereas SCIN-A failed to block eqC3 conversion (**Figure 3A**). We further characterized the dose-dependent inhibition of eqC3bBb across eqSCIN concentrations ranging from 0.04 to 10 µM, which yielded a half-maximal inhibitory concentration (IC_{50}) of 0.61 µM (**Figure 3B**). These data strongly suggest that eqSCIN binds and interferes with activation of eqC3bBb.

Since C3bBb has a short half-life that causes rapid dissociation of Bb, this protease is not normally detected on target surfaces following opsonization. The binding of SCIN to C3bBb was found to stabilize this otherwise labile complex (11). We therefore examined whether eqSCIN, like human SCIN-A, could also stabilize C3bBb enzymes on bacterial surfaces. To

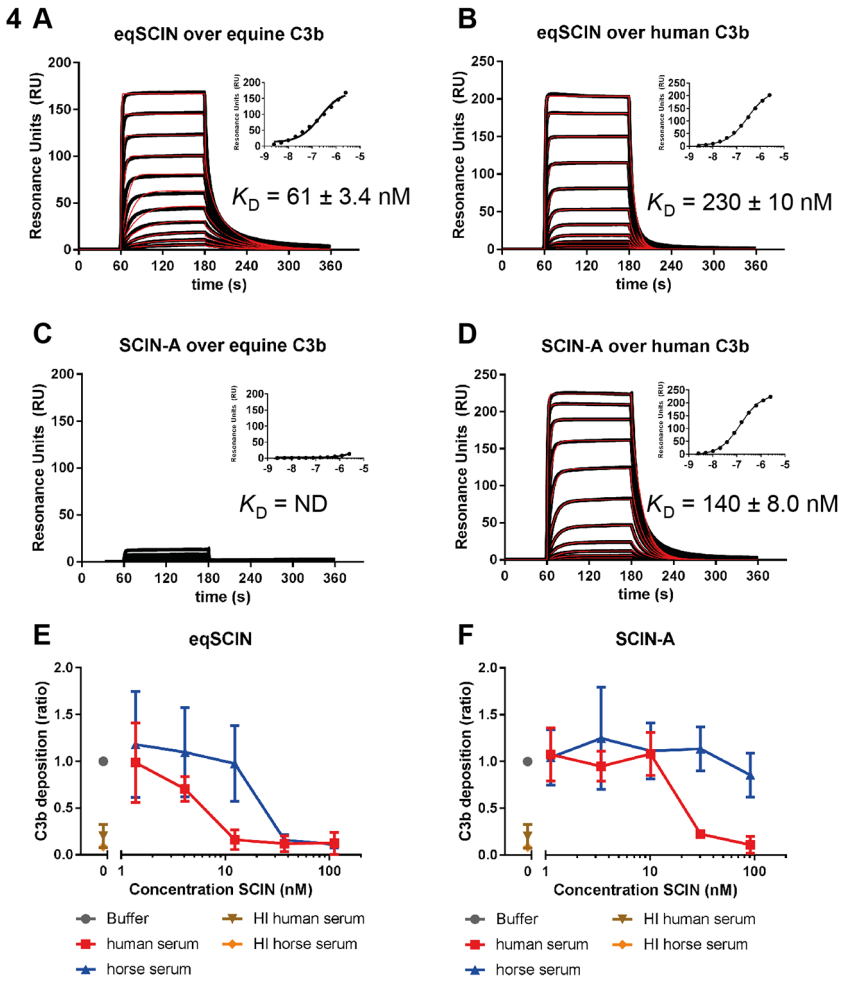

Figure 4: eqSCIN binds equine and human C3b. Characterization of eqSCIN (**A and B**) or SCIN-A (**C and D**) binding to human C3b or eqC3b by SPR. eqSCIN binds to both equine and human C3b, whereas SCIN-A binds to only human C3b. (**E**) eqSCIN inhibits C3b deposition on *S. aureus* in both 20% human and 20% horse serum, whereas SCIN-A (**F**) inhibits C3b deposition only in human serum. As control, HI serum from both human and horses does not lead to C3b deposition.

Table 1: Surface Plasmon Resonance: SCIN/C3b binding parameters.

Immobilized Ligand	Analyte	$K_D^{SPR,kin}$ (nM)	k_a ($M^{-1}s^{-1}$)	k_d (s^{-1})	$K_D^{SPR,ss}$ (nM)
Equine C3b					
	eqSCIN	61 ± 3.4	(1.8 ± 1.0) x 10^6	(1.1 ± 0.65) x 10^{-1}	220 ± 6.0
	SCIN-A	ND	ND	ND	29,000 ± 1700
Human C3b					
	eqSCIN	220 ± 6.0	(5.5 ± 0.01) x 10^5	(1.3 ± 0.04) x 10^{-1}	300 ± 12
	SCIN-A	140 ± 8.0	(6.3 ± 2.6) x 10^5	(9.2 ± 4.3) x 10^{-2}	140 ± 4.0
	eqSCIN	230 ± 10	(5.5 ± 0.01) x 10^5	(1.3 ± 0.04) x 10^{-1}	300 ± 12
	SCIN-A	140 ± 8.0	(6.3 ± 2.6) x 10^5	(9.2 ± 4.3) x 10^{-2}	140 ± 4.0

k_a = association rate constant
k_d = dissociation rate constant
$K_D^{SPR,kin}$ = equilibrium dissociation constant derived from rate constants (kd/ka)
$K_D^{SPR,ss}$ = equilibrium dissociation constant derived from steady-state fitting
ND = not determined, could not be calculated

address this question, we incubated *S. aureus* cells with equine serum in the presence of eqSCIN and, after washing, surface bound Bb molecules were detected using western blotting. While human SCIN-A did not affect eqC3bBb stability at the bacterial surface, we found that eqSCIN lead to stabilization of convertases on *S. aureus* cells (**Figure 3C**). Together, these data indicate that eqSCIN blocks complement activation in equine serum by stabilization of an inhibited form of the equine AP C3 convertases.

eqSCIN binds equine and human C3b

Following verification that eqSCIN indeed functions as a convertase inhibitor in horses, we wondered whether this molecule has similar host-restricted specificity as human SCIN-A molecules. We therefore performed surface plasmon resonance (SPR) to compare the affinity of eqSCIN with C3b molecules from equine and human origin (**Figures 4A, 4B and Table 1**). C3b was non-covalently captured on streptavidin biosensor chips using a previously described method where biotin is site-specifically linked to the thioester domain of C3b that normally anchors C3b to a target surface (12, 13). We found that eqSCIN binds with a comparably high affinity to both eqC3b and human C3b (K_D=61 nM and 230 nM, respectively) (**Figures 4A and 4B**). In concordance with previous reports, we observed that SCIN-A binds very weakly to eqC3b (K_D= ND), but quite highly to human C3b (K_D=140 nM) (**Figures 4C, 4D and Table 1**).

These C3b binding analyses suggest that SCIN-A is specific for human complement, and that eqSCIN might have activity against both human and equine complement. To investigate this further we examined the ability of eqSCIN to inhibit the human complement system. We first

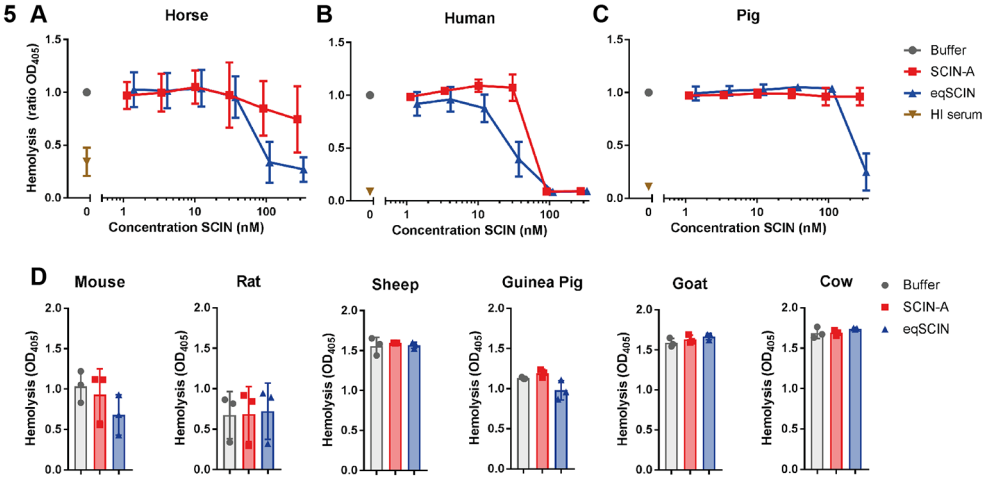

Figure 5: eqSCIN blocks hemolysis in horses, humans and pigs. eqSCIN is able to inhibit AP-dependent hemolysis of erythrocytes caused by complement system of pigs (**A**), horses (**B**), and humans (**C**), whereas SCIN-A inhibits the complement system of only humans (C). As a control, HI serum did not lead to hemolysis of the erythrocytes. HI = heat-inactivated serum (**D**) Both SCIN-A and eqSCIN (concentration of 1 µM was used) do not significantly block hemolysis in mouse, rat, sheep, guinea pig, goat, and cow serum. Bars express SD with N=3. Significance relative to buffer control was determined by one-way ANOVA with Bonferroni post-test correction for multiple comparison.

measured C3b deposition on *S. aureus* cells using human and horse sera in the presence or absence of eqSCIN and SCIN-A (Fig. 4E and 4F). In agreement with the SPR results, 100 nM eqSCIN fully inhibited (AP-dependent) C3b deposition in human and horse serum (**Figure 4E**), while an identical concentration of SCIN-A only blocked C3b deposition by human serum (**Figure 4F**). Examination of eqSCIN and SCIN-A across a range of concentrations revealed that eqSCIN (IC_{50} = 5.1 nM) (**Figure 4E**) was 5 times more potent as an inhibitor of human complement compared to SCIN-A (IC_{50} = 26.1 nM) (**Figure 4F**).

eqSCIN blocks human, equine and pig complement

The C3b-binding data described above suggested that eqSCIN is capable of inhibition of the complement system of multiple host species. To further explore the species specificity of eqSCIN, we used an assay of complement-dependent erythrocyte lysis to also test sera of other animals (mouse, rat, sheep, guinea pig, goat, cow and pig). We initially verified that eqSCIN could inhibit complement activation in the presence of both equine (**Figure 5A**) and human serum (**Figure 5B**) in this assay, whereas SCIN-A only blocked human complement effectively. We also found that eqSCIN inhibited complement activity in pig serum (**Figure 5C**), albeit at only the highest concentration of inhibitor tested. Testing a broader range of animals (mouse, rat, sheep, guinea pig, goat and cow) revealed that eqSCIN only blocked equine, human, and pig complement, while SCIN-A inhibited the human complement system exclusively (**Figure 5D**). As a control, HI serum did not show any hemolysis (**Supplemental Figure 2**). Together, these data established that eqSCIN is not specific for equine complement, but also targets the

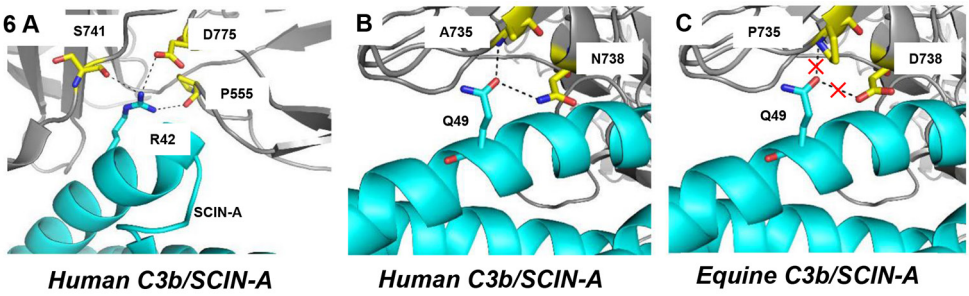

Figure 6: Modeling a putative SCIN-A/eqC3b Interface. To gain insight into the human specific nature of SCIN-A activity, the co-crystal structures of SCIN-A (cyan) in complex with human C3b (grey) were used to model an interaction between equine C3b and SCIN-A. (**A**) SCIN-A R42 forms hydrogen bonds with three human C3b residues (P555, S741, and D775, marked in yellow) and is critical for mediating high-affinity SCIN-A/C3b interaction. An arginine residue is encoded at an equivalent position in eqSCIN and C3b residues which directly contact R42 are conserved between equine and human C3b. (**B**) In contrast to the conserved R42-mediated interaction, the Q49 residue of SCIN-A forms a salt bridge with human C3b residues A735 and N738 (shown in yellow), whereas in equine C3b (**C**) this interaction would be abrogated by A735P and N738D substitutions. The equivalent eqSCIN position encodes a Tyr residue rather than a Gln.

AP C3 convertase of humans and pigs as well.

DISCUSSION

In this study, we identified a variant of the *S. aureus* virulence factor SCIN-A in equid isolates. Interestingly, we observed that eqSCIN was 5 times more potent as an inhibitor of human complement compared to SCIN-A (**Figure 4E and 4F**). This could be explained by the fact that SCIN has two major interaction sites in the C3 convertase (C3bBb). In contrast to SCIN-A orthologues found in human *S. aureus* isolates that only block human complement (16), this newly identified eqSCIN acts on a broader range of host species, and is able to inhibit equine, human and pig complement. These data on eqSCIN support previously observed broad species specificities of equine-adapted *S. aureus* immune evasion proteins (14, 20). Previous work on staphylococcal leukocidins and clotting factors in equid *S. aureus* isolates has identified that equine-adapted immune evasion proteins are not strictly horse-specific but have the ability to interact with immune mediators of multiple host species. For example, the equine-adapted leukocidin LukPQ kills equine neutrophils with higher efficiency than its closest relative in human isolates (LukED) (14). However, LukPQ also has the ability to lyse neutrophils of other animals (humans and cows), albeit less efficiently, in contrast to the ϕSa2-encoded leukocidin PVL that specifically kills human neutrophils (21). Similarly, a broader host range was observed for the equine variant of the von Willebrand factor binding protein compared to similar molecules from ruminant strains (20). The observed broader species specificity of equine virulence factors like eqSCIN as opposed to the human-specific activity of molecules like SCIN-A is interesting and may result from similarities between the complement proteins of these hosts, or possibly result from more frequent/recent host equine/human host jumps of these *S. aureus* lineages. Further research may be able to address these questions. Genome

sequencing of wider collections of *S. aureus* strains isolated from equids over time will help to further investigate the evolution of equid-associated *S. aureus* lineages and their virulence factors.

While SCIN-A and eqSCIN are only 58% identical (**Figure 1B**), human C3b and eqC3b share nearly 80% identity at the amino acid sequence level. We were interested in understanding if differences in amino acids on either side of the SCIN-A/C3b interface may provide an underlying structural explanation for the human specific activity of SCIN-A. Previous work in our labs has produced crystal structures for SCIN-A, SCIN-A/C3bBb, SCIN-A/C3b, and SCIN-A/C3c (11, 22, 23). These studies have been extended to naturally occurring SCIN variants found in human-associated staphylococcal isolates and include atomic-resolution structures of an inactive SCIN protein known as SCIN-D (12, 24). We leveraged this information to model a putative SCIN-A/eqC3b complex. In the context of our previous structural and biochemical studies on SCIN-A/human C3b this approach afforded several potential insights into the human specific nature of SCIN-A.

First, we noted that a key SCIN-A/C3b interaction involving SCIN-A Arg-42 (25) is conserved in the eqSCIN/eqC3b model (**Figure 6A**). Despite its relative importance in driving overall C3b affinity, multiple lines of evidence from our studies involving SCIN variants indicate that residues other than Arg-42 are also critical in mediating C3b interaction and complement inhibitory activity (25). This point is underscored by the observation that SCIN-D, which possesses an equivalently positioned Arg residue, fails to interact with C3b and does not inhibit complement (11, 12). Next, we examined the C3b side of the interface. Of the twelve residues which bury more than 10% of total surface area in the SCIN-A/C3c crystal structure (as judged by the EBI PISA server (26) using PDB: 3L3O), four are non-conserved in eqC3b. These include human to horse substitutions of V554L, A735P, N738D, and V740I. While V554 contacts SCIN-A Tyr-39, V740 makes contact with side chain atoms of SCIN-A Lys-41 and Arg-42. Each of these SCIN-A residues is conserved in eqSCIN and analysis of a putative SCIN-A/eqC3b interface reveals that the similar hydrophobic contacts mediated by each C3b residue are likely to be formed even with the V554L and V740I equine substitutions. Together these observations suggest that these positions are unlikely to significantly alter the affinity of SCIN-A for eqC3b. In contrast, residues A735 and N738 mediate a salt bridge interaction with SCIN-A Gln-49 (**Figure 6B**). This interaction is abrogated in the SCIN-A/eqC3b model as P735 lacks the backbone amide and D738 lacks the side-chain amino group that participate in the Gln-49 salt bridge (**Figure 6C**). Interestingly, eqSCIN encodes a Tyr residue at this position and thus may be able to maintain high affinity for eqC3b via compensatory interactions.

It seems likely that subtle changes in structure resulting from altered sequences of SCIN proteins along with corresponding sequence differences in C3b give rise to their differing specificity profiles. While our model seemingly implicates the A735P/N738D substitutions and the corresponding SCIN-A to eqSCIN Q49Y substitution, however, this alone does not explain

the large differences in affinity that we observe for SCIN-A/C3b vs. SCIN-A/eqC3b (data not shown). It is important to note several limitations inherent in this analysis. First, while we have only considered the primary SCIN-A/C3b site, a second SCIN-A/C3b-binding site involving residues of the N-terminus of SCIN-A is present in all SCIN-A/C3b or C3c crystal structures. We have shown previously that this site contributes to the overall affinity of SCIN proteins for C3b (24) and candidate interactions analogous to the one described above can be identified (i.e. where substitutions on both sides of the SCIN/C3b interface are present). Second, an assumption of this type of analysis is that larger scale structural changes are absent in eqSCIN or eqC3b relative to SCIN-A or human C3b, respectively. To this point, the crystal structure of the inactive SCIN-D protein revealed a change in the secondary structure of the second alpha-helix relative to SCIN-A as well as a significantly different surface charge profile (12). We cannot rule out that higher order structural differences contribute to the C3b-specificity observed for SCIN-A vs. eqSCIN. Thus, future structure/function studies involving eqSCIN and eqC3b are needed to address the underlying structural basis for the human specific activity of SCIN-A more comprehensively.

When considered as a whole, our functional experiments suggest an important role for eqSCIN in the evasion of the innate immune defense against *S. aureus* in horses. The close association of eqSCIN with LukPQ on phage ϕSaeq1 implies that these molecules may act in concert to evade the equine neutrophil response and contribute to *S. aureus* infections in horses. However, further evaluation of the clinical impact of both LukPQ and eqSCIN is clearly required to test this idea. Importantly, zoonotic transmission of equine isolates has been documented between hospitalized horses and their personnel (27–29). In Europe, an epidemic subclone of CC398 MRSA of almost exclusively spa-type t011 was shown to spread within and between equine hospitals (29). Interestingly, we demonstrated in our previous work that the prevalence of LukPQ in equid isolates of this spa-type (t011) was relatively high (14). We can speculate that molecules like LukPQ and eqSCIN that block innate immune responses in horses and humans may facilitate zoonotic transmission of *S. aureus* in settings like the veterinary hospital. The same molecules may also facilitate host jumps between horses and other susceptible host species, like pigs (30). A follow up study focusing on the population distribution of prophage ϕSaeq1 in *S. aureus* isolates of horses, humans and pigs may reveal if there is an association between ϕSaeq1 and *S. aureus* host switching, like was previously shown for other staphylococcal MGE (31, 32). While our understanding of *S. aureus* host adaptation is still largely incomplete, this study provides new insights into the ability of *S. aureus* to evade immune responses in a host-adaptive manner.

MATERIALS & METHODS

Bacterial strains and genomic analysis

The collection of sequenced *S. aureus* genomes used in this study has been described earlier in our previous work

(14). In short, strains used in this study were collected as part of routine surveillance in the United Kingdom or were part of previous/ongoing studies in Switzerland (33), Tunisia (34, 35) and Brazil (36). BLASTn analysis was performed to identify the *scn-eq* gene in the genome collection and the *scn-eq* sequence of isolate 3711 was used as reference throughout the study. The complete sequence of the ϕSaeq1 phage of isolate 3711 is available in the Sequence Read Archive database of the European Nucleotide Archive (Accession Number LT671578). We furthermore used Wood 46 (ATCC-10832) for phagocytosis, C3b deposition and convertase stabilization.

Proteins

Recombinant SCIN with and without a his tag was prepared as described before (9). The protein without his tag was used in the phagocytosis assay, while the his-tagged protein was used for the C3b deposition and hemolysis assay. A gel with the purified proteins is shown in **Supplemental Figure 3**. The eqSCIN coding sequence excluding the signal peptide sequence was amplified from strain 3711 using Phusion polymerase (Thermo Scientific). PCR products were ligated into a slightly modified expression vector pRSETB (Invitrogen Life Technologies) with a non-cleavable N-terminal 6xHis tag. Plasmids were transformed in *E. coli* (Rosetta-gami(DE3)pLysS (Novagen, Merck Biosciences) and protein expression was induced using 1 mM Isopropyl β-D-1-isogalactopyranoside (IPTG). Bacterial pellets were lysed using 200 µg/ml lysozyme and three freeze-thaw cycles in 20 mM sodium phosphate (pH 7.8) to isolate the eqSCIN protein. His-tagged protein was purified using nickel-affinity chromatography (HiTrap chelating, HP, GE Healthcare) with an imidazole gradient ranging from 10-250 mM (Sigma-Aldrich). Finally, purified eqSCIN was dialyzed to PBS and stored at -20°C.

Phagocytosis and C3b deposition on *S. aureus*

Informed consent for blood draw was obtained from all subjects, in accordance with the Declaration of Helsinki. Approval from the medical ethics committee of the University Medical Center Utrecht was attained (METC-protocol 07-125/C approved on 1 March 2010). Blood was collected immediately upon death from four healthy horses during the slaughter process in tubes containing 3 mM EDTA anticoagulant. Equine neutrophils were isolated using 70% Percoll gradients as described before (37). Phagocytosis assays were carried out as described before (38). In short, 2.5 x 10^5 cells of *S. aureus* Wood expressing GFP were incubated with 1 µM SCIN-A or eqSCIN (or buffer control without SCIN-A/eqSCIN), 0-0.5% (v/v) serum, and freshly isolated neutrophils for 15 min at 37°C.

For C3b deposition, 20% horse and 20% human serum were pre-incubated with 30 nM SCIN-A or 37 nM eqSCIN and added to 2.5 x 10^7 washed cells of *S. aureus* Wood WT. Surface-bound C3b was stained with anti-C3 conjugated with FITC (protos immunoresearch) and measured by flow cytometry analysis as geometric mean fluorescence of the gated bacteria. The buffer used for C3b deposition was veronal buffered saline (140 mM NaCl) pH 7.4, 5 mM $MgCl_2$, 10 mM EGTA, and 0.05% (v/v) BSA.

Conversion of C3

An equimolar solution of eqC3b and equine factor B (250 nM) was mixed with 100 nM human factor D to form an equine AP convertase (eqC3bBb). Equine C3 (2 µM) was mixed in the presence or absence of 1 µM eqSCIN or SCIN-A for 1 hour at 37°C in 20 mM HEPES (7.3), 140 mM NaCl, 5 mM NiCl2. The conversion of eqC3 α-chain to α' was monitored on a reducing SDS-PAGE gel. A two-fold serial dilution of eqSCIN (0.04 to 10 µM) was incubated with eqC3bBb and the band corresponding to the eqC3 α'-chain was quantitated by densitometry using ImageJ with the invariant eqC3 β-chain to normalize each lane. All assays were performed in duplicate and an IC_{50} was calculated using variable non-linear regression in GraphPad Prism 5.

Convertase stabilization

Convertase C3bBb stabilization experiments were done as described before (9). In short, 2.5 x 107 cells of *S.*

aureus Wood were incubated for 20 min at 37°C in veronal buffered saline pH 7.4 containing 1 mM $MgCl_2$ and 1 mM $CaCl_2$ plus 0.1% (v/v) BSA with different concentrations of horse serum and 1 µM SCIN-A, eqSCIN, or buffer control). After centrifugation, bacterially-associated proteins were separated by SDS-PAGE, followed by immunoblot. Horse Bb was detected with goat anti-human factor B (Complement Technology) followed by peroxidase-conjugated anti-goat IgG (Santa Cruz Biotechnology).

Hemolysis assay

The alternative pathway hemolytic assay was performed by incubating 20% serum of different animals (30% for horse serum) with various concentrations of SCIN-A or eqSCIN (0 - 1 µM) or one fixed concentration of 1 µM and 2 x 10^7 rabbit erythrocytes (Biotrading) for 1 h at 37°C in veronal-buffered saline containing 5 mM $MgCl_2$ and 10 mM EGTA. OD_{450} nm was measured from supernatant of lysed cells.

Protein-protein interaction assays by SPR

Direct binding of SCIN-A and eqSCIN to human or eqC3b was assessed by SPR on a Biacore T200 instrument. All experiments were performed at 25°C in a running buffer of 20 mM HEPES (pH 7.3), 140 mM NaCl, 0.005% (v/v), Tween-20 (HBS-T) using a flowrate of 30 µl min-1. Site-specifically biotinylated human and eqC3b was prepared using protocols previously described (12, 13). C3b surfaces were prepared by capturing biotinylated C3b on a CMD-200 sensor chip (Xantec) which had previously been coupled with neutravidin (Sigma-Aldrich). EqC3b-biotin was captured at 3,000 RU and human C3b-biotin at 4,200 RU. A reference surface was generated by injecting with biotin only. SCIN-A or eqSCIN were injected for 2 min over each C3b surface in two-fold serial dilutions ranging from 2.5 to 2,500 nM. The dissociation of SCIN/C3b complexes was monitored for 3 min. Baseline signal was achieved without use of regeneration solutions. Each injection series was performed in triplicate. Data were fit to a 1:1 kinetic model of binding (red lines) as well a steady-state binding model (inset plots) using BiaEvaluation T200 Software. In the case of SCIN-A/eqC3b data could not be fit to a kinetic model and thus a steady-state affinity was estimated. As the concentrations used for SCIN-A/eqC3b were sub-saturating this was achieved by fitting these data using a constant maximal observable signal (Rmax) based on the eqSCIN/eqC3b interaction.

Statistical analyses

Statistical analyses was performed with Graphpad Prism version 7. Statistical significance was calculated using one-way ANOVA and Student's t test.

ACKNOWLEDGEMENTS

We thank Dr. Bryan Wee for providing us with bio-informatic advice and Prof. Ross Fitzgerald for critical review of the manuscript. This research was supported by a grant from the U.S. National Institutes of Health (AI113552 and GM121511 to B.V.G.), by an ERC starting grant (#639209 to S.H.M.R.) and this publication presents independent research supported by the Health Innovation Challenge Fund (WT098600, HICF-T5-342), a parallel funding partnership between the Department of Health and Wellcome Trust. The views expressed in this publication are those of the author(s) and not necessarily those of the Department of Health or Wellcome Trust.

CONFLICT OF INTEREST

The authors declare that they have no conflicts of interest with the contents of this article.

AUTHOR CONTRIBUTIONS

N.W.M.d.J. designed and performed functional experiments, analyzed data, and wrote the manuscript. M.V. designed and performed functional experiments, analyzed data, and wrote the manuscript. B.L.G. designed and performed biochemical experiments, analyzed data, and wrote the manuscript. G.K. analyzed epidemiological data and critically reviewed the manuscript. M.B. designed and performed biochemical experiments and analyzed data. P.C.A. produced and isolated recombinant proteins. M.R. performed functional experiments and analyzed data. J.A.G.v.S. designed and analyzed the outcome of functional experiments. M.H. analyzed data and critically reviewed the manuscript. E.M.H. analyzed data and critically reviewed the manuscript. B.V.G. designed the overall scope of the study, analyzed the data, and wrote the manuscript. S.H.M.R. designed the overall scope of the study, analyzed the data, and wrote the manuscript.

REFERENCES

1. Lowy, F. D. (1998) *Staphylococcus aureus* infections. N. Engl. J. Med. 339, 520–532
2. Fitzgerald, J. R. (2012) Livestock-associated *Staphylococcus aureus*: Origin, evolution and public health threat. Trends Microbiol. 20, 192–198
3. Bradley, a. J. (2002) Bovine mastitis: An evolving disease. Vet. J. 164, 116–128
4. Weese, J. S., and van Duijkeren, E. (2010) Methicillin-resistant *Staphylococcus aureus* and Staphylococcus pseudintermedius in veterinary medicine. Vet. Microbiol. 140, 418–429
5. Spaan, A. N., Surewaard, B. G. J., Nijland, R., and van Strijp, J. a G. (2013) Neutrophils versus *Staphylococcus aureus*: a biological tug of war. Annu. Rev. Microbiol. 67, 629–50
6. Van Wamel, W. J. B., Rooijakkers, S. H. M., Ruyken, M., Van Kessel, K. P. M., and Van Strijp, J. A. G. (2006) The innate immune modulators staphylococcal complement inhibitor and chemotaxis inhibitory protein of *Staphylococcus aureus* are located on β-hemolysin-converting bacteriophages. J. Bacteriol. 188, 1310–1315
7. Cuny, C., Abdelbary, M., Layer, F., Werner, G., and Witte, W. (2015) Prevalence of the immune evasion gene cluster in *Staphylococcus aureus* CC398. Vet. Microbiol. 177, 219–223
8. Sung, J. M. L., Lloyd, D. H., and Lindsay, J. a. (2008) *Staphylococcus aureus* host specificity: Comparative genomics of human versus animal isolates by multi-strain microarray. Microbiology. 154, 1949–1959
9. Rooijakkers, S. H. M., Ruyken, M., Roos, A., Daha, M. R., Presanis, J. S., Sim, R. B., van Wamel, W. J. B., van Kessel, K. P. M., and van Strijp, J. A. G. (2005) Immune evasion by a staphylococcal complement inhibitor that acts on C3 convertases. Nat. Immunol. 6, 920–927
10. Gasque, P. (2004) Complement: A unique innate immune sensor for danger signals. Mol. Immunol. 41, 1089–1098
11. Rooijakkers, S. H. M., Wu, J., Ruyken, M., van Domselaar, R., Planken, K. L., Tzekou, A., Ricklin, D., Lambris,

J. D., Janssen, B. J. C., van Strijp, J. a G., and Gros, P. (2009) Structural and functional implications of the alternative complement pathway C3 convertase stabilized by a staphylococcal inhibitor. Nat. Immunol. 10, 721–727

12. Garcia, B. L., Summers, B. J., Lin, Z., Ramyar, K. X., Ricklin, D., Kamath, D. V., Fu, Z. Q., Lambris, J. D., and Geisbrecht, B. V. (2012) Diversity in the C3b convertase contact residues and tertiary structures of the staphylococcal complement inhibitor (SCIN) protein family. J. Biol. Chem. 287, 628–640
13. Ricklin, D., Tzekou, a., Garcia, B. L., Hammel, M., McWhorter, W. J., Sfyroera, G., Wu, Y.-Q., Holers, V. M., Herbert, a. P., Barlow, P. N., Geisbrecht, B. V., and Lambris, J. D. (2009) A Molecular Insight into Complement Evasion by the Staphylococcal Complement Inhibitor Protein Family. J. Immunol. 183, 2565–2574
14. Koop, G., Vrieling, M., Storisteanu, D. M. L., Lok, L. S. C., Monie, T., van Wigcheren, G., Raisen, C., Ba, X., Gleadall, N., Hadjirin, N., Timmerman, A. J., Wagenaar, J. A., Klunder, H. M., Fitzgerald, J. R., Zadoks, R., Paterson, G. K., Torres, C., Waller, A. S., Loeffler, A., Loncaric, I., Hoet, A. E., Bergström, K., De Martino, L., Pomba, C., de Lencastre, H., Ben Slama, K., Gharsa, H., Richardson, E. J., Chilvers, E. R., de Haas, C., van Kessel, K., van Strijp, J. A. G., Harrison, E. M., and Holmes, M. A. (2017) Identification of LukPQ, a novel, equid-adapted leukocidin of *Staphylococcus aureus*. Sci. Rep. 7, 40660
15. Joisel, F., Leroux-Nicollet, I., Lebreton, J. P., and Fontaine, M. (1983) A hemolytic assay for clinical investigation of human C2. J. Immunol. Methods. 59, 229–235
16. Jongerius, I., Köhl, J., Pandey, M. K., Ruyken, M., van Kessel, K. P. M., van Strijp, J. a. G., and Rooijakkers, S. H. M. (2007) Staphylococcal complement evasion by various convertase-blocking molecules. J. Exp. Med. 204, 2461–2471
17. Nauseef, W. M. (2007) How human neutrophils kill and degrade microbes: An integrated view. Immunol. Rev. 219, 88–102
18. Xu, Y., Narayana, S. V, and Volanakis, J. E. (2001) Structural biology of the alternative pathway convertase. Immunol. Rev. 180, 123–135
19. Garcia, B. L., Tzekou, A., Ramyar, K. X., McWhorter, W. J., Ricklin, D., Lambris, J. D., and Geisbrecht, B. V. (2009) Crystallization of human complement component C3b in the presence of a staphylococcal complement-inhibitor protein (SCIN). Acta Crystallogr. Sect. F Struct. Biol. Cryst. Commun. 65, 482–485
20. Viana, D., Blanco, J., Tormo-Más, M. Á., Selva, L., Guinane, C. M., Baselga, R., Corpa, J. M., Lasa, Í., Novick, R. P., Fitzgerald, J. R., and Penadés, J. R. (2010) Adaptation of *Staphylococcus aureus* to ruminant and equine hosts involves SaPI-carried variants of von Willebrand factor-binding protein. Mol. Microbiol. 77, 1583–1594
21. McCarthy, A. J., Witney, A. a, and Lindsay, J. a (2012) *Staphylococcus aureus* temperate bacteriophage: carriage and horizontal gene transfer is lineage associated. Front. Cell. Infect. Microbiol. 2, 6
22. Rooijakkers, S. H. M., Milder, F. J., Bardoel, B. W., Ruyken, M., van Strijp, J. a G., and Gros, P. (2007) Staphylococcal complement inhibitor: structure and active sites. J. Immunol. 179, 985–994
23. Garcia, B. L., Ramyar, K. X., Tzekou, A., Ricklin, D., McWhorter, W. J., Lambris, J. D., and Geisbrecht, B. V. (2010) Molecular Basis for Complement Recognition and Inhibition Determined by Crystallographic Studies of the Staphylococcal Complement Inhibitor (SCIN) Bound to C3c and C3b. J. Mol. Biol. 402, 17–29
24. Garcia, B. L., Summers, B. J., Ramyar, K. X., Tzekou, A., Lin, Z., Ricklin, D., Lambris, J. D., Laity, J. H., and Geisbrecht, B. V. (2013) A structurally dynamic n-terminal helix is a key functional determinant in staphylococcal complement inhibitor (SCIN) proteins. J. Biol. Chem. 288, 2870–2881
25. Summers, B. J., Garcia, B. L., Woehl, J. L., Ramyar, K. X., Yao, X., and Geisbrecht, B. V. (2015) Identification of peptidic inhibitors of the alternative complement pathway based on *Staphylococcus aureus* SCIN proteins. Mol. Immunol. 67, 193–205
26. Krissinel, E., and Henrick, K. (2007) Inference of Macromolecular Assemblies from Crystalline State. J. Mol. Biol. 372, 774–797
27. Cuny, C., Strommenger, B., Witte, W., and Stanek, C. (2008) Clusters of infections in horses with MRSA ST1, ST254, and ST398 in a veterinary hospital. Microb.Drug Resist. 14, 307–310
28. Van Duijkeren, E., Moleman, M., Sloet van Oldruitenborgh-Oosterbaan, M. M., Multem, J., Troelstra, a., Fluit, a. C., van Wamel, W. J. B., Houwers, D. J., de Neeling, a. J., and Wagenaar, J. a. (2010) Methicillin-

resistant *Staphylococcus aureus* in horses and horse personnel: An investigation of several outbreaks. Vet. Microbiol. 141, 96–102

29. Abdelbary, M. M. H., Wittenberg, A., Cuny, C., Layer, F., Kurt, K., Wieler, L. H., Walther, B., Skov, R., Larsen, J., Hasman, H., Fitzgerald, J. R., Smith, T. C., Wagenaar, J. a., Pantosti, A., Hallin, M., Struelens, M. J., Edwards, G., Böse, R., Nübel, U., and Witte, W. (2014) Phylogenetic analysis of *Staphylococcus aureus* CC398 reveals a sub-lineage epidemiologically associated with infections in horses. PLoS One. 9, 31–36

30. Islam, M. Z., Espinosa-Gongora, C., Damborg, P., Sieber, R. N., Munk, R., Husted, L., Moodley, A., Skov, R., Larsen, J., and Guardabassi, L. (2017) Horses in Denmark are a reservoir of diverse clones of methicillin-resistant and -susceptible *Staphylococcus aureus*. Front. Microbiol. 8, 1–10

31. Guinane, C. M., Zakour, N. L. Ben, Tormo-Mas, M. a., Weinert, L. a., Lowder, B. V., Cartwright, R. a., Smyth, D. S., Smyth, C. J., Lindsay, J. a., Gould, K. a., Witney, A., Hinds, J., Bollback, J. P., Rambaut, A., Penadés, J. R., and Fitzgerald, J. R. (2010) Evolutionary genomics of *Staphylococcus aureus* reveals insights into the origin and molecular basis of ruminant host adaptation. Genome Biol. Evol. 2, 454–466

32. Lowder, B. V, Guinane, C. M., Ben Zakour, N. L., Weinert, L. a, Conway-Morris, a, Cartwright, R. a, Simpson, a J., Rambaut, a, Nübel, U., and Fitzgerald, J. R. (2009) Recent human-to-poultry host jump, adaptation, and pandemic spread of *Staphylococcus aureus*. Proc.Natl.Acad.Sci.U.S.A. 106, 19545–19550

33. Sieber, S., Gerber, V., Jandova, V., Rossano, A., Evison, J. M., and Perreten, V. (2011) Evolution of multidrug-resistant *Staphylococcus aureus* infections in horses and colonized personnel in an equine clinic between 2005 and 2010. Microb. Drug Resist. 17, 471–8

34. Gharsa, H., Ben Sallem, R., Ben Slama, K., Gomez-Sanz, E., Lozano, C., Jouini, a, Klibi, N., Zarazaga, M., Boudabous, a, and Torres, C. (2012) High diversity of genetic lineages and virulence genes in nasal *Staphylococcus aureus* isolates from donkeys destined to food consumption in Tunisia with predominance of the ruminant associated CC133 lineage. BMC Vet Res. 8, 203

35. Gharsa, H., Ben Slama, K., Gómez-Sanz, E., Lozano, C., Zarazaga, M., Messadi, L., Boudabous, A., and Torres, C. (2015) Molecular characterization of *Staphylococcus aureus* from nasal samples of healthy farm animals and pets in Tunisia. Vector Borne Zoonotic Dis. 15, 109–15

36. Aires-de-Sousa, M., Parente, C. E. S. R., Vieira-da-Motta, O., Bonna, I. C. F., Silva, D. a., and De Lencastre, H. (2007) Characterization of *Staphylococcus aureus* isolates from buffalo, bovine, ovine, and caprine milk samples collected in Rio de Janeiro State, Brazil. Appl. Environ. Microbiol. 73, 3845–3849

37. Siemsen, D. W., Schepetkin, I. A., Kirpotina, L. N., Lei, B., and Quinn, M. T. (2007) Neutrophil Isolation From Nonhuman Species. in Book, pp. 21–34, 10.1007/978-1-59745-467-4_3

38. Rooijakkers, S. H. M., Van Wamel, W. J. B., Ruyken, M., Van Kessel, K. P. M., and Van Strijp, J. a G. (2005) Anti-opsonic properties of staphylokinase. Microbes Infect. 7, 476–484

SUPPLEMENTAL DATA

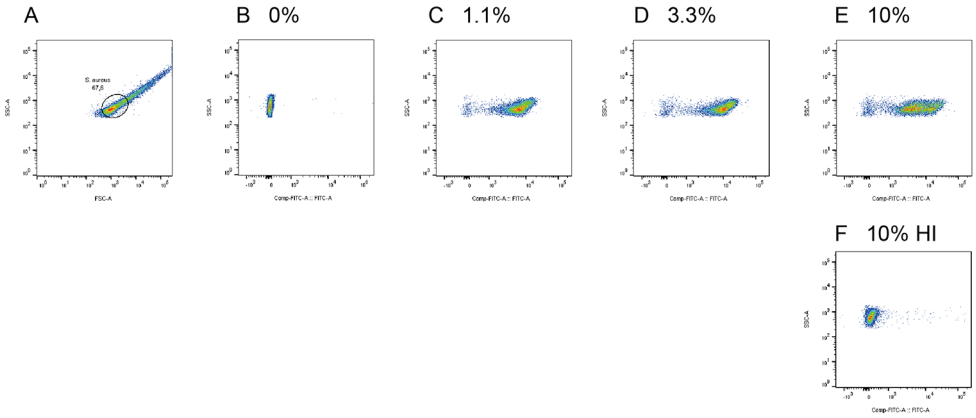

Supplemental Figure 1: Representative flow plots for C3b deposition with equine serum. (**A**) Representation of gating *S. aureus* Wood in each well. (**B-E**) Detection of surface-bound C3b with anti-C3 conjugated with FITC and measured by flow cytometry analysis as geometric mean fluorescence of the gated bacteria after addition of various concentrations of equine serum. (**F**) 10% HI serum does show any C3b deposition, by the lack of FITC signal.

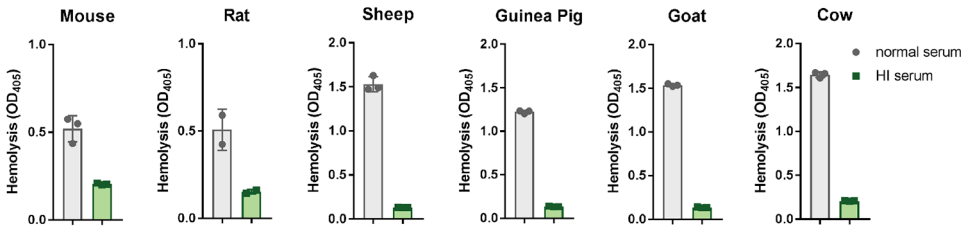

Supplemental Figure 2: HI serum lacks ability to lyse erythroyctes compared to normal serum. The serum of the different animals used in **Figure 5D** were heat-inactivated and tested in the hemolysis assay. The complement in the sera of all animals lacked activity to lyse erythrocytes, while normal serum had active complement to lyse the erythrocytes.

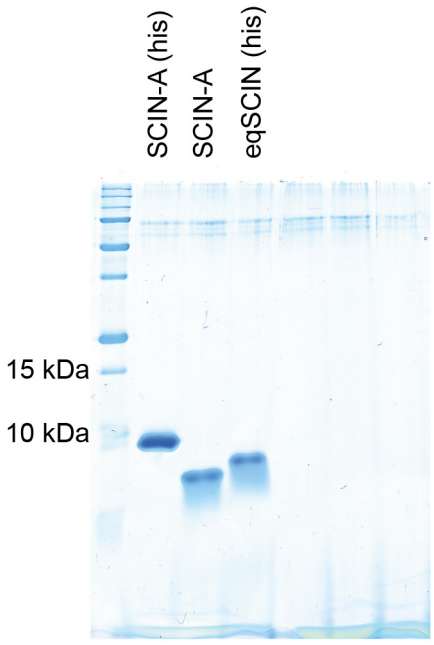

Supplemental Figure 3: Protein gel with purified proteins used in this paper. Purified SCIN-A without his tag (lane 1) was used in the phagocytosis assay, while the his-tagged protein was used for the C3b deposition and hemolysis assay (lane 2). The protein in lane 3 is eqSCIN with non-cleavable 6xHis tag. The concentration of the proteins is 150 µg/ml.

Supplemental Table 1: *scn-eq* is present in *Staphylococcus aureus* strains from different clonal complexes (CC) and different countries. For *scn-eq*, the gene location (prophage/chromosome), % identity to the reference (3711), single nucleotide polymorphisms (SNPs) and insertions (INS) are indicated. Furtermore, the presence of lukPQ and other scns are reported.

						scn-eq								*lukPQ*		
						SNPs							INS			
Strain ID	CC	Country	Host species	Location	Identity (%)	75[ns]	103[ns]	157[ns]	189[s]	198[ns]	254[ns]	318[s]	87	*lukP*	*lukQ*	Ref.
KM595-06	1	Switzerland	Horse	Prophage	98,261	G	A	G	A	C	G	T		+	+	(34)
KM777-07	1	Switzerland	Horse	Prophage	98,261	G	A	G	A	C	G	T		+	+	(34)
KM489-05	1	Switzerland	Horse	Prophage	98,261	G	A	G	A	C	G	T		+	+	(34)
m-25-21 2.3	1	UK	Cow	Prophage	98,261	G	A	G	A	C	G	T		+	+	(14)
m-25-21 2.11	1	UK	Cow	Prophage	98,261	G	A	G	A	C	G	T		+	+	(14)
8205	1	UK	Horse	Prophage	98,261	G	A	G	A	C	G	T		+	+	(14)
1928	1	UK	Horse	Prophage	98,261	G	A	G	A	C	G	T		+	+	(14)
8231	1	UK	Horse	Prophage	98,261	G	A	G	A	C	G	T		+	+	(14)
8182	1	UK	Horse	Prophage	98,261	G	A	G	A	C	G	T		+	+	(14)
VetBz55B	133	Brazil	Buffalo	Chromosome	100	T	G	A	T	G	A	T		+	+	(37)
VetBz63	133	Brazil	Buffalo	Chromosome	100	T	G	A	T	G	A	T		+	+	(37)
c3388	133	Tunisia	Donkey	Prophage	100	T	G	A	T	G	A	T		+	+	(35)
c3401	133	Tunisia	Donkey	Prophage	100	T	G	A	T	G	A	T		+	+	(35)
c3403	133	Tunisia	Donkey	Prophage	100	T	G	A	T	G	A	T		+	+	(35)
c4439	133	Tunisia	Donkey	Prophage	100	T	G	A	T	G	A	T		+	+	(35)
c4444	133	Tunisia	Donkey	Prophage	100	T	G	A	T	G	A	T		+	+	(35)
c4445	133	Tunisia	Donkey	Prophage	100	T	G	A	T	G	A	T		+	+	(35)
c4451	133	Tunisia	Donkey	Prophage	100	T	G	A	T	G	A	T		+	+	(35)
c4452	133	Tunisia	Donkey	Prophage	100	T	G	A	T	G	A	T		+	+	(35)
c3815	133	Tunisia	Goat	Prophage	100	T	G	A	T	G	A	T		+	+	(35)
7107	133	UK	Horse	Prophage	100	T	G	A	T	G	A	T		+	+	(14)
7540	133	UK	Horse	Prophage	100	T	G	A	T	G	A	T		+	+	(14)
5431	133	UK	Horse	Prophage	100	T	G	A	T	G	A	T		+	+	(14)
8401	133	UK	Horse	Prophage	100	T	G	A	T	G	A	T		+	+	(14)
3711	133	UK	Horse	Prophage	100	T	G	A	T	G	A	T		+	+	(14)
8572	350	UK	Horse	Prophage	98,261	G	A	G	A	C	G	T		+	+	(14)
3507	522	UK	Horse	Prophage	99,42	T	G	A	A	G	A	C		+	+	(14)
8571	522	UK	Horse	Prophage	98,261	G	A	G	A	C	G	T		+	+	(14)
KM1549-2-06	1660	Switzerland	Horse	Prophage	95,763	G	A	G	A	C	G	T	AAAG CAGTA	+	+	(34)

[ns] = non-synonymous; [s] = synonymous

Chapter 8

GENERAL DISCUSSION – Expanding the staphylococcal evasion repertoire

Nienke W. M. de Jong[1]

[1] Department of Medical Microbiology, University Medical Center Utrecht, Utrecht University, Utrecht, the Netherlands

Manuscript accepted for publication:
Adapted from Gram-positive pathogens, 3rd Edition, Section III: the Staphylococcus
Novick R. et al., Eds.

EXPANDING THE STAPHYLOCOCCAL EVASION REPERTOIRE

Staphylococcal innate immune evasion

Bacteria adapt to their environment. Pathogenic bacteria adapt to survival in their host. In the human host this means that they have evolved various virulence strategies to overcome innate and adaptive immunity. These virulence strategies are: (i) camouflage of the microbial surface to avoid immune recognition by the production of an inert capsule, often composed of sugars; (ii) hiding from the immune system by adapting to an intracellular life style in immune cells or other cells; or (iii) secretion of small proteins that inhibit specific elements of the immune system (1). These approaches all have advantages and disadvantages. Production of a capsule requires a considerable amount of energy. Next to that, at some stages during infection, the bacteria need to remove their capsule, for example for adherence to host cells, thereby exposing themselves to the immune system. Hiding from the immune system through survival inside cells is also a challenge by the presence of multiple microbicidal enzymes and proteins inside these cells. Moreover, discovery of intracellular TLRs, NOD-like receptors, and inflammasomes revealed that bacteria can also be recognized at the inside of cells (2). Therefore the production of small secreted inhibitory proteins is, by itself or in combination with the other strategies, a strong evasion strategy to survive within the host and works extracellularly as well as intracellularly. *S. aureus* has extensively evolved proteins to evade all facets of the initial attack by the host immune system, as described in **Chapter 1**.

S. aureus remains a leading cause of bacterial infections and has an inclining risk for human health with the rise of antibiotic resistance in community-acquired strains. Also, the financial burden grows due to increasing pressure on the health-care system. Research toward immune evasion molecules is very important, since these proteins determine staphylococcal virulence and pathogenesis. Understanding the mode of action of these evasion molecules will help us to find new therapeutics for prophylaxis or will improve treatment against *S. aureus*, since a functional vaccine is still lacking.

So many evasion molecules; luxury or necessity

To date, the functions of around forty immune evasion proteins are identified and this number is still growing, as reviewed in **Chapter 1**. These evasion molecules are present in clinical isolates and are expressed in the human host, since healthy carriers and non-carriers in adults and even young children have antibodies against these proteins (3, 4). Some of these evasion molecules were detected by high resolution mass spectrometry from nasal polyp tissue from patients with chronic rhinosinusitis (5). One question arising from this observation is; why is *S. aureus* expressing so many evasion molecules? It seems a waste of time and energy for the bacterium to produce and secrete all of these proteins. Most of them target different specific parts of the immune system. We think that this demonstrates the strength, the significance, and the redundancy of our innate immune system. A very efficient and redundant immune

system can only be overcome by a redundant counterattack. Moreover, other microbes have different methods to avoid recognition and killing by the immune system. As said before, a thick capsule is an efficient method to hide and sterically hinder access to the highly immunogenic surface, for example masking the binding of C3 fragments to the complement receptor. This leads to decreased opsonization, phagocytosis and subsequently killing of the micro-organisms by neutrophils (6). Gram-negative bacteria such as Neisseria meningitides and Gram-positive bacteria such as Group A *Streptococcus* and *Streptococcus pneumoniae*, are known to produce this thick capsule (6–8). A typical capsule is encoded by at least 15 large glycosyltranferases that are encoded by 3-4% of all basepairs in the genome, because the average size of a glycosyltransferase is between 200-300 kDa. Evasion proteins are much smaller, typically between 10-30 kDa and encoding 40 of these therefore will take less than 1% of the whole *S. aureus* genome. Also the production and maintenance of a thick polysaccharide capsule consumes a large amount of energy. Therefore, the production of 40 small proteins that directly attack the immune system is "cheaper" for the bacterium than the strategy to make a thick capsule.

Another explanation for the enormous amount of different immune evasion proteins is variability in the human's defense. The arsenal of immune evasion molecules makes it easier to fight the immune system of different individuals with variable antigens and genomic variation in their immune response. In addition, the expression of the various evasion molecules is tightly regulated via multiple regulation systems and this results in differential expression during different growth stages. Interestingly, some of these relative small molecules have multiple functions as seen in **Chapter 1**. The total number of secreted proteins in *S. aureus* is 100-200 and many of these proteins still have no known function (9). Thus, it is likely that not only new evasion molecules will be identified in the future, but also that new functions will be addressed to already known proteins (9). In this thesis we have identified the function of SPIN (in **Chapter 4**), but it might be that in the future another function will be addressed to SPIN. Addressing a second function to SPIN in immune evasion could help us in explaining some unpublished data where there was a significant difference in virulence between wild-type bacteria and Δ*spn* knock-out bacteria *in vivo* in mice. Mice injected with Δ*spn* knock-out bacteria developed less abscesses compared to mice injected with wild-type bacteria. This is quite striking since we extensively tested that SPIN does not have any inhibitory function on murine myeloperoxidase (MPO) (**Chapter 4** and unpublished data).

Despite the fact that *S. aureus* produces so many evasion molecules, the majority of colonized individuals will not suffer a staphylococcal infection. This tells us how complex and efficient our own immune system is. Invading micro-organisms can already be cleared within minutes by our innate immune system, possibly before some immune evasion proteins are produced. The pathogens are recognized by pattern recognition receptors and opsonized by components of the complement system and immunoglobulins. These immunoglobulins from the adaptive immune system are also able to neutralize bacterial components, such as superantigens,

toxins and other immune evasion proteins. The opsonized bacteria are efficiently ingested by neutrophils and killed by oxidative and non-oxidative proteins, which are safely stored inside their granules.

In conclusion, it seems that there is a delicate balance between the immune system and *S. aureus* in their ongoing battle to fight each other. However, *S. aureus* is gaining ground due to the rise of antibiotic resistance, community-acquired and highly virulent strains.

Identification of a newly identified protein evading neutrophil killing

Since there were indications that there are still yet unidentified evasion proteins and there were unknown factors which led to a decrease in neutrophil reactive oxygen species (ROS) production (**Chapter 3**), we used a new high-throughput screening method in our search to find yet unidentified evasion proteins. This method, called secretome phage display, has been used before in the discovery of SEIX and SSL6 which were shown to bind specific neutrophil surface receptors (10). In **Chapter 4**, we successfully identified SPIN by using secretome phage display, where we found that SPIN was binding to the degranulate of activated neutrophils. There we observed an enrichment in 36 out of 48 clones with this protein. Nowadays this screening method has been optimized for deep sequencing, which gives the possibility to discover other potential evasion proteins which first remained in the background (unpublished data). This is a novel, unbiased and successful method to screen for particularly secreted proteins. It is a screening method and therefore not all evasion proteins will be detected via this technique, but it might give us other novel identified evasion proteins in the future.

Thus, we identified and characterized SPIN, where we observed that SPIN is able to bind and inhibit MPO. The role of MPO in intracellular bacterial killing is controversial. In the early 1970s it was thought that MPO is the main factor in killing of *S. aureus* by HOCl production, because MPO deficient patients showed a log difference in bacterial survival after phagocytosis (11). However, this process is incompletely understood and reproducible results are lacking. Later, MPO showed to contribute poorly to the pulmonary defence in MPO-deficient mice against *S. aureus*, whereas other micro-organisms (e.g. *C. albicans, C. tropicalis, P. aeruginosa*) where significantly less cleared in MPO-deficient mice compared to wild-type mice (12). Back then it was believed that the pH inside the phagosome dropped to 4.0 (13). Later the pH inside the phagosome was believed to be pH 7.8 and later dropped till pH 6.9 after 15 minutes of phagocytosis (14), or lowered to pH 5.7 after 60 minutes (15). Recently, data revealed that the pH becomes even more alkaline due to K^+ influx, which is optimal for granules proteases (16), bringing in debate the role of MPO in bacterial killing because an alkaline pH results in a virtual absence of peroxidase and chlorinating activity of MPO (17). It is possible that MPO has two different functions *in vivo*, one is peroxidase activity at pH ~6 when the neutrophil is unable to fully engulf an organism, or a SOD (18) or catalase (19) activity in an alkaline milieu in a fully enclosed vacuole with a pH ~9 to favor conditions for the neutrophil serine proteases (NSPs) (e.g. proteinase 3, cathepsin G, and elastase) (20). MPO could also protect the microbicidal

enzymes against oxidative damage, so both oxygen-dependent and oxygen-independent machineries inside the phagosome synergize to most effectively killing of microbes.

In **Chapter 4**, we have demonstrated that the MPO-dependent part in killing of *S. aureus* in neutrophils is 26% in the first 60 minutes. Therefore, the contribution of SPIN to MPO-mediated killing after phagocytosis is modest. In order for us to observe a SPIN-dependent effect on bacterial survival, we boosted the SPIN expression to make sure that all MPO inside the phagosome was inhibited. We therefore used the highly efficient promoter of LukM instead of its own promoter for overexpression of SPIN (21). This led to a super producing SPIN strain as observed in **Chapter 4**. This vector was modified from the promoter reporter vector from **Chapter 2** where the *sarA*-P1 promoter was replaced by promoter of LukM and the fluorescent signal sGFP was swapped for *spn*. This stable plasmid has also been modified to study the expression of SPIN in **Chapter 4**, with sGFP under the control of *spn* promoter.

Despite the moderate SPIN-dependent effect on bacterial survival after phagocytosis, the mechanism by which SPIN inhibits MPO is very unique. This mechanism is described in **Chapter 4** where we solved the co-crystal structure SPIN/MPO. The N-terminus of SPIN forms a molecular plug to prevent substrate access of MPO at its active site. In **Chapter 5** we zoomed into the binding and inhibiting characteristics of SPIN toward MPO. There we observed that the N-terminus of SPIN is not structured in the unbound state, as found with NMR studies. This floppy N-terminus is susceptible for cleavage by NSPs, which cleaves the N-terminus as detected with MALDI-TOF. However, *S. aureus* secretes Eap which inhibits the NSPs (22) as shown in **Chapter 5**. There we suggest that Eap can have a protective role for SPIN inside the phagosome, but are both of them expressed there? **Chapter 4** showed eightfold upregulation of *spn* expression after phagocytosis compared with samples without neutrophils. This effect was similar as in an earlier microarray study where enhanced *spn* expression was observed after exposure to azurophilic granule proteins (23). Interestingly, the increase in *spn* expression in **Chapter 4** was not detected when we used SaeR/S knock-out bacteria, which is known to regulate the expression of multiple virulence factors (24). This suggests that SPIN is largely regulated by the SaeR/S regulation system and likely contributes to the SaeR/S-dependent reduction of neutrophil ROS as described in **Chapter 3**. Interestingly, Eap (MW1880) is highly upregulated as well in the same microarray study, after exposure to azurophilic granules. This upregulation was even three times higher compared to SPIN (11-fold upregulation after 15 minutes exposure for SPIN compared to 30-fold for Eap) (23). Also, it has been shown before that the SaeR/S regulation system is essential for Eap expression (25). Therefore, it is likely that SPIN and Eap are expressed together inside the phagosome after phagocytosis, where Eap protects the N-terminal region of SPIN from NSP degradation as described in **Chapter 5**.

In **Chapter 6** we looked with a biochemical view at natural occurring SPIN variants in other staphylococci to broaden our knowledge in structure/function principles of SPIN/MPO. There we investigated binding to and inhibition of human MPO of eight SPIN homologs, where three

of them showed more or less inhibition to human MPO. These SPIN proteins derived from other staphylococci may have a function toward MPO from their preferred host. MPO from these different hosts (for example dogs and farm animals) should be produced and tested in a similar experimental approach in order to address this hypothesis with a more biological view. Interestingly, SPIN-sciuri colonizes both animals (e.g. pigs) and humans (26, 27), but this SPIN variant did not bind nor inhibit human MPO (**Chapter 6**). In **Chapter 6** we observed that SPIN-agnetis bond MPO with a SPR-derived KD of 41.8 nM, but SPIN-agnetis did not show any MPO inhibition. Comparing the sequences, revealed that the highly conserved Q37 and N38 in multiple SPIN variants was changed to K37 and S38 in SPIN-agnetis. This suggests that these amino acids are crucial for inhibiting MPO, but that it does not play a significant role in binding to MPO. The function characteristics of this SPIN variant closely resembles a site-directed mutant of SPIN-aureus where the conserved sidechains of H43, D44, and D45 were simultaneously changed to alanine (**Chapter 5**). This mutant also revealed a clear difference between binding and inhibition; $SPIN^{43\text{-}45\rightarrow AAA}$ was still able to bind MPO, whereas there was completely no inhibition of MPO.

It is quite striking that homologs of SPIN are found in so many other staphylococcal species. For example, SCIN is only found in *S. argenteus*, which only recently separated from *S. aureus* (28). Sequence identities between the homologs used in **Chapter 6** vary between 38% and 57%. The sequence identity is much higher (between 98% and 100%) if we compare SPIN-*aureus* with SPIN in *S. argenteus, S. schweitzeri, S. haemolyticus*. The latter species are found in humans and non-human primates (28, 29), where SPIN probably inhibits human MPO. In contrast, SPIN in the human commensal *S. epidermidis* resulted in only 34% sequence identities. Interestingly, we observe that the SSL next to SPIN on the genome, SSL11, only has homologs in *S. argenteus, S. schweitzeri*, and *S. haemolyticus* and not in the other less related staphylococcal species, when we used BLAST search on SSL11. This indicates that SPIN is more conserved among staphylococcal species compared to SSL11. However, more research needs to be done to identify the importance of SPIN other less related staphylococcal species.

Identification of a horse adapted complement evasion protein

S. aureus is not restricted to the human host, since it can also colonize and infect various mammalian species (30). It can successfully adapt to its host through a combination of allelic diversification, gene loss and the acquisition of mobile genetic elements (MGEs), such as pathogenicity islands (SaPIs) and prophages (31). These MGE-encoded immune evasion genes are generally more restricted to one host, whereas genes encoded in the core variable genome are immobile and have a broader species specificity (32). For example when looking at two leukocidins both targeting C5aR; Panton-Valentine leukocidin (PVL) is found on a prophage which is strongly related to human strains, whereas Hemolysin-gamma CB (HlgCB) is encoded in the core genome and shows a broad species specificity (33). LukPQ is another leukocidin which was identified from an equid-specific prophage (termed ϕSaeq1). LukPQ is adapted to horses by lysing equine neutrophils, similar as eqSCIN which is located on the same prophage

and inhibits the equine complement system as shown in **Chapter 7**. These are not the first examples on host adaptation, because ruminant and equine *S. aureus* isolates contain mobile pathogenicity islands with host-specific variants of the von Willebrand factor-binding protein that specifically causes clotting of ruminant and equine blood (34, 35).

Whereas human SCIN is restricted to the human host, eqSCIN is the first animal-adapted SCIN variant that shows a broader species specificity, by inhibiting the complement system of horses, humans, and pigs, as shown in **Chapter 7**. Similarly, LukPQ also lyses neutrophils of other animals, such as humans and cows, albeit less efficiently (36). Still, many evasion proteins have high affinity binding capacity to only human targets. These high affinity protein-protein interactions between virulence factor and target cause lack of affinity in targets in other, less related hosts. Because multiple immune evasion proteins are restricted to the human host, it leads to difficulties in studying *S. aureus* infections *in vivo*, such as mice. Subsequently, this leads to the lack of a highly reliable animal model and makes it difficult to study human infections, this is in the case of for example SCIN, CHIPS, SAK, PVL, and SPIN (as seen in **Chapter 4**). However, some isolated virulence factors are not human specific and do allow studies in other species, for example Ecb and Efb in a murine infection model (37).

Evasion proteins and therapeutic strategies

Over the past two decades we have gained in-depth knowledge about the existence, the importance and the molecular mode of action of many immune evasion proteins, now, what can we do with this knowledge? As illustrated below, one crucial goal is to find a treatment specifically against staphylococcal infections, but these immune evasion proteins can also be used to dampen the immune response in inflammatory diseases.

Combating *S. aureus* with (new) antibiotics is a challenge, since the bacterium has the extraordinary ability to develop resistance against antibiotics and the discovery of new antibiotics is declining (38). Vaccination is a strategy that could solve much of the problems that we encounter with antibiotic resistance. A few vaccine candidates have already been tested in clinical trials, however, none of them successfully passed phase III studies (39). For example, the vaccine candidates against the relative small capsule of *S. aureus*, capsular polysaccharides type 5 and 8, have not passed clinical trials yet (40). This is possible due to the presence of natural non-opsonic antibodies to another *S. aureus* cell surface polysaccharide, poly-N-acetylglucosamine (PNAG), in human serum and this interferes with the vaccine (41). Other vaccines targeting a single cell surface-associated antigen already failed clinical trials, for example the iron surface determinant B (IsdB). Antibody against IsdB showed good tolerance in healthy volunteers, but in phase III studies patients administered with this vaccine were more susceptible for developing *S. aureus* infections and were five times more likely to die than unvaccinated patients with *S. aureus* infections (42). A recent overview of vaccine candidates and the status of their clinical trials was described and this shows that although there is still ongoing research in this field, no functional vaccine will be available in the near

future (39).

Another way to neutralize evasion molecules is by the generation of small inhibitory peptides or neutralizing antibodies via passive immunization, which is short-term immunity provided by antibodies obtained outside the body. For example, a CCR5 antagonist often used in HIV treatment, maraviroc, also protects T cells and myeloid cells from LukED-mediated toxicity (43). Thus, these types of drugs could also be used as therapeutic alternatives against staphylococcal infections. Also, it might be a good approach to target one of the toxins produced by *S. aureus*. Currently, there are three anti-staphylococcal monoclonal antibodies in clinical trials. Two of them target the secreted virulence factor alpha-toxin, which has recently shown to protect against *S. aureus*-induced pneumonia (44). Unfortunately, until now antibody-based therapy did not pass clinical trial phase two. Earlier research focused on single antigens displayed at the bacterial surface, but recently this has moved toward agents targeting multiple *S. aureus* proteins, for example immune evasion molecules and intracellular reservoirs of the bacterium (45). For example, the monoclonal antibody 6D4 interferes with the activity of SCIN, but it is likely that this will not be the only target in anti-staphylococcal therapy since SCIN-deficient *S. aureus* strains still cause infections (46). Nevertheless, despite the lack of a functional monoclonal antibody/antibodies at this moment, antibody-based therapy is a promising therapeutic agent against staphylococcal infections in the future (47).

The fact that, so-far the development of an anti-staphylococcal vaccine has failed can be contributed to several factors. Vaccines targeting single antigens without adjuvants were insufficient to give protection. This is likely due to the secretion of the manifold evasion molecules. Therefore, research focus has switched to developing a vaccine against a combination of proteins. Another reason for the failure of previous vaccination attempts is the existence of immune evasion by itself, which leads to lower local immunity. Even if the vaccine raises sufficient opsonizing antibodies during this lowered local immunity, the induced antibodies cannot confer protection by lack of an effector system (such as complement and neutrophils). A way to overcome this is to incorporate evasion molecules into the vaccine and raise neutralizing antibodies against these evasion molecules. Inhibit the inhibitor and restore local immunity could be a solution to solve vaccination issues in the future. Nevertheless, redundancy of immune evasion molecules and a good animal model remain obstacles to be resolved.

The evasion molecules can also be used as an anti-inflammatory therapy in diseases where there is a deflecting immune activation. This is a growing area of research due to its increased prevalence in Western countries. There are numerous inflammatory diseases, for example; allergy, asthma, autoimmune diseases, vasculitis, and inflammatory bowel disease. A lot of evasion molecules inhibit central players in human inflammatory diseases, such as some GPCRs, complement components, and Toll-like receptors and are therefore interesting therapeutic targets (48–50). Interestingly, microscopic polyangiitis (MPA) and Churg Strauss

syndrome (CSS) are autoimmune diseases which are characterized with systemic vascular inflammation (vasculitis) of the small-sized blood vessels (51). A hallmark for this vasculitis is the presence of pathogenic, circulating autoantibodies (ANCAs) directed against MPO or NSPs, such as proteinase 3. Though it is currently not understood how antibodies against MPO and proteinase 3 are induced, clinical findings suggest development of ANCAs may be triggered by infection with bacteria such as *S. aureus* (52). More specifically, these autoantibodies can arise from the proteins SPIN (inhibits MPO) and Eap (inhibits NSPs) secreted by *S. aureus*. Investigating if these evasion molecules specifically trigger the formation of ANCAs could help us in understanding why these autoantibodies are produced. Immune evasion proteins as a target for therapeutics has already been used in several studies, for example, SCIN-derived peptides were screened for complement inhibition through phage display in order to develop new complement-directed therapies (53). However, the evasion molecules are immunogenic by itself. So, we need something else that is based on these evasion proteins, such as small peptides or derivatives which are no longer immunogenic. The (co)-crystal structure is known from many evasion molecules and this shows us where the exact binding interface at amino acid level is between the staphylococcal protein and its binding partner of the immune system (32). This is very helpful in designing (structured) peptides.

Another way to use peptides from evasion molecules is in anticancer strategies. Some of these immune receptors promote cancer growth, such as FPR1 in brain tumours. Thus, the staphylococcal inhibitor of FPR1, CHIPS, is a potential anticancer drug target. Recent research with mice expressing human FPR1 on astrocytoma cells treated with CHIPS indeed showed increased survival of the mice and reduced tumour growth (54).

CONCLUDING REMARKS

Studying immune evasion has revealed hidden parts of pathogenesis. We have summarized the function of the many immune evasion proteins which are known so far, while there is still more to discover. Unravelling the pathogenesis of *S. aureus* helps us to develop new therapeutics.

REFERENCES

1. Finlay, B. B., and McFadden, G. (2006) Anti-immunology: Evasion of the host immune system by bacterial and viral pathogens. Cell. 124, 767–782

2. Kawai, T., and Akira, S. (2010) The role of pattern-recognition receptors in innate immunity: update on Toll-like receptors. Nat. Immunol. 11, 373–384

3. Verkaik, N. J., de Vogel, C. P., Boelens, H. a, Grumann, D., Hoogenboezem, T., Vink, C., Hooijkaas, H., Foster, T. J., Verbrugh, H. a, van Belkum, A., and van Wamel, W. J. B. (2009) Anti-Staphylococcal Humoral Immune Response in Persistent Nasal Carriers and Noncarriers of *Staphylococcus aureus*. J. Infect. Dis.

199, 625–632

4. Verkaik, N. J., Lebon, a., de Vogel, C. P., Hooijkaas, H., Verbrugh, H. a., Jaddoe, V. W. V., Hofman, a., Moll, H. a., van Belkum, a., and van Wamel, W. J. B. (2010) Induction of antibodies by *Staphylococcus aureus* nasal colonization in young children. Clin. Microbiol. Infect. 16, 1312–1317
5. Schmidt, F., Meyer, T., Sundaramoorthy, N., Michalik, S., Surmann, K., Depke, M., Dhople, V., Gesell Salazar, M., Holtappels, G., Zhang, N., Bröker, B. M., Bachert, C., and Völker, U. (2017) Characterization of human and *Staphylococcus aureus* proteins in respiratory mucosa by *in vivo*- and immunoproteomics. J. Proteomics. 155, 31–39
6. Rajagopal, M., and Walker, S. (2015) Envelope Structures of Gram-Positive Bacteria. in Current Topics in Microbiology and Immunology, pp. 1–44, 404, 1–44
7. Lo, H., Tang, C. M., and Exley, R. M. (2009) Mechanisms of avoidance of host immunity by Neisseria meningitidis and its effect on vaccine development. Lancet Infect. Dis. 9, 418–427
8. Stollerman, G. H., and Dale, J. B. (2008) The Importance of the Group A *Streptococcus* Capsule in the Pathogenesis of Human Infections: A Historical Perspective. Clin. Infect. Dis. 46, 1038–1045
9. Kusch, H., and Engelmann, S. (2014) Secrets of the secretome in *Staphylococcus aureus*. Int. J. Med. Microbiol. 304, 133–141
10. Fevre, C., Bestebroer, J., Mebius, M. M., de Haas, C. J. C., van Strijp, J. a G., Fitzgerald, J. R., and Haas, P. J. A. (2014) *Staphylococcus aureus* proteins SSL6 and SElX interact with neutrophil receptors as identified using secretome phage display. Cell. Microbiol. 16, 1646–1665
11. Klebanoff, S. J. (1972) Role of myeloperoxidase-mediated antimicrobial systems in intact leukocytes. J. Reticuloendothel. Soc. 12, 170–196
12. Aratani, Y., Kura, F., Watanabe, H., Akagawa, H., Takano, Y., Suzuki, K., Maeda, N., and Koyama, H. (2000) Differential host susceptibility to pulmonary infections with bacteria and fungi in mice deficient in myeloperoxidase. J. Infect. Dis. 182, 1276–1279
13. Jensen, M. S., and Bainton, D. F. (1973) Temporal changes in pH within the phagocytic vacuole of the polymorphonuclear neutrophilic leukocyte. J. Cell Biol. 56, 379–388
14. Dri, P., Presani, G., Perticarari, S., Albèri, L., Prodan, M., and Decleva, E. (2002) Measurement of phagosomal pH of normal and CGD-like human neutrophils by dual fluorescence flow cytometry. Cytometry. 48, 159–166
15. Cech, P., and Lehrer, R. I. (1984) Phagolysosomal pH of human neutrophils. Blood. 63, 88–95
16. Reeves, E. P., Lu, H., Jacobs, H. L., Messina, C. G. M., Bolsover, S., Gabella, G., Potma, E. O., Warley, A., Roes, J., and Segal, A. W. (2002) Killing activity of neutrophils is mediated through activation of proteases by K+ flux. Nature. 416, 291–297
17. Levine, A. P., Duchen, M. R., De Villiers, S., Rich, P. R., and Segal, A. W. (2015) Alkalinity of neutrophil phagocytic vacuoles is modulated by HVCN1 and has consequences for myeloperoxidase activity. PLoS One. 10, 1–20
18. Kettle, A. J., Anderson, R. F., Hampton, M. B., and Winterbourn, C. C. (2007) Reactions of superoxide with myeloperoxidase. Biochemistry. 46, 4888–4897
19. Kettle, a. J., and Winterbourn, C. C. (2001) A kinetic analysis of the catalase activity of myeloperoxidase. Biochemistry. 40, 10204–10212
20. Levine, A. P., and Segal, A. W. (2016) The NADPH Oxidase and Microbial Killing by Neutrophils, With a Particular Emphasis on the Proposed Antimicrobial Role of Myeloperoxidase within the Phagocytic Vacuole. Microbiol. Spectr. 4, 1–14
21. Vrieling, M., Koymans, K. J., Heesterbeek, D. a, Aerts, P. C., Rutten, V. P., de Haas, C. J., van Kessel, K. P., Koets, a P., Nijland, R., and van Strijp, J. a (2015) Bovine *Staphylococcus aureus* Secretes the Leukocidin LukMF' To Kill Migrating Neutrophils through CCR1. MBio. 6, e00335
22. Stapels, D. a C., Kuipers, a., Von Köckritz-Blickwede, M., Ruyken, M., Tromp, a. T., Horsburgh, M. J., de Haas, C. J. C., Van Strijp, J. a G., Van Kessel, K. P. M., and Rooijakkers, S. H. M. (2016) *Staphylococcus aureus* protects its immune-evasion proteins against degradation by neutrophil serine proteases. Cell. Microbiol. 18, 536–545
23. Palazzolo-Ballance, a. M., Reniere, M. L., Braughton, K. R., Sturdevant, D. E., Otto, M., Kreiswirth, B. N.,

Skaar, E. P., and DeLeo, F. R. (2007) Neutrophil Microbicides Induce a Pathogen Survival Response in Community-Associated Methicillin-Resistant *Staphylococcus aureus*. J. Immunol. 180, 500–509

24. Voyich, J. M., Vuong, C., DeWald, M., Nygaard, T. K., Kocianova, S., Griffith, S., Jones, J., Iverson, C., Sturdevant, D. E., Braughton, K. R., Whitney, A. R., Otto, M., and DeLeo, F. R. (2009) The SaeR/S gene regulatory system is essential for innate immune evasion by *Staphylococcus aureus*. J. Infect. Dis. 199, 1698–706

25. Harraghy, N., Kormanec, J., Wolz, C., Homerova, D., Goerke, C., Ohlsen, K., Qazi, S., Hill, P., and Herrmann, M. (2005) sae is essential for expression of the staphylococcal adhesins Eap and Emp. Microbiology. 151, 1789–1800

26. Chen, S., Wang, Y., Chen, F., Yang, H., Gan, M., and Zheng, S. J. (2007) A highly pathogenic strain of Staphylococcus sciuri caused fatal exudative epidermitis in piglets. PLoS One. 2, 1–6

27. Stepanović, S., Ježek, P., Vuković, D., Dakić, I., and Petráš, P. (2003) Isolation of Members of the Staphylococcus sciuri Group from Urine and Their Relationship to Urinary Tract Infections. J. Clin. Microbiol. 41, 5262–5264

28. Tong, S. Y. C., Schaumburg, F., Ellington, M. J., Corander, J., Pichon, B., Leendertz, F., Bentley, S. D., Parkhill, J., Holt, D. C., Peters, G., and Giffard, P. M. (2015) Novel staphylococcal species that form part of a *Staphylococcus aureus*-related complex: the non-pigmented Staphylococcus argenteus sp. nov. and the non-human primate-associated Staphylococcus schweitzeri sp. nov. Int. J. Syst. Evol. Microbiol. 65, 15–22

29. Cavanagh, J. P., Hjerde, E., Holden, M. T. G., Kahlke, T., Klingenberg, C., Flægstad, T., Parkhill, J., Bentley, S. D., and Ericson Sollid, J. U. (2014) Whole-genome sequencing reveals clonal expansion of multiresistant Staphylococcus haemolyticus in European hospitals. J. Antimicrob. Chemother. 69, 2920–2927

30. Fitzgerald, J. R. (2012) Livestock-associated *Staphylococcus aureus*: Origin, evolution and public health threat. Trends Microbiol. 20, 192–198

31. Guinane, C. M., Penadés, J. R., and Fitzgerald, J. R. (2011) The role of horizontal gene transfer in *Staphylococcus aureus* host adaptation. Virulence. 2, 241–243

32. Koymans, K. J., Vrieling, M., Gorham, R. D., and van Strijp, J. A. G. (2016) Staphylococcal Immune Evasion Proteins: Structure, Function, and Host Adaptation. Curr. Top. Microbiol. Immunol. 6, 23–27

33. Spaan, A. N., Schiepers, A., de Haas, C. J. C., van Hooijdonk, D. D. J. J., Badiou, C., Contamin, H., Vandenesch, F., Lina, G., Gerard, N. P., Gerard, C., van Kessel, K. P. M., Henry, T., and van Strijp, J. a. G. (2015) Differential Interaction of the Staphylococcal Toxins Panton–Valentine Leukocidin and γ-Hemolysin CB with Human C5a Receptors. J. Immunol. 195, 1034–1043

34. Viana, D., Blanco, J., Tormo-Más, M. Á., Selva, L., Guinane, C. M., Baselga, R., Corpa, J. M., Lasa, Í., Novick, R. P., Fitzgerald, J. R., and Penadés, J. R. (2010) Adaptation of *Staphylococcus aureus* to ruminant and equine hosts involves SaPI-carried variants of von Willebrand factor-binding protein. Mol. Microbiol. 77, 1583–1594

35. Guinane, C. M., Zakour, N. L. Ben, Tormo-Mas, M. a., Weinert, L. a., Lowder, B. V., Cartwright, R. a., Smyth, D. S., Smyth, C. J., Lindsay, J. a., Gould, K. a., Witney, A., Hinds, J., Bollback, J. P., Rambaut, A., Penadés, J. R., and Fitzgerald, J. R. (2010) Evolutionary genomics of *Staphylococcus aureus* reveals insights into the origin and molecular basis of ruminant host adaptation. Genome Biol. Evol. 2, 454–466

36. Koop, G., Vrieling, M., Storisteanu, D. M. L., Lok, L. S. C., Monie, T., van Wigcheren, G., Raisen, C., Ba, X., Gleadall, N., Hadjirin, N., Timmerman, A. J., Wagenaar, J. A., Klunder, H. M., Fitzgerald, J. R., Zadoks, R., Paterson, G. K., Torres, C., Waller, A. S., Loeffler, A., Loncaric, I., Hoet, A. E., Bergström, K., De Martino, L., Pomba, C., de Lencastre, H., Ben Slama, K., Gharsa, H., Richardson, E. J., Chilvers, E. R., de Haas, C., van Kessel, K., van Strijp, J. A. G., Harrison, E. M., and Holmes, M. A. (2017) Identification of LukPQ, a novel, equid-adapted leukocidin of *Staphylococcus aureus*. Sci. Rep. 7, 40660

37. Jongerius, I., Von Kockritz-Blickwede, M., Horsburgh, M. J., Ruyken, M., Nizet, V., and Rooijakkers, S. H. M. (2012) *Staphylococcus aureus* virulence is enhanced by secreted factors that block innate immune defenses. J. Innate Immun. 4, 301–311

38. DeLeo, F. R., Otto, M., Kreiswirth, B. N., and Chambers, H. F. (2010) Community-associated meticillin-resistant *Staphylococcus aureus*. Lancet. 375, 1557–1568

39. Pozzi, C., Olaniyi, R., Liljeroos, L., Galgani, I., Rappuoli, R., and Bagnoli, F. (2016) Vaccines for *Staphylococcus*

aureus and Target Populations. in Current topics in microbiology and immunology, pp. 23–27, 6, 23–27

40. Bagnoli, F., Bertholet, S., and Grandi, G. (2012) Inferring Reasons for the Failure of *Staphylococcus aureus* Vaccines in Clinical Trials. Front. Cell. Infect. Microbiol. 2, 2–5

41. Skurnik, D., Kropec, A., Roux, D., Theilacker, C., Huebner, J., and Pier, G. B. (2012) Natural antibodies in normal human serum inhibit *staphylococcus aureus* capsular polysaccharide vaccine efficacy. Clin. Infect. Dis. 55, 1188–1197

42. Fowler, V. G., Allen, K. B., Moreira, E. D., Moustafa, M., Isgro, F., Boucher, H. W., Corey, G. R., Carmeli, Y., Betts, R., Hartzel, J. S., Chan, I. S. F., McNeely, T. B., Kartsonis, N. a., Guris, D., Onorato, M. T., Smugar, S. S., DiNubile, M. J., and Sobanjo-ter Meulen, A. (2013) Effect of an Investigational Vaccine for Preventing *Staphylococcus aureus* Infections After Cardiothoracic Surgery. Jama. 309, 1368

43. Alonzo III, F., Kozhaya, L., Rawlings, S. A., Reyes-Robles, T., DuMont, A. L., Myszka, D. G., Landau, N. R., Unutmaz, D., and Torres, V. J. (2012) CCR5 is a receptor for *Staphylococcus aureus* leukotoxin ED. Nature. 493, 51–55

44. Hua, L., Hilliard, J. J., Shi, Y., Tkaczyk, C., Cheng, L. I., Yu, X., Datta, V., Ren, S., Feng, H., Zinsou, R., Keller, a., O'Day, T., Du, Q., Cheng, L., Damschroder, M., Robbie, G., Suzich, J., Stover, C. K., and Sellman, B. R. (2014) Assessment of an anti-alpha-toxin monoclonal antibody for prevention and treatment of *Staphylococcus aureus*-induced pneumonia. Antimicrob. Agents Chemother. 58, 1108–1117

45. Sause, W. E., Buckley, P. T., Strohl, W. R., Lynch, a. S., and Torres, V. J. (2016) Antibody-Based Biologics and Their Promise to Combat *Staphylococcus aureus* Infections. Trends Pharmacol. Sci. 37, 231–241

46. Hoekstra, H., Romero Pastrana, F., Bonarius, H. P. J., van Kessel, K. P. M., Elsinga, G. S., Kooi, N., Groen, H., van Dijl, J. M., and Buist, G. (2017) A human monoclonal antibody that specifically binds and inhibits the staphylococcal complement inhibitor protein SCIN. Virulence. 0, 1–13

47. François, B., Barraud, O., and Jafri, H. S. (2017) Antibody-based therapy to combat *Staphylococcus aureus* infections. Clin. Microbiol. Infect. 23, 219–221

48. Du, C., and Xie, X. (2012) G protein-coupled receptors as therapeutic targets for multiple sclerosis. Cell Res. 22, 1108–1128

49. Ricklin, D., and Lambris, J. D. (2013) Complement in Immune and Inflammatory Disorders: Pathophysiological Mechanisms. J. Immunol. 190, 3831–3838

50. Liu, Y., Yin, H., Zhao, M., and Lu, Q. (2014) TLR2 and TLR4 in autoimmune diseases: a comprehensive review. Clin. Rev. Allergy Immunol. 47, 136–147

51. Kallenberg, C. G. M. (2008) Pathogenesis of PR3-ANCA associated vasculitis. J. Autoimmun. 30, 29–36

52. Glasner, C., De Goffau, M. C., Van Timmeren, M. M., Schulze, M. L., Jansen, B., Tavakol, M., Van Wamel, W. J. B., Stegeman, C. a., Kallenberg, C. G. M., Arends, J. P., Rossen, J. W., Heeringa, P., and Van Dijl, J. M. (2017) Genetic loci of *Staphylococcus aureus* associated with anti-neutrophil cytoplasmic autoantibody (ANCA)-associated vasculitides. Sci. Rep. 7, 1–9

53. Summers, B. J., Garcia, B. L., Woehl, J. L., Ramyar, K. X., Yao, X., and Geisbrecht, B. V. (2015) Identification of peptidic inhibitors of the alternative complement pathway based on *Staphylococcus aureus* SCIN proteins. Mol. Immunol. 67, 193–205

54. Boer, J. C., Domanska, U. M., Timmer-Bosscha, H., Boer, I. G. J., de Haas, C. J. C., Joseph, J. V, Kruyt, F. a E., de Vries, E. G. E., den Dunnen, W. F. a, van Strijp, J. a G., and Walenkamp, a M. E. (2013) Inhibition of formyl peptide receptor in high-grade astrocytoma by CHemotaxis Inhibitory Protein of *S. aureus*. Br. J. Cancer. 108, 587–596

&

Closing pages

NEDERLANDSE SAMENVATTING

INTRODUCTIE

Staphylococcus aureus is een Gram-positieve bacterie die de huid en neusholtes van de mens koloniseert. Veel mensen merken niks van deze kolonisatie, maar soms kan deze bacterie ernstige infecties veroorzaken zoals abcessen, endocarditis, sepsis, bacteriemie en longontsteking. *S. aureus* heeft het buitengewone vermogen om resistent te worden voor antibiotica, zoals de meticilline-resistente *Staphylococcus aureus* (MRSA). Deze bacterie werd eerst alleen in patiënten die in ziekenhuizen opgenomen waren gevonden, maar later werd deze bacterie ook gevonden in gezonde mensen buiten ziekenhuizen. Momenteel neemt de economische last toe en is *S. aureus* een ernstige bedreiging voor de gezondheid van de mens geworden. Dit resulteerde in meer onderzoek naar de pathofysiologie van deze bacterie in de afgelopen jaren wat tot gevolg heeft gehad dat ongeveer veertig eiwitten zijn ontdekt en gekarakteriseerd die verschillende processen in het aangeboren en adaptieve immuunsysteem ontwijken, de zogenaamde evasie eiwitten. De meeste van deze evasie eiwitten zijn specifiek gericht tegen het aangeboren immuunsysteem.

Grootschalige studies aan het proteoom van *S. aureus* (alle eiwitten geproduceerd door *S. aureus*) hebben voorspeld dat ongeveer 100 tot 200 eiwitten uitgescheiden worden door de bacterie. Van velen is de functie momenteel niet bekend. Al deze eiwitten zijn potentiële immune evasie eiwitten, dus de ongeveer 40 evasie eiwitten die we tot nu toe geïdentificeerd hebben zijn misschien nog maar het 'topje van het ijsberg'.

Het immuunsysteem is een verdedigingsmechanisme van ons lichaam dat indringers van buitenaf, zoals bacteriën, bestrijdt. Neutrofielen zijn onderdeel van het aangeboren immuunsysteem en deze cellen zijn zeer belangrijk tijdens een acute infectie. Neutrofielen vormen de grootste groep van leukocyten en maken ongeveer 60% uit van het totale aantal dat in een gezond lichaam aanwezig is. Ze zijn de eerste immuuncellen die aankomen bij een infectie en kunnen bacteriën 'opeten' (fagocyteren). Alleen bacteriën die gelabeld zijn kunnen gefagocyteerd worden. Dit labelen (opsonizeren) van bacteriën wordt gedaan door het complementsysteem. Het complementsysteem is een groep van ongeveer 30 eiwitten die na activatie door middel van een kettingreactie complement activatieproducten afzetten op de oppervlakte van de bacterie (het opsonizeren van bacteriën). Het complementsysteem kan daarnaast immuuncellen, zoals neutrofielen, activeren en aantrekken en Gram-negatieve bacteriën doden door het vormen van een lytische porie, genaamd het 'membrane attack complex' (dit laatste is natuurlijk niet het geval bij *S. aureus*, omdat het een Gram-positieve bacterie is).

Nadat de bacteriën geopsonizeerd zijn door het complementsysteem kunnen ze worden gefagocyteerd door neutrofielen. Eenmaal in de neutrofiel belanden de bacteriën in een holte, het zogeheten 'fagosoom'. Wanneer bacteriën in het fagosoom belanden kan de neutrofiel verschillende granula met antimicrobiële inhoud laten fuseren met het fagosoom waardoor deze belandt in het fagosoom. Hierna kan de neutrofiel zuurstofradicalen produceren die de bacterie aanvallen en daardoor (hopelijk) de bacterie doden. Echter, *S. aureus* heeft van de vele evasie eiwitten ook eiwitten die specifiek ingrijpen tegen de aanval van zuurstofradicalen van de neutrofiel. Een nieuw eiwit dat we kunnen toevoegen aan dit arsenaal is 'Staphylococcal Peroxidase INhibitor' (SPIN), waar hieronder meer over staat geschreven bij hoofdstukken 3 t/m 6. De hoofdstukken 2 en 7 beschrijven andere studies die ik heb gedaan tijdens mijn promotieonderzoek. In hoofdstuk 1 en 8 zijn de introductie en algemene discussie beschreven.

Hoofdstuk 1

Dit hoofdstuk geeft een opsomming van de verschillende immune evasie eiwitten van *Staphylococcus aureus* die op het aangeboren immuunsysteem werken. De verschillende fasen van de immuunrespons die start door een acute infectie worden besproken waarna wordt uitgelegd hoe de verschillende eiwitten van *S. aureus* deze processen tegengaan (inhiberen). Dit resulteert in een overzicht van het immuun evasie repertoire en wat we kunnen doen met deze kennis met betrekking tot het ontwikkelen van therapieën tegen *S. aureus*.

Hoofdstuk 2

In dit hoofdstuk beschrijven we een methode hoe *S. aureus* gelabeld kan worden met 6 verschillende fluorescente kleuren, namelijk mAmetrine, CFP, sGFP, YFP, mCherry en mKate. Deze kleuren hebben we zonder een marker in het genoom van de bacterie gekregen, waardoor de fluorescente kleuren constitutief tot expressie worden gebracht. Verder hebben we ook een vector gecreëerd waarbij een bekende promoter van *S. aureus*, SarA, geplaatst is voor de verschillende fluorescente kleuren. Deze vector kan gebruikt worden voor expressie studies waarbij SarA vervangen kan worden door elke andere gewenste promoter. Deze tools kunnen gebruikt worden om de expressie van eiwitten te monitoren en bacteriën zichtbaar te maken met behulp van maar liefst 6 verschillende fluorescente kleuren.

Hoofdstuk 3

In de studie beschreven in dit hoofdstuk hebben we geobserveerd dat *S. aureus* een factor produceert die invloed heeft op het verlagen van reactieve zuurstofradicalen in neutrofielen. Deze factor wordt gereguleerd door het SaeR/S regulatiesysteem. Dit regulatiesysteem in *S. aureus* is gelinkt aan de regulatie van meerdere evasie eiwitten. We suggereren dat de gevonden factor te maken heeft met het inhiberen van myeloperoxidase (MPO), een eiwit dat betrokken is met reactieve zuurstofradicalen tegen bacteriën in de neutrofiel. Echter, deze factor is niet geïdentificeerd in dit paper.

Hoofdstuk 4

In dit hoofdstuk identificeren en karakteriseren we een eiwit dat we 'Staphylococcal Peroxidase Inhibitor' (SPIN) hebben genoemd. We hadden aanwijzingen dat *S. aureus* eiwitten produceert die specifiek het overleven van de bacterie binnen de neutrofiel vergroten. Daarom hebben we een screen opgezet en we hebben daarbij het eiwit SPIN gevonden. SPIN kan MPO binden en inhiberen. Omdat MPO belangrijke rol speelt bij het doden van bacteriën wanneer ze gefagocyteerd zijn door neutrofielen, is SPIN belangrijk voor het overleven van de bacteriën die in de neutrofielen zitten. We hebben aanwijzingen dat SPIN gereguleerd wordt door het SaeR/S regulatiesysteem, dus de factor beschreven in hoofdstuk 3, is zeer waarschijnlijk SPIN. Bovendien hebben we de kristalstructuur van SPIN in combinatie van MPO kunnen bepalen waardoor we konden zien hoe SPIN precies MPO inhibeert. In de kristalstructuur zien we dat het einde van SPIN (de C-terminus) 3 spiralen (alfa-helices) vormt. Het begin van het eiwit (de N-terminus) gaat naar binnen in de actieve site van MPO en vormt daar 2 bèta-sheets. Hierdoor wordt voorkomen dat het substraat van MPO bij de actieve site kan komen en is MPO inactief.

Hoofdstuk 5

In dit hoofdstuk hebben we de binding en inhibitie mechanismen van SPIN naar MPO verder gekaraktiseerd. We hebben mutanten gemaakt van SPIN om te kijken welke delen van het eiwit belangrijk zijn voor binding en/of inhibitie van MPO. We hebben o.a. gevonden dat de C-terminus belangrijk is voor de binding aan MPO, terwijl de N-terminus verantwoordelijk is voor de inhibitie van MPO. We hebben ook gezien dat de N-terminus alleen niet voldoende is om MPO te inhiberen, het heeft namelijk wel de C-terminus nodig om te binden, waarna de N-terminus in de actieve site gaat en daar de werking van MPO tegengaat. Bovendien hebben we met NMR studies gevonden dat de N-terminus van SPIN niet gestructureerd is wanneer het eiwit niet gebonden is aan MPO, dat gebeurt pas wanneer SPIN aan MPO bindt.

Hoofdstuk 6

In dit hoofdstuk hebben we gekeken naar homologen van SPIN in andere stafylokokken. Door te kijken naar deze natuurlijke mutanten van SPIN kunnen we de moleculaire eigenschappen bepalen die de specificiteit beïnvloeden van de SPIN eiwitten naar MPO. We hebben in dit hoofdstuk gevonden dat SPIN uit S*taphylococcus delphini* ook humaan MPO kan inhiberen, terwijl de homologie tussen de twee eiwitten (SPIN van *S. delphini* en SPIN van *S. aureus*) maar ~50% is. Omdat SPIN van *S. delphini* (SPIN-*delphini*) kan binden met humaan MPO, hebben we hierbij ook de kristalstructuur kunnen oplossen.

Hoofdstuk 7

In dit hoofdstuk hebben we een ander evasie eiwit van *S. aureus* gekarakteriseerd, namelijk een nieuwe variant van 'Staphylococcal Complement INhibitor' (SCIN). Het was al bekend dat SCIN geïsoleerd uit humane stafylokokken de activatie van het complementsysteem kan inhiberen. Dit leidt tot verminderde C3b depositie en daardoor ook verminderde

capaciteit van de neutrofielen om bacteriën te fagocyteren. Deze nieuwe variant van SCIN is gevonden in stafylokokken uit paarden en wij hebben gevonden dat deze equine SCIN (eqSCIN) geëvolueerd is om het complementsysteem van paarden te inhiberen. Het eqSCIN is daarmee de eerste beschreven variant van SCIN is die aangepast is aan dieren. *S. aureus* kan namelijk ook veel verschillende dieren infecteren, zoals bijvoorbeeld koeien, schapen, geiten, gevogelte, konijnen en paarden en de bacterie zorgt voor veel problemen in bijvoorbeeld de zuivelindustrie. We hebben ook gevonden dat de werking van eqSCIN zich niet beperkt tot één gastheer, omdat het ook het complementsysteem van mensen en varkens kan inhiberen. Het veranderen van het eiwit SCIN speelt een belangrijke rol in de adaptatie van *S. aureus* naar andere gastheren.

Hoofdstuk 8

In dit hoofdstuk bediscussiëren we de rol van de nieuw ontdekte immune evasie eiwitten uit bovenstaande hoofdstukken. Hoe belangrijk is het voor de bacterie om deze eiwitten te hebben, zijn er nog meer niet ontdekte evasie eiwitten en kan onderzoek hiernaar uiteindelijk leiden tot therapeutische middelen om infecties door *S. aureus* tegen te gaan?

DANKWOORD

Jeej KLAAR! Nu rest mij nog het schrijven van het meest gelezen onderdeel van mijn boekje; het dankwoord. Ik had mijn promotie nooit alleen kunnen doen en ik wil daarbij iedereen bedanken die mij tijdens het werk heeft geholpen, maar ook naast het werk voor de nodige ontspanning heeft gezorgd. Allereerst wil ik mijn promotor **Jos** en copromotor **Kok** bedanken:

Bedankt **Jos** dat je het vertrouwen had, en dat ik ondanks dat ik de beurs niet had gekregen, toch bij jou in de groep kon komen promoveren. Ik wil je bedanken dat ik de vrijheid heb gekregen om te doen wat in mijn voorstel stond en heb ik in mijn eerste screen toch maar lekker SPIN gevonden! Ondanks deze vliegende start mislukte alles in mijn 3de jaar, maar mede dankzij jouw steun en onuitputtelijke enthousiasme kwam alles bij elkaar de laatste paar maanden. Ik heb veel dingen geleerd in het lab, maar ook daarbuiten over mezelf. Ik vond de trip naar Amerika een unieke ervaring, binnen een dag naar Manhattan, New York, naar Manhattan, Kansas. Bedankt voor alles!

Kok, ik vond het heel leuk dat je afgelopen zomer zei dat je mijn 'officiële' copromotor wilde zijn. Eigenlijk is er niks veranderd behalve dat je op 29 maart terecht achter de tafel kan zitten. Ik wil je enorm bedanken voor alle hulp met het bedenken van experimenten, zoveelste keer de FACS uitleggen met het maken van een nieuw experiment, maar vooral voor het meedenken wanneer de killingsassays helemaal niet wilde lukken. Bedankt voor je hulp toen Jos wat langer thuis was. Ik denk niet dat het SPIN verhaal in PNAS zou zijn belandt als die killingsassays niet zouden zijn gelukt.

Daarna wil ik natuurlijk mijn 2 paranimfen bedanken die straks op 29 maart naast mij zullen staan. Lieve **Kirsten**, samen Bachelor en Master gedaan, ook eerste stage gedeeld en daarna in dezelfde groep gepromoveerd. Ik heb ooit eens gelezen dat als je 10 jaar lang vrienden bent, dat je dan voor altijd bevriend blijft. Volgens mij zijn we die 10 jaar net gepasseerd en ik hoop daarom ook dat onze vriendschap nog heel lang blijft bestaan. Bedankt dat ik jouw paranimf mocht zijn en dat jij die van mij wilt zijn en voor al je hulp en steun tijdens mijn promotie, steun en gezelligheid tijdens congressen, de bijklets-thee'tjes en ontspanning naast het onderzoek.

Lieve **Seline**, wat ontzettend leuk dat je een paar jaar geleden bij ons in de groep kwam en ik vind het geweldig dat je naast me zal staan tijdens mijn verdediging. Je enthousiasme en vrolijkheid is aanstekelijk! Ook je creativiteit is geweldig, alle briefjes die je achterlaat op de kamer, maar ook het bedenken van de 'cactus outfits' van afgelopen Koepel. Ik hoop dat we elkaar nog lang zullen zien wanneer ik niet meer op de MMB ben en dat ik je dan ook zoveel mogelijk kan helpen met het afronden van jouw promotie.

During my PhD I have been collaborating intensively with Kansas State University. Dear **Brian**, I want to thank you so much for everything you have done. This thesis would be very empty without you. That beautiful cocrystal is only solved because of your perseverance. Thank you for your extensive emails and unstoppable enthusiasm for this project and later also for the SCIN project. I liked it a lot when Jos and I visited Kansas and I really enjoyed working with you. **Kasra**, also special thanks to you for welcoming us in Kansas and your great contribution. **Brandon**, the eqSCIN paper would definitely not be so interesting without your input. Thank you so much for looking at it with a more biochemical view. **Nicoleta**, I am glad we have met last summer. Thanks for solving the NMR structure and good luck with finishing your thesis!

I also want to say a special thank you to **Jovanka Voyich** and **Fermin**. Thank you for your contribution to the SPIN paper and that you added me as a coauthor on the JLB paper. Good luck **Kyle** with all the fish experiments and thank you for our skype sessions.

Verder wil ik iedereen bedanken van de **MMB**! Ik denk dat je niet overal zo'n warme afdeling tegenkomt waarbij menig feestje goed wordt gevierd. Ik heb er ook heel veel zin in dit met jullie te vieren eind maart! Er zijn een aantal mensen in het bijzonder die ik wil bedanken: Bedankt **Suzan** voor het oppikken en begeleiden van het paarden-SCIN project, zonder jou was het niet (zo snel) af geweest. **Carla**, bedankt voor alle clone-'tips en tricks' waar ik vooral veel aan heb gehad aan het begin van mijn PhD. **Reindert**, bedankt voor je hulp met fibrine gelen onder de microscoop, alle gekleurde aureus'jes, maar natuurlijk ook voor je gezelligheid. **Pieter-Jan**, bedankt voor je kennis over phage display. **Lisette**, ik wil jou ook heel erg bedanken dat je me de phage display op onze afdeling hebt geleerd. Super leuk dat we nu weer samen aan fagen werken! Bedankt **Karlijn** voor alle administratieve zaken en de gezellige gesprekken! Alles werd meteen geregeld, het was zo fijn om jou op de afdeling te hebben, heel veel succes komende tijd als ZZP'er! Bedankt **Maartje** voor het uitleggen van de complement assays en het runnen van het lab 406. **Anneroos** en **Adinda**, bedankt voor jullie vrolijkheid in het lab! **Piet**, we zijn een goed isolatie team geweest, later ook samen met **Rob**, op de donderdagochtend met het afleveren van perfecte neutro's. Thanks **Alex** for helping me with alignments, really nice you joined our Department. Thanks for you hospitality **Julia**, I really liked our trip to Tübingen. **Bart** (Bartacus), het is altijd gezellig als jij bij een feestje erbij bent. Bedankt voor het luisteren en sparren over de killingsassays.

Bedankt lieve (oud) kamergenootjes van G04.560! Inmiddels is de meidenkamer helemaal veranderd, maar het is nog steeds even gezellig. **Evelien**, jij bent zo'n lief persoon en je hebt een super reden om niet op mijn promotie aanwezig te kunnen zijn! Ik hoop je weer snel te zien wanneer jullie weer in Nederland wonen. **Daphne**, super leuk dat weer terug komt op onze afdeling! Jij bent echt een aanwinst voor het onderzoek en ik hoop dat je nog lang in de wetenschap kan blijven. **Anne**, thanks for all the sweets and good luck at Yale! Lieve **Arie**, bedankt voor je gezelligheid, gelach en creativiteit (vooral met het maken van Koepel outfits!). **Maaike**, leuk om te zien dat alles zo goed gaat in Zeist samen met Hidde en Anton! Thank you

Fernanda for our talks, I am really happy you could stay at the Department. **Patrique**, thanks for the Feuerzangenbowle. Lieve **Jasper**/Jappo/Soppe/Sopje, sorry voor het irriteren terwijl je brak op het werk zat (of toch niet….). Je bent zo'n harde werker en ik hoop dat je straks een super mooi (en misschien heel dik?) boekje hebt, hea. **Dani**, het zonnetje van de kamer en op het lab. Bedankt voor het Broabants praten en je enthousiasme over je MAC. Ik hoop dat je ooit C10 nog zal vinden! **Ron** the American, super gezellig dat je afgelopen jaren mijn buurman was en voor je 'make that the cat wise' Dutch/English. It was always fun when you were explaining me some Dutch grammar rules, vèrrèkkes super dankjewel! I hope you and **Kaila** will find a lovely new home in America.

Bedankt alle **(ex-)aio's van de MMB**! Lieve **Steef**, heel leuk dat we elkaar soms 's ochtends nog tegenkomen om weer zoals vanouds naar de uithof te fietsen. **Rutger** aka Gerrie, het spuiten met alcohol in het lab of ijs in mijn nek heb ik toch niet gemist, wel je aanwezigheid bij de laatste feestjes. Bedankt **Gentje** voor de vele racefiets-ritjes en skype sessies over zebravissen, succes in the windy city! **Nienke Plantinga**, heel leuk dat ik afgelopen jaar een paar keer mee ben gegaan met vrouwenwielrennen, ik ga mijn best doen om komend seizoen zo vroeg mogelijk te beginnen. Succes met het afronden van je promotie! Buurvrouw in het lab, **Manouk**, het was altijd gezellig om samen proefjes te doen. Bedankt voor je grote bijdrage aan het SCIN project en ik vind het super leuk dat je straks achter de tafel zit tijdens de verdediging! **Bas**, veel plezier in Calgary. Zoals je kan lezen in mijn general discussion, is er toch wat van het vele werk van de muizenproeven in het boekje gekomen. Ik vond het super gezellig tijdens de Gordon in Italië! Bedankt **Wouter**, voor alle zin en onzin verhalen en geluidsberichtjes die ik kon meeluisteren op **Kobus'** zijn telefoon. **Dennis**, kei gezellig dat je op de afdeling bent gebleven na je stage! **Elise**, heel veel succes begin mei en veel plezier alvast in Canada!

Verder wil ik ook een aantal vrienden bedanken die voor de nodige ontspanning hebben gezorgd naast het werk:

De meisjes van 'le lait'. Inmiddels is het al super lang geleden dat we in het huisje in de Ardennen zaten en de naam 'le lait' werd geboren. **Kirsten**, **Jarka** (leuk om te zien dat je met zoveel enthousiasme lesmateriaal ontwikkeld en lesgeeft), **Vera** (je bent zo'n lief vriendinnetje!) en **Dieke** (succes met je promotie!).

Marjolein en **Helen**, de BMW meisjes van dag 1. Bedankt voor alle gezellige etentjes en feestjes en het jaarlijkse sauna-uitstapje. Lieve **Lotte**, ik vind het zo leuk dat je ook klaar bent met je promotie en dat je een opleidingsplek in Utrecht hebt gekregen. **Helen**, **Lotte** en **Emile**, ik vond het altijd super leuk om met jullie mee te gaan naar feestjes.

Natuurlijk kunnen de dames van **Femme Fatale** hier niet ontbreken. Bedankt voor een enthousiast bestuur elk jaar, borrels, etentjes en (de laatste tijd) carrièregesprekken. Heel leuk om te zien hoe ons gezelschap verandert in de jaren, terwijl er een nieuwe aanwas van jonge

leden blijft komen.

Na ongeveer 18 jaar mee te hebben gedaan met de Brabantse Dag (en ook de eerste jaren van mijn promotie nog te hebben meegedaan), kan deze groep natuurlijk ook niet ontbreken. **Vriendenkring de Rijten**, ontzettend bedankt voor de gezelligheid, grote hoeveelheden bier en het warme welkom wat ik meteen bij deze groep voelde. Misschien dat ik in de toekomst wel weer mee kan doen, ik kom in ieder geval altijd kijken. Vriendenkring de Rijten…..bedankt! Lieve **Marcelle**, lief vriendinnetje, heel gezellig dat je ook in Utrecht woont en dat we elkaar nog steeds zien. Ik ga mijn best doen om vaker af te spreken!

Lieve **papa** en **mama**, bedankt dat ik uit een enorm warm Brabants nest kom en voor jullie onvoorwaardelijke steun en liefde. Ik vind het altijd fijn om thuis te komen in Heeze, waarbij de deur altijd openstaat. Zonder jullie was dit boekje er echt niet geweest. **Sander** en **Niels** (Nelis), bedankt broertjes voor het dollen, maar op zijn tijd ook goede gesprekken. Broers-zus dag moeten we er zeker inhouden! **Familie Bosman**, bedankt dat ik me altijd welkom voel!

Lieve **Kobi**, ik ben ontzettend blij dat ik je op de afdeling heb leren kennen. Het zijn soms niet de allerbeste omstandigheden om met iemand samen te wonen die ook promoveert (en ook op dezelfde afdeling), maar het is ons super goed afgegaan. Bedankt voor je steun, het relativeren en de vele vakanties die we samen al hebben gehad. Ik vind het heel fijn met je en hoop er over een half jaar net zo voor je te staan als jij nu voor mij. Bedankt schatje.

LIST OF PUBLICATIONS

Related to this thesis

Ploscariu, N. T., **de Jong, N. W. M.**, van Kessel, K. P. M., van Strijp, J. A. G., Geisbrecht, B. V., Identification and Structural Characterization of a Novel Myeloperoxidase Inhibitor from *Staphylococcus delphini*. *(Under revision, Archives of Biochemistry and Biophysics)*

de Jong, N. W. M.*, Vrieling, M.*, Garcia, B. L., Koop, G., Brettmann, M., Aerts, P. C., Ruyken, M., van Strijp, J. A. G., Holmes, M., Harrison, E. M., Geisbrecht, B. V., and Rooijakkers, S. H. M. (2018) Identification of a Staphylococcal Complement Inhibitor with broad host specificity in equid *S. aureus* strains. *J. Biol. Chem.* 10.1074/jbc.RA117.000599

de Jong, N. W. M., van Kessel, K. P. M., van Strijp, J. A. G., (2018) Immune evasion by *Staphylococcus aureus*. Book chapter in Gram-positive pathogens, 3rd Edition, Section III: the *Staphylococcus,* Novick R. *et al*., Eds. *(Manuscript accepted for publication)*

de Jong, N. W. M.*, Ploscariu, N. T.*, Ramyar, K. X., Garcia, B. L., Herrera, A. I., Prakash, O., Katz, B. B., Leidal, K. G., Nauseef, W. M., van Kessel, K. P. M., van Strijp, J. A. G., and Geisbrecht, B. V. (2018) A Structurally Dynamic N-terminal Region Drives Function of the Staphylococcal Peroxidase Inhibitor (SPIN). *J. Biol. Chem.* 10.1074/jbc.RA117.000134

de Jong, N. W. M., Ramyar, K. X., Guerra, F. E., Nijland, R., Fevre, C., Voyich, J. M., McCarthy, A. J., Garcia, B. L., van Kessel, K. P. M., van Strijp, J.A.G., Geisbrecht, B.V.[#], and Haas, P. J. A.[#] (2017) Immune evasion by a staphylococcal inhibitor of myeloperoxidase. *Proc. Natl. Acad. Sci.* 10.1073/pnas.1707032114

de Jong, N. W. M., van der Horst, T., van Strijp, J. A. G., and Nijland, R. (2017) Fluorescent reporters for markerless genomic integration in *Staphylococcus aureus. Sci. Rep.* 7, 1–10

Guerra, F. E., Addison, C. B., **de Jong, N. W. M.**, Azzolino, J., Pallister, K. B., van Strijp, J. A. G., and Voyich, J. M. (2016) *Staphylococcus aureus* SaeR/S-regulated factors reduce human neutrophil reactive oxygen species production. *J. Leukoc. Biol.* 100, 1–6

Other publications

Wilson, D. W., Goodman, C. D., Sleebs, B. E., Weiss, G. E., **de Jong, N. W. M.**, Angrisano, F., Langer, C., Baum, J., Crabb, B. S., Gilson, P. R., McFadden, G. I., and Beeson, J. G. (2015) Macrolides rapidly inhibit red blood cell invasion by the human malaria parasite, Plasmodium falciparum. *BMC Biol.* 13, 52

Weiss, G. E.*, Gilson, P. R.*, Taechalertpaisarn, T., Tham, W. H., **de Jong, N. W. M.**, Harvey, K. L., Fowkes, F. J. I., Barlow, P. N., Rayner, J. C., Wright, G. J., Cowman, A. F., and Crabb, B. S. (2015) Revealing the Sequence and Resulting Cellular Morphology of Receptor-Ligand Interactions during *Plasmodium falciparum* Invasion of Erythrocytes. *PLoS Pathog.* 11, 1–25

Dekkers, J. F., Wiegerinck, C. L., de Jonge, H. R., Bronsveld, I., Janssens, H. M., De Winter-De Groot, K. M., Brandsma, A. M., **de Jong, N. W. M.**, Bijvelds, M. J. C., Scholte, B. J., Nieuwenhuis, E. E. S., van den Brink, S., Clevers, H., van der Ent, C. K., Middendorp, S., and Beekman, J. M. (2013) A functional CFTR assay using primary cystic fibrosis intestinal organoids. *Nat. Med.* 19, 939–945

* equal contribution
[#] shared supervision

CURRICULUM VITAE

Nienke Wilhelmina Maria de Jong was born on the 10th of March, 1988 in Waalre, the Netherlands. She graduated from her pre-university education (VWO) in 2006 at the Strabrecht College in Geldrop. In the same year she started her study of Biomedical Sciences at Utrecht University and obtained her Bachelor of Science degree in 2009. During the end of her Bachelors, she got accepted for the Master Infection & Immunity at Utrecht University, which she started in September 2009. Her first internship took place in Utrecht, at the Department of Immunology, in the group of Prof.dr. Linde Meyaard under the supervision of Dr. Tessa Steevels. Therein she studied the activation, adhesion, and dimerization properties of the inhibitory immune receptor LAIR-1. After the first year of her Masters, she wanted to travel and learn to speak Spanish. Therefore, from September till December 2010, she worked as a Junior technician at the Department of Biomolecular Imaging to fund a three-month Spanish course in Buenos Aires, after which she traveled through Peru and Bolivia for another 3 months. In September 2011 she continued the Master's program Infection & Immunity, where she traveled to Melbourne, Australia, for her second internship. During this internship she studied receptor-ligand interactions during and after invasion of malaria parasites into human red blood cells under the supervision of Dr. Paul Gilson and Dr. Paul Sanders. Back in the Netherlands she wrote her Master thesis under the supervision of Dr. Daphne Stapels in the group of Dr. Suzan Rooijakkers and Prof.dr. Jos van Strijp where she realized she wanted to continue working in microbiology and especially immune evasion. She graduated from the Master's in 2012 and worked for 7 months at QVQ BV to producing Llama antibodies against a specific target by using phage display. In April 2013, she started as a technician in the group of Prof.dr. Jos van Strijp at the Department of Medical Microbiology where she continued working on phage display to screen yet unidentified immune evasion proteins. She continued her work as a PhD candidate in January 2014, under the supervision of Prof.dr. Jos van Strijp and Dr. Kok van Kessel. Her research focused on staphylococcal immune evasion and the results of her studies are described in this thesis and published in peer-reviewed scientific journals. At this moment, Nienke is still working at the Department of Medical Microbiology as a postdoctoral researcher and helps setting up a clinical trial with bacteriophages against *P. aeruginosa* in Cystic Fibrosis patients.

&